FP7-ICT-2009-4/248454

QoSMOS

D3.5

Radio Context Acquisition algorithms – Final version

Contractual Date of Delivery to the CEC:	30-Nov-2012
Actual Date of Delivery to the CEC:	02-Dec-2012
Editor(s):	David Depierre (TCS)
Author(s):	Kazushi Muraoka, Hiroto Sugahara, Masayuki Ariyoshi (NEC), David Depierre (TCF), Matthieu Gautier, Dominique Noguet, Vincent Berg, Jean-Baptiste Doré (CEA), Johanna Vartiainen, Janne Lehtomäki (UOULU), Kamran Arshad, Olasunkanmi Durowoju (UNIS), Dorin Panaitopol, Abdoulaye Bagayoko (NTUK), Luis Gonçalves, Atílio Gameiro, Adão Silva, Carlos Ribeiro (IT)
Internal Reviewers:	Rainer Wansch (Fraunhofer IIS), Arturo Medela (TST)
EAB reviewers:	Alexandre Kholod
Workpackage:	WP3
Est. person months:	105
Security:	PU
Nature:	R
Version:	Issue 2.0
Total number of pages:	140

Abstract:

This deliverable gives a complete overview of the sensing algorithms to acquire and process the radio environment that were developed in the framework of the QoSMOS project. It describes and gives performance estimations for several innovative local and distributed methods.

Keyword list:

Cognitive Radio, Sensing, Radio Context Models

The research leading to these results was derived from the European Community's Seventh Framework Programme (FP7) under Grant Agreement number 248454 (QoSMOS)

Table of Content

1 EXECUTIVE SUMMARY 9

2 SENSING GENERALITIES 11

2.1 STATE OF THE ART REVIEW 11
2.1.1 Introduction 11
2.1.2 Waveform Recognition 12
2.1.2.1 Frequency Localization 12
2.1.2.2 Modulation Identification 12
2.1.3 OFDM Detection 12
2.1.3.1 LTE Detection 14
2.2 MATHEMATICAL AND ALGORITHMIC NOTATIONS 15
2.2.1 General Mathematical Notations 15
2.2.2 Notations for OFDM Waveform 15
2.2.3 Notations for PMSE Waveform 16
2.2.4 Notations for Cyclostationarity Properties 18
2.3 SIMULATION AND EVALUATION METRICS 18

3 LOCAL SENSING ALGORITHMS 20

3.1 SIGNAL DETECTION 20
3.1.1 OFDM Detection 20
3.1.1.1 Two-Stage Hybrid Detection for OFDM 20
3.1.1.2 Parallel Sensing using Antenna Array Processing 27
3.1.2 PMSE Detection 36
3.1.2.1 Wireless Microphone Detection 36
3.1.2.2 White Band Frequency Domain Detection 42
3.1.2.3 Generalized Higher-Order Cyclostationary Feature Detector 48
3.1.2.4 Two-Stage Hybrid Detection for PMSE 52
3.1.3 Spectrum Sensing Based on Statistical Tests 54
3.1.3.1 Fast and Reliable Signal Detection with Background Process for Noise Estimation 54
3.1.3.2 Robust Spectrum Sensing for Cognitive Radios Based on Statistical Tests 60
3.1.4 GFDM Sensing 68
3.1.5 Sensing in Code 70
3.1.5.1 Concept 70
3.1.5.2 UMTS/HSDPA Downlink Channels Structure 70
3.1.5.3 UMTS Traffic Channel Detection 71
3.1.5.4 HSDPA Traffic Channel Detection 74
3.1.5.5 Conclusion 77
3.2 INTERFERENCE MONITORING 78
3.2.1 Overview of Interference Monitoring 78
3.2.2 Interference Measurement Using Quiet Period-Based Power Estimation 79
3.2.3 Interference Measurement Using Cell-specific Reference Signals 81
3.2.4 Comparison of the QP Method with Cell-Specific RS Methods 81
3.3 IDENTIFICATION OF OPPORTUNISTIC SYSTEMS 84
3.3.1 Generalities 84
3.3.2 Watermarking 85
3.3.2.1 State of the Art 86
3.3.2.2 Signal Detection Using Watermark Insertion 86
3.3.2.3 Theoretical Performance 89
3.3.2.4 Simulation Results 91

3.3.2.5 Conclusion ... 93
3.4 BLIND FREQUENCY LOCALIZATION ... 93

4 DISTRIBUTED PROCESSING AND DATA FUSION ... 97

4.1 INFLUENCE OF METRICS PARAMETERIZATION ... 97
4.1.1 Scenario and Main Issues ... 97
4.1.2 One Shot Detection ... 98
4.1.3 Sequential Detection ... 100
4.1.4 Quantization ... 101
4.1.5 Selective Reporting Algorithm ... 102
4.1.5.1 Review of the Basics ... 102
4.1.5.2 Cooperative Sensing with Censorship ... 104
4.1.5.3 Cooperative Sensing with Silence Periods ... 104
4.1.5.4 Analysis ... 106
4.1.5.5 Information Theoretic Interpretation of the Sensing Scheme ... 107
4.1.5.6 Algorithm Behaviour with Fading Channels ... 107
4.1.5.7 Numerical Results ... 108
4.1.6 Selective Reporting Based on State Transitions ... 112
4.1.6.1 State Models for the Case of Constant Underlying Process ... 112
4.1.6.2 Influence of the Reliability of the Reporting Channel ... 114
4.1.6.3 Numerical Results ... 116
4.1.7 Conclusions ... 116
4.2 COLLABORATIVE SPECTRUM SENSING BASED ON BETA REPUTATION SYSTEM ... 117
4.2.1 Introduction ... 117
4.2.2 System Model ... 118
4.2.3 Beta Reputation System ... 119
4.2.4 Proposed Reputation Based Mechanism at Fusion Centre ... 120
4.2.5 Simulation Results and Discussions ... 120
4.3 DISTRIBUTED PROCESSING TO HANDLE MOBILITY ... 122
4.3.1 Introduction ... 122
4.3.2 System Model ... 122
4.3.3 Spectrum Sensing ... 123
4.3.3.1 Measurement Statistics ... 123
4.3.3.2 Hypothesis Testing ... 124
4.3.3.3 Performance Analysis ... 124
4.3.4 Numerical Results ... 125
4.3.5 Remark ... 126

5 CONCLUSIONS ... 127

6 ACRONYMS ... 128

7 REFERENCES ... 132

List of Figures

Figure 2-1: Illustration of cyclic prefix extension in OFDM systems 16
Figure 2-2: RC (left hand side) and RRC (right hand side) impulse response 17
Figure 2-3: Normalized QPSK Signal Spectrum for a roll-off factor 0.1 (left) and 0.9 (right) 17
Figure 2-4: T_S as a function of roll-off factor β, for a constant 400 kHz frequency bandwidth 17
Figure 3-1: Energy detector algorithm 20
Figure 3-2: Energy detector under uncertainty, for PFA_{target}=0.1 21
Figure 3-3: CAF of an OFDM signal 24
Figure 3-4: Comparison between ED and CD for an OFDM signal 24
Figure 3-5: ED and CD feasibility area 25
Figure 3-6: Two-stage hybrid detection concept 25
Figure 3-7: PD versus SNR, for ED and CD, for several sensing duration, with or without error on noise estimation 26
Figure 3-8: Hybrid detection performance on OFDM signals with AWGN channel and 512 carriers compared to ED or CD detection 27
Figure 3-9: Serial sensing vs. parallel sensing 28
Figure 3-10: Scenario for sensing with interference rejection in CR 29
Figure 3-11: Orientation convention for the measure of angles 31
Figure 3-12: Probability of detection vs. SNR when using 1 to 5 antennas for a mono-path stationary channel (left) and the EPA channel (right) and for a PFA=1%, in presence of one cyclostationary signal and AWGN 35
Figure 3-13: Probability of detection vs. SIR when using 1 to 5 antennas for a mono-path stationary channel (left) and the EPA channel (right) and for a PFA=1%, in presence of one cyclostationary signal and one non-cyclostationary signal 35
Figure 3-14: Detection probability versus SNR for various detectors and 2 PFAs (1% and 10%) 38
Figure 3-15: Structure of the narrow-band filter-bank based detector 39
Figure 3-16: PD versus PFA for different window bandwidths of the narrow band power detection, the narrow-band autocorrelation detection and the narrow-band Teager-Kaiser detection 40
Figure 3-17: Detection probability versus SNR for various narrow-band detectors and 2 PFAs (1% and 10%) 41
Figure 3-18: Experimental test bench of wireless microphone sensing 41
Figure 3-19: Measured detection probability versus SNR for various detectors 42
Figure 3-20: Architecture of the wide-band frequency domain detection 43
Figure 3-21: Frequency analysis block for Teager-Kaiser detection 44
Figure 3-22: Bias versus ratio between Input size and FFT size 45
Figure 3-23: Sensitivity in SNR versus number of sub-channel 45
Figure 3-24: Detection probability versus SNR 46
Figure 3-25: Complexity in number of real multiplications versus FFT size 47

Figure 3-26: OFDM cyclostationarity detection – comparison of CD2 and CD4 49
Figure 3-27: CAF4 Best Peak Position is a function of β (RRC Implementation) 50
Figure 3-28: Proposed Detection algorithm for QPSK PMSE with unknown roll-off factor 50
Figure 3-29: Detection probability (PD) - CD4 vs. CD2 for β=0.1 51
Figure 3-30: Example of a knowledge base computed with the help of the ratio R, when RRC filter (left) and RC filters (right) are used 52
Figure 3-31: CAF of a QPSK Signal 52
Figure 3-32: CAF of a FM Signal 53
Figure 3-33: PMSE cyclostationarity detection, PFA=0.1 53
Figure 3-34: Hybrid detector for PMSE 54
Figure 3-35: Trigger periods representation for short and long term (background) components 55
Figure 3-36: Fast energy detection scheme using a background process for noise estimation 55
Figure 3-37: Adjacent sub-band B_i detection using kurtosis, as a function of INR and of analysed frequency band occupancy 58
Figure 3-38: Adjacent sub-band B_i detection using kurtosis. Use case involving 3 narrow-band interferers (FM) each with INR=-15dB 58
Figure 3-39: Membership probabilities used for adjacent sub-band B_i detection, after 40 iterations of the EM algorithm; INR=0dB 59
Figure 3-40: Mixing probabilities are indicating 10% of the analysed B_i band as occupied by signal and 90% only by noise 59
Figure 3-41: Kurtosis and cyclostationary methods compared to an ED computed with noise uncertainty – PD in terms of SNR (in B_0), for INR=-10dB (in B_i) 60
Figure 3-42: ROC curves with system model used in [Wang09_2], N=28 and SNR= -2dB 67
Figure 3-43: ROC curves with N=32 and SNR=-10dB (AWGN) 67
Figure 3-44: ROC curves with N=32 and SNR=-10dB (Laplacian Noise) 67
Figure 3-45: OFDM and GFDM Structure for a load with N_L=3 OFDM symbols 68
Figure 3-46: GFDM cyclostationary properties for β=0.1 (left) and β=0.3 (right), $T_G=T_D/4$, N_L=16 .. 68
Figure 3-47: Detection probability for GFDM signals - Comparison of cyclostationary Detectors on the Side Peak (SP), for 10 ms GFDM signals, for different β and different cyclic prefix lengths. PFA_{target} has been considered 0.1 69
Figure 3-48: Detection probability for GFDM Signals - Comparison between energy and cyclostationarity detectors on both Side Peak (SP) and Normal Peak (NP), for 10 ms GFDM signals, for different β and different cyclic prefix lengths. PFA_{target} has been considered 0.1 69
Figure 3-49: Structure of a DPCH 71
Figure 3-50: UMTS demodulator structure 72
Figure 3-51: CDMA signal configuration for simulation 73
Figure 3-52: UMTS traffic detection criteria without pilot bits (left) and with pilot bits (right) 73
Figure 3-53: UMTS traffic detection performance when using the method with and without pilots bits, for a mono-path and a Vehicular A propagation channel 74

Figure 3-54: HS-SCCH channel coding chain 75
Figure 3-55: HS-PDSCH identification chain 76
Figure 3-56: HSDPA signal configuration for simulation 76
Figure 3-57: Probability to have a correct or incorrect CRC depending on the decoding weight 77
Figure 3-58: Percentage of correct CRC depending on the SNR 77
Figure 3-59: Concept of interference monitoring 79
Figure 3-60: Quiet period allocation 79
Figure 3-61: RMSE performance 81
Figure 3-62: Description of cell-specific RS method using correlation in time-domain 82
Figure 3-63: Comparison between cell-specific RS method I and cell-specific RS method II, assuming perfect synchronization (τ=0) 83
Figure 3-64: Comparison between cell-specific RS methods and QP methods 83
Figure 3-65: PDF of the measurement error [dB] for QP (left hand side) and cell-specific RS method II (right hand side) for 200 ms 84
Figure 3-66: Comparison between cell-specific RS method II and QP method, under fading effect 84
Figure 3-67: System model of the watermark insertion in the signal of User 1 and its detection by User 2 86
Figure 3-68: Implementation of the watermark insertion 88
Figure 3-69: Implementation of the detector 88
Figure 3-70: Output of the averaging filter 88
Figure 3-71: Insertion sensibility: BER versus E_b/N_0 for several watermark power WSR 90
Figure 3-72: Density of probability of the correlation output for H_0 and H_1 90
Figure 3-73: False alarm probability and non-detection probability versus detection threshold 91
Figure 3-74: Detection probability versus SNR for different WSR 92
Figure 3-75: Detection probability versus SNR for different integration time N 92
Figure 3-76: Detection sensibility in SNR versus integration time N 92
Figure 3-77: The FCME threshold setting procedure. The threshold separates signal samples (dots) into two sets: the noise set and thenarrow-band signal(s) set 93
Figure 3-78: The LAD and the LAD ACC methods. Red circle denotes the sample(s) that ACC allows to go below the lower threshold without breaking the signal 94
Figure 3-79: Flowchart of the LAD methods 95
Figure 4-1: System and concept under analysis 97
Figure 4-2: Two thresholds for cooperative sensing with censorship 104
Figure 4-3: Operation of type 1 (left) sensor and type 2 (right) 105
Figure 4-4: Illustration of the selective reporting scheme with two sensors of different types 105
Figure 4-5: Two sensor scheme for interpretation of the behaviour of the selective reporting algorithm 107

Figure 4-6: Distribution of the number of transmissions for the type 2 nodes a) and type 1 b), Hypothesis H_0 109

Figure 4-7: Distribution of the total number of transmissions. Hypothesis H_0 109

Figure 4-8: Distribution of the total number of transmissions. Hypothesis H_0 and probability of false alarm designed for 0.3 110

Figure 4-9: Distribution of the number of transmissions for the type 2 nodes a) and type 1 b). Hypothesis H_1 and no fading 110

Figure 4-10: Distribution of the total number of transmissions. Hypothesis H_1 110

Figure 4-11: Average number of transmissions as a function of the SNR. Hypothesis H_1 and no fading 111

Figure 4-12: Distribution of the number of transmissions for the type 2 nodes a) and type 1 b). Hypothesis H_1 and fading leading to SNR uniformly distributed in [-8; 10] dB 111

Figure 4-13: Distribution of the total number of transmissions. Hypothesis H_1 and fading leading to SNR uniformly distributed in [-8; 10] dB 111

Figure 4-14: Average number of transmissions as a function of the SNR. Hypothesis H_1 and fading leading to different spans for the SNR 112

Figure 4-15: State diagram for underlying hypothesis H_0 113

Figure 4-16: State diagram for underlying hypothesis H_1 113

Figure 4-17: State diagram with message labelling 114

Figure 4-18: State diagram including errors in the reporting channel 115

Figure 4-19: ROC for the conventional detector and transition / periodic reporting 116

Figure 4-20: Simulation results showing the performance of CF-CSS 122

Figure 4-21: Proposed structure of detector 124

Figure 4-22: Probability of miss detection versus speed 126

Figure 4-23: Probability of miss detection versus number of measurements N 126

Figure 4-24: Probability of miss detection versus received power 126

List of Tables

Table 3-1: Advantages and drawbacks of an energy detector 22
Table 3-2: Extended Pedestrian A propagation model characteristics 34
Table 3-3: CAF2 and CAF4 peaks 49
Table 3-4: Input parameters for identification of bands B_i 56
Table 3-5: Cyclic frequencies for different signal types 57
Table 3-6: Number of different pilot patterns for a DPCH 71
Table 3-7: Vehicular A propagation channel characteristics 74
Table 3-8: Simulation conditions for QP-based power estimation 80
Table 3-9: Simulation results in the multi-path case for the LAD and LAD ACC methods 96

1 Executive Summary

WP3 deals with technologies related to spectrum measurement, modelling, sensing and interchange of sensing information. Task 3.3 is focused on algorithms for radio context acquisition. In this deliverable, a complete set of algorithms to acquire and process radio environment information is provided. This ranges from classical radio context acquisition (i.e. local sensing) to disseminated sensing with exchange of collaboratively or cooperatively collected context data.

A plethora of local sensing algorithms is proposed in the literature. They are classically sorted in three main categories: energy detection, matched filtering and cyclostationary feature detection. New approaches, based on these three categories are investigated in this deliverable as well as their context of usage:

- **Statistical test theory**: For energy detection, in order to improve noise level estimation when it follows some distribution properties, statistical test theory is useful. Several tests are proposed including Anderson-Darling and Kolmogorov-Smirnov approaches. It has been shown that the detection probability is almost the same as for a perfect energy detection - which is not affected by any noise uncertainty.
- **Improved energy detection**: Based on speech characteristics, the energy detection algorithm for PMSE can be improved.
- **Generalized higher-order cyclostationary feature detector**: For PMSE, the 4^{th} order cyclostationarity detector outperforms the 2^{nd} order cyclostationarity detector when using shaping functions.
- **Hybrid detection**: It consists in mixing energy detection and cyclostationary feature detection. It has been developed for both PMSE and OFDM. It will be proved to outperform the performance of both techniques taken separately.
- **Parallel sensing based on antenna processing**: Classical cyclostationary feature detection is extended to the multi-antenna case. It will be shown that smart antenna techniques not only improve the detection sensitivity but also allow non-OFDM spatial rejection permitting an opportunistic user to perform sensing on incumbent network without managing quiet periods.
- **Sensing on GFDM**: GFDM signals have been presented in WP4. As a joint contribution with WP4, WP3 studied the cyclostationary properties of GFDM signals. Improved detection probability on peaks specific to cyclostationary GFDM characteristics has been shown. As opposed to OFDM, GFDM also allows lowering the cyclic prefix and thus increasing the total amount of transmitted data, without affecting the detection probability.
- **Sensing in code**: For CDMA standards, the downlink bands are always fully used by common channels even if no user is using them. This means that there might be a potential available resource (unused orthogonal codes) that classical sensing algorithms cannot detect. In order to use these codes, the opportunistic system must be able to detect them (that is to detect the used spreading factors and spreading codes). Several algorithms for the detection of UMTS and HSDPA downlink traffic channels are proposed and their performance evaluated.
- **Opportunistic system detection by watermarking**: The detection of opportunistic users may be considered by the joint approach of the design of the physical layer of opportunistic users and the design of their detection. The proposed solution relies on the following proposal: the detection can be considered by the explicit introduction of specific signatures (or watermark) in the transmitted signal.
- **Blind frequency localisation**: The proposed method is the Localization Algorithm based on Double-thresholding (LAD) with Adjacent Cluster Combining (LAD ACC). The iteratively

operated LAD method is able to operate in any transform domain, for example, in the frequency domain. The only requirement is that in the considered data there have to be some noise samples. That is, the signal is not allowed to cover the whole studied band.

In the case of the TV white space reuse, classical sensing (meaning the detection of the presence of a signal in a given frequency band) might not be sufficient. Indeed, to verify that the reuse of the TV channel will not cause harmful interference to the incumbent receiver, the opportunistic system has to estimate the Carrier to Interference Ratio (CIR) of the incumbent receiver to determine the allowable transmit power. In order to do so a reliable CIR estimation technique is presented.

Distributed sensing is often presented as an alternative to improve local sensing performance in presence, for example, of shadowing (presence of an obstacle between the sensing device and the emitter to be sensed). The issues addressed here are no longer the detection performance by itself but how to transmit the sensing metrics to the fusion centre and how to merge numerous / various sensing metrics in an optimal way. In this deliverable, several key aspects of distributed sensing are addressed:

- **The quantization of the metrics sent to the fusion centre**: What is the metrics resolution to use in order not to degrade sensing performance and not to use too much resource for metrics transmission.
- **The impact of the time variance caused by the mobility** (key point of the QoSMOS project) of cognitive radios on the sensitivity of spectrum sensing algorithms. It is a new approach as most of the actual works suppose a stationary cognitive radio. Mobility driven collaborative spectrum sensing mechanism using Neyman-Pearson's criterion is considered and a framework for local spectrum sensing is proposed in order to exploit spatio-temporal diversity due to the user mobility.
- How can the fusion centre deal with **malfunctioning or misbehaving sensing nodes**? A solution based on a **beta reputation system** is proposed. The performance of the proposed credibility based scheme is compared with the case of equal weight combining.

2 Sensing Generalities

2.1 State of the Art Review

2.1.1 Introduction

The fundamental task of a Cognitive Radio (CR) user, in a most primitive sense, is to detect incumbent users if they are present, and identify the available spectrum if they are absent. To achieve this, CRs should have abilities including spectrum sensing and dynamic spectrum selection. One of the most critical functionality of CR is spectrum sensing, because a CR should utilise a spectrum band only when it can detect and monitor the activity of incumbent users reliably and quickly [Arshad10]. However, detecting either an incumbent user or other opportunistic users in a certain frequency band using spectrum sensing is a challenging task for many reasons. For example, since Signal to Noise Ratio (SNR) in the receiver may be very low, time and frequency dispersion of the channel causes fluctuations in the received signal power, there is uncertainty about the noise power, to mention a few.

To address these challenges, numerous spectrum sensing algorithms have been proposed in literature. Each algorithm has its own operational requirements, advantages and disadvantages. A comprehensive survey has recently been published [Yücek09]. In traditional systems, three main sensing techniques are used, namely Energy Detection (ED), Matched Filtering (MF), and Cyclostationary Feature Detection (CFD) [Goh07], [Sutton08].

Energy detection is a common method to detect unknown signals in additive noise [Arshad10]. This method is optimal if the exact noise power is known but is susceptible to errors otherwise [Tandra08]. In addition to narrow-band sensing, energy detection has been used for Multi-band Joint Detection (MJD) in wide-band sensing by employing an array of energy detectors (sensing all bands in parallel), each of which detects one frequency band [Quan09]. The MJD method enables CR users to simultaneously detect incumbent user signals across multiple frequency bands for efficient management of wide-band spectrum resource at the cost of detection hardware.

Matched filtering sensing corresponds to the search of a known pattern (reference signal, pilot bits, pilot carrier, etc.) on the processed signal. Therefore, it requires a-priori knowledge of the incumbent user signal and needs perfect frequency synchronisation between incumbent transmitter and the opportunistic user [Cabric06].

In contrast to the noise process which is stationary, cyclostationary features of communication signals can be exploited to distinguish noise from signals using cyclostationary feature detection. Contrarily to the MF method, CFD does not require perfect frequency synchronisation and sampling. But its major drawback is that it demands long sensing durations and high signal processing capabilities [Sutton08]. Two possibilities can be envisaged. The first one is blind spectrum sensing, based on a source separation algorithm, which does not need any incumbent information but suffers from high computational complexity [Zheng09]. The other possibility is oriented sensing which requires knowledge of the waveform characteristics of the incumbent user, which is not always available.

Another approach is sensing based on the Likelihood Ratio Test (LRT). It is optimal but it needs the distribution of both th source signal and thenoise which is unobtainable in practice [Chair86]. In this case, composite hypothesis testing can be used and the most common approach is called Generalized LRT (GLRT). In GLRT, the unknown parameters are estimated by the Maximum Likelihood Estimates (MLE). In [Zarrin09], the Rao test and the locally most powerful test are proposed for detecting weak incumbent signals. The Rao test is asymptotically equivalent to GLRT and does not require the MLE of unknown parameters.

Classical sensing techniques are not valid for multi-channel sensing due to hardware limitations (e.g. sampling rate). Recent advances in compressed sensing [Donoho06], [Candes06], [Tian07] enables the sampling of wide-band signals at sub-Nyquist rate to relax the Analog to Digital Converter (ADC)

requirements. Similarly, an alternative approach for spectrum reconstruction based on fast Fourier sampling has been proposed in [Gilbert02], [Tachwali10], [Tropp07].

2.1.2 Waveform Recognition

2.1.2.1 Frequency Localization

The binary sensing methods simply decide if a signal is present or not. Frequency localization gives much more detailed information about the signal as it estimates both the centre frequencies and bandwidths. Frequency localization has many applications including military, surveillance and CR. More generally, a waveform of a signal can be represented by several parameters such as carrier frequency, bandwidth, modulation, symbol rate, etc. [Le06]. Identification of the modulation, such as Binary Phase-Shift Keying (BPSK), of the received signal also has many applications, such as in military, surveillance, software defined radio and CR.

Frequency localization can be performed in several ways. [Wiley93] described thresholding with hysteresis. Therein, the main purpose is to avoid separation of the signal into two or more signals in the presence of noisy data. The threshold for the current samples is reduced or increased if the previous sample is above or below the threshold. This method requires a noise level estimation because reduction and accretion depend on the noise level. In [Mustafa03], three methods were presented for automatic detection of active radio stations. The methods are based on frequency domain information and detected radio station's bandwidths as well as centre frequencies are estimated.

One method for blind frequency localization is the Localization Algorithm based on Double-thresholding (LAD) with Adjacent Cluster Combining (LAD ACC) [Vartiainen10_2]. The iteratively operated LAD method is able to operate in any transform domain, for example, in the frequency domain. The only requirement is that, in the considered data, there have to be some noise samples. That is, the signal is not allowed to cover the whole studied band.

2.1.2.2 Modulation Identification

The problem of recognizing the modulation has been called Modulation Identification (MOD ID), Automatic Modulation Classification (AMC), and modulation recognition, among others. One of the key approaches for the MOD ID problem is Likelihood Based (LB) MOD ID, based on Bayesian decision theory. In [Wei00], Wei and Mendel presented a theoretical performance analysis of a maximum likelihood based MOD ID. In general, although theoretically optimal, the Maximum Likelihood (ML) based approach may have problems in terms of implementation complexity and robustness. In [Huan95] and [Leinonen04], quasi-log likelihood ratio based classifiers have been investigated for reducing the complexity. In practice, when applying the ML based MOD ID methods, pre-processing, e.g., carrier frequency estimation, SNR estimation, inter-symbol-interference cancellation, and extracting the desired base-band signal, is necessary. When comparing different methods, complete systems including the pre-processing should be used depending on the application and/or the objection of the MOD ID.

The second main approach for MOD ID is Feature-Based (FB) MOD ID. For example, in [Swami00], high order moment parameter cumulant is used to identify the modulation type. Results showed robustness against carrier phase and frequency offsets and also impulsive non-Gaussian noise. In [Dobre05], Dobre has proposed a cyclic cumulant based classifier for digital linear modulation types.

In [Dobre05], several MOD ID methods from the above two approaches have been reviewed and guidelines for choosing an appropriate MOD ID method are presented. However, it is usually difficult to conclusively say which MOD ID method is the most suitable for a given situation.

2.1.3 OFDM Detection

In OFDM systems, sensing may be performed in several ways. For example, [Khambekar07] utilizes the guard interval of OFDM symbols at the transmitter thus detecting incumbent Digital Terrestrial

Television (DTT) signals. The drawback is that at the transmitter, no cyclic prefix is employed but a different type of guard interval.

In [Chen08_2], they utilize the cyclic prefix nature of the OFDM modulated signals. Also, pilot tones based on time-domain symbol cross-correlation of two OFDM symbols are employed. The proposed scheme is accurate, easy to implement, has a low-complexity and is able to operate at low SNR values. Comparisons with cyclic prefix correlation based method showed superior performance in various channel models when unknown symbol timing was assumed. FFT based detection (i.e. considering frequency domain samples) was used in [Demirdogen10]. The method outperforms the conventional Power Spectral Density (PSD) system [Aldirmaz09] but is also more complex. The PSD system presented in [Aldirmaz09] performed better with block-based allocation than with scattered allocation. In addition, the threshold setting is a critical issue in PSD system.

In [Koufos09], sensing is based on autocorrelation using the uniform approximation for the distribution of the power of incumbent signal without any additional knowledge about the incumbent signal. Cyclic Prefix Correlation Coefficient (CPCC) which is simple but ineffective in multi-path scenarios was presented in [Bokharaiee10]. In the same reference, also a multi-path-based constrained generalized likelihood radio test (MP-based GLRT) that outperforms the CPCC in a rich multi-path environment was proposed. According to simulations in [Bokharaiee10], both CPCC and MP-based GLRT outperform energy detection in an environment with noise uncertainty. In [Noh08], a cyclic prefix and an idle period containing no information symbols are used. It was noted that the method improved sensing accuracy when compared to the system that uses only an idle period. Receiver-aided Spectrum Sensing scheme with Spatial Differentiation (RaSSSD) was proposed in [Wang10]. Therein, an opportunistic deployed area is divided into two sub-areas based on opportunistic user SINR, and after that, RaSSSD is described according to the locations of opportunistic user transmitters and receivers. In [Zhou10], the probabilistic information of channel availability obtained from sensing is used to assist resource allocation. Embedded pilot sub-carriers were used in [Zahedi10]. Therein, cyclic prefix was not used. According to [Zahedi10], the presented method outperforms the methods presented in references, [Sohn07], [Tu07], [Öner07] and [Lunden08].

Different allocation methods could be studied to get the Probability of Detection (PD) / Probability of False Alarm (PFA) performance. Allocation methods include, for example, block-like, scattered and striping. Usually, more block-like allocations are suitable for cognitive radios because there are less affected sub-carriers with non-idealistic assumptions such as time and frequency offsets, mainly those adjacent to each block would be affected. In OFDMA systems, available periods in the time domain can be detected with vertical striping, where the allocation is first performed in the frequency domain, and afterward the last sub-channel is filled [Gronsund09]. According to [Gronsund09] vertical striping is a more suitable scheduling technique for incumbent systems from the opportunistic user's perspective than horizontal striping or rectangular allocation. That is, because in the vertical striping it is possible to allocate the whole bandwidth for operation over a dedicated time interval. Instead, detection of available frequency is a more complex issue because of the sub-carrier distribution. One possible solution is to utilize the first symbol after the latest partially occupied symbol, so the frequency is intensive until this symbol is detected and close to zero for the rest of the sub-frame. According to [Gronsund09] this method can be implemented with all sensing methods (matched filter, energy or cyclostationary feature detection).

Building on the study in [Gronsund09], dynamic spectrum access for opportunistic users coexisting with incumbent OFDMA systems was considered in [Pha10]. A dynamic spectrum access scheme called DSA-alpha was proposed. DSA-alpha allows an opportunistic user to access the whole bandwidth during the last consecutive symbols of each incumbent OFDMA sub-frame. It is assumed that the opportunistic user is scheduled promptly or perfect spectrum sensing is implemented in order to access each sub-frame promptly. The proposed scheme was simulated in a modified WiMAX simulator.

The knowledge of resource blocks is also an important issue. The sensing performance will be improved if blind block size estimation is known or performed. In [Sahin10], resource elements (resource blocks) have the same occupancy status and the synchronization of the incumbent is known. Actually, similar ideas are probably applicable in time slotted cognitive radios to resources blocks. Therein, the beginning of each slot (here first symbol(s) of a resource block) is first sensed. Then, if it is found that the channel is vacant, the remainder of this slot (here the remainder of the resource block) is guaranteed to be unoccupied (assuming perfect sensing).

In [Lien10], a kind of "prediction" has been proposed for OFDMA small cellular base stations called femto-cells. First, one frame (sensing frame) is sensed and that information is used for accessing some subsequent frames (data frames). As mentioned in [Lien10], the performance depends on the correlation of resource block allocations of the macro Base Station (BS), here the incumbent user BS. It seems that opportunistic use of this method would require high correlation (or constant resource block allocation for some period of time) for sufficient incumbent protection. Therein, perfect sensing was assumed.

2.1.3.1 LTE Detection

In OFDM systems, it has just to be decided if there is a signal present or not. However, it is not necessary that all the sub-carriers are occupied. Therefore, sensing may be performed separately for each sub-carrier to find out if the sub-carrier is unoccupied. After that, the assumed unoccupied sub-carriers may be utilized for transmission. The sub-carriers are not independent since several sub-carriers are allocated to each user so that joint decision may be performed for all sub-carriers used by the same user if these are known – or estimated. In block based allocation several adjacent sub-carriers are allocated to the same user whereas in scattered allocations the user's sub-carriers are spread over the whole set of sub-carriers. A question that arises is how rapidly and randomly the sub-carrier allocations change. Also, even a tiny carrier frequency offset from the cognitive transmitter compared to the potentially mobile (Doppler) incumbent receiver may destroy the orthogonality of sub-carriers, so that guard bands around the occupied sub-carriers may be necessary.

LTE is a potential technique for future cognitive radio communications to mitigate the spectrum scarcity issue. In LTE, OFDMA is used in downlink and DFT-spread OFDM, i.e., Single Carrier Frequency Division Multiple Access (SC-FDMA) which has better peak-to-average power ratio properties is used in uplink. The main difference between OFDM and SC-FDMA is that as the first one is a multi-carrier transmission scheme, the latter one is a single-carrier transmission scheme. In the SC-FDMA, DFT-spreading of data symbols is performed in the frequency domain. The modulation schemes include QPSK, 16QAM and 64QAM (downlink) and BPSK, QPSK, 8PSK and 16QAM (uplink). Incumbent user sensing based on 3GPP LTE wireless sensor networks has been considered in [Li09]. Therein, cooperative sensing based on energy detection was used. According to [Li09], an energy detector in a single antenna cognitive radio leads to poor detection performance when SNR is low thus causing interference to the incumbent. According to simulation results, cooperative frequency spectrum sensing in OFDM with multiple antennas and a square-law-combining energy detector offers an improvement in detection performance.

In [Lotze09], spectrum sensing on LTE consumer-deployed home base stations (femto-cells) for GSM spectrum re-farming using Xilinx Field-Programmable Gate Arrays (FPGA) was considered. LTE-systems (femto-cells) with GSM as the incumbent are considered. Also, sensing the LTE signal to avoid using the same channels as other LTE femto-cells in the same GSM cell was considered. Therein, robust sensing to achieve interference-free operation of neighbouring LTE femto-cells was considered. The proposed approach for LTE femto-cell deployment included, for example, an operation specific database using GSM macro-cell id and a sensing method to identify unoccupied channels. The proposed sensing algorithm is based on signal detection using a time-averaged PSD estimate. It computes the square magnitudes of instantaneous FFT and averages over a time period, then smooths the PSD and correlates the PSD with the expected LTE footprint (i.e., moving the average filter). Then, it finds the width of the area above the threshold and makes the occupancy

decision based on that. According to [Lotze09] there is no need to decode the control channels of neighbouring femto-cells over the air.

Coarse spectrum sensing for LTE systems was considered in [Abdelmonem10]. Therein, the whole LTE signal bandwidth sensing was proposed to be performed using Fast Wavelet Transform (FWT) and a multiple resource block sensing. An FFT-based method was used as a point of comparison. Simulations stated that FWT and FFT had almost the same performance. With realistic probabilities of false alarms, FFT had a better performance. It was noticed in [Abdelmonem10] that the sensing can be performed in two stages. The first stage performs coarse sensing, for example, energy detection or wavelet-based sensing. The second stage performs fine sensing using feature detection, pilot-based sensing, or sensing based on known signal preambles. After selecting the sensing method, a database could be used for predicting the resource block usage in the future, e.g., the next frame, based on historical and current sensing. Two-stage sensing has also been proposed in [Vartiainen10_1], where a detection history database and a signal detection with power level and full signal detection (for example, using the LAD method for narrow-band and cyclostationary or maximum-minimum eigenvalue detector for wide-band signals) are used.

Effects of imperfect sensing could also be studied by starting with exact (perfect) data from the BS (of the test network) and then studying the effects of imperfect sensing on the accuracy of the predictions. For forming the predictions, some papers in the literature try to find the pattern of the incumbent access, such as fixed on and off periods. This may be applicable to LTE.

For predicting, it may be suitable to think ways for the incumbent base stations to help CRs without changes to the incumbent MSs.

2.2 Mathematical and Algorithmic Notations

The goal of this section is to describe common mathematical notations used in this deliverable for algorithmic descriptions.

2.2.1 General Mathematical Notations

- Scalars and functions are in italic: α
- Vectors are underlined: $\underline{\mathrm{v}}$
- Matrices are in capital and bold: $\mathbf{M}$
- $\mathbf{M}^*$ is the conjugate of the matrix $\mathbf{M}$
- $\mathbf{M}^T$ is the transpose of the matrix $\mathbf{M}$
- $\mathbf{M}^H$ is the transpose-conjugate of the matrix $\mathbf{M}$
- $\hat{\alpha}$ is an estimate of α
- $E[x(t)]$ is the mathematical expectation of $x(t)$
- F_e is the sampling frequency, T_e the sampling period
- The continuous-time signal $x(t)$ sampled at rate F_e is written $x[n] = x(nT_e)$

2.2.2 Notations for OFDM Waveform

As illustrated in Figure 2-1, in an OFDM symbol:

- T_G is the cyclic prefix duration in seconds (N_G in samples)
- T_D is the useful data duration in seconds (N_D in samples). One can underline that for a non-over-sampled signal, N_D corresponds to the total number of sub-carriers and to the order of the FFT.
- T_S is the OFDM symbol duration in seconds (N_S in samples)

Let us call the $s(t)$ the transmit continuous-time OFDM signal:

$$s(t) = \frac{1}{\sqrt{N_D}} \sum_{k \in \mathbf{Z}} \sum_{n=0}^{N_D-1} a_{k,n} e^{-2j\pi n \frac{(t-T_G-kT_S)}{T_D}} g(t - kT_S) \quad \text{Eq. 2-1}$$

Where $a_{k,n}$ is the transmitted symbol on sub-carrier n and OFDM symbol k and $g(t)$ the shaping function equal to 1 if $0 \leq t \leq T_S$ and 0 otherwise.

After D/A conversion and RF modulation, the signal is passed through the mobile radio channel which can be modelled as a time-variant linear filter with impulse response:

$$h(t) = \sum_{l=1}^{L} h_l(t) \delta(t - \tau_l) \quad \text{Eq. 2-2}$$

where L is the number of channel paths and τ_l is the delay of each path.

At the receiver, the signal is received along with noise. It can be formulated as:

$$r(t) = e^{j2\pi\Delta_f t} \sum_{l=1}^{L} s(t - \tau_l)\, h_l(t) + n(t) \quad \text{Eq. 2-3}$$

Where $n(t)$ is the additive white Gaussian noise with zero mean and variance of σ_n^2 and Δ_f the frequency offset.

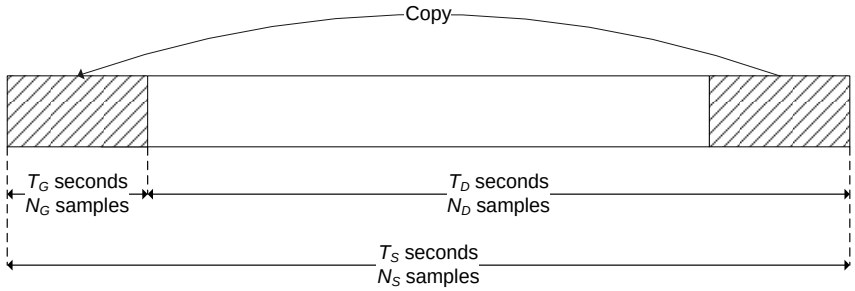

Figure 2-1: Illustration of cyclic prefix extension in OFDM systems

2.2.3 Notations for PMSE Waveform

Programme Making and Special Events (PMSE), typically wireless microphones, can use digital modulations such as Quadrature Phase Shift Keying (QPSK) or analogue modulation such as Frequency Modulation (FM) [ETSI06].

In QPSK modulation, the information is encoded in the phase of the transmitted signal. The complex constellation after sampling at the QPSK symbol period T_S can be written as [Proakis95]

$$a \in \left\{ A\cos\left(2\pi \frac{n-1}{4}\right) + jA\sin\left(2\pi \frac{n-1}{4}\right) \right\} \quad \text{Eq. 2-4}$$

where $n \in \{1,2,3,4\}$ and $A^2/2$ is the symbol power.

For simulation purposes QPSK transmissions can consider a rectangular shaping filter [Proakis95] but a more realistic approach which allows decreasing adjacent spectral side lobes is to use Nyquist filters and more precisely Raised Cosine (RC) or Root Raised Cosine (RRC) filters which are defined as in [Proakis95] and represented in Figure 2-2 for different roll-off factors β.

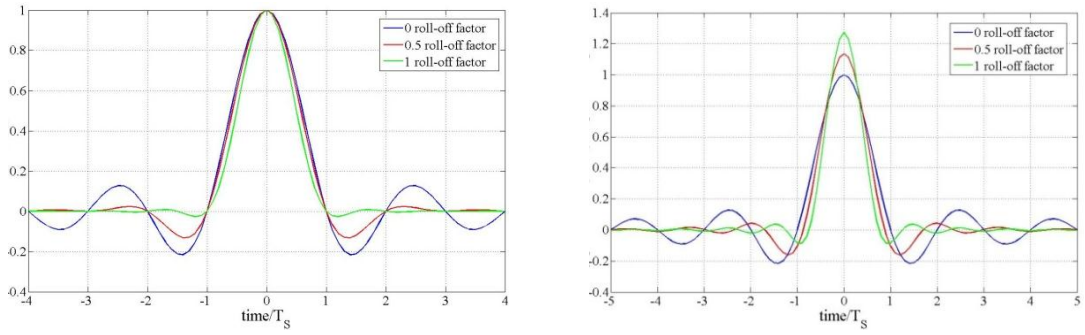

Figure 2-2: RC (left hand side) and RRC (right hand side) impulse response

Please note that the RC filtering can be distributed between the transmitter Tx and the receiver Rx. In the transmitter, a RRC filter is used as a shaping filter and in the receiver another RRC filter is used as a matched filter. At the receiver side, the sampling period T_e might be chosen (but not compulsory) equal to the symbol period T_S.

For exemplification purposes a digital transmission is described, using β=0.1 (see Figure 2-3 left) and β=0.9 (see Figure 2-3 right) with the same symbol period T_S. A QPSK signal has been further considered, with T_S=1/(200×10^{-3})sec with rectangular shaping function (black), square root (green) and square root raised cosine (red) shaping functions respectively**.** The bandwidth of the signal is given by both symbols period T_S and roll-off factor β.

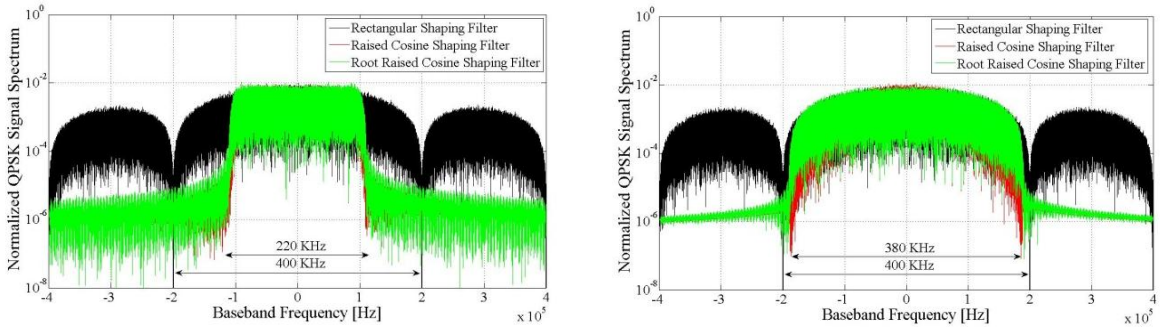

Figure 2-3: Normalized QPSK Signal Spectrum for a roll-off factor 0.1 (left) and 0.9 (right)

When designing a PMSE QPSK Tx using Nyquist filtering, the choice of the frequency bandwidth is given by the combination of the symbol period T_S and the roll-off factor β. This aspect is represented in Figure 2-4, for a constant bandwidth of 400 kHz.

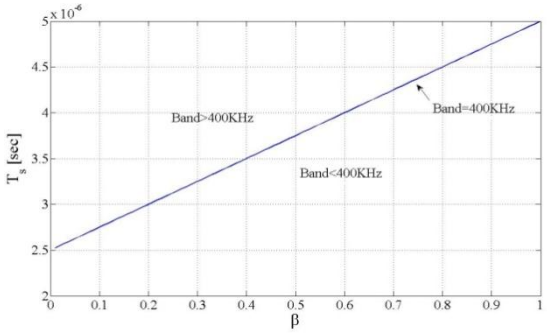

Figure 2-4: T_S as a function of roll-off factor β, for a constant 400 kHz frequency bandwidth

Some other kind of wireless microphones use analogue FM modulations [Chen08_1]. The FM PMSE signal has a spectral bandwidth B_s of 200 kHz, contrary to digital transmissions which are allowed for a higher spectral bandwidth (usually they have a 400 kHz bandwidth but they can be up to 600 kHz).

Most of the FM PMSE signal energy is concentrated in a bandwidth of 40 kHz. The transmit power is a few tens of mW. Therefore, the coverage area is relatively low, about 500 meters for the most powerful microphones. Their detection is difficult to achieve.

The signal from the microphone $s(t)$ can be modelled as follows:

$$s(t) = A\cos\left(2\pi f_0 t + 2\pi\frac{f_d}{x_m}\int_0^t x(\tau)d\tau\right) \quad \text{Eq. 2-5}$$

where f_0 is the carrier frequency, f_d the frequency deviation of the FM modulation, and $x(t)$ the modulating signal having an maximum amplitude x_m. The signal $s(t)$ has a power σ_s^2 equals to $A^2/2$.

Let $r(t)$ be the microphone signal received by the opportunist receiver and $n(t)$ an Additive White Gaussian Noise (AWGN) with a zero mean and a variance σ_n^2:

$$r(t) = s(t) + n(t) \quad \text{Eq. 2-6}$$

$s(t)$ and $n(t)$ being independent, the SNR received by the opportunistic user is:

$$SNR = \frac{\sigma_s^2}{\sigma_n^2} = \frac{A^2}{2\sigma_n^2} \quad \text{Eq. 2-7}$$

2.2.4 Notations for Cyclostationarity Properties

A zero mean complex cyclostationary signal $\mathrm{r(t)}$ is characterized by a time varying autocorrelation function $R_{rr}(t,\tau) = E[r(t)r^*(t+\tau)]$, which is periodic in time *t* and can be represented as a Fourier series :

$$R_{rr}(t,\tau) = \sum_{\alpha} R_{rr}^{\alpha}(\tau)e^{j2\pi\alpha t} \quad \text{Eq. 2-8}$$

where the sum is taken over integer multiples of fundamental frequencies α. τ corresponds to the lag parameter (i.e. the time delay of the autocorrelation function). $R_{rr}^{\alpha}(\tau)$ is called the cyclic autocorrelation function.

Characterizing the cyclostationarity of a signal is finding the right non-null couple (τ,α), (τ_0,α_0) for which

$$R_{rr}^{\alpha_0}(\tau_0) \neq 0 \quad \text{Eq. 2-9}$$

2.3 Simulation and Evaluation Metrics

In this document, numerous sensing algorithms are described for various types of waveforms and standards. Different detection techniques are investigated and simulated: energy detection, cyclostationarity-based techniques, reference-based techniques, etc. Nevertheless, whatever the algorithm is, the global approach is the same and the way results are presented can be homogenized. Indeed all sensing methods consist in elaborating a detection criterion and compare it to a threshold in order to determine the presence or absence of a given signal. The choice of the threshold is a tricky problem. It is a trade-off between the Probability of False Alarm (PFA, the probability to detect a signal while it is not present) and the Probability of Detection (PD, the probability to detect a signal which is present). In this document, in order for the algorithms to be more easily comparable target PFA, PD and performance representation curves are standardized.

First of all, simulations can be run in presence of thermal noise and/or interference, for AWGN or multi-path fading channels. In any case, for fixed PFA representations, the thresholds are set to target **PFAs equal to 1% or 10%**. Likewise when reached noise levels or interference levels are given, they are for a target **PD equal to 90% or 99%**.

In presence of thermal noise, the noise level is given by the SNR which corresponds to the received power of the signal of interest over the power of noise in the bandwidth of the signal of interest.

In presence of interference, the interference level is given by the Signal to Interference Ratio (SIR) which corresponds to the received power of the signal of interest over the power of the interfering signal in the bandwidth of the signal of interest. In contrast with the spectrum sensing for incumbent signal detection, interference monitoring can use the Root Mean Square Error (RMSE) of the interference measurements as an evaluation metric for the local sensing algorithms. Since the interfering signal is subject to the measurement in the interference monitoring, the interference level is given by the Interference to Signal Ratio (ISR). The definition of I and S is the same for both SIR and ISR. In both cases, the interference term does not include thermal noise. Nevertheless, simulations in presence of interference do include a certain level of noise corresponding to an SNR of 30 dB. This level is intentionally high so that only the interfering signal impacts the algorithm performance.

3 Local Sensing Algorithms

In this section, various local sensing algorithms are studied and their performances are described. Local sensing corresponds to the classical context acquisition where the sensing metrics are measured in one single location. This will consider simple energy detection to more advanced algorithms that explore the features of the radio signals expected to be encountered in the environment.

This section is divided into four subsections corresponding to:

- **Signal detection**, with a focus on various methods for OFDM signal detection, PMSE detection and sensing based on statistical tests.
- **Interference monitoring**, checking the carrier to interference ratio of the incumbent receiver.
- **Identification of opportunistic systems** using the watermarking method.
- **Blind frequency localization**, to detect where the signal is located in a frequency band**.**

3.1 Signal Detection

3.1.1 OFDM Detection

3.1.1.1 Two-Stage Hybrid Detection for OFDM

This section first presents the Energy Detector (ED) and the Cyclostationarity Detector (CD). For each detector, the strong and the weak points are listed, showing the benefit of using a two-stage hybrid detection. Finally, simulation results show that the two-stage hybrid detection performs better than both the ED and CD only in certain conditions.

3.1.1.1.1 Energy Detector

Instead of relying on the a priori knowledge of the signal, energy detectors are independent of the nature of the signal. As presented in Figure 3-1, the energy detector performs an energy computation or power computation, compares the energy value (or power value respectively) to a threshold and decides whether the useful incumbent signal is present or not.

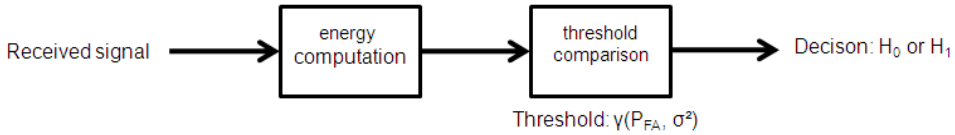

Figure 3-1: Energy detector algorithm

Energy detection [Urkowitz67] is a well-known detection method mainly used because of its simplicity. The basic functional method involves an energy computation block (i.e., a squaring device and an integrator) and comparison block, as shown in Figure 3-1.

The threshold γ is chosen according to a desired PFA and when performing power computation the threshold is given by:

$$\gamma = \frac{\sqrt{2}}{\sqrt{N}}\sigma_n^2 Q^{-1}\left(PFA_{target}\right) + \sigma_n^2 \qquad \text{Eq. 3-1}$$

where N is the number of samples of the digital signal and σ_n^2 is the noise variance. We denote by Q^{-1} the inverse of the Q function defined by:

$$Q(t) \equiv \frac{1}{\sqrt{2\pi}}\int_t^{\infty}\exp\left(-\frac{u^2}{2}\right)du = \frac{1}{2}\left(1 - erf\left(\frac{t}{\sqrt{2}}\right)\right) \qquad \text{Eq. 3-2}$$

It can be shown that the performance of the energy detector decreases when the noise variance increases (for low SNRs). Subsequently, a precise knowledge of the noise variance is necessary to determine the threshold value.

Introducing a noise uncertainty ε in the variance of the estimated noise has an interesting effect. With the noise uncertainty (here, linearly represented) one can notice that the value of the threshold changes according to the following equation:

$$\gamma = \frac{\sqrt{2}}{\sqrt{N}}\left(\sigma_n^2 \cdot \varepsilon\right)Q^{-1}\left(PFA_{target}\right)+\left(\sigma_n^2 \cdot \varepsilon\right) \qquad \text{Eq. 3-3}$$

For the same value of the threshold, one can get the same performance by using another detector which incorporates the uncertainty in the PFA value:

$$\gamma = \frac{\sqrt{2}}{\sqrt{N}}\left(\sigma_n^2\right)Q^{-1}\left(PFA_{equivalent}\right)+\left(\sigma_n^2\right) \qquad \text{Eq. 3-4}$$

Please note that Eq. 3-4 corresponds to an ideal detector where the noise uncertainty has been perfectly estimated but the real PFA is no longer the target PFA. Comparing Eq. 3-3 to Eq. 3-4 one could see that increasing the noise uncertainty ε will impact the real PFA by decreasing it:

$$PFA_{equivalent} = Q\left(\varepsilon \cdot Q^{-1}\left(PFA_{target}\right)+\frac{\sqrt{N}}{\sqrt{2}}\left(\varepsilon-1\right)\right) \qquad \text{Eq. 3-5}$$

Please also note that when ε=1, the real PFA becomes the desired (target) PFA. Therefore, it has been shown that a precise knowledge of the noise variance is necessary in order to compute the threshold value γ. Subsequently, a wrong computed threshold value is affecting both the detection probability PD and the real false alarm probability PFA, which differs from the target PFA.

As one can see in Figure 3-2, increasing the number of samples for an ED under noise uncertainty has limited benefits:

- Many more samples are needed to get a 1 dB performance improvement.
- There is anyway an asymptotic bound that cannot be crossed.

Also, note that all curves from Figure 3-2 converge to PD = 0 and cross at PD = PFA (while in the case where the noise variance is perfectly known, all curves would asymptotically converge to PFA). From all these above remarks, the advantages and disadvantages of using an energy detector as a detection solution have been summarized in Table 3-1.

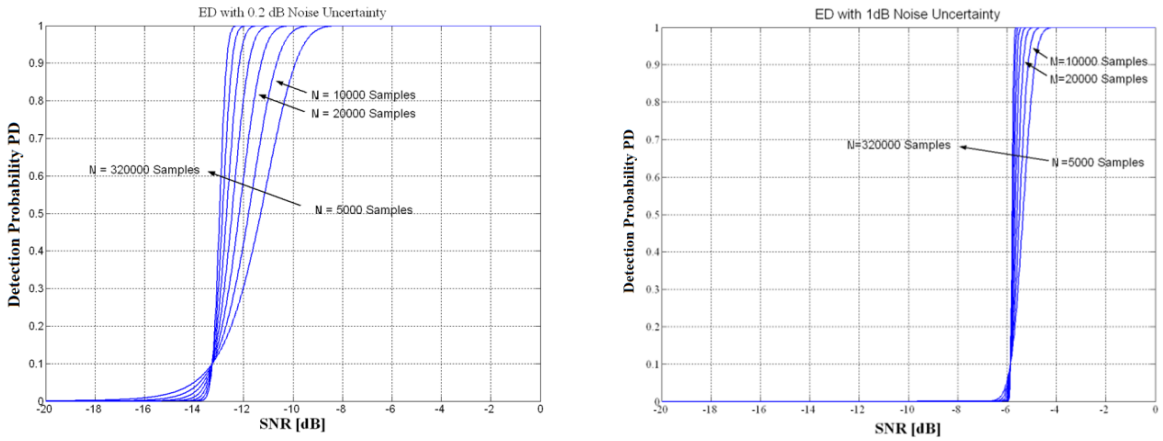

Figure 3-2: Energy detector under uncertainty, for PFA_{target}=0.1

Table 3-1: Advantages and drawbacks of an energy detector

Advantages	Drawbacks
• Very easy to implement • Low complexity • No signal characteristics needed	• Inefficient in low SNR conditions • Noise variance σ_n^2 needs to be estimated accurately

3.1.1.1.2 Second Order Cyclostationary Feature Detector

The autocorrelation function can be represented by Fourier series expansion, which is expressed as:

$$R_{ss}(t,\tau) = \sum_{\alpha \in \psi} R_{ss}^{\alpha}(\tau) \exp(j2\pi\alpha t) \quad \text{Eq. 3-6}$$

where α is a cyclic frequency, and $R_{ss}^{\alpha}(\tau)$ is the Fourier coefficient, also called Cyclic Autocorrelation Function (CAF). The CAF of the second order autocorrelation function can be written as:

$$R_{ss}^{\alpha}(\tau) = \lim_{T\to\infty} \frac{1}{T} \int_{-\frac{T}{2}}^{\frac{T}{2}} s(t)s^*(t-\tau)\exp(-j2\pi\alpha t)dt = \lim_{T\to\infty} \frac{1}{T} \int_{-\frac{T}{2}}^{\frac{T}{2}} s^*(t)s(t+\tau)\exp(-j2\pi\alpha t)dt \quad \text{Eq. 3-7}$$

Similarly, one could define CAFs for every autocorrelation function previously described. The expression described above could be time-discrete approximated by:

$$R_{ss}^{\alpha}(d) = \frac{1}{N} \sum_{n=0}^{N-1} s^*[n]s[n+d]\exp(-j2\pi\alpha n T_e) \quad \text{Eq. 3-8}$$

where *d* represents the delay time normalized by the sampling period T_e.

Let us denote $r(t)$ the received signal, where $r(t) = s(t) + n(t)$, with $s(t)$ being the useful transmitted signal and $n(t)$ being the noise. Then, the Generalized Likelihood Ratio Test (GLRT) algorithm for cyclostationarity detection [Dandawate94] can be re-written as:

- Compute the value of the CAF $R_{rr}^{\alpha}(\tau)$ for a given delay τ and a cyclic frequency α. The delays τ and cyclic frequencies α could be used directly from a database (see the definition of inputs) or they could be estimated if necessary [Bouzegzi08]. Take the real and the imaginary part of this CAF:

$$\underline{r}_{rr}^{\alpha}(\tau) = \left[\mathrm{Re}\left\{R_{rr}^{\alpha}(\tau)\right\}, \mathrm{Im}\left\{R_{rr}^{\alpha}(\tau)\right\}\right] \quad \text{Eq. 3-9}$$

- Compute $Q_1^{\alpha}(\tau)$ and $Q_2^{\alpha}(\tau)$ defined by:

$$Q_1^{\alpha}(\tau) = \frac{1}{NL} \sum_{l=-\frac{L-1}{2}}^{\frac{L-1}{2}} w(l) F_{rr}\left(\alpha - \frac{l}{NT_e}\right) F_{rr}\left(\alpha + \frac{l}{NT_e}\right) \quad \text{Eq. 3-10}$$

and

$$Q_2^{\alpha}(\tau) = \frac{1}{NL} \sum_{l=-\frac{L-1}{2}}^{\frac{L-1}{2}} w(l) F_{rr}^{*}\left(\alpha + \frac{l}{NT_e}\right) F_{rr}\left(\alpha + \frac{l}{NT_e}\right) \quad \text{Eq. 3-11}$$

where *w* is a Kaiser window and *L* its length. $F_{rr}(f)$ is defined by:

$$F_{rr}(f) = \sum_{n=0}^{N-1} r^{*}[n] r[n+d] \exp(-j2\pi f n T_e) \quad \text{Eq. 3-12}$$

where *N* is the number of samples and T_e is the sampling period. Please note that $F_{rr}(f)$ has the same meaning as $R_{rr}^{f}(d)$, for a fixed *d* (the delay time normalized by the sampling period), and normalized with *N*. Higher order CAF (e.g., from autocorrelation functions with four multiplications, with no conjugation or two conjugations) will have similar expressions.

- Compute the covariance matrix $\sum_r(\alpha)$:

$$\begin{bmatrix} \mathrm{Re}\left(\frac{Q_1^{\alpha}(\tau)+Q_2^{\alpha}(\tau)}{2}\right) & \mathrm{Im}\left(\frac{Q_1^{\alpha}(\tau)-Q_2^{\alpha}(\tau)}{2}\right) \\ \mathrm{Im}\left(\frac{Q_1^{\alpha}(\tau)+Q_2^{\alpha}(\tau)}{2}\right) & \mathrm{Re}\left(\frac{Q_2^{\alpha}(\tau)-Q_1^{\alpha}(\tau)}{2}\right) \end{bmatrix} \quad \text{Eq. 3-13}$$

- Compute the test statistic:

$$T_{GLRT}(r,\alpha) = N \cdot \underline{r}_{rr}^{\alpha}(\tau) \cdot inv\left(\sum_r(\alpha)\right) \cdot \underline{r}_{rr}^{\alpha}(\tau)^T \quad \text{Eq. 3-14}$$

where inv is the inversion operation of the covariance matrix.

The test statistic is compared with a threshold γ. This threshold is computed according to the following equation: PFA = 1 – Γ(1,γ/2) where Γ is the incomplete gamma function.

For the simulations, a base-band OFDM signal has been used, with the following parameters:

- Number of sub-carriers: 512
- Useful symbol duration: T_D
- Cyclic prefix length: T_G = ¼ T_D
- (Maximum) sensing time: $T_{sensing}$ = 5ms
- Number of OFDM symbols: $T_{sensing}$ / (T_D +T_G)
- PFA: 0.1
- Delays: τ = +/- T_D
- Cyclic positions: $\alpha = k / (T_D + T_G)$, *k* = +/- 0,1,2,… ; the value *k* = +/-1 is used here
- Sampling period T_e : with respect to the Nyquist theorem (and at least a number of samples per symbol equal to the number of sub-carriers).
- Number of samples *N*: $T_{sensing}$ / T_e
- *L*=101
- Tests were done under AWGN channels but multi-path can be tested using the channel model from standards (as LTE).

For an OFDM signal, the peaks in the CAF are dependent on T_D and the total symbol duration which is $T_D + T_G$. For a sum of multiple OFDM signals with different parameters (different T_D and different $T_D + T_G$), multiple distinct peaks should appear on the cyclic autocorrelation function (cf. Figure 3-3).

The cyclostationary feature based detection methods use periodic characteristics (e.g., symbol time, cyclic prefix) of the transmitted radio signals. Such processing can deal with low SNR signals and is less sensitive to background noise. Cyclostationary detectors can also provide signal classification capabilities of the detected signal such as the number of detected signals, their symbol rate, modulation type, and so on. However, the disadvantage of such detectors is their computational complexity which is very high. Therefore, a quick detection is not achievable.

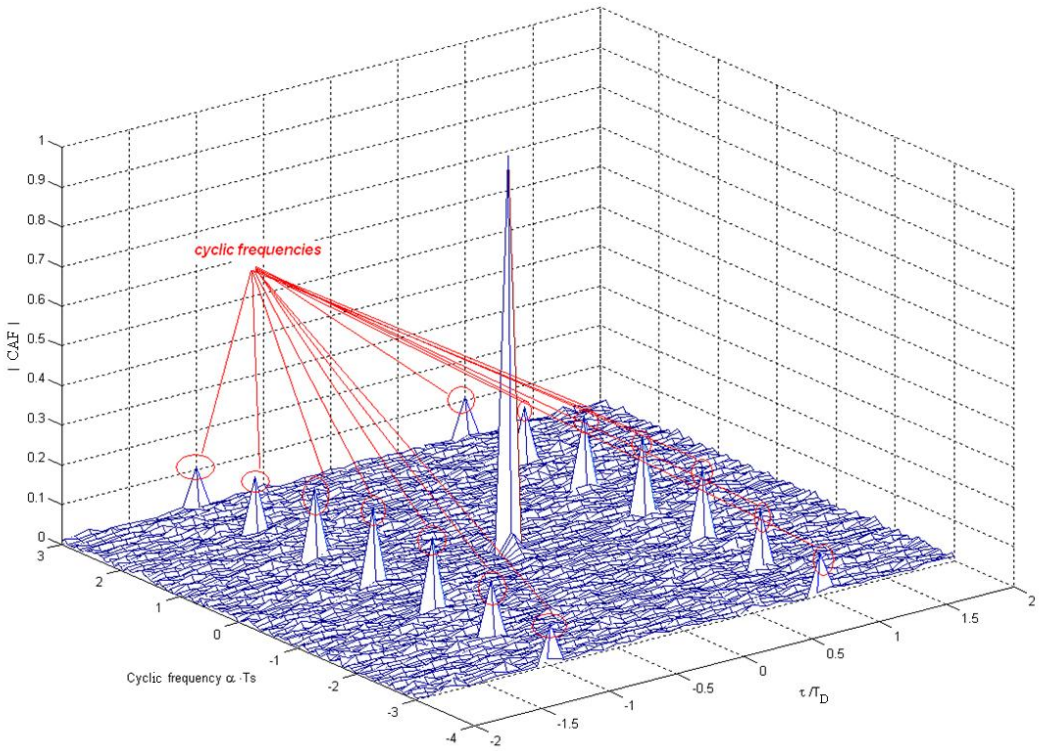

Figure 3-3: CAF of an OFDM signal

Preliminary results, presented in Figure 3-4, show that in the case with perfect noise estimation for the ED, CD has to acquire a larger number of samples in order to outperform ED.

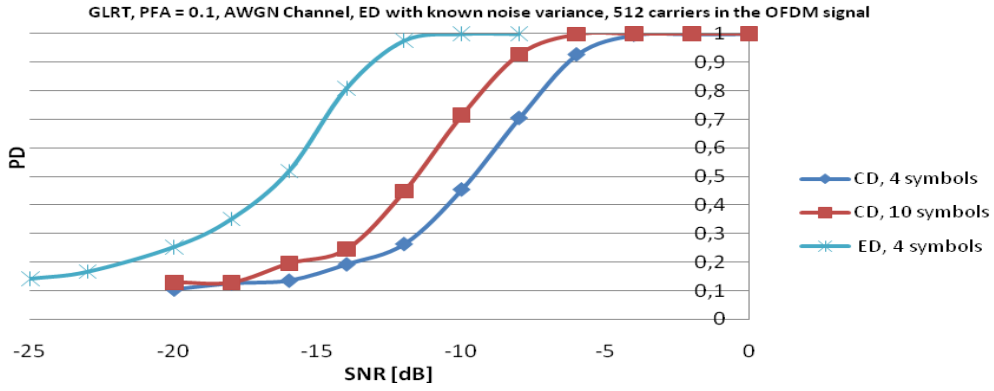

Figure 3-4: Comparison between ED and CD for an OFDM signal

3.1.1.1.3 On the Two-Stage Hybrid Detection

As shown in the previous sections, combining ED and CD in a common architecture can be motivated through the graph from Figure 3-5. It shows that it is worthwhile to use ED when the uncertainty is weak (when the noise variance is accurately known) and for a short sensing time to perform a quick sensing. On the other hand, it is worthwhile to use the CD when the noise uncertainty is considerable and for a longer sensing time.

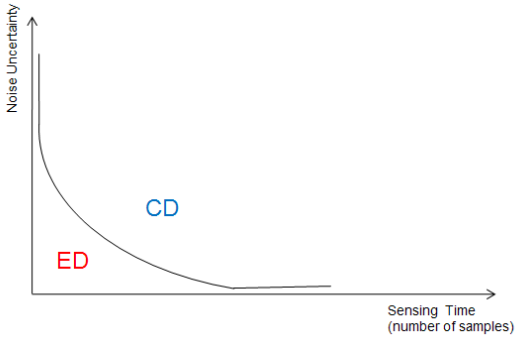

Figure 3-5: ED and CD feasibility area

The graph from Figure 3-5 shows that the ED is asymptotically limited by the noise uncertainty wall, while the CD is not. For this reason, the CD is used in the second stage (see Figure 3-6) to compensate the weakness of the ED under noise uncertainty conditions. Under this approach, the CD is used only if the ED is not able to detect any incumbent user

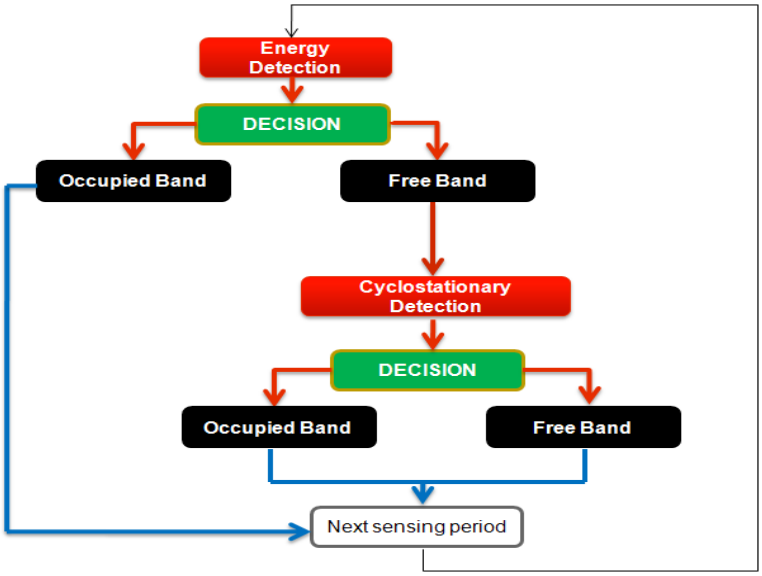

Figure 3-6: Two-stage hybrid detection concept

After some analysis and several simulations, it has been proved that it makes sense to use the two-stage detector in the following scenarios:

- Scenario 1: The **sensing time** for ED is **shorter** than the sensing time used by CD.
- Scenario 2: The **noise estimation** is **uncertain** (the noise variance is not perfectly known which is always in practice).

Scenarios 1 and 2 (see Figure 3-7) helped identifying the most important parameters that might affect the performance of the detector. In practice, a two-stage hybrid detector works on a combination of scenarios 1 and 2. That is because not only ED and CD could be used for coarse sensing (a faster

process) and for fine sensing respectively (only if necessary, and it is a longer process) which corresponds to the 1st scenario, but it can also be proved that noise estimation uncertainty is quite common (and is higher than 1dB) which corresponds to the 2nd scenario.

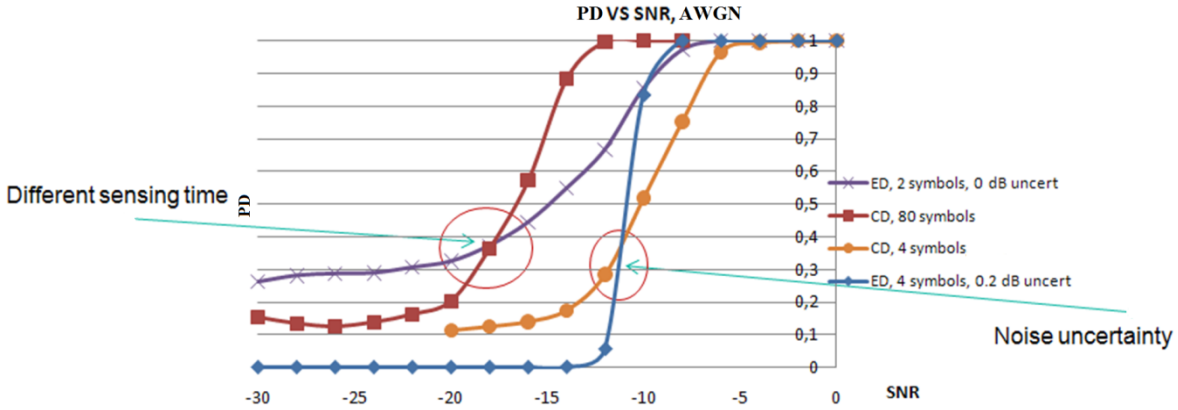

Figure 3-7: PD versus SNR, for ED and CD, for several sensing duration, with or without error on noise estimation

When ED and CD are combined as a two-stage detector, it is worthwhile to determine in which conditions it makes sense to use this new hybrid detector. The hybrid detector is expected to perform better than ED and CD respectively, but this can be achieved only if we meet some requirements. The overall PD and PFA of the two-stage detector can be expressed as follows:

$$PD = PD_{ED} + (1 - PD_{ED}) \cdot PD_{CD} \quad \text{Eq. 3-15}$$

$$PFA = PFA_{ED} + (1 - PFA_{ED}) \cdot PFA_{CD} \quad \text{Eq. 3-16}$$

where:

- PD_{ED} denotes the PD of the Energy Detector.
- PFA_{ED} denotes the PFA of the Energy Detector.
- PD_{CD} denotes the PD of the Cyclostationary Detector.
- PFA_{CD} denotes the PFA of the Cyclostationary Detector.

From Eq. 3-15 and Eq. 3-16 one can see that using a two-stage hybrid detector will not only increase the probability of detection but it also increases the probability of false alarm. Therefore, a two-stage hybrid detector could be seen as a compromise in terms of complexity and performance between ED and CD.

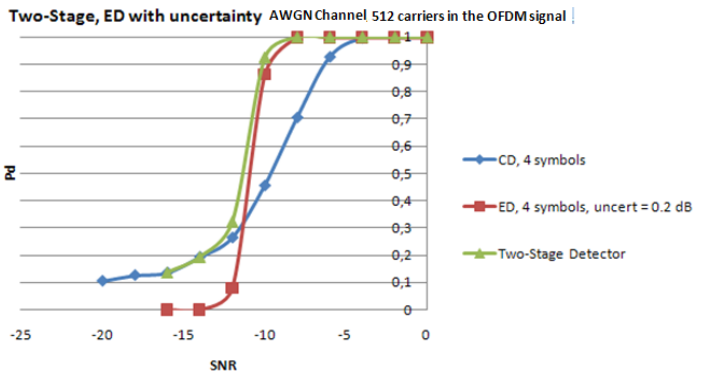

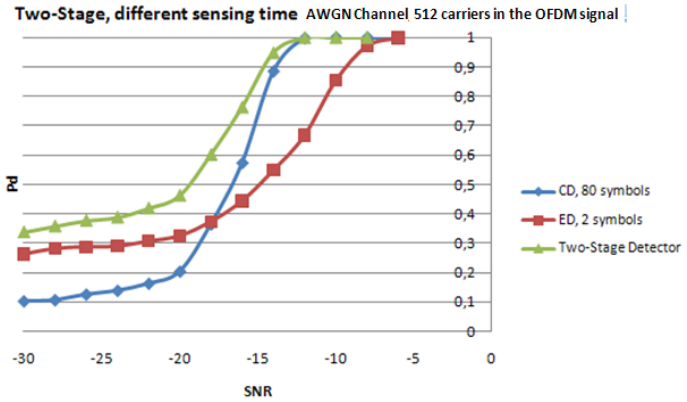

Figure 3-8: Hybrid detection performance on OFDM signals with AWGN channel and 512 carriers compared to ED or CD detection

3.1.1.2 Parallel Sensing using Antenna Array Processing

3.1.1.2.1 Introduction

In a coexistence use case, where in the same frequency band the incumbent user and the opportunistic user can coexist, the latter must ensure that the incumbent system is protected and that it will not be interfered in by the opportunistic user. To do so, it must first find an available frequency band. It must then periodically check that an incumbent system is not present in the band it is using by performing in-band sensing.

In this section an approach to perform efficient in-band parallel sensing (parallel sensing in the band currently in use) based on the use of an antenna array and on the spatial rejection abilities of smart antenna processing is proposed. The assumption is made that the incumbent system presents cyclostationary features known by the opportunistic system. First, a comparative presentation of the advantages and drawbacks of parallel sensing versus serial sensing is proposed. The use of antenna processing techniques to perform parallel sensing is also depicted and a practical use case is described. Then an extension to the classical cyclostationary feature detection algorithm to the multi-antenna case is proposed and evaluated.

3.1.1.2.2 Parallel versus Serial Sensing

In classical CR systems, the cognitive waveform of an opportunistic system is designed in a way such that the opportunistic user is able to detect an incumbent system using its frequency band. In order to do so, periodic time slots are allocated in the opportunistic user's frame during which the cognitive system is not communicating. These time periods, referred as quiet periods (QP), are used by the opportunistic user to perform in-band sensing without being interfered by the signal it receives. This way to proceed is called serial sensing. The main advantage of serial sensing is that it is usually performed at high Signal to Interference Ratio (SIR). Therefore basic sensing algorithms such as energy detection can be used and have a good sensitivity. Nevertheless, the waveform needs to be redesigned in order to insert and properly use the QPs, thus increasing the system complexity and reducing the payload rate of the system. Another way to proceed is to directly sense the communication signal by parallel sensing as described in Figure 3-9. This way, there is no rate reduction and sensing can be performed without any adjustment in the waveform. Of course, a more robust sensing algorithm must be used as it has to operate at low SIR since the opportunistic communication signal always generates a high level of interference.

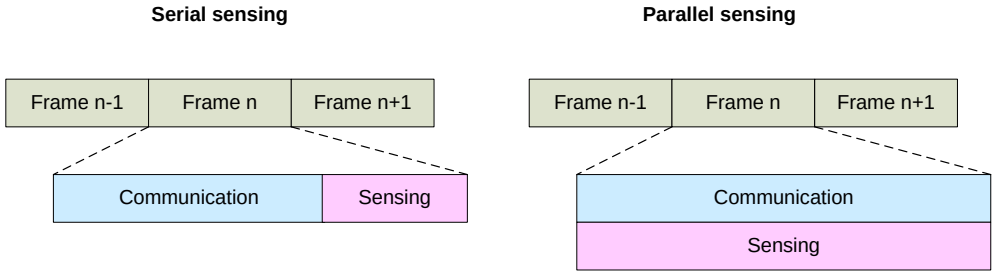

Figure 3-9: Serial sensing vs. parallel sensing

3.1.1.2.3 Interference Rejection

As stated previously, the main drawback of in-band parallel sensing is that the opportunistic sensing device has to be able to detect the incumbent system while being highly jammed by the signal it receives from its own system (a downlink signal from its RATs base station). The concept developed here is to use the interference rejection abilities of multi-antenna processing to spatially reject the opportunistic signal and only keep the signal of interest (in this case, the signal to be detected, that is the incumbent signal).

Antenna processing turns out to increase detection performance by several means. Firstly, the detection is more robust to fast fading thanks to spatial diversity. Secondly, it can reduce the noise floor of the detection criterion by averaging it over the sensors of the array. But the most important aspect for parallel sensing is that signal separation can be performed thanks to the characteristics of the sensed signal. This allows detecting a given signal even with very low SIR. Indeed, when the antenna array receives several sources emitted from different directions of arrival, the multi-antenna processing can recombine the signals received on the different antennas in order to detect one given source – the other ones are considered as interference that the processing can spatially reject. This process is often called **interference rejection**. In this study, it is assumed that the incumbent signal presents known cyclostationarity properties that will be useful to implement reliable multi-antenna detection.

3.1.1.2.4 Use Case for Parallel Sensing

Figure 3-10 describes a cognitive radio use case for parallel sensing. It can be decomposed into three phases:

- Phase 1: A mobile opportunistic system is located in a white space. It identifies the spectrum band B_0 as free and decides to use it. In order to ensure the protection of an eventual incumbent user; it has to periodically sense B_0.
- Phase 2: The mobile opportunistic system has moved and is no longer in the white space. On B_0, it is now interfering with the incumbent system. The opportunistic system is not aware of the presence of the incumbent Tx yet and is still communicating. For the opportunistic Rx, the signal coming from the incumbent Tx is seen as an interference.
- Phase 3: The opportunistic Rx is performing sensing on B_0. The goal of this phase is to detect the incumbent Tx. The signal coming from the incumbent Tx is now the signal of interest (signal to be detected) and the signal from the opportunistic Tx, the interference (it is jamming the sensing process). As the opportunistic Rx has interference rejection capabilities, it can perform sensing even if the opportunistic Tx is emitting and still be able to detect the incumbent Tx. As proved in the following, this is true even if the received signal level from the opportunistic Tx is more than 40 dB above the one from the incumbent Tx.

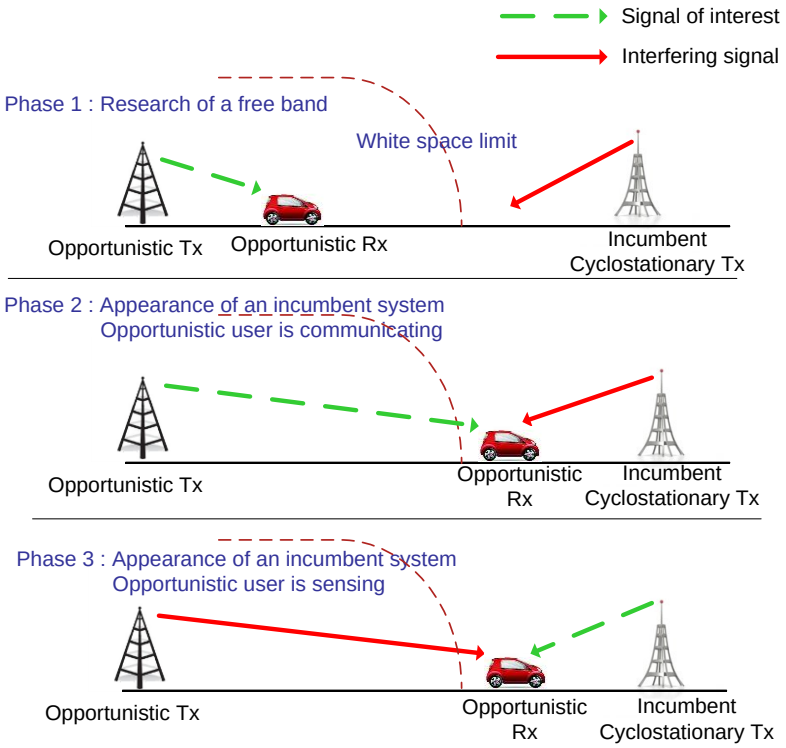

Figure 3-10: Scenario for sensing with interference rejection in CR

3.1.1.2.5 Spatial Propagation Channel Model

In the context of mobile communications, it is well established that the distortions induced by the propagation channel between the transmitter and the receiver deeply influence the performance of the demodulation algorithms. Moreover as the algorithm proposed in section 3.1.1.2.6 is using an antenna arrays, it is thus crucial to be able to reliably simulate the propagation channels between the active emitters and the *M* receivers. The multi-channel propagation model used for the algorithmic study is an extension of the classical Clarke mono-channel model [Clarke68].

The Clarke model allows taking into account the situation of a moving device at speed *v*. The antenna array receives different plane waves due to multiple reflections on various obstacles (near or far obstacles):

- with random amplitudes,
- with random phases,
- with random directions of arrival.

At the propagation channel output, the received signal in base-band is given by the following expression:

$$\underline{x}(t) = \sum_{l=1}^{L} a_l d(t-\tau_l) \left[\sum_{n=1}^{N_l} c_{n,l} e^{j\left(2\pi v/\lambda \cos(\theta_{n,l}-\gamma)t+\varphi_{n,l}\right)} \underline{s}_{n,l} \right] \qquad \text{Eq. 3-17}$$

where:

- $d(t)$ is the useful modulated signal,

- $\underline{x}(t)$ is the received signal vector,
- L is the number of paths,
- a_l is the attenuation of the l^{th} path (a path is due to a reflection on a far obstacle),
- τ_l is the delay of the l^{th} path,
- N_l is the number of elementary sub-paths associated to the l^{th} path. The sub-paths are due to the multiple reflections typically all around the device. All sub-paths associated to a path are considered to have the same delay (the delay differences are negligible compared to the inverse of the signal bandwidth),
- $c_{n,l}$ is the attenuation of the n^{th} sub-path associated to the l^{th} path,
- v is the device speed,
- γ is the angle between the device speed and the North (randomly uniformly distributed [0, 2π]),
- λ is the wavelength,
- $\theta_{n,p}$ is the azimuth of the n^{th} sub-path associated to the l^{th} path, (see Figure 3-11 for the orientation conventions),
- $\varphi_{n,l}$ is the phase of the n^{th} sub-path associated to the l^{th} path (randomly uniformly distributed [0, 2π]),
- $\underline{s}_{n,l}$ is the steering vector of the n^{th} sub-path associated to the l^{th} path. The steering vector depends on the array geometry and on the direction of arrival of the sub-path:

$$\underline{s}_{n,l} = \left[e^{j\Delta\phi_{n,l,1}} \cdots e^{j\Delta\phi_{n,l,M}}\right]^{\mathrm{T}},$$

where:

  - M is the number of antennas
  - $\Delta\phi_{n,l,k}$ is the geometric phase shift of the n sub-path associated to the l^{th} path between the k^{th} antenna and the array centre:
  - $\Delta\phi_{n,l,k} = 2\pi(R_k/\lambda)\cos(\theta_{n,l} - \alpha_k)$,

    where:

    - (R_k, α_k) are the polar co-ordinates of antenna k.

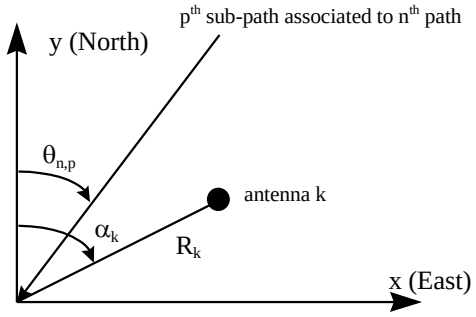

Figure 3-11: Orientation convention for the measure of angles

In this model, all the parameters are stationary. The only variations are due to the device speed, which generates a fading variation of the received signal on each antenna. When the device is not moving, there is spatial diversity (each antenna has its own fading level), but this spatial diversity is stationary.

In short, our propagation model can be used to simulate various scenarios, including:

- Stationary propagation conditions: N_l = 1. The user chooses all the parameters for the simulation. This simple scenario is essentially used in order to validate the algorithms.
- Rayleigh fading: all the paths have the same number of sub-paths (N_l = 10 for all the simulations) with the same amplitude: $c_{n,l}$ = 1/sqrt(N_l).
- Rice fading: the first sub-path has a higher amplitude than the other paths ($c_{0,l} > c_{n,l}$ = 1/sqrt(N_l). The relative amplitude of the different sub-paths is an input parameter.

Finally, the various angles of arrival $\theta_{n,l}$ are chosen randomly and uniformly distributed in a angular reception cone.

3.1.1.2.6 Cyclostationary Feature Detection

Let us first start by describing the detection criterion in the mono-antenna case. Let $r[n]$ be the discrete time signal received at time nT_s (T_s being the sampling frequency). For each α, $\hat{R}_{rr}^{\alpha}(N,\tau)$ represents the empirical estimate of $R_{rr}^{\alpha}(\tau)$ (Cf. section 2.2.4 for notations) given by:

$$\hat{R}_{rr}^{\alpha}(N,\tau) = \frac{1}{N}\sum_{n=1}^{N} r[n]r^{*}[n+\tau]e^{j2\pi\alpha n} \qquad \text{Eq. 3-18}$$

where N, is the integration duration in samples. A simple estimate of the cyclostationarity properties (τ_0, α_0) is found by maximizing $\hat{R}_{xx}^{\alpha}(N,\tau)$ [Gardner88]. Therefore, one can deduce a mono-antenna detection criterion:

$$C(N) = \frac{\left|\hat{R}_{xx}^{\alpha_0}(N,\tau_0)\right|}{\left|\hat{R}_{xx}^{0}(N,0)\right|} \qquad \text{Eq. 3-19}$$

This criterion is normalized in order to be independent of the received signal power and be easily compared to a threshold, depending only on the integration duration N. This threshold is computed by simulation, by calculating the criterion, on a large number of drawings, in presence of a non-cyclostationary signal. The threshold is chosen to target a given PFA. It is important to highlight that a frequency offset due to inaccurate frequency synchronization with the received signal does not impact the criterion. Moreover, this criterion does not require synchronization; contrarily to a classical reference-based detection criterion, one single value is computed.

Let us now extend the criterion of Eq. 3-19 to the multi-antenna case. In order to simplify the readability, let us use matrix notations.

Let us call

$$\underline{\rho}[n,M] = \begin{bmatrix} r^{(1)}[n] \\ \vdots \\ r^{(M)}[n] \end{bmatrix} \quad \text{Eq. 3-20}$$

the received snapshot vector on the *M* antennas of the array at time *n*.

The received snapshot matrix on *M* antennas and on the time horizon *N* is then built:

$$\mathbf{P}[N,M] = \begin{bmatrix} \underline{\rho}[1,M] & \cdots & \underline{\rho}[N,M] \end{bmatrix} \quad \text{Eq. 3-21}$$

By introducing the sampled received signal on antenna *m*, delayed by the lag parameter $\tau_0 = T_D$ and shifted in frequency by the cyclic frequency $\alpha_0 = 1/T_S$:

$$u^{(m)}[n] = r^{(m)}[n + N_D]e^{j2\pi n/N_S} \quad \text{Eq. 3-22}$$

The snapshot vector and the snapshot matrix can be introduced the same way:

$$\underline{\upsilon}[n,M] = \begin{bmatrix} u^{(1)}[n] \\ \vdots \\ u^{(M)}[n] \end{bmatrix} \quad \text{Eq. 3-23}$$

and

$$\mathbf{Y}[N,M] = [\underline{\upsilon}[1,M] \quad \cdots \quad \underline{\upsilon}[N,M]] \quad \text{Eq. 3-24}$$

Let us now introduce the $M \times M$ estimated autocorrelation and cross-correlation matrices:

$$\mathbf{R_{PP}} = \mathbf{P}[N,M]\mathbf{P}^H[N,M] \quad \text{Eq. 3-25}$$

$$\mathbf{R_{YY}} = \mathbf{Y}[N,M]\mathbf{Y}^H[N,M] \quad \text{Eq. 3-26}$$

$$\mathbf{R_{YP}} = \mathbf{Y}[N,M]\mathbf{P}^H[N,M] \quad \text{Eq. 3-27}$$

$$\mathbf{R_{PY}} = \mathbf{P}[N,M]\mathbf{Y}^H[N,M] \quad \text{Eq. 3-28}$$

In [Gardner90], it is shown that the detection test of the number of common sources *l* in r and u is based on the following test statistic:

$$Q(l) = -N\log \prod_{j=l+1}^{M} (1-\mu_j) \quad \text{Eq. 3-29}$$

with μ_j is the j[th] eigenvalue of the matrix

$$\mathbf{R} = \mathbf{R_{YP}}\mathbf{R_{PP}^{-1}}\mathbf{R_{PY}}\mathbf{R_{YY}^{-1}} \quad \text{Eq. 3-30}$$

The presence of one single common source in r and u (meaning in our case that *r* is cyclostationary) can be tested by applying $l = 0$ in equation Eq. 3-29.

As $\prod_{j=1}^{M}(1-\mu_j) = \det(\mathbf{I}_M - \mathbf{R})$, we can deduce our multi-antenna cyclostationarity detector as being:

$$C(N,M) = 1 - \det\left(\mathbf{I}_M - \mathbf{R}_{\mathbf{YP}}\mathbf{R}_{\mathbf{PP}}^{-1}\mathbf{R}_{\mathbf{PY}}\mathbf{R}_{\mathbf{YY}}^{-1}\right) \quad \text{Eq. 3-31}$$

where det(.) is the determinant function and $\mathbf{I}_M$ is the $M \times M$ identity matrix. As in the mono-antenna case, this criterion does not require synchronization and it is computed only once, not on a search horizon.

For this criterion, a coherent integration is made over *N* samples. It is important to highlight that when using this criterion, as autocorrelation is computed, a frequency offset due to the inaccurate frequency synchronization with the received signal does not impact the performance. Therefore, the length of the coherent integration is not limiting as it is the case when using a reference-based criterion.

In [Öner04], it has been shown that an OFDM signal exhibits non-conjugate cyclostationarity with cycle frequencies $\alpha = k/T_S$ with peaks at $\tau = \mp T_D$ (Cf. section 2.2.2 for notations). Therefore, this criterion can be applied to detect any OFDM waveform.

Parallel with the reference-based algorithm

It is interesting to notice that this criterion is a generalization of the reference-based criterion (as used in [E3_D5.3]), in the case where no reference is known but only the cyclostationary properties. Indeed, when a reference $d[n]$ of the processed signal is known (pilot bits, pilot channel, synchronization signal, etc.), instead of using the vector $\underline{\upsilon}[n,M]$, one can simply use the scalar $d[n]$ (the reference is the same on each antenna of the array).

Then, the correlation matrix $\mathbf{R}_{\mathbf{YP}}$ is replaced by the correlation vector $\underline{\mathrm{r}}_{d\mathbf{P}} = \underline{\mathrm{r}}_{\mathbf{P}d}^H$ and the correlation matrix $\mathbf{R}_{\mathbf{YY}}$ by the scalar $\left\|\underline{\mathrm{d}}\right\|^2$.

The $\mathbf{R}_{\mathbf{YP}}\mathbf{R}_{\mathbf{PP}}^{-1}\mathbf{R}_{\mathbf{PY}}\mathbf{R}_{\mathbf{YY}}^{-1}$ matrix becomes

$$\frac{\underline{\mathrm{r}}_{\mathbf{P}d}^H\mathbf{R}_{\mathbf{PP}}^{-1}\underline{\mathrm{r}}_{\mathbf{P}d}}{\left\|\underline{\mathrm{d}}\right\|^2}$$

This expression being a scalar, the detection criterion becomes:

$$C(N,M) = \frac{\underline{\mathrm{r}}_{\mathbf{P}d}^H\mathbf{R}_{\mathbf{PP}}^{-1}\underline{\mathrm{r}}_{\mathbf{P}d}}{\left\|\underline{\mathrm{d}}\right\|^2} \quad \text{Eq. 3-32}$$

which is the optimal reference-based spatial detector as demonstrated in [E3_D5.3].

3.1.1.2.7 Knowledge of the Cyclostationarity Properties

As stated previously, it is assumed, in this section, that the cyclostationary properties of the incumbent radio access system to be sensed are known. In practice, this knowledge can be acquired by two means.

The first one consists in estimating these properties. Several methods have been proposed in the literature (for example, in the OFDM case, in [Yücek07]). Nevertheless, they always present two drawbacks. They increase the computational complexity of the algorithm and as they are not 100% reliable, in the case of bad estimation, they degrade the probability of detection.

The second one consists in finding this information in a database. Indeed, in September 2010, FCC published a report [FCC10] with the scope of finalizing rules to make the unused spectrum in the TV bands available for unlicensed broadband wireless devices. This report is favourable to geo-location with database approach, but leaves a backdoor open for any other contribution from the spectrum sensing research field. It can be therefore envisaged that the opportunistic system finds in the database a list of the incumbent systems it might encounter at its location, with their characteristics. It could then apply the proposed method using the cyclostationary properties of the listed systems.

3.1.1.2.8 Simulation Performance

3.1.1.2.8.1 Determination of the Thresholds

A detection criterion needs a threshold to be compared to in order to determine the presence or absence of the searched signal. The threshold depends on the detector parameters, i.e. in our case the number of samples N and the number of antennas M.

The threshold choice is led by the PFA. 10,000 draws are run in absence of the searched signal (AWGN only). This allows having significant statistics for PFA down to 10^{-3}.

3.1.1.2.8.2 Detection Performance

Two phases of the scenario presented in section 3.1.1.2.4 are simulated: Phase 1 during which the opportunistic user is searching for an available frequency band and phase 3 during which the opportunistic user is performing parallel sensing to verify the presence or not of an incumbent user on the frequency band it is using. Phase 1 corresponds to simulations in presence of the cyclostationary incumbent signal and AWGN. Phase 3 corresponds to simulations in presence of the cyclostationary incumbent signal, the non-cyclostationary opportunistic signal and AWGN. It allows quantifying the interference rejection capabilities of the multi-antenna algorithm. The presented algorithm is also working if the opportunistic system is cyclostationary but only if it does not present the same cyclostationary properties as the incumbent system.

Simulations are run using an OFDM signal as the incumbent signal to be detected. As shown in [Öner04], OFDM signals exhibit non-conjugate cyclostationarity due to the insertion of the cyclic prefix. The FFT order is set to 1024 with a cyclic prefix of 1/8.

For phase 1 sensing simulations, AWGN is added in order to target an SNR varying from -20 dB to 5 dB. For phase 3 sensing simulations, SIR varies from -70 dB to +20 dB. AWGN is also added to the OFDM signal, to target an SNR equal to +30 dB.

Two propagation channel models are simulated, a mono-path stationary channel and one of the models recommended by the LTE standard [3GPP 36.521], the Extended Pedestrian A (EPA) model. The characteristics of the EPA model are described in Table 3-2.

Table 3-2: Extended Pedestrian A propagation model characteristics

Number of channel taps	Delay spread	Maximum Doppler Frequency	Excess tap delay [ns]	Relative power [dB]
7	45 ns	5 Hz	0	0.0
			30	-1.0
			70	-2.0
			90	-3.0
			110	-8.0
			190	-17.2
			410	-20.8

The detection criterion is integrated over 20 OFDM symbols ($N = 20 \times 1024(1 + 1/8) = 23040$), using from 1 to 5 antennas. The detection thresholds are set in order to target a PFA equal to 1%.

Figure 3-12 presents the sensing performance during phase 1, that is the PD versus SNR for the two propagation channels. First of all, one can notice that the detection performance improves while the number of antennas increases. With a mono-path stationary channel, the gain is equal to 4.3 dB, when using five antennas instead of one, for a target PD of 90%. It must be underlined that this case is the less favourable for antenna processing as there is no antenna diversity (the propagation channel is stationary) and no interference rejection (absence of any interference). For the EPA channel model, the gain is higher, 6.3 dB, due mainly to the spatial diversity gain. As the EPA channel model is tougher,

the reachable SNR for a target PD of 90% is lower than with the mono-path channel (-9 dB vs. -11.1 dB when using five antennas).

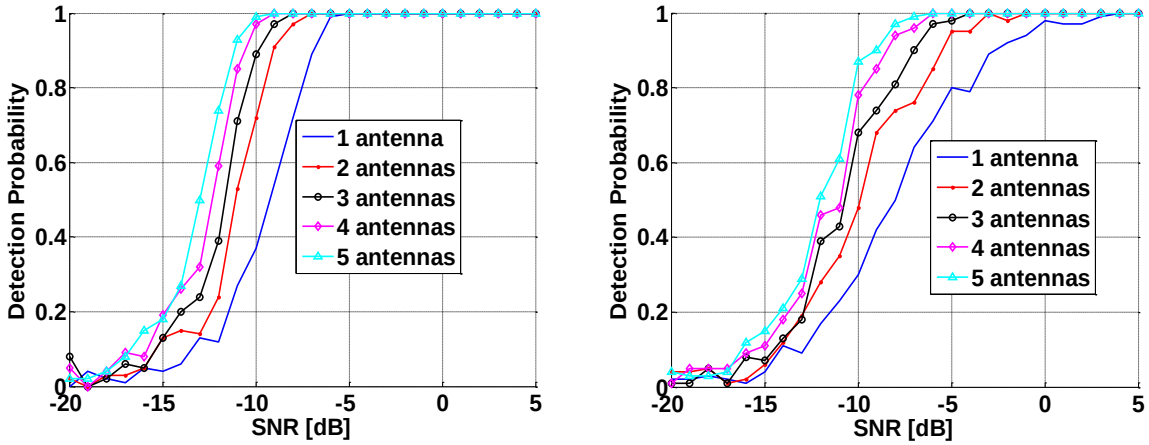

Figure 3-12: Probability of detection vs. SNR when using 1 to 5 antennas for a mono-path stationary channel (left) and the EPA channel (right) and for a PFA=1%, in presence of one cyclostationary signal and AWGN

Figure 3-13 presents the sensing performance during phase 3, that is the PD versus SIR for the two propagation channels. With a mono-path propagation channel, the interference rejection ability of the algorithm is clear. With only two antennas, the gain for a target PD of 90% is equal to 54 dB (higher than 65 dB with five antennas). The opportunistic signal can be rejected with a SIR down to -62 dB (around -75 dB with five antennas). In this case, it is clear that parallel sensing is conceivable.

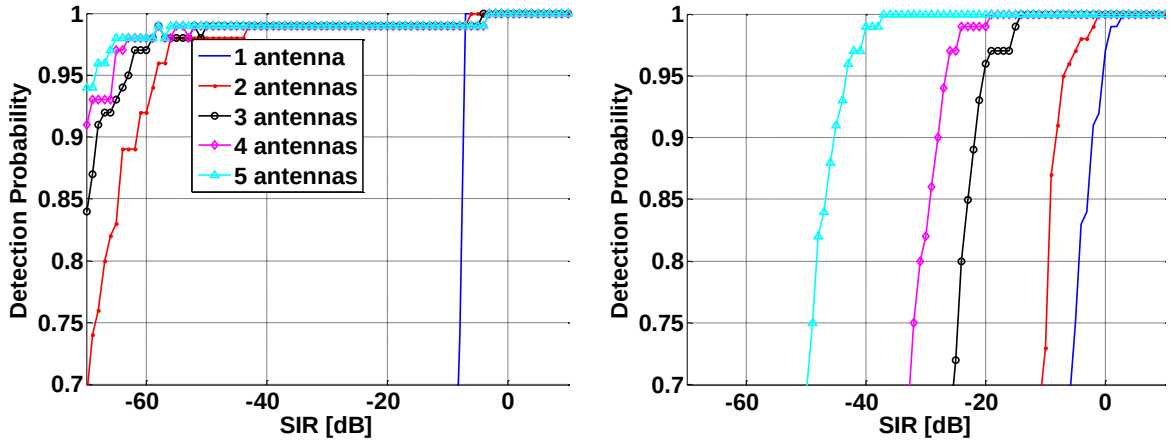

Figure 3-13: Probability of detection vs. SIR when using 1 to 5 antennas for a mono-path stationary channel (left) and the EPA channel (right) and for a PFA=1%, in presence of one cyclostationary signal and one non-cyclostationary signal

For the EPA channel model, the gain is lower (only 7.3 dB with two antennas but 43 dB with five antennas). It is due to the fact that the algorithm can reject *M-1* sources with *M* antennas. It is important to underline that two paths from the same emitter are considered as two sources. This explains the results obtained with the EPA channel model. Indeed with two antennas, the algorithm is only able to reject the most powerful path. The remaining six paths are significant enough to disrupt the detection performance. In the EPA model, it can considered that the first four paths are the really disrupting, that is why we observe a gain of nearly 25 dB when using five antennas instead of four (the last significant path has been rejected thanks to the fifth antenna). With five antennas, the opportunistic user can be rejected down to a SIR equal to -45 dB for a PD of 90%.

3.1.1.2.9 Conclusion

An innovative approach for parallel sensing based on the use of antenna array and antenna processing was presented. It shows that thanks to the interference rejection capabilities of a multi-antenna system, in-band sensing can be performed by an opportunistic user without having to integrate quiet periods in its waveform.

An extension of the cyclostationary feature detection algorithm in the multi-antenna case is proposed. With a realistic propagation channel model such as the extended pedestrian A (recommended by the LTE standard), the cyclostationary incumbent system can be detected with a SIR down to -45 dB with five antennas (lower than -70 dB with a mono-path channel). These values are promising for practical application. The proposed method can be used on FDD systems of TDD systems but only on the reception time slots.

The limitation of the proposed method is that the opportunistic signal must not have the same cyclostationarity properties as the incumbent.

3.1.2 PMSE Detection

3.1.2.1 Wireless Microphone Detection

In this section, the wireless microphone sensing is addressed for incumbent detection in the TV white space. The suggested approach is based on an efficient semi-blind detection of narrow-band FM modulation signals.

The base-band microphone signal is generated following the model of section 2.2.3 in which the parameters are set as follows:

- the frequency bandwidth of *x(t)* is set to 20 kHz
- the FM deviation f_d is set to 3
- the carrier frequency f_0 is equal to 100 kHz, in a 8 MHz band
- the noise power σ_n^2 is set to 0 dBm

Under these conditions, the transmitted microphone signal *s(t)* has a frequency bandwidth around 100 kHz.

Based on the European UHF band channelization, the observation window is 8 MHz (narrow-band conditions) and the proposed algorithms considers N = 4096 samples (approximately 0.5 ms for 8 MHz). Moreover, it is considered there is at most one wireless microphone in the observation band.

In this study, two steps are evaluated to achieve wireless microphone sensing. The first step consists of the validation of a new detector which takes into account the FM modulation characteristics of the signal and to use the appropriate Teager-Kaiser energy operator. This algorithm is tested over an 8 MHz channel. The second step consists of analysing how detection can be improved by narrowing down the considered bandwidth using a filter-bank. This second step is applied to the new algorithm as well as the classical approaches.

3.1.2.1.1 State of the Art

TV band incumbent detection has been an active research topic over the past few years. Most of them concentrate on DTT (Digital Terrestrial Television) detection, which is the incumbent operating system in these bands. DTT signal is well suited to feature detectors. For instance, [Bouzegzi08] has proposed a cyclostationarity detector for OFDM signals, which is the modulation used by the European DTT system (DVB-T). Wireless microphones are opportunistic users of the TV band. However, they must be preserved interference free by any opportunistic system that would operate in this band. Microphone sensing raises new challenges due to its analog FM modulation and very low power operation. In particular, the modulation hardly exposes any feature that could be exploited by

enhanced feature detectors. For these reasons, most of the literature references suggest blind detectors for the specific case of the wireless microphones [Chen08_1]. These studies are based on eigenvalue decomposition [Xu08], spectral correlation [Han06] and energy detection [Ghosh08].

A selection of two classical blind detectors is introduced as the baseline for the sake of comparison with the proposed algorithms. These methods lie on a stationary and deterministic model of the signal mixed with a stationary noise.

- Energy detection: The energy detector computes a variable which is proportional to the energy of the received signal [Urkowitz67]. The test statistic T of the energy detector is given by:

$$T = \frac{1}{N}\sum_{n=0}^{N-1} |r[n]|^2 \qquad \text{Eq. 3-33}$$

  where *N* is the number of samples of the analysed signal. The test statistic is then compared to a threshold.

- Autocorrelation detection: This method tests the stationary properties of the signal by calculating the autocorrelation function. When no signal is present and assuming AWGN conditions, the second order moment of the signal is a Dirac distribution. The receiver estimates the autocorrelation function y[k] of the received signal:

$$y[k] = E[r[n]r^*[n-k]], \quad k = 0, \pm 1, \pm 2, \ldots \pm N, \qquad \text{Eq. 3-34}$$

  In practice, the autocorrelation is an approximation of the second order momentum with finite integration time.

There are several test statistics that can be used. The most efficient one [Shellhammer08] uses the sum of the square of the amplitude of all components of the autocorrelation function and the square of the amplitude of the central sample (k=0). Thus, the following decision variable is calculated:

$$T = \frac{\sum_{k=0}^{N-1} |y[k]|^2}{|y[0]|^2} \qquad \text{Eq. 3-35}$$

When no signal is present, the two terms should be roughly equal (assuming AWGN conditions), since the non-central values ($k \neq 0$) should be approximately zero. When the wireless microphone signal is present, the signal is no longer white and the statistical test should increase.

One of the common properties of these algorithms is that they assume the detection of wide-band signals. However, the European TV band is composed of 48 channels of 8 MHz bandwidth. Each band has to be analysed for the detection of both the TV signals and the microphones and a decision variable will be provided to the CR system which takes the final decision of using one band or not. The analysed TV channel is wide compared to the frequency band occupied by the microphone signal. Thus, an important assumption of our study is that the detection of the wireless microphones deals with narrow-band signals.

3.1.2.1.2 Teager-Kaiser Energy Detector

First, a new method for energy detection suitable to detect microphones is proposed . Instead of using the conventional energy detector, we suggest using the Teager-Kaiser energy operator to measure the energy activity over a certain time. This operator better captures the energy of FM signals.

Introduced in [Kaiser90], Kaiser uses the results of Teager [Teager89] which show the non-linear model of the speech. These changes of the characteristics of the speech signal can be modelled as a linear combination of AM and FM signals. Based on this model, Kaiser has proposed a very simple and fast algorithm [Kaiser90] to estimate energy, called the Teager-Kaiser energy operator, since the

restriction related to the bandwidth of the signal (narrow-band signal) is respected. The Teager-Kaiser energy operator Ψ extracts directly the energy from the instantaneous signal *s*, it is expressed by:

$$\Psi\{s[k]\} = s[k]^2 - s[k+1]s[k-1] \quad \text{Eq. 3-36}$$

Adding white Gaussian noise *n(t)*, the operator can be expressed as:

$$\Psi\{r[k] = s[k] + n[k]\} = \Psi\{s[k]\} + \Psi\{n[k]\} + 2\Psi\{s[k], n[k]\} \quad \text{Eq. 3-37}$$

where $\Psi[s(k), n(k)]$ is the cross energy operator defined as:

$$\Psi\{s[k], n[k]\} = s[k]n[k] - \frac{1}{2}s[k+1]n[k-1] - \frac{1}{2}s[k-1]n[k+1] \quad \text{Eq. 3-38}$$

$\Psi\{s(k), n(k)\} = 0$ if *s(t)* and *n(t)* are uncorrelated.

Then, the average value of the operator *r*[*k*] is:

$$E[\Psi\{r[k]\}] = E[\Psi\{s[k]\}] + E[\Psi\{n[k]\}] = E[\Psi\{s[k]\}] + \sigma_n^2 \quad \text{Eq. 3-39}$$

Eq. 2-5 shows that the wireless microphone signal is an FM modulation of a speech signal, so the Teager-Kaiser energy detector should be adapted to this kind of signal. From Eq. 3-39, the semi-blind detection could be performed by computing the test $T = E[\Psi\{r[k]\}]$.

Figure 3-14 shows the performance of the Teager-Kaiser energy detector. The detection probability is computed versus the SNR for two false alarm probabilities (PFA= 1% and 10%).

The performance is compared with those of the classical energy detector and the autocorrelation detector. For PFA=10% and PD=90%, the simulation results show that the Teager-Kaiser energy detector can detect SNR down to -12dB. This algorithm is compared with the energy detection algorithm in order to check if the energy model is non-linear and if this detector provides a better estimate of an FM signal energy. Figure 3-14 shows that the energy detector can detect SNR down to -9 dB for PFA=10% and PD=90%.

Then, the Teager-Kaiser energy detector allows a 3 dB detection gain. Note that this detector does not induce an important increase of the computational complexity compared to the energy detector.

Results also show that the autocorrelation detection achieves the most interesting performance. It can detect SNR down to -14 dB for PFA=10% and PD=90%. However, this performance is achieved at an important cost of the complexity compared to the other two detectors.

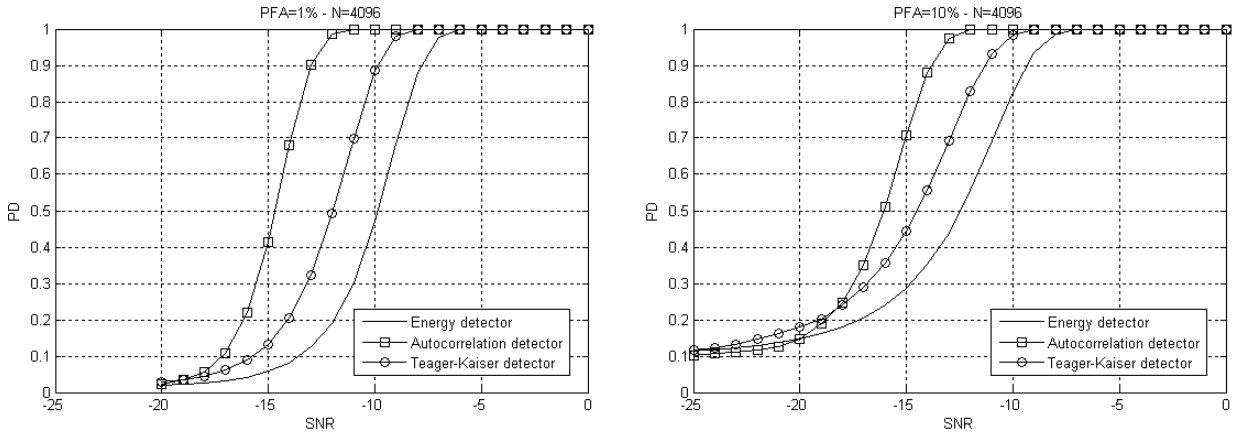

Figure 3-14: Detection probability versus SNR for various detectors and 2 PFAs (1% and 10%)

3.1.2.1.3 Adapted Counterparts of the Wide-Band Algorithms

The first proposed solution improves the detection by using the Teager-Kaiser energy operator which takes into account the non-linear model of speech. The second approach deals with the narrow-band characteristics of the wireless microphone signal, a filter-bank based technique splits the analysis of the wide-band signal into sub-bands in order to increase the accuracy of the algorithms.

The narrow-band detection is derived from wide-band detections by filtering the signal into sub-bands. Figure 3-15 describes the structure of the adapted detector using a filter-bank structure. Once filtered, each sub-band is processed by a detector and a test statistic T_i is computed for each sub-band. The final decision is made on the maximum of these test statistics.

This structure depends on the filters' bandwidth *B*.

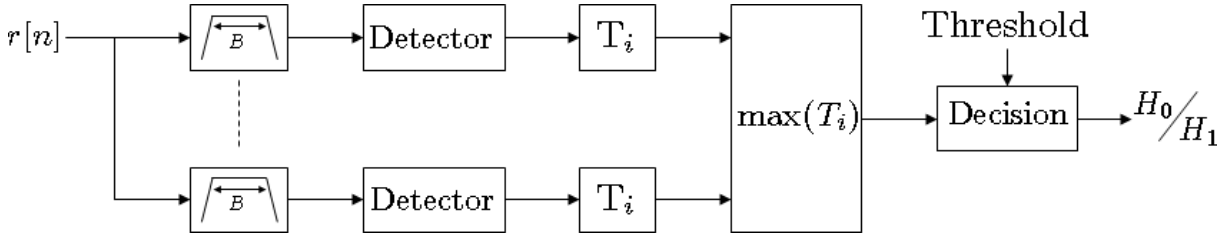

Figure 3-15: Structure of the narrow-band filter-bank based detector

As detectors, it is proposed to use the energy detector, the autocorrelation detector and the Teager-Kaiser energy detector.

In the specific case of the energy detector [Neihart07], the energy calculation could be performed in the frequency domain. Then, the filter-bank is replaced by a Fast Fourier Transform (FFT) which analyses the spectral content of the signal.

The FFT size is chosen to have sufficient frequency resolution in the signal band:

$$\frac{B_c}{N_{FFT}} << B_s \qquad \text{Eq. 3-40}$$

where N_{FFT} is the size of the transform and B_s the microphone signal bandwidth in the channel bandwidth B_c.

Once the FFT is performed, the energy detection is computed on each sub-band. This algorithm is called the "narrow-band energy detector".

For the autocorrelation detector and the Teager-Kaiser energy detector, the test statistic must be computed in the time domain, so these detectors must use a filter-bank as shown in Figure 3-15.

These new algorithms are called the "narrow-band autocorrelation detector" and the "narrow-band Teager-Kaiser energy detector".

For the three structures, the optimum width *B* of the frequency window has to be set. Obtained by simulation, PD is plotted versus PFA for different frequency bandwidths. Performance is compared to the one obtained with the algorithm without filtering (curves *B*= 8 MHz). The results are shown in Figure 3-16.

- For the narrow-band energy detection using a FFT, the curves are obtained for SNR=-15 dB and for B set from 20 kHz up to 160 kHz. First, these simulations show the improvement of the new algorithm. Indeed, when the frequency window is not used, detection is clearly impossible. Then, the results show that the size of the frequency window gives the best results

for 80 kHz. When the bandwidth is too small or too large compared to the signal bandwidth, performance is degraded. In the following, a bandwidth of 80 kHz will be used.

- For the autocorrelation algorithm using a filter-bank, the curves are obtained for SNR=-16 dB and for B=200 kHz, 400 kHz and 800 kHz. The best bandwidth is obtained for 400 kHz.
- For the narrow-band Teager-Kaiser energy detector, the curves are obtained for SNR=-16 dB and for B=50 kHz, 100 kHz and 200 kHz. These simulations show that the detection is clearly impossible when the filter-bank is not used. Then, the results show that a bandwidth of 100 kHz provides the best results, this value will be used thereafter.

The bandwidth obtained for each method is, in an obvious way, in the same order as the bandwidth of the wireless microphone signal. The difference of bandwidth between each method results from the filter-bank coefficients that have been recomputed for each method.

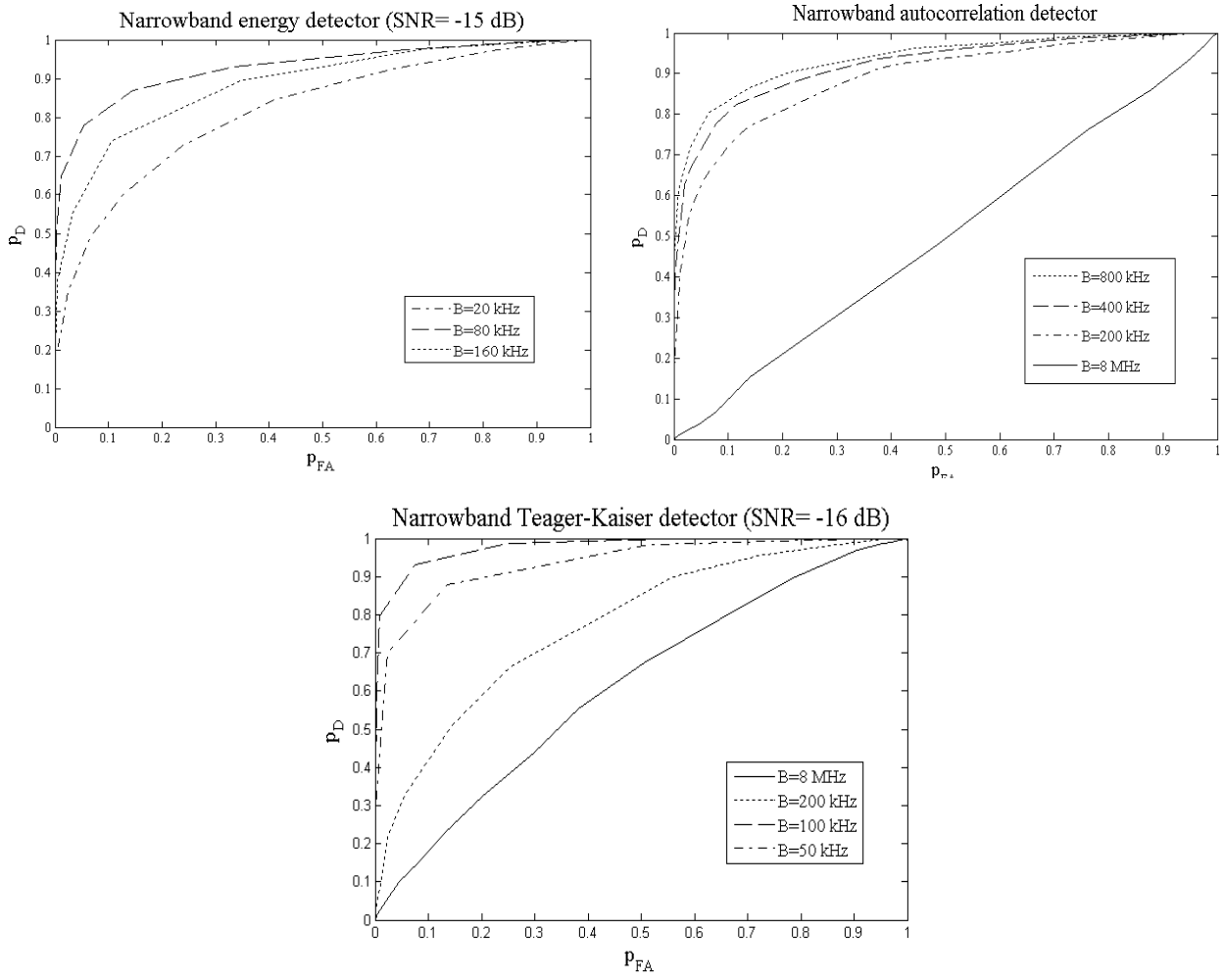

Figure 3-16: PD versus PFA for different window bandwidths of the narrow band power detection, the narrow-band autocorrelation detection and the narrow-band Teager-Kaiser detection

After setting the bandwidth *B* for each narrow-band detector, the performance of these detectors is computed and introduced on Figure 3-17. This figure shows the detection probability PD versus the SNR for two false alarm probabilities (PFA= 1% and 10%).

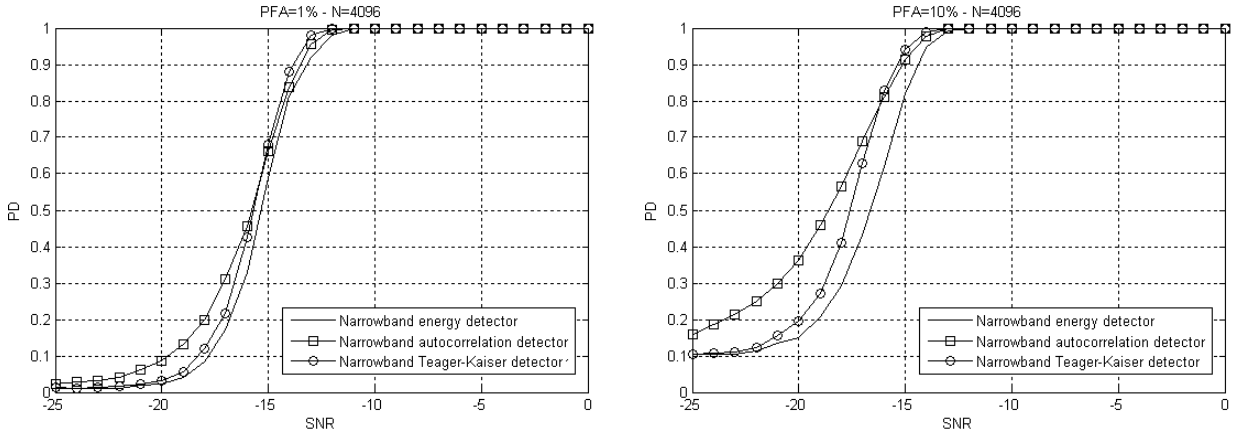

Figure 3-17: Detection probability versus SNR for various narrow-band detectors and 2 PFAs (1% and 10%)

Compared to the simulation results of Figure 3-14, the simulation results show that, for PFA=10% and PD=90%:

- The narrow-band energy detector enables the detection of signals with SNR= -14 dB, leading to a 5 dB improvement of the energy detector.
- The narrow-band autocorrelation detector enables the detection of signals with SNR= -15.5 dB, leading to a 2 dB improvement of the autocorrelation detector.
- The narrow-band Teager-Kaiser energy detector enables the detection of signals with SNR= -15 dB, leading to a 3 dB improvement of the Teager-Kaiser energy detector.

Narrowing down the bandwidth under analysis allows a significant increase of the minimal SNR that could be detected. The FFT based implementation of the narrow-band energy detector is a promising solution. Indeed, in the case of the other narrow-band detectors, the implementation of the filter-bank structure will increase the complexity of the detector.

3.1.2.1.4 Experimental Validation

In order to test the proposed algorithms on real signals, an experimental validation is presented in this section. The experimental test bench is described in Figure 3-18. It consists of a wireless microphone (Sennheiser ew100) equipped with a UHF antenna and a microphone, it can transmit on 1440 frequencies (with a step of 25 kHz) between 518 and 866 MHz at a power of 15 dBm. The signal from the microphone is received by the spectrum analyser Tektronix RSA 3408B. This analyser can record base-band signals on a 12.8 MHz band (in our case). The line-of-sight channel is considered to be an AWGN one. Using the MATLAB software, the recorded signals are then processed by the algorithms described previously.

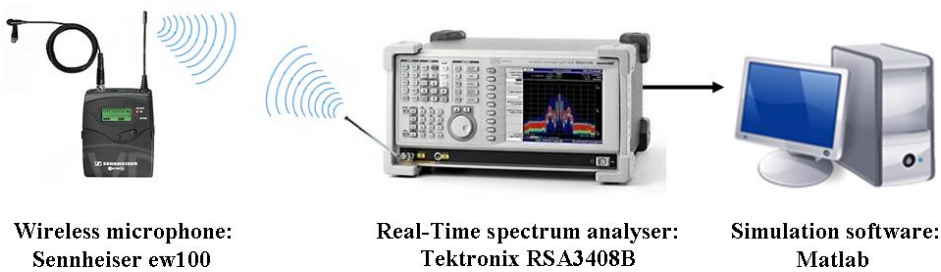

Figure 3-18: Experimental test bench of wireless microphone sensing

Measurements are recorded for different microphone signal powers. For each record, the detection probability is computed (the threshold is set such that PFA=1%) for various detectors. Results are shown in Figure 3-19. The detection probability PD is plotted versus the different received SNR. The measurement results are consistent with those obtained from simulation. The curves with squares show that the narrow-band algorithms outperform their initial counterparts. The measurements also show the improvement of the use of the Teager-Kaiser energy operator instead of the energy detector. The autocorrelation detector is still the most efficient solution; however, it considerably increases the complexity of the detector.

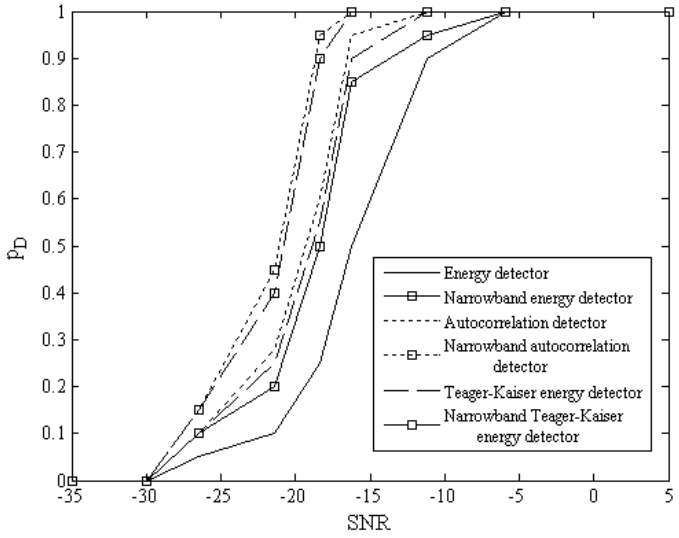

Figure 3-19: Measured detection probability versus SNR for various detectors

3.1.2.2 White Band Frequency Domain Detection

The main purpose of this study is to analyse the band in the frequency domain by using a wide-band FFT operator. First, the general architecture of the detector is introduced. Its application to Teager-Kaiser detection is then detailed.

3.1.2.2.1 General Architecture

The proposed scheme follows the idea of spectrum pooling introduced in [Wei04]. Proposed as a transmission technique used by an opportunist user, the idea is to match the bandwidth of one sub-band with an integer multiple of the carrier spacing. Two key advantages can be identified for the transceiver architecture [Noguet11]. First, the input of the IFFT can be fed with zeros at frequencies where incumbent users are present, while vacant sub-bands are used for transmission by the opportunistic radio. Second, the FFT operation required at the receiver to invert the modulation may also be used to monitor spectral activity of the other users. The proposed architecture is based on this second idea.

Figure 3-20 shows the general architecture of the proposed detector. It is composed of 3 main blocks: an "FFT operation", a "Frequency Bin Selection" block and several "Frequency Analysis blocks".

In order to compute a large FFT, the signal is split into N_t slots of size N_{FFT} which is the size of the FFT. The outputs of the FFT operation are:

$$R(\nu) = \sum_{k=0}^{N_{FFT}-1} r[k] e^{-j2\pi \frac{\nu}{N_{FFT}} k} \qquad \text{Eq. 3-41}$$

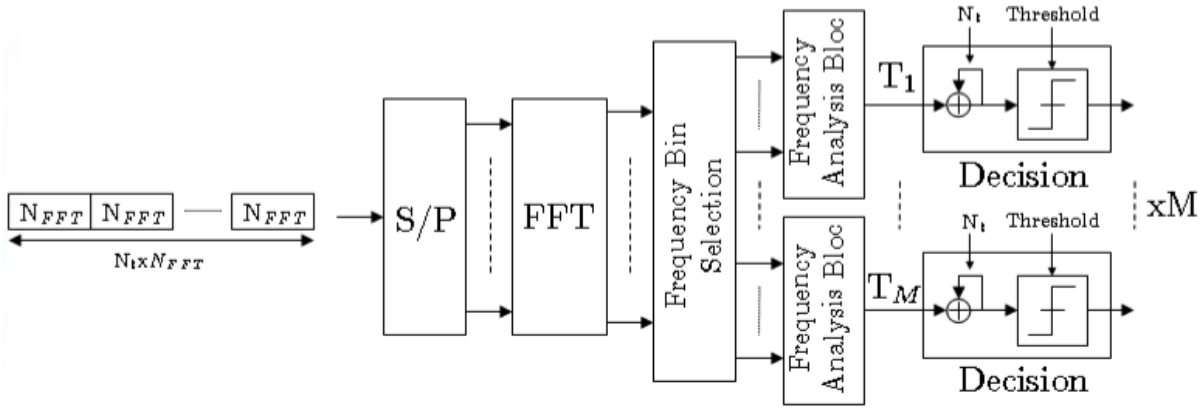

Figure 3-20: Architecture of the wide-band frequency domain detection

The "Frequency Bin Selection" manages the way of scanning the whole band. Its parameters are the number of sub-bands *M* and the Overlapping Ratio (*OR*) between 2 adjacent bands. In that case, the number of frequency bins per sub-bands (denoted by *N*) is:

$$N = \frac{N_{FFT}}{M(1-OR)} \qquad \text{Eq. 3-42}$$

Theses parameters are set according to the signal. For example, if a 40 MHz band is analysed and an 8 MHz DVB-T signal is sensed, *M*=5 sub-bands and no overlapping *OR*=0 are needed. If wireless microphone signals are sensed in an 8 MHz band, overlapping is needed because of the random frequency position of the signal and the bandwidth of each sub-band must be set to 200 kHz.

The "Frequency Analysis block" provides a test statistic from the frequency bins selected by the previous block. One bloc uses *N* samples to compute the metric.

Several test statistics can be computed in the frequency domain. Starting with the detectors introduced as the state of the art for wireless microphone detection, two test statistics are firstly introduced in the frequency domain.

The frequency domain energy detection could be directly computed from the frequency bins *R(ν).* It is defined by the following metric:

$$\mathrm{T_i} = \frac{1}{N}\sum_{\nu=B_i}^{B_i+N-1} |\mathrm{R}(\nu)|^2 \qquad \text{Eq. 3-43}$$

$B_i=N(1-OR)_i$ being the first sample of the sub-band *i* (*i*= 0,… *M*-1).

Contrary to energy detection, the autocorrelation detection must be computed in the time domain by using an IFFT of size *N*. From the frequency bins *R(ν)*, the autocorrelation function is computed by:

$$C_i[\tau] = \sum_{\nu=B_i}^{B_i+N-1} R(\nu)R^*(\nu)e^{j2\pi\frac{\nu}{N}\tau} \qquad \text{Eq. 3-44}$$

After the frequency analysis block, the decision is made on the mean of the N_t FFT frames.

3.1.2.2.2 Application to Teager-Kaiser detection

In the particular case of detection of wireless microphones, an architecture of the frequency analysis block based on the Teager-Kaiser energy operator is proposed.

Using the autocorrelation function, the Teager-Kaiser detector could be written in the time domain by:

$$T = E\left\langle \Psi\{r[k]\}\right\rangle = E\left\langle r[k]^2\right\rangle - E\left\langle r[k+1]r^*[k-1]\right\rangle = C_r[0] - C_r[2] \qquad \text{Eq. 3-45}$$

$C_r[0]$ is the energy of the signal and $C_r[2]$ is the tap 2 of the autocorrelation function.

So to compute the Teager-Kaiser energy operator from the FFT of the signal, the two following terms should be calculated:

$$C_r[0] = \sum_{\nu=0}^{N-1} R(\nu)R^*(\nu) \qquad \text{Eq. 3-46}$$

and

$$C_r[2] = \sum_{\nu=0}^{N-1} R(\nu)R^*(\nu)e^{j2\pi\frac{\nu}{N}2} \qquad \text{Eq. 3-47}$$

Figure 3-21 describes the structure of the frequency analysis block in the case of the Teager-Kaiser detection.

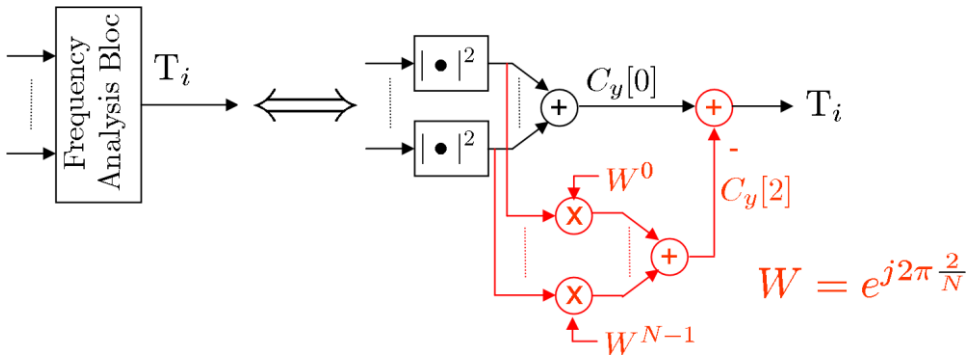

Figure 3-21: Frequency analysis block for Teager-Kaiser detection

3.1.2.2.3 Architecture settings

In the following, the wireless microphone study case is used to analyse the proposed architecture. Based on the European UHF band specifications, the bandwidth is 8 MHz. A large FFT of 4096 bins is used as a fixed parameter of the system. The baseband microphone signal is generated following the model introduced in section 3.1.2.1 with these parameters: the frequency bandwidth of *x(t)* is 20 kHz, the FM deviation κ_f is 3, the carrier frequency f_0 is equal to 100 kHz and the noise power σ_n is set to 0 dBm. Under these conditions, the transmitted microphone signal *s(t)* has a frequency bandwidth around 100 kHz.

The first characteristic that must be specified is the number of input samples that can be analysed by this architecture. Indeed, according to the test statistic, a bias could appear between the time and the frequency domain computations of the metric. For example, a FFT size of N_{FFT} can be used to compute the frequency domain energy of N_{FFT} input samples without any bias. However, for the autocorrelation and Teager-Kaiser metrics, a bias may appear according the size of the inputs samples.

Figure 3-22 gives the total bias for both metrics as a function of the ratio between the input and FFT sizes. Results show that, for the autocorrelation function, a bias appears for a ratio over 0.5 and increases with the input size while, for the Teager-Kaiser energy operator, only a ratio closed to 1 leads to a bias and this bias is lower than the autocorrelation's one at the same ratio.

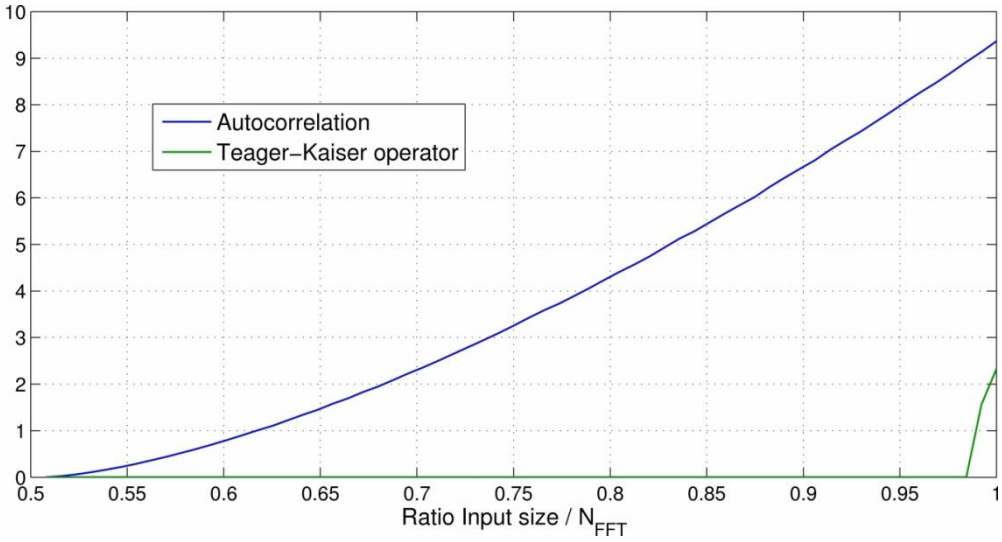

Figure 3-22: Bias versus ratio between Input size and FFT size

This analysis outlines that the comparison of the different "Frequency Analysis block" is not obvious. Indeed, using a fixed FFT size, the same number of samples could not be analysed without any bias. Thus, in the following, only the energy detection and the Teager-Kaiser detection will be computed in the frequency domain. For the Teager-Kaiser detection, 2 samples (insignificant compared to the FFT size of 4096) will not be used in order to have no bias.

In a second step, the number of sub-bands *M* has to be set. Obtained by simulation, the sensitivity of the two frequency domain detectors is plotted versus the number of sub-bands. The sensitivity is the minimum SNR that the detector could sense with PD=95% and PFA=1%. The results are shown in Figure 3-23 for an *OR* of 20% and N_t=1.

Simulation results show that the sensitivity increases with the number of sub-channel. For large number of sub-channel, the SNR decrease with a lower step and seem to reach a SNR floor. This appears when the sub-band bandwidth becomes smaller that the signal bandwidth. In the following, *M*=16 will be used.

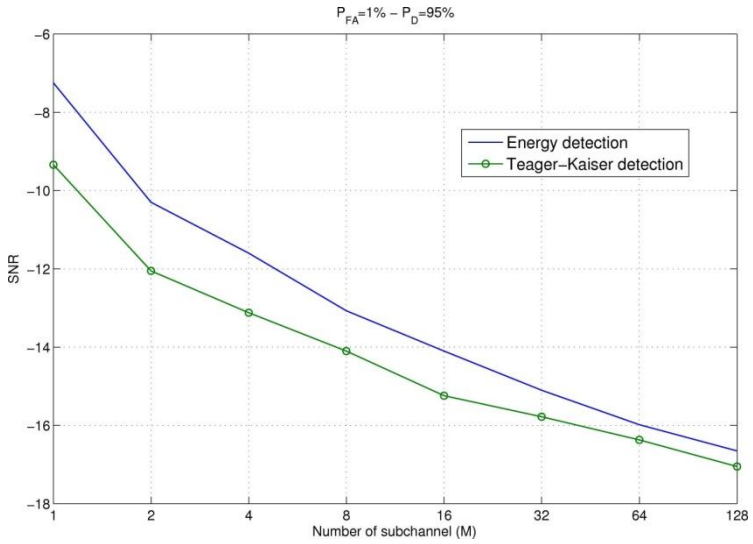

Figure 3-23: Sensitivity in SNR versus number of sub-channel

3.1.2.2.4 Performance analysis

Detection sensitivity

The main feature of a detector is its sensitivity in SNR that it achieve. Figure 3-24 shows the performance of the two frequency domain algorithms. Performance is compared with the time domain algorithms. The PD is computed versus the SNR of the wireless microphone received signal. The architecture settings are M=16, OR=20%, N_t=1 and N_{FFT}=4096 and the PFA is 1%.

For a target PD of 95% the simulation results show that:

- the frequency domain energy detector enables the detection of signals with SNR=-14 dB, leading to a 6.5 dB improvement of the energy detector,
- the frequency domain Teager-Kaiser detector enables the detection of signals with SNR=-15.5 dB, leading to a 6 dB improvement of the Teager-Kaiser detector,
- both frequency domain detectors outperform the autocorrelation detector with a 4 dB gain for Teager-Kaiser detector and a 2.5 dB gain for the energy detector.

These algorithms allow an interesting increase of the minimal SNR that could be detected.

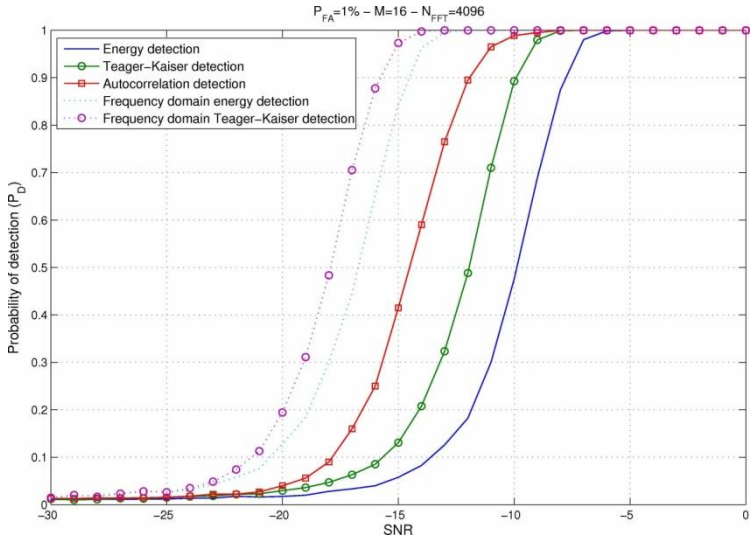

Figure 3-24: Detection probability versus SNR

Complexity evaluation

After the sensitivity evaluation, the complexity of the frequency domain algorithms needs to be evaluated and compared to their time domain counterpart. A simple way to estimate complexity is to determine the total number of real multiplications for each algorithm. Assuming split-radix implementation of the FFT, the number of real multiplications to process N_{FFT} samples is:

- for the frequency domain energy detector:

$$N_{FFT} \times \log_2(N_{FFT}) + N_{FFT} \qquad \text{Eq. 3-48}$$

- for the frequency domain Teager-Kaiser detector:

$$(N_{FFT} + 2) \times \log_2(N_{FFT} + 2) + 2 \times (N_{FFT} + 2) \qquad \text{Eq. 3-49}$$

The complexity is compared with the one of a filter-bank based architecture as introduced in [Gautier10]. In order to split the frequency band into sub-bands, an alternative to FFT is the use of a filter-bank in order to channelise the wide band. To understand the requirements on the filter used by the filter-bank, a rejection requirement A (in dB) on the filter is derived and then extrapolate the

number of taps required for a finite impulse response implementation of the filter. The filter length L_{filter} is estimated using an equi-ripple low-pass implementation. Using a low complexity dyadic implementation of the filter-bank [Akansu01], the complexity of this structure is:

$$L_{filter} \times M \times \log_2(M) \times N_{FFT}/M \qquad \text{Eq. 3-50}$$

to process N_{FFT} samples. Then, N_{FFT} and $2N_{FFT}$ real multiplications must be added to compute the channelised energy detection and the channelised Teager-Kaiser detection respectively.

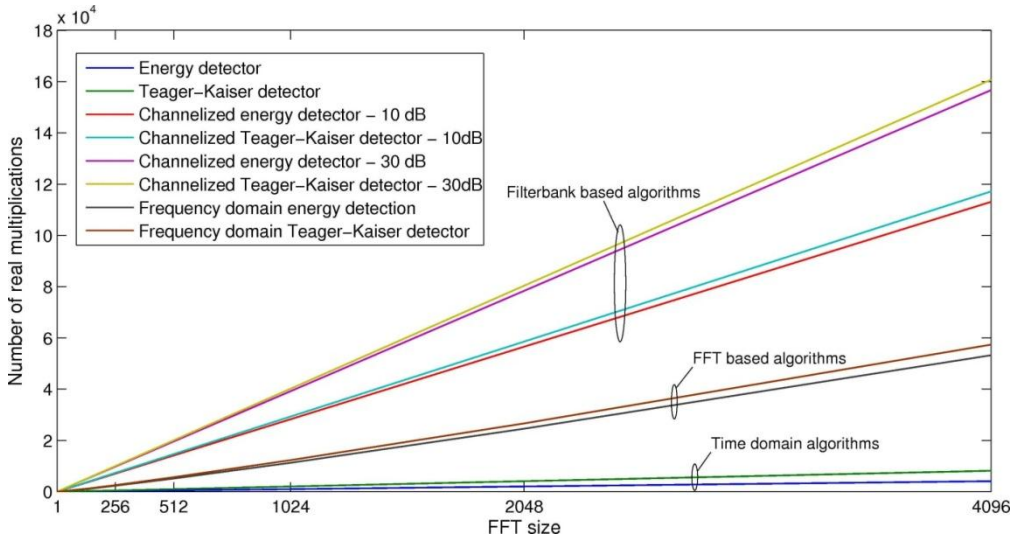

Figure 3-25: Complexity in number of real multiplications versus FFT size

Figure 3-25 shows the complexity of each option as a function of the FFT size. For the channelised structure, two rejection requirements are used: A=10 dB and A=30 dB. It is obvious that the time domain algorithms have lower complexity when no channelisation is done. However, the results underline that the proposed FFT based detector has a lower complexity compared with the filter-bank based architecture.

Furthermore, this study does not take into account the fact that the FFT operation could be performed with the same FFT operation as the demodulation scheme. In that case, the FFT comes for free and the frequency domain detectors have nearly the same complexity as their time domain counterpart.

3.1.2.2.5 Conclusions

In this study, the detection of narrow-band wireless microphone signals has been addressed. The motivation of this study is to identify a wireless microphone detector that could be implemented with an acceptable complexity. This study focuses on the complexity-performance trade-off of the algorithms.

Two main points are revealed. The first is the use of a FFT operation to monitor wide-band signal. Considering a mutualised FFT implementation for both communication and sensing schemes, this leads to a low complexity detector. In the wireless microphone study case, the proposed architecture leads to a 6 dB gain compared to time domain detectors.

The second point is the computation of the Teager-Kaiser energy operator in the frequency domain. The implementation of this operator in the frequency domain allows a further 1.5 dB gain compared to frequency domain energy detection.

3.1.2.3 Generalized Higher-Order Cyclostationary Feature Detector

Several authors such as [Marchand98] have suggested that higher order cyclostationarity detection might be used to increase the detection performance. Below, the cyclic properties and cyclic algorithms that could be used are described .

The second order autocorrelation function of a signal *s* is described by:

$$R_{ss,2,1}(t,\tau) = E\left[s(t)s^*(t-\tau)\right] = \int_{-\infty}^{\infty} s(t)s^*(t-\tau)dt \qquad \text{Eq. 3-51}$$

The fourth order autocorrelation function with two conjugates is described by:

$$\begin{aligned} R_{ss,4,2}(t,\tau_1,\tau_2,\tau_3) &= E\left[s(t)s(t-\tau_1)s^*(t-\tau_2)s^*(t-\tau_3)\right] \\ &= \int_{-\infty}^{\infty} s(t)s(t-\tau_1)s^*(t-\tau_2)s^*(t-\tau_3)dt \end{aligned} \qquad \text{Eq. 3-52}$$

The fourth order autocorrelation function with no conjugates is described by:

$$\begin{aligned} R_{ss,4,4}(t,\tau_1,\tau_2,\tau_3) &= E\left[s(t)s(t-\tau_1)s(t-\tau_2)s(t-\tau_3)\right] \\ &= \int_{-\infty}^{\infty} s(t)s(t-\tau_1)s(t-\tau_2)s(t-\tau_3)dt \end{aligned} \qquad \text{Eq. 3-53}$$

The input signal could be:

- Base-band: In this case, $R_{ss,2,1}(t,\tau)$ and/or $R_{ss,4,2}(t,\tau_1,\tau_2,\tau_3)$ should be considered for testing
- RF (with the carrier f_0): In this case, $R_{ss,4,4}(t,\tau_1,\tau_2,\tau_3)$ should be considered for testing

The fourth order CAF with no conjugations can be expressed as:

$$R^{\alpha}_{ss,4,0}(n,d_1,d_2,d_3) = \frac{1}{N}\sum_{n=0}^{N-1} s[n]s[n+d_1]s[n+d_2]s[n+d_3]\exp(-j2\pi\alpha nT_e) \qquad \text{Eq. 3-54}$$

where d_1, d_2, d_3 are representing the delay times normalized by the sampling period T_e.

Higher order detectors can be implemented also in time domain. The detector proposed in [Renard10] averages the lag-product of the received sequence over time:

$$R_{ss,4,4}(n,d_1,d_2,d_3) = \frac{1}{N}\sum_{n=0}^{N-1} s[n]s[n+d_1]s[n+d_2]s[n+d_3] \qquad \text{Eq. 3-55}$$

This detector is simpler to implement than the previous one (no Fourier transform of the signal is required since we work in the time domain), which results in a computational complexity evolving as *N*, the total number of samples. In [Renard10] it is stated that it benefits from the same immunity to noise uncertainty and is suited for operations at low SNR.

The goal of this study is to see if higher order cyclostationary properties could be used to increase the detection probability. It has been found that both second order CAF (CAF2) and fourth order CAF (CAF4) properties are different for QPSK PMSE signals using Nyquist filtering and that these properties can be used to improve detection probability. However, this is not the case for OFDM signals, as shown in Figure 3-26. It clearly shows that for OFDM signals the cyclostationarity detector of order 2 (CD2) outperforms the cyclostationarity detector of order 4 (CD4).

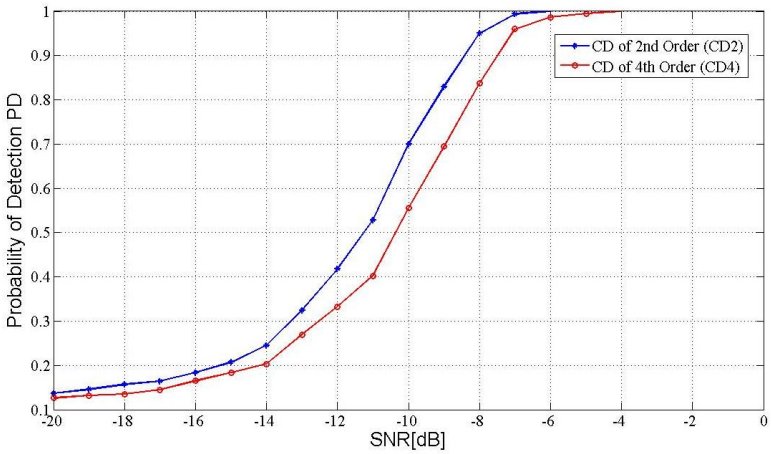

Figure 3-26: OFDM cyclostationarity detection – comparison of CD2 and CD4

The next three sections provide CAF2 and CAF4 results for QPSK PMSE along with 2 possible applications: improved cyclostationarity detection for QPSK PMSE with unknown shaping filter and bandwidth estimation for QPSK PMSE.

3.1.2.3.1 CAF2 and CAF4 Properties for QPSK PMSE using Nyquist Filtering

The same CAFs have been obtained for 2nd and 4th orders, with cyclic frequencies at $\pm k/T_S$, and delay $\tau = \pm(1/2)\ T_S$, for k=1. This representation also explains that CD4 does not outperform CD2.

However, the delays and the peaks are no longer the same for the other shaping functions. It is shown that the cyclic peaks change with the shaping function used, as shown in Figure 3-27 and further in Table 3-3 where complete results are provided.

Table 3-3: CAF2 and CAF4 peaks

CAF Type	Delays for CAF with Rectangular Shaping Function	β	Delays for CAF with Raised Cosine Shaping Function	Delays for CAF with Root Raised Cosine Shaping Function
CAF2	$\pm (1/2)T_S$ for k=1	1	$0T_S$ for k=1	$0T_S$ for k=1
		0.01	None (very small)	None (very small)
		0.22	Constant	Constant
CAF4	$\pm (1/2)T_S$ for k=1	1	$0T_S$ for k=1 (k=2 is not optimal)	$0T_S$ for k=1 (k=2 is not optimal)
		0.01	$0T_S$ for k=1	$0T_S$ for k=1
		0.22	$\pm T_S$ for k=1 ($0T_S$ not optimal)	$\pm T_S$ for k=1 ($0T_S$ not optimal)

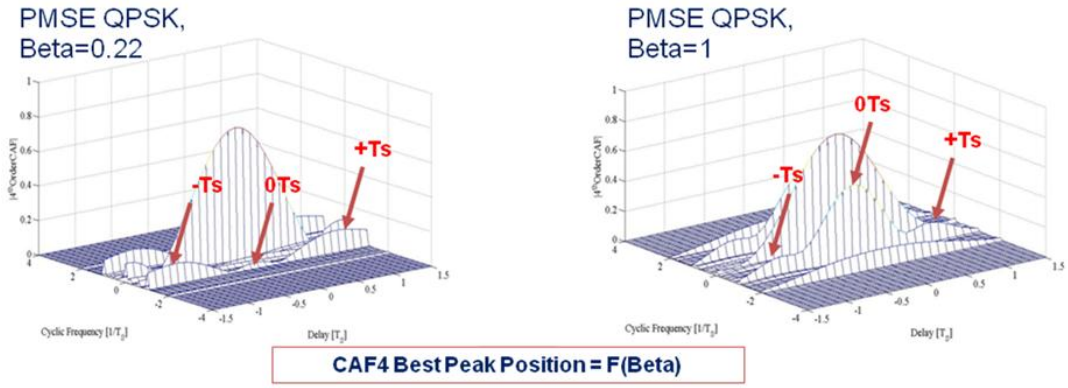

Figure 3-27: CAF4 Best Peak Position is a function of β (RRC Implementation)

3.1.2.3.2 Improved Cyclostationary Detection for QPSK PMSE using Nyquist Filtering

When Nyquist filter is used by the PU, CD2 is no longer reliable below a certain roll-off factor β. In this situation, CD4 is improving the detection result but the position of the highest peak is a function of β. The most powerful peak of a CAF2/CAF4 when PU (root) raised cosine shaping function is used is either for a delay $0T_S$ or $\pm T_S$ (undetermined) depending on β value.

In this situation, CD4 may improve detection result but the position of the highest CAF peak is a function of β (as seen in Figure 3-27). When PU (root) raised cosine shaping function is used, for a non-zero cyclic frequency (which is used for the testing purposes in a noisy environment), the highest peak of a CAF2/CAF4 function is either for the delay $0T_S$ or the delays $\pm T_S$ (undetermined) depending on β value.

Therefore the detection algorithm represented in Figure 3-28 is proposed. It is further described as follows:

1. A β estimation block provides the roll-off factor employed by the transmission. This block can be embedded on the device and can estimate in real time. Another alternative will be a knowledge base which provides the value of β as output.
2. The proposal considers a "β equilibrium" for which a detector using CD4 has the same performance as a detector using CD2.
3. Once the beta equilibrium is determined (from a knowledge base for example), a comparison block decides if the highest peak is for the delays $0T_S$ or $\pm T_S$.
4. The last block decides which order and which CD is used (CD can be performed on multiple peaks, using different implementations such as GLRT, etc).

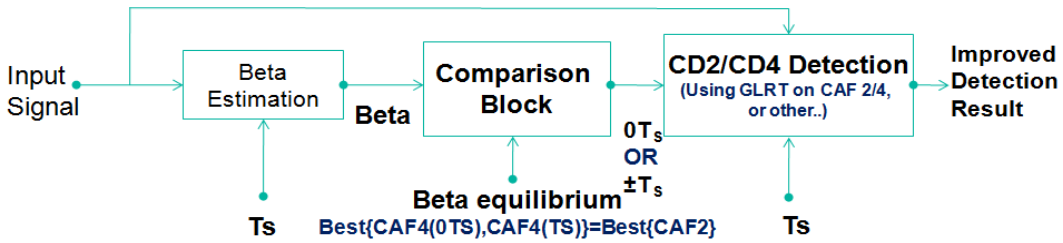

Figure 3-28: Proposed Detection algorithm for QPSK PMSE with unknown roll-off factor

Figure 3-29 shows detection probability results for different CD implementations with different orders and different delays, when β=0.1. The results have been obtained for a 400 kHz modulated QPSK PMSE signal, for 18340 samples (which is almost equal to 2.4 ms if the sampling frequency is 7.6 MHz or and to 4.8 ms if the sampling frequency is 3.84 MHz).

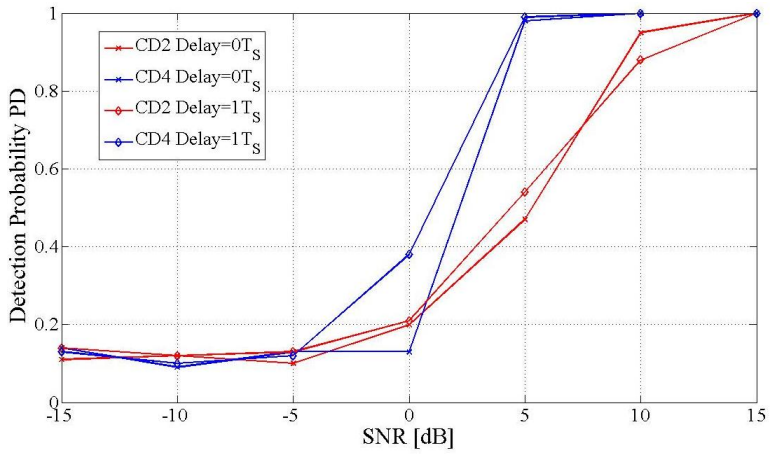

Figure 3-29: Detection probability (PD) - CD4 vs. CD2 for β=0.1

3.1.2.3.3 Bandwidth Estimation for QPSK PMSE

In order to estimate the bandwidth of the received signal *r(t)*, the following assumptions are considered:

- T_S is known from database or determined from another process (e.g. differential T_S recovery),
- The method uses a knowledge base and compares it with an estimated real-time value, which might be:

  1. the estimated cyclostationary autocorrelation function of order 4(CAF4) in $0T_S$ and $\alpha=1/T_S$ (for example):

$$R_{rr,4,2}^{\alpha=1/T_S}(n,0,0,0T_S)=\frac{1}{N}\sum_{n=1}^{N} r^*[n]r^*[n]r[n]r[n+0T_S]e^{-j2\pi n\frac{1}{T_S}T_e}\cong F(\beta,T_e) \qquad \text{Eq. 3-56}$$

  However, as described by the above equation, CAF4 in $0Ts$ is a function of both β and sampling period T_e and it might not be very convenient to use it in such form. Therefore a second method based on a ratio is proposed.

  2. the estimated ratio R of 2 CAF4 functions in $\alpha=1/T_S$:

$$\hat{R}=\frac{R_{rr,4,2}^{\alpha=1/T_S}(n,0,0,0T_S)}{R_{rr,4,2}^{\alpha=1/T_S}(n,0,0,+T_S)}=\frac{\sum_{n=1}^{N} r^*[n]r^*[n]r[n]r[n]e^{-j2\pi n\frac{1}{T_S}T_e}}{\sum_{n=1}^{N} r^*[n]r^*[n]r[n]r[n+T_S]e^{-j2\pi n\frac{1}{T_S}T_e}}\cong F(\beta) \qquad \text{Eq. 3-57}$$

  Herein we have used the ratio of CAF4 in delay $0T_S$ and CAF4 in delay $+T_S$. It can be proved that this ratio R is no longer dependent on the sampling period T_e, and it is only a function depending on β only. This has the advantage of simplifying the algorithm and the knowledge base used to estimate the bandwidth.

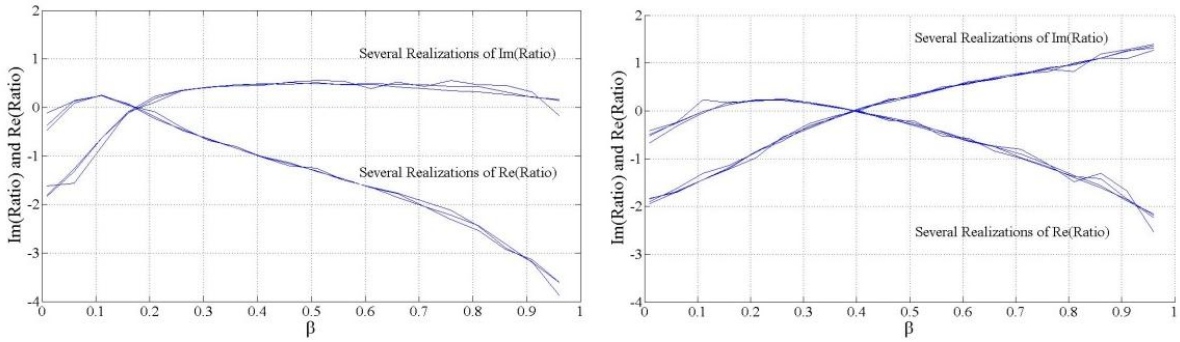

Figure 3-30: Example of a knowledge base computed with the help of the ratio R, when RRC filter (left) and RC filters (right) are used

3.1.2.4 Two-Stage Hybrid Detection for PMSE

3.1.2.4.1 PMSE Cyclostationarity

It is important to notice that both QPSK and FM signals exhibit cyclostationary properties. For QPSK modulations the second order CAF is represented in Figure 3-31, and for FM modulations the second order CAF is represented in Figure 3-32. From Figure 3-31 one can easily notice that for QPSK, the cyclic frequencies α are multiples of $1/T_S$ (where T_S is the symbol period as presented in the introductory chapter). On the contrary, for FM the cyclic frequencies α can be found for $\pm 2f_0$ (f_0 being the carrier frequency) as it can be seen in Figure 3-32.

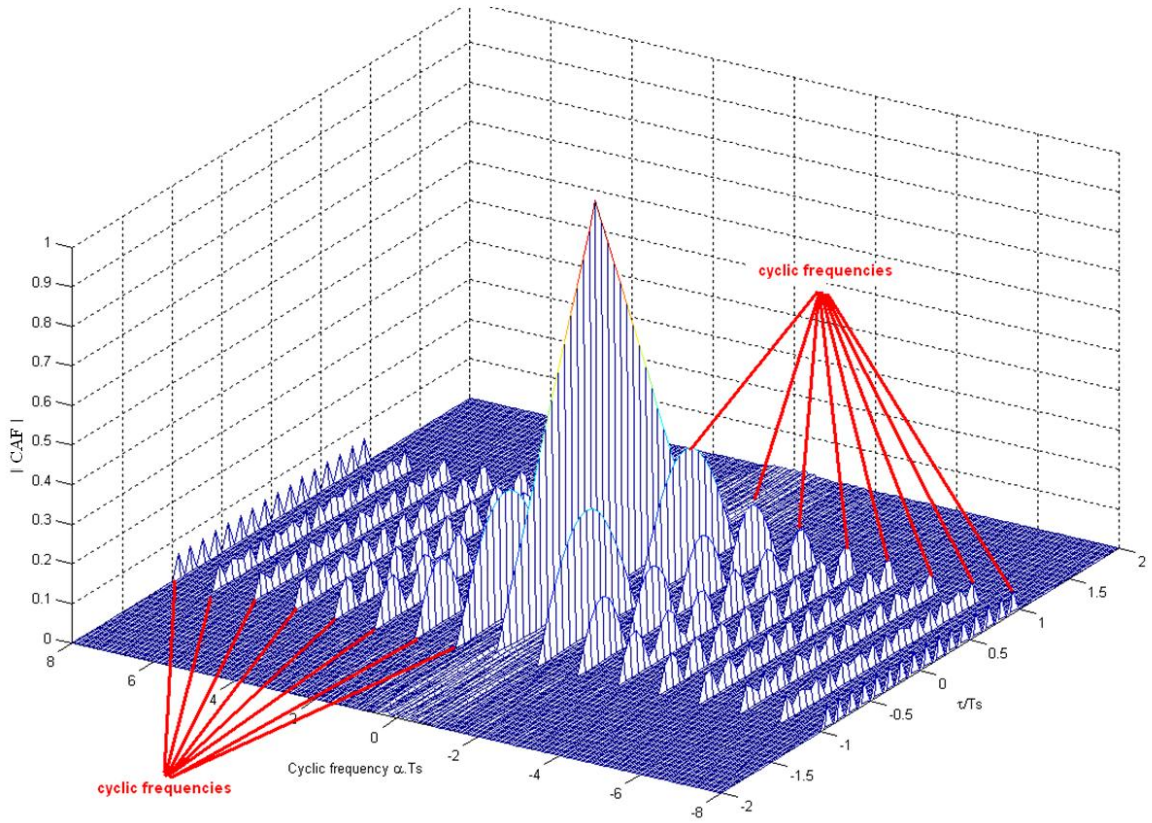

Figure 3-31: CAF of a QPSK Signal

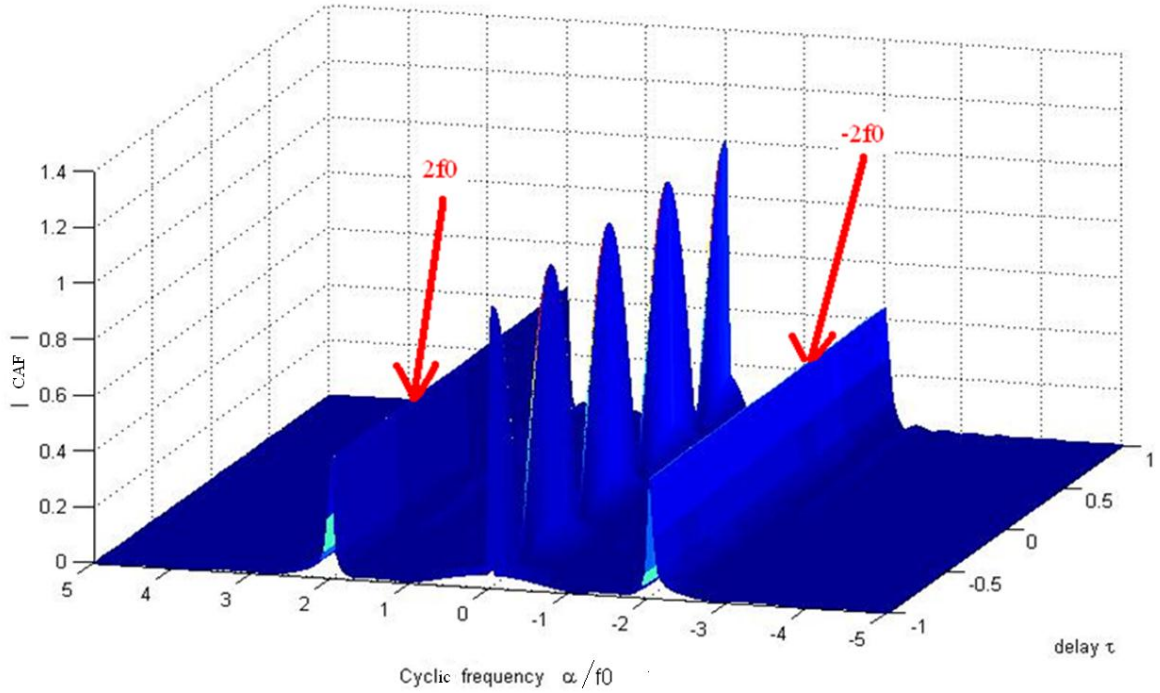

Figure 3-32: CAF of a FM Signal

Since both QPSK and FM exhibit cyclostationary properties, we can use CD in order to detect them. For this, we are using the GLRT algorithm presented in Section 3.1.1.1.2, for one cyclic frequency (i.e. $1/T_S$ for QPSK and $2f_0$ for FM). It can be easily seen in Figure 3-33 that the detection performance in the case of FM is a bit higher, this result being the effect of higher peaks in the CAF.

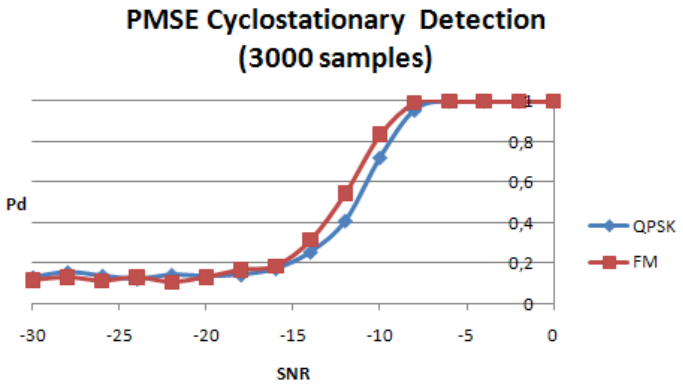

Figure 3-33: PMSE cyclostationarity detection, PFA=0.1

3.1.2.4.2 Hybrid Detector for PMSE Signals

The two-stage detector is now applied for PMSE signals. A noise uncertainty of 0.1dB is introduced to fit the conditions where the use of the two-stage makes sense. The results are shown in Figure 3-34.

As presented previously with the OFDM signal, the two-stage detector performs better than the energy detector and the cyclostationarity detector respectively.

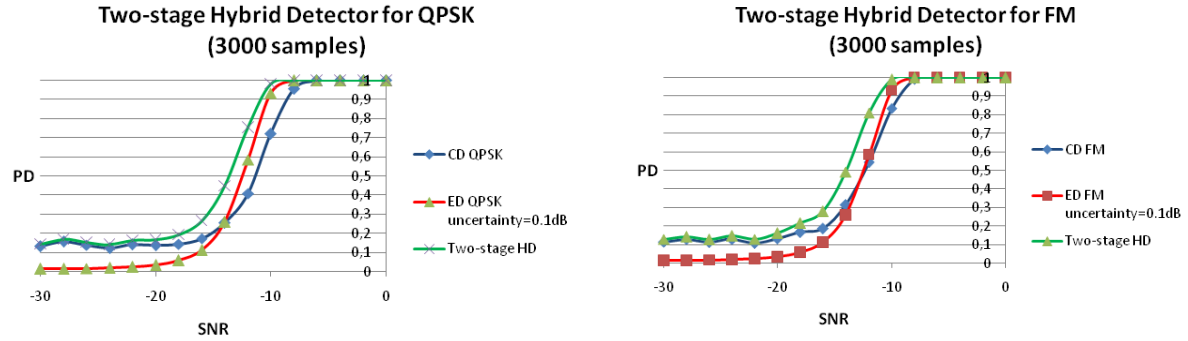

Figure 3-34: Hybrid detector for PMSE

3.1.3 Spectrum Sensing Based on Statistical Tests

3.1.3.1 Fast and Reliable Signal Detection with Background Process for Noise Estimation

In September 2010 FCC published a report 10-174 [FCC10] with the scope of finalizing rules to make the unused spectrum in the TV bands available for unlicensed broadband wireless devices. The report was favourable to geo-location with database approach, but leaves a backdoor open for any other contribution from the spectrum sensing research field.

If the geo-location database access method is not providing sufficient adequate and reliable protection, spectrum sensing should be used in order to help identifying the white spaces in the considered frequency band.

In this context, a mobile radio system occupies as an opportunistic user a given band of spectrum, which is denoted by B_0. This means that the opportunistic user is currently using B_0 to transmit and receive data because the owner of the band, the incumbent user, was previously detected as absent from its band.

The opportunistic user is allowed to occupy B_0 provided that it is able to stop using it immediately if the incumbent user decides to use it. This implies that the opportunistic system may have sensing capabilities able to detect the incoming incumbent user very quickly and with a very high reliability.

As explained in section 2.1.1, the main drawback of the energy detector is to reliably estimate the noise variance. That is why the current state of the art consists in making a trade-off: either use a fast detector and accept that the ED performance is possibly affected by a bad noise variance estimate, or choose a detector different from ED which in turn will be slower, to obtain very high performance. In other words, having a very high probability of detection and a fast algorithm altogether still remains a challenge.

It can be shown that a precise knowledge of the noise variance is necessary in order to compute the threshold value γ. Subsequently, a wrong computed threshold value is affecting both the detection probability PD and the real false alarm probability PFA_{real}, which differs from the PFA_{target}. In the next subsections we are going to study reliable noise estimation methods which are using the statistical properties of the received signal.

Hence, the solution will consist of two main components, which do not operate in the same timescale, and not in the same band:

(a) A long term component, in charge of monitoring the bands B_i in the neighbourhood of B_0, in order to identify a band where there is only noise, and estimate the noise variance in the identified band. This component is triggered every T_2.

(b) A short term component, in charge of detecting an incumbent signal in B_0 as soon as it appears. This detector is an ED detector whose input is the noise variance estimated in the

component (a). This component is triggered every T_1. As represented in Figure 3-35, typically $T_1 << T_2$: it is assumed that the noise variance is stationary during T_2.

The solution consists in using the ED because it is fast, but the detection is reliable only when it has very good noise variance estimates. In order to achieve this goal, two main aspects are implemented:

- The noise variance can be well estimated on portions of bands (different from the band of interest B_0) in which we have previously identified that no signal was present.
- The noise variance is assumed to vary slower than the periodicity T_1 at which the ED must be triggered.

Because of the second condition, one can address the first one by implementing algorithms which are able to detect the presence of a signal very reliably, without knowing the noise variance, and which take possibly much more time than T_1.

Figure 3-35: Trigger periods representation for short and long term (background) components

In the component (a), two main modules are present:

(a_1) The module which performs the identification of the suitable band for noise variance estimation (see Figure 3-36). This module may consist of any algorithm able to decide with a good reliability about the presence of a signal, without any prior knowledge of the noise variance.

(a_2) The module which performs the noise variance estimation, once an empty band B_i has been identified by module (a_1). This is performed through very classical averaging of the observed noise spectral density over the whole identified band B_i.

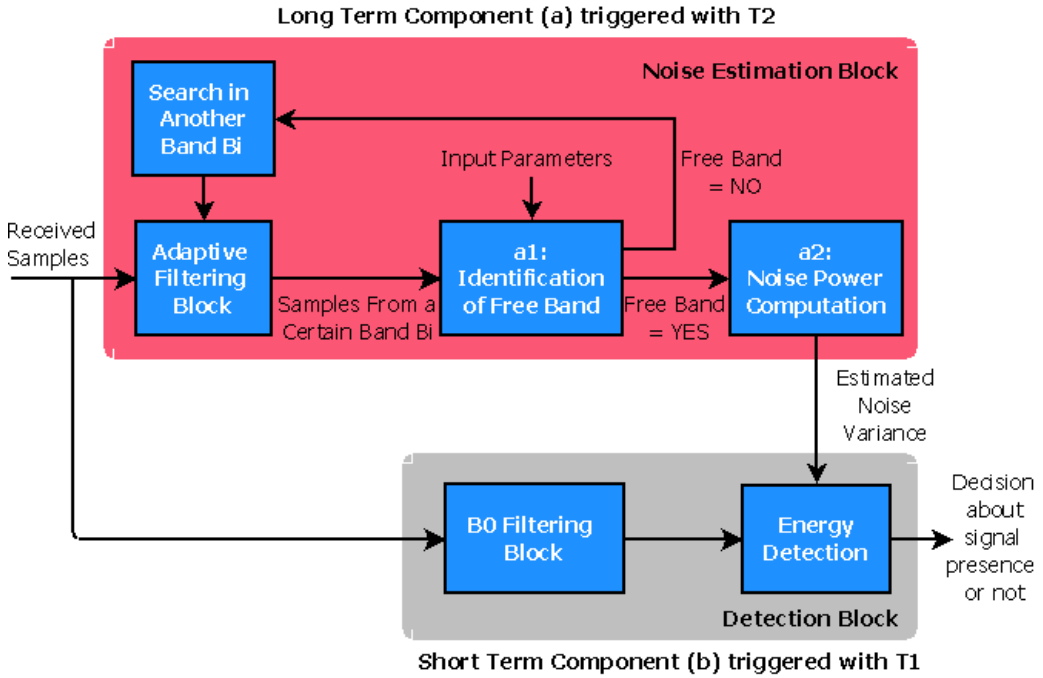

Figure 3-36: Fast energy detection scheme using a background process for noise estimation

Algorithms used by (a_1) can be statistical based (e.g. kurtosis computation, expectation maximization) or could exploit for example cyclostationary properties. All these methods use different input parameters described in Table 3-4.

Table 3-4: Input parameters for identification of bands B_i

Method	FFT needed?	Input parameters
Expectation Maximization	Yes	A Mixture of 2 distributions assumption
Kurtosis	Yes	Gaussian noise assumption
Cyclic Cyclostationary	No	Cyclic frequencies knowledge

The methods described in Table 3-4 are further explained in the next paragraphs:

1) Kurtosis computation [Panaitopol10_1], which exploits the fact that the kurtosis (well known 4th order statistic) is null for a Gaussian signal. So if the kurtosis is different from 0, a priori it means that there is a signal in addition to the noise (see Figure 3-38).

   It is known that the kurtosis K of a random variable ζ with zero mean has the expression

$$K \overset{Def}{=} \frac{E\left[\zeta^4\right]}{E\left[\zeta^2\right]^2} - 3 \qquad \text{Eq. 3-58}$$

   The kurtosis computation is made on the samples of the FFT of the incoming signal (the FFT of a Gaussian signal is Gaussian), therefore the variable ζ is related to the frequency samples from the analysed band.

2) Expectation Maximization (EM) algorithm [Moon06], [Panaitopol10_2] which checks if the incoming signal in bands $B_i \neq B_0$ is from a mixture composed of 2 Probability Density Functions (PDF) with 2 variances and 2 mixing probabilities. If so, it means that there is not only noise in the considered band. The benefit of using the EM algorithm for module (a_1) is that it is very easy to implement in a completely blind context (no assumption about what to look for), and it can also provide the band occupancy. Therefore, it can be performed for narrow frequency bands identification. Note the same as in kurtosis implementation, EM operates on the samples of the FFT of the incoming signal. In [Panaitopol10_2] it is shown that EM can be used for more complex mixtures such as generalized Gaussian Mixtures, but herein we suppose a mixture of two Gaussians.

   For a fixed number of available FFT samples m, if **Z** is a variable denoting which one of the 2 distributions the sample ζ_j (with $j = 0 \ldots m-1$) belongs to, one can describe the estimation steps such as:

   Initialization: For $\forall\ i$=1,2, at the incremental time t=0, set variance $\sigma_i^{t=0}$, mixing probabilities $p_i^{t=0}$ and means $\mu_i^{t=0}$ as in [Panaitopol10_2]. Let the Θ_{1x6} be the vector of the unknown parameters $\Theta_{1x6} = [(\mu_1,\mu_2),(\sigma_1,\sigma_2),(p_1,p_2)]$.

   E-Step: The computation of the membership probabilities

$$p\left(z_j = i \middle| \zeta_j, \Theta^t\right) = \frac{p\left(\zeta_j \middle| z_j = i, \Theta^t\right) p_i^t}{\sum_{k=1}^{2} p\left(\zeta_j \middle| z_j = k, \Theta^t\right) p_k^t} \quad \text{Eq. 3-59}$$

for $j = 0 \ldots m-1$ and $i = 1, 2$.

M-Step: The upgrades on the means

$$\mu_i = \frac{\sum_{j=0}^{m-1} p\left(z_j = i \middle| \zeta_j, \Theta^t\right) \zeta_j}{\sum_{j=0}^{m-1} p\left(z_j = i \middle| \zeta_j, \Theta^t\right)} \quad \text{Eq. 3-60}$$

the upgrades on the variances

$$\sigma_i^2 = \frac{\sum_{j=0}^{m-1} p\left(z_j = i \middle| \zeta_j, \Theta^t\right) \left|\zeta_j - \hat{\mu}_i\right|^2}{\sum_{j=0}^{m-1} p\left(z_j = i \middle| \zeta_j, \Theta^t\right)} \quad \text{Eq. 3-61}$$

and the upgrades on the mixing probabilities

$$p_i = \frac{\sum_{j=0}^{m-1} p\left(z_j = i \middle| \zeta_j, \Theta^t\right)}{\sum_{k=1}^{2} \sum_{j=0}^{m-1} p\left(z_j = k \middle| \zeta_j, \Theta^t\right)} \quad \text{Eq. 3-62}$$

for $i = 1, 2$.

3) Cyclostationarity detector [Dandawate94], [Birru10], which checks if the incoming signals in bands $B_i \neq B_0$ exhibit some cyclic frequencies. Herein the generalized likelihood ratio test is used [Dandawate94] for one non null cyclic frequency, from Table 3-5. If the signal exhibits cyclic properties, this means that there is not only noise in the considered band, because the noise is stationary. The cyclic frequencies are determined from signal parameters (see Table 3-5). For OFDM, [Bouzegzi08] is proposing several algorithms for parameter recognition.

Table 3-5 presents examples of the cyclic frequencies adequate for the most common types of radio signals:

Table 3-5: Cyclic frequencies for different signal types

Type of Signal	Cyclic frequencies
OFDM	k/Ts, $k = \pm 0,1,2,\ldots$
FM	$\pm 2f_0$
QPSK	k/Ts, $k = \pm 0,1,2,\ldots$
Noise	0

Please note that the kurtosis is computed from the real and the imaginary parts of FFT, separately. In Figure 3-37 one can see that the kurtosis value is highly dependent on the band occupancy. If the band occupancy is low, kurtosis becomes high. For example, for 10% band occupancy, an interferer cannot be detected (i.e., transmitter in the noise estimation band B_i) with INR below -14dB. Therefore, this

method should be preferred for detecting narrow-band signals (FM by definition, or OFDM signals only if the analysed band is wide enough).

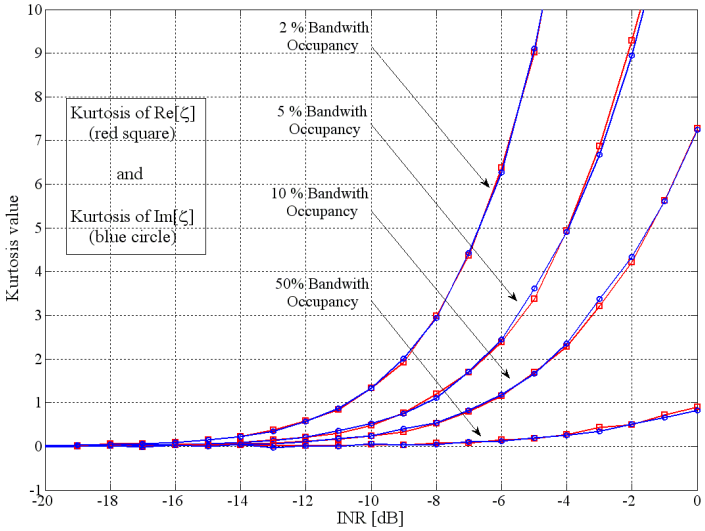

Figure 3-37: Adjacent sub-band B_i detection using kurtosis, as a function of INR and of analysed frequency band occupancy

In Figure 3-38 the kurtosis detection method is presented, by estimating the kurtosis in a sliding window 10 times larger than the interferer frequency band. Since the sliding window is smaller than the total bandwidth, the captured noise is smaller and the INR is decreased to about -8dB. This graph clearly shows that kurtosis increases where there are interferers.

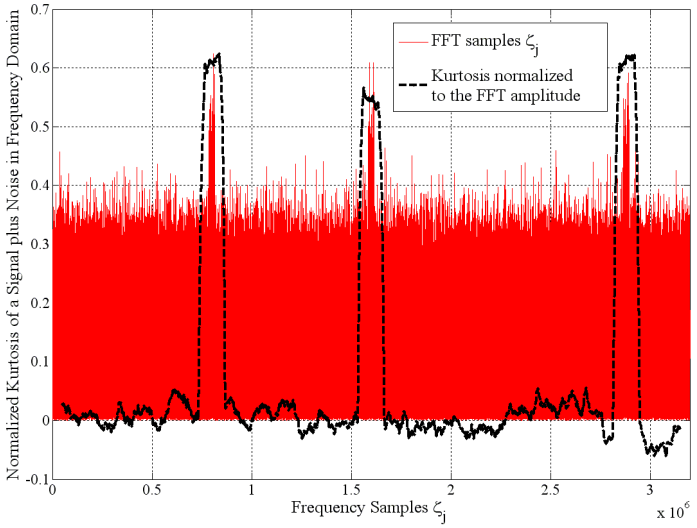

Figure 3-38: Adjacent sub-band B_i detection using kurtosis. Use case involving 3 narrow-band interferers (FM) each with INR=-15dB

In Figure 3-39, OFDM symbols with 512 sub-carriers and $T_G=T_D/4$ are used. Moreover, the signal is over-sampled with a factor of 2. The band occupancy of the interferer is only 10%, result also found when representing the mixing probabilities convergence as seen in Figure 3-40. The simulations showed that EM cannot provide a good identification of the interferers in the adjacent bands for INR<-10dB.

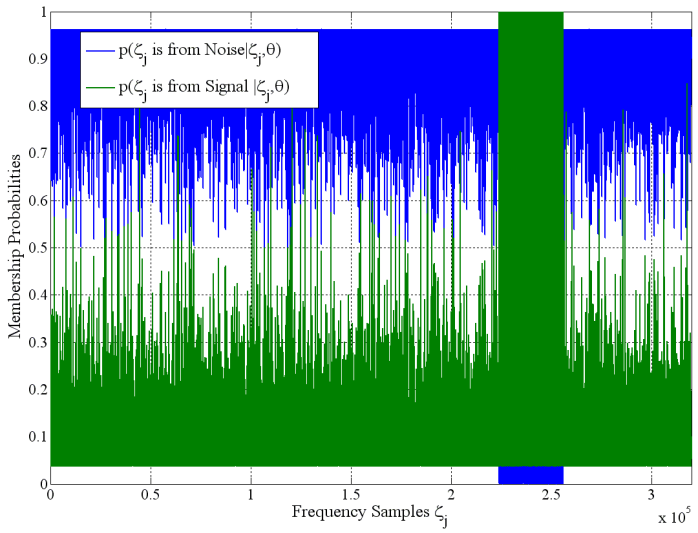

Figure 3-39: Membership probabilities used for adjacent sub-band B_i detection, after 40 iterations of the EM algorithm; INR=0dB

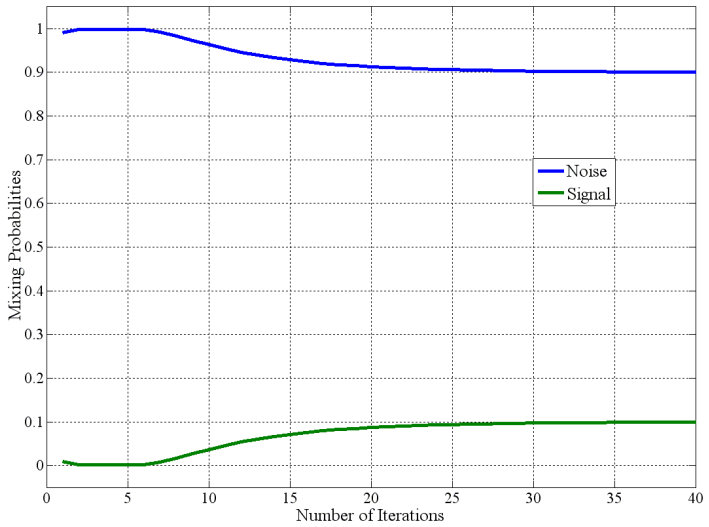

Figure 3-40: Mixing probabilities are indicating 10% of the analysed B_i band as occupied by signal and 90% only by noise

In Figure 3-41 the proposed algorithms with the bound given by the ED are compared to perfect noise estimation. For this simulation an interferer with INR=-10dB and a background process time $T_2=15T_1$ is considered. Since the INR is high (about -10dB in B_i) and the B_i occupancy is small (about 10%), the kurtosis method is the most reliable, but one can expect an improvement of the cyclostationary method when we are dealing with $T_2>>T_1$ and higher band occupancy. In this scenario, for a low INR, the kurtosis method will no longer be able to detect the interferers from opportunistic bands B_i.

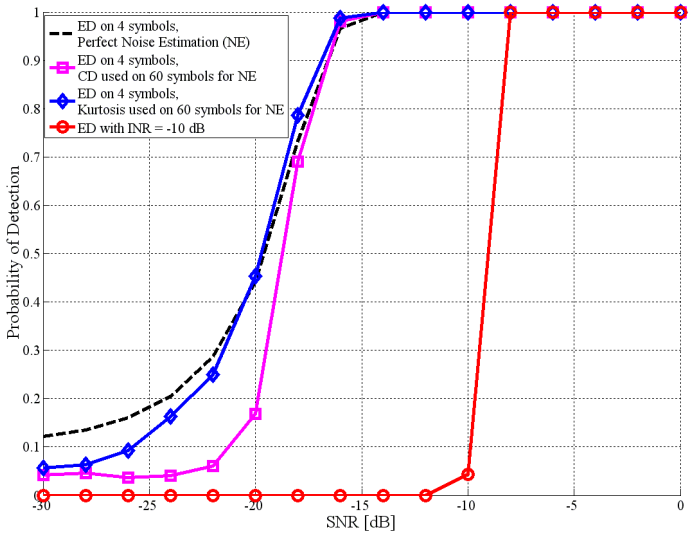

Figure 3-41: Kurtosis and cyclostationary methods compared to an ED computed with noise uncertainty – PD in terms of SNR (in B_0), for INR=-10dB (in B_i)

3.1.3.2 Robust Spectrum Sensing for Cognitive Radios Based on Statistical Tests

The work presented here is based on a novel local sensing algorithm using statistical test theory. The proposed algorithm is treated for the case of known noise probability, unknown noise and non-Gaussian noise with results outperforming both the energy detector and Anderson detector especially in low SNR regimes.

3.1.3.2.1 Introduction

A CR can utilise a spectrum band only when it can detect and monitor the activity of incumbent users reliably and quickly using spectrum sensing [Arshad10]. However, detecting either an incumbent user or other opportunistic users in a certain frequency band is a challenging task for many reasons. For example, received SNR may be very low, time and frequency dispersion can cause channel fluctuations in the received signal power, uncertainty about the noise power, and so on.

To address these challenges a number of spectrum sensing algorithms have been proposed in literature and each algorithm has its own operational requirements, advantages and disadvantages; a comprehensive survey has recently been published by [Yücek09]. For example, sensing based on the likelihood ratio test is optimal but it needs the distribution of source signal and noise which is unobtainable in practice [Chair86]. Sensing based on matched filtering not only requires a-priori knowledge of the incumbent user signal but also needs perfect synchronisation between incumbent transmitter and the opportunistic user [Cabric06]. Energy detection is a common method to detect unknown signals in additive noise [Arshad10]. This method is optimal if the exact noise power is known but is susceptible to errors in noise power [Tandra08]. In contrast to the noise process which is wide-sense stationary, Cyclostationary features of communication signals can be exploited to distinguish noise from the signals using Cyclostationary Feature Detection (CFD).

The major drawback of CFD sensing is that knowledge of the incumbent user signal is required, which is not always available. Spectrum sensing for CRs based on the Anderson-Darling (AD) test has been proposed in [Wang09_1]. The authors consider the spectrum sensing problem as a goodness-of-fit testing problem and use an AD test to check whether the received samples are drawn from the known noise distribution. From a mathematical point of view, the AD test is asymptotically distribution-free which means that for large sample sizes, the threshold is independent of the distribution and can be calculated in advance for any arbitrary noise distribution [Wang09_1]. For AD-sensing, the noise distribution does not necessarily have to be Gaussian, but it should be known a priori. In practice, this

is not a viable assumption, as the exact noise distribution is largely unknown and the presence of noise uncertainty could significantly degrade the performance of AD-sensing.

What is hitherto investigated is the spectrum sensing problem by exploiting the theory of statistical testing. In particular, Two sensing algorithms derived from the Kolmogorov-Smirnov test (KS-sensing) and Student's t-test (t-sensing) are proposed. The sensing performance of these algorithms are compared with the well-known ED-sensing and with AD-sensing as recently proposed in [Wang09_1]. For KS-sensing the assumption is made that noise probability distribution is known to the CR, as assumed in AD-sensing [Wang09_1]. KS-sensing has been chosen for the following reasons:

- KS test is a distribution-free test [Kolmogoroff33]; that is, calculation of decision threshold does not depend on the specific noise distribution.
- KS test is widely used if the sample sizes are small [Conover99] — this is interesting for CR applications as spectrum sensing duration should be short.
- KS test is the only goodness-of-fit test with exact derivable confidence bounds [Quade65]. Our simulation results show that under similar conditions and assumptions, KS-sensing gives better performance than AD-sensing.

In most practical scenarios, noise can be modelled by a zero-mean Gaussian random process; hence another spectrum sensing method based on Student's t-test is proposed. With exact analysis and support from simulation results, it is shown that t-sensing is asymptotically robust and can be applied to an arbitrary noise distribution (including non-Gaussian noise). For t-sensing no information of noise probability distribution and noise power is required. Hence it is unsusceptible of noise uncertainty. Simulation results show that t-sensing performs much better than AD and ED sensing with low computational complexity, particularly at low SNR in Gaussian noise. For the purpose of clarity, $\mathrm{F}(x)$ and $f(x)$ denote the distribution and density function of x respectively and $\Phi(\cdot)$ represent the distribution function of standard Gaussian random process. The notation $\mathcal{H}_n$ represents hypothesis n and $x \mid \mathcal{H}_n$ indicate x given $\mathcal{H}_n$.

3.1.3.2.2 System Model

Suppose that the bandwidth of interest for a CR is B, which is scanned in observation time T. Let N be an integer close to $T \times B$. The spectrum sensing problem can then be formulated as a binary hypothesis testing problem as follows [Arshad10]:

$$z_i = \begin{cases} n_i, & \mathcal{H}_0 \\ h_i \times s_i + n_i, & \mathcal{H}_1 \end{cases} \qquad \text{Eq. 3-63}$$

where $i \in \boldsymbol{\mathcal{S}} = \{1, 2, \ldots, N\}$, n_i is the noise sample of zero mean and variance σ_n^2, h_i is the amplitude gain of the channel, and s_i is the transmitted signal. The term transmitted signal is used for the signal transmitted by the incumbent user or other competing opportunistic users. Further, $\mathcal{H}_0$ represents the null hypothesis that only noise is present, and $\mathcal{H}_1$ represents the alternate hypothesis that a transmitted signal and noise is present. Assume $r_i = h_i \times s_i$ and probability density of the amplitude of r_i is denoted by $f(r)$. Let $\mathbf{y} = [y_1, y_2, \cdots, y_N]^{\mathrm{T}} = \mathrm{sort}(\mathbf{z})$ where $\mathrm{sort}(\cdot)$ represents sorting function such that $y_1 \leq y_2 \leq \cdots \leq y_N$.

The assumption is made that noise samples n_i and n_j for all $i, j \in \boldsymbol{\mathcal{S}}$ are independent of each other and cumulative distribution function of the noise is continuous. The exact form of distribution of $\mathbf{y}$ depends on the channel conditions as well on the noise distribution, for example, for the case of additive white Gaussian noise and a Rayleigh fading channel:

$$f(\mathbf{y}|\mathcal{H}_0) = (2\pi\sigma_n^2)^{-\frac{N}{2}} \exp\left\{-\sum_{k=1}^{N} \frac{y_k^2}{2\sigma_n^2}\right\} \quad \text{Eq. 3-64}$$

$$f(\mathbf{y}|\mathcal{H}_1) = f(\mathbf{r}) * f(\mathbf{y}|\mathcal{H}_0) \quad \text{Eq. 3-65}$$

where $*$ represents the convolution operation and $f(\mathbf{r})$ is the joint probability density function of $r_i \; \forall \; i \in \mathcal{S}$,

$$f(r_i) = \frac{r_i}{\sigma_r^2} \exp\left\{-\frac{r_i^2}{2\sigma_r^2}\right\}, \quad r_i \geq 0 \quad \text{Eq. 3-66}$$

Where σ_r is the expected value of r_i^2.

Let $f(y)$ and $F(y)$ be the empirical density and distribution function of the received signal y:

$$F(y) = \frac{1}{N}\sum_{i=1}^{N} I_{y_i \leq y}, \quad \text{Eq. 3-67}$$

where $I_{y_i \leq y}$ is the indicator function and is defined as:

$$I_{y_i \leq y} = \begin{cases} 1, & \text{if } y_i \leq y \\ 0, & \text{otherwise} \end{cases} \quad \text{Eq. 3-68}$$

For any spectrum sensing algorithm, first a test statistic is calculated; that is, $\mathfrak{T}(\mathbf{y})$. This test statistic is then compared with a decision threshold λ to decide if the transmitted signal is present; $\mathfrak{T}(\mathbf{y}) > \lambda$ indicates that a signal is present and vice versa. In the framework of spectrum sensing, the probability of false alarm, PFA, indicates the probability that an empty spectrum band is falsely declared as occupied; that is, PFA denotes the percentage of spectrum bands that are available but cannot be used by opportunistic users. A good sensing method will make PFA as small as possible. Similarly, the probability of detection PD is the probability that a frequency band is declared as occupied when it is really occupied. Lower values of PD induce harmful interference to incumbent or competing opportunistic users. Thus, the probability of detection must be as high as possible. The Receiver Operating Characteristics (ROC) curve is an important metric to evaluate the performance of a spectrum sensing algorithm. The ROC curves considered plots PD on the y-axis versus PFA on the x-axis [Arshad10].

$$\text{PFA} = \text{Prob}\{\mathfrak{T} > \lambda \mid \mathcal{H}_0\}, \quad \text{Eq. 3-69}$$

$$\text{PD} = \text{Prob}\{\mathfrak{T} > \lambda \mid \mathcal{H}_1\} \quad \text{Eq. 3-70}$$

Energy detection is a common method to detect an unknown signal in additive noise. But energy itself is a relative quantity and requires a reference noise energy level for comparison to decide the existence of a transmitted signal embedded in noise. Hence, when an exact noise estimate is available, the detection performance can be significantly improved. Unfortunately, an energy detector performs poorly in the presence of noise uncertainty and when the SNR of received samples is low, because at low signal power it is difficult to distinguish between the energy of signal and noise [Tandra08].

Test statistics and decision rules in this case are given by [Arshad10]:

$$\mathfrak{T}_{\text{ED}} \triangleq \frac{1}{N}\sum_{i=1}^{N} |y(i)|^2 \underset{\mathcal{H}_0}{\overset{\mathcal{H}_1}{\gtrless}} \lambda_{\text{ED}} \quad \text{Eq. 3-71}$$

Based on the decision rule defined in Eq. 3-71, PFA and PD for ED-sensing can be derived as [Urkowitz67]:

$$\text{PFA} = \frac{\Gamma(N, \frac{\lambda_{\text{ED}}}{2})}{\Gamma(N)} \triangleq \mathcal{G}(\lambda_{\text{ED}})$$
$$\text{PD} = \mathcal{Q}_m\left(\sqrt{2N \times SNR}\,, \quad \sqrt{\mathcal{G}^{-1}(\text{PFA})}\right) \qquad \text{Eq. 3-72}$$

where $\Gamma(a)$ is the gamma function, $\Gamma(a,x)$ is the incomplete gamma function and $\mathcal{Q}_m(a,b)$ is the generalised Marcum $\mathcal{Q}$- function (for definition, see [Gradshteyn80]).

3.1.3.2.3 Spectrum Sesing Based on Statistical Tests

In many practical situations, the knowledge of incumbent and/or other opportunistic user signals is limited, incomplete or imprecise. Hence, a sensor which is designed for a specific signal type may suffer drastic degradation in performance when sensing other signals.

Proposed spectrum sensing methods using statistical tests are robust in a sense that they are totally independent of the transmitted signal. When there is no signal transmission, the received samples $\mathbf{y}$ are a sequence of samples drawn independently from the noise $f(\mathbf{y} \mid \mathcal{H}_0)$. Similarly under $\mathcal{H}_1$ the received samples are drawn from the density $f(\mathbf{y} \mid \mathcal{H}_1)$, defined in Eq. 3-65, such that $f(\mathbf{y} \mid \mathcal{H}_0) \neq f(\mathbf{y} \mid \mathcal{H}_1)$. Hence, the spectrum sensing problem can be transformed into a simple problem of testing the null hypothesis $\mathcal{H}_0$; if we cannot reject $\mathcal{H}_0$ under the given constraints, then the null hypothesis is retained and the channel is available for opportunistic use.

In the sequel, spectrum sensing algorithms based on statistical tests are described. An introduction to AD-sensing (as proposed in [Wang09_1]) is given. KS-Sensing is then described, under the assumption that noise probability density function is known, that is, $f(\mathbf{y} \mid \mathcal{H}_0)$ is an arbitrarily (but known) distribution. The assumption of known noise density is later relaxed, and t-sensing is proposed. It is also asymptotically robust for any noise distribution. It is further shown by simulation results that t-sensing gives similar performance in the presence of non-Gaussian noise.

3.1.3.2.3.1 AD Sensing

The AD test is used to check whether the received samples at a CR come from a known noise distribution $F(\mathbf{y} \mid \mathcal{H}_0)$.

The AD test statistic is given by [Anderson52]:

$$\mathfrak{T}_{\text{AD}} \triangleq N \times \int_{-\infty}^{+\infty} (F(\mathbf{y})F(\mathbf{y} \mid \mathcal{H}_0)^2)\, \psi(F(\mathbf{y} \mid \mathcal{H}_0))\ \mathrm{d}F(\mathbf{y} \mid \mathcal{H}_0) \qquad \text{Eq. 3-73}$$

where $\psi(x) = (x(1-x))^{-1}$ is a weight function defined over $0 \leq x < 1$. The integral in Eq. 3-73 can be performed and a simplified form of $\mathfrak{T}_{\text{AD}}$ is obtained as:

$$\mathfrak{T}_{\text{AD}} = \frac{-1}{N}\left(N^2 + \sum_{i=1}^{N}(2i-1)(\ln Z_i + \ln[1 - Z_{N-i+1}])\right) \qquad \text{Eq. 3-74}$$

where $Z_i = F(y_i \mid \mathcal{H}_0)$. The asymptotic distribution of $\mathfrak{T}_{\text{AD}}$ under $\mathcal{H}_0$ can be derived as [Anderson52]:

$$F\{\mathfrak{T}_{\text{AD}} \mid \mathcal{H}_0;\, x\} = \frac{\sqrt{2\pi}}{x}\sum_{i=0}^{\infty} a_i(4i+1)e^{-\frac{(4i+1)^2\pi^2}{8x}} \int_0^{+\infty}\left(\frac{x}{8(w^2+1)} - \frac{(4i+1)^2\pi^2 w^2}{8x}\right)dw \qquad \text{Eq. 3-75}$$

where $a_i = (-1)^i \, \Gamma\left(i + \frac{1}{2}\right) / \, \Gamma\left(\frac{1}{2}\right) i!$. From Eq. 3-69 and Eq. 3-75, the threshold can be calculated for a given $\overline{\text{PFA}}$ using Eq. 3-76:

$$\overline{\text{PFA}} \; = \; 1 - F\{ \, \mathfrak{T}_{\text{AD}} \; | \mathcal{H}_0; \; \lambda_{\text{AD}} \} \qquad \text{Eq. 3-76}$$

Hence, for large N, Eq. 3-75 and Eq. 3-76 give the values of the thresholds for different values of probability of false alarm; a table is given in [Stephens74]. Finally, $\mathfrak{T}_{\text{AD}}$ is compared with λ_{AD} to check if $\mathcal{H}_0$ can be rejected at given $\overline{\text{PFA}}$ and a decision is made as follows: if $\mathfrak{T}_{\text{AD}} > \lambda_{\text{AD}}$ the null hypothesis is rejected and the channel is considered as occupied; alternatively the null hypothesis is accepted and the channel is assumed to be unoccupied.

3.1.3.2.3.2 KS Sensing

Like the AD test, the KS test also evaluates the hypothesis that received signal samples, $\mathbf{y}$, with distribution function $F(\mathbf{y})$ is drawn from a given distribution function of noise; that is, $F(\mathbf{y} \mid \mathcal{H}_0)$. Under the same assumption that noise distribution is completely known to the CR, estimated cumulative distribution function of received signal is compared with the given CDF of noise. Graphically, the KS test statistic is the maximum vertical distance between the two distributions; that is, $F(\mathbf{y})$ and $F(\mathbf{y} \mid \mathcal{H}_0)$.

$$\mathfrak{T}_{\text{KS}} = \sup_{y} |F(\mathbf{y} \mid \mathcal{H}_0) - F(\mathbf{y})| \qquad \text{Eq. 3-77}$$

The distribution-free property of the KS test means that $\mathfrak{T}_{\text{KS}}$ has a distribution function that is totally independent of the distribution of noise under $\mathcal{H}_0$. In Kolmogorov's paper [Kolmogoroff33], there are formulas which show how to calculate statistics for small values of N and also for asymptotic distribution as $N \to \infty$ under $\mathcal{H}_0$

$$\text{Prob}\left(\sqrt{N} \, \mathfrak{T}_{\text{KS}} \leq \lambda_{\text{KS}}\right) = \sum_{i=-\infty}^{+\infty} (-1)^i \exp(-2i^2 \lambda_{KS}^2) \qquad \text{Eq. 3-78}$$

According to the Glivenko-Cantelli theorem, under the null hypothesis $\mathcal{H}_0$, the test statistic tends to zero as follows [Durbin73]:

$$\text{Prob}\left(\lim_{N \to \infty} \mathfrak{T}_{\text{KS}} = 0\right) = 1 \qquad \text{Eq. 3-79}$$

which proves that the test will reject a false hypothesis with probability 1 as more and more samples are included to calculate the test statistic.

From Eq. 3-69 and Eq. 3-78, the threshold for KS-sensing for a given PFA can be calculated as:

$$\overline{\text{PFA}} \; = \; 1 - \text{F}\{ \, \mathfrak{T}_{\text{KS}} \; | \mathcal{H}_0; \; \lambda_{\text{KS}} \} \qquad \text{Eq. 3-80}$$

Massey [Massey51] provides tables and recursive expressions to calculate the threshold λ_{KS} for a given $\overline{\text{P}}_{\text{f}}$ using Eq. 3-80.

3.1.3.2.3.3 t-Sensing

Thermal noise in communication channels is widely modelled as AWGN process with zero mean and an unknown variance. Under the hypothesis $\mathcal{H}_1$, the probability density function of received signal is dependent on the channel conditions and the distribution of noise, as defined in Eq. 3-65. It is well known that absolute values of received signal variations at a receiver, typically encountered in a wireless environment can be accurately modelled using a Rayleigh distribution [Boccuzzi07]. Hence the distribution of $\mathbf{r}$ is considered as a multivariate Rayleigh distribution where the density function of each r_i is given by Eq. 3-65. Initially, it is also assumed that the noise is AWGN, apply the central limit theorem, and assume that distribution of $\mathbf{y}$ under $\mathcal{H}_1$ can also be approximated by a Gaussian

distribution with unknown parameters (i.e. unknown location μ and scale parameter σ). Applying the central limit theorem involves a limiting approximation, but the theorem itself gives no guide to the accuracy of this approximation. Further work will be needed to determine this. Under these assumptions, Eq. 3-65 becomes:

$$f(y \mid \mathcal{H}_1) = (2\pi\sigma^2)^{\frac{-N}{2}} \exp\left\{-\sum_{k=1}^{N} \frac{(y_k - \mu)^2}{2\sigma^2}\right\} \quad \text{Eq. 3-81}$$

Since the values of μ and σ are unknown, these parameters need to be estimated by maximising the density functions with respect to the unknown parameters. In order to derive an optimal detector in the Neyman-Pearson sense, the likelihood ratio (or logarithm of likelihood ratio) needs to be calculated:

$$\mathcal{L}(y) = \frac{f(y \mid \mathcal{H}_1)}{f(y \mid \mathcal{H}_0)} \quad \text{Eq. 3-82}$$

Substituting all unknown and estimated values in Eq. 3-82, the test statistics for t-sensing can be written as follows [Lehmann05]:

$$\mathfrak{T}_t = \frac{\sum_{i=1}^{N} y_i}{\sqrt{N}\left(\frac{1}{N-1}\sum_{i=1}^{N}\left(y_i - \frac{1}{N}\sum_{i=1}^{N} y_i\right)\right)} \quad \text{Eq. 3-83}$$

It is not difficult to verify that under the hypothesis $\mathcal{H}_0$, the test statistic of t-sensing has a limiting Gaussian distribution with zero mean and unit variance. Hence the decision threshold λ_t for a given probability of false alarm, $\overline{PFA}$, can be computed asymptotically as:

$$\Phi(\lambda_t) = 1 - \overline{PFA} \quad \text{Eq. 3-84}$$

For small values of N, the threshold λ_t can be exactly calculated from Eq. 3-69:

$$\overline{PFA} = Prob\{\mathfrak{T}_t > \lambda_t \mid \mathcal{H}_0\} = 1 - \mathcal{F}(\lambda_t)$$

$$\lambda_t = \mathcal{F}^{-1}(1 - \overline{PFA}) \quad \text{Eq. 3-85}$$

where $\mathcal{F}$ is the distribution function of Student's t distribution [Lehmann05]. Although t-sensing test statistics as defined in Eq. 3-83 derived from the Neyman-Pearson lemma and use maximum likelihood estimates of unknown parameters, it can be shown that t-sensing is the Uniformly Most Powerful (UMP) unbiased test [Fraser57].

The test statistic of t-sensing is derived under the assumption of Gaussian noise, so the probability of false alarm, in general, will not remain constant for non-Gaussian noise. However $\mathfrak{T}_t$ shows some interesting properties for larger values of N. The bracketed term in the denominator of Eq. 3-83 can be shown to converge in probability to σ^2 asymptotically. By applying central limit theorem, it can be shown that under $\mathcal{H}_0$ the distribution of $\sum_{i \in \mathcal{S}}(y_i/\sqrt{N})$ has a distribution of mean zero and variance σ^2. Since t-sensing statistic is asymptotically Gaussian, if the threshold is chosen according to Eq. 3-84 the probability of false alarm will remain constant for an arbitrarily noise distribution. Hence, the proposed t-sensing is asymptotically non-parametric. It is noted here that $t-$sensing is not as vulnerable to noise uncertainty as AD, KS, or ED sensing. Accuracy of AD sensing and KS-sensing is highly dependent on the given noise distribution function. If the noise power fluctuates and so also does the noise distribution function, AD and KS sensing will produce inaccurate results. However, in t-sensing parameters are estimated from the measurement data and hence t-sensing algorithm provides resistance to noise uncertainty problem.

3.1.3.2.4 Simulation Results

Simulation results are presented to evaluate the performance of proposed sensing algorithms earlier described. AD-sensing, KS-sensing and $t-$sensing are considered. ED-sensing is used as a reference

for comparison purposes. Monte-Carlo simulations are performed and compared to the results using ROC curves. It is assumed that $\sigma_n = 1$ in all simulation results. In [Wang09_1], it was shown by simulations that AD-sensing performs much better than ED-sensing at low SNR. The signal model used in [Wang09_1] is simple and under both hypothesis $\mathcal{H}_0$ and $\mathcal{H}_1$ the received signal energy will remain the same. Hence, it is not fair to compare AD-sensing with ED-sensing under such conditions. It is interesting to note that with the system model defined in [Wang09_1], the spectrum sensing problem can be formulated as a location testing problem and hence t-sensing performs better than AD-sensing with less complexity.

This is indeed confirmed by our simulations as shown in Figure 3-42, where the same parameters and model are used as used in [Wang09_1]. The goodness-of-fit based sensing methods are very difficult to implement in real time even with a fast processor [Bacut84]; while on the other hand t-sensing statistic and threshold calculations are straightforward. Figure 3-43 depicts the complementary ROC curves in the low SNR region (i.e. received SNR is -10dB and the number of received samples is 32). Here, it is assumed that the channel is Rayleigh fading channel and noise process is modelled as a Gaussian process with zero mean and variance σ_n^2. It is clear that t-sensing outperforms ED, AD and KS based spectrum sensing at low SNR. For example, at PFA $= 10^{-1}$, the probability of detection for t-sensing is 82%, while for ED-sensing, the probability of detection is only 32%. The detection probability of AD-sensing and KS-sensing at PFA $= 10^{-1}$ is around 69% and 74% respectively.

Despite of the fact that AD-sensing and KS-sensing require a-priori information about the noise distribution, their performance is inferior compared to t-sensing in AWGN noise. Our simulation results show that the proposed t-sensing performs better than AD, KS and ED based sensing, even though they are more complex to implement on a real hardware. Furthermore, our proposed sensing scheme is also robust asymptotically and gives similar performance if the noise is non-Gaussian. To show the robustness of our proposed method, we consider another type of noise commonly present in communication systems, it should be noted here that conclusion remains valid for any other type of noise as well. Recent studies have shown that non-Gaussian noise is present in indoor environments and a Laplace distribution is widely used for modelling such noise [Marks78]. In simulations, it is considered a situation where the corrupting noise is nominally zero-mean Laplacian noise and defined by:

$$f(x) = \frac{\gamma}{2}\exp(-\gamma|x|) \qquad \text{Eq. 3-86}$$

where γ is a positive parameter. A detector is called robust if it shows the same performance irrespective of noise distribution. To see how t-sensing performs under Laplacian noise, ROC curves are plotted with same parameters, for sample size $N = 32$, and SNR −10dB, in Figure 3-44. Although, $\mathfrak{T}_t$ is derived for Gaussian noise, it gives similar performance in non-Gaussian noise as seen in Figure 3-44. An interesting observation that can be derived from Figure 3-44 is that asymptomatic behaviour is seen even for $N = 32$, our simulation study shows that t-sensing is robust for $N \geq 25$. For example, at PFA $= 10^{-1}$, the detection probability for t-sensing is still 92%; while in this case AD-sensing and KS sensing perform better than t-sensing. However, the exact noise distribution is often unknown in real situations and AD and KS based sensing work only if the exact noise distribution is known a-priori. Hence under such conditions t-sensing is the most suitable choice.

3.1.3.2.5 Remark

Spectrum sensing algorithms based on statistical tests are discussed in this sub-section and proposed KS-sensing and t-sensing. The efficacy of the proposed sensing schemes has been demonstrated by simulations. Simulation result show that proposed t-sensing outperforms energy-detection based spectrum and AD sensing proposed in literature, with less complexity. It is shown that if the noise distribution is known and Gaussian, then t-sensing is superior in terms of detection probability, while with known non-Gaussian noise distribution KS-sensing is a better alternative. It is further emphasised that proposed t-sensing is robust asymptotically and gives similar performance for an unknown non-

Gaussian noise distribution while AD and KS sensing is applicable only if the exact noise distribution is known. As future work, it would be interesting to quantify the complexity of all algorithms and implement all sensing techniques on real hardware.

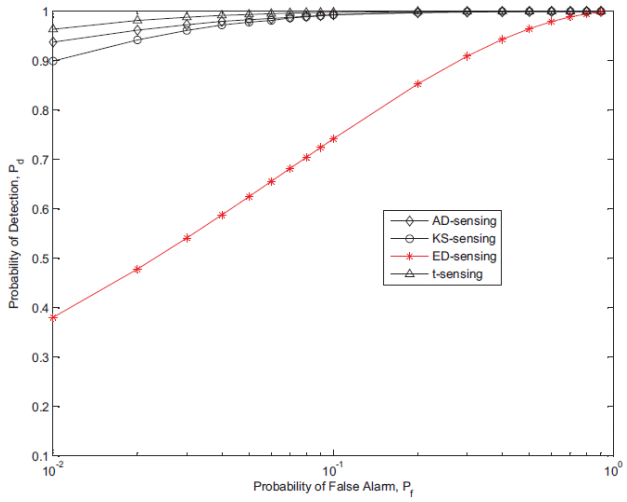

Figure 3-42: ROC curves with system model used in [Wang09_2], *N*=28 and SNR= -2dB

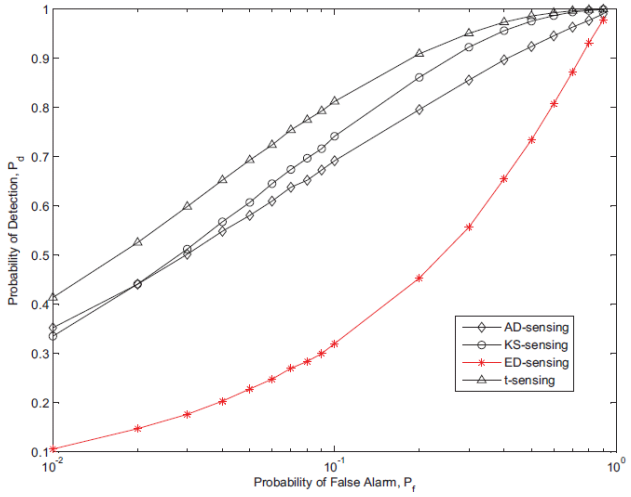

Figure 3-43: ROC curves with *N*=32 and SNR=-10dB (AWGN)

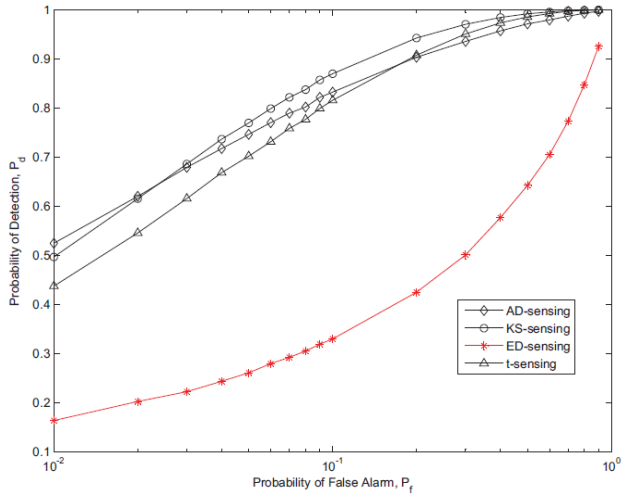

Figure 3-44: ROC curves with *N*=32 and SNR=-10dB (Laplacian Noise)

3.1.4 GFDM Sensing

This section is a joint-WP work between WP3 and WP4. Please note that the Generalized Frequency Division Multiplexing (GFDM) description can be found in [QoSMOS_D4.3] As described in WP4, GFDM is a recent multi-carrier modulation technique with extremely low out-of-band radiation that makes it an attractive choice for the PHY layer of cognitive radio. It has a flexible pulse shaping technique which reduces the out of band leakage.

GFDM also has an innovative tail biting Cyclic Prefix (CP) which shows unique circular detection properties. Figure 3-45 shows the OFDM transmission structure and the GFDM transmission structure for a load of N_L=3 OFDM symbols. The OFDM symbol is composed from one guard period $T_{G,OFDM}$ and one useful period $T_{D,OFDM}$. However, a GFDM symbol is composed from one guard period $T_{G,GFDM}$ and N_L useful periods $T_{D,OFDM}$. Please note that in the example from Figure 3-45, OFDM presents three CPs, one for each symbol, while GFDM presents only one.

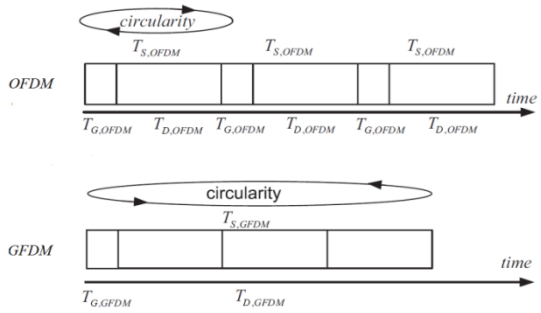

Figure 3-45: OFDM and GFDM Structure for a load with N_L=3 OFDM symbols

In [Panaitopol12], the CAF of GFDM signals is graphically presented. It has been showed for the first time the existence of side peaks in GFDM CAF.

The classic cyclostationarity detection approach would have been to use the cyclostationary properties resulting from the presence of cyclic prefix and not the symmetric side peaks obtained from using the shaping filters. Figure 3-46 represents the GFDM CAF for the roll-off factors β=0.1 and β=0.3. The peaks resulted from the presence of CP are called Normal Peaks (NP), while the peaks resulted from using the shaping filters are called Side Peaks (SP). For simplicity, in the following paragraphs T_D and T_S represents the GFDM useful period and the GFDM symbol period respectively.

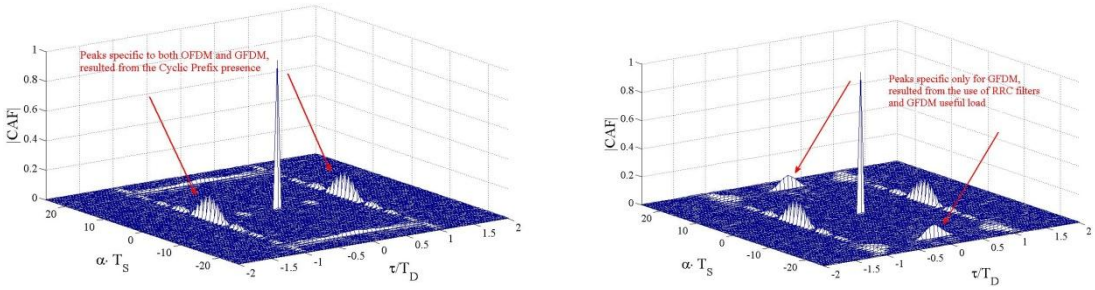

Figure 3-46: GFDM cyclostationary properties for β=0.1 (left) and β=0.3 (right), T_G=T_D/4, N_L=16

In this section the impact of RRC design on detection results is analysed. It is also shown that if the RRC coefficient is properly designed, this can increase the detection even when the CP is very small, thus allowing to transmit more useful data without decreasing system detection capabilities.

Figure 3-47 and Figure 3-48 show PD plots for different CD with different CP lengths and varying roll-off factor β. The results therefore show the impact of the RRC pulse shaping design on cyclostationarity detection of GFDM signal.

In Figure 3-47 it is shown that when performing cyclostationarity detection on the side peaks, for a fixed β, the performance is the same with respect to different CP lengths. However, in Figure 3-48 it is seen that CD on normal peaks for $T_G = T_D/4$ is better than the one when $T_G = T_D/16$. If the length of the cyclic prefix is small then obviously the CD performance will be worse. Now, if CD performance based on side peaks are compared, it can be seen that the performance gets better as the roll-off factor increases. Moreover, compared to the performance on normal peaks, the detection performance is better if done on the side peaks even for $T_G = T_D/16$. For the case when $T_G = T_D/4$, the cyclostationarity detection based on side peaks shows improvements as the roll-off factor increases from 0.3 to 0.9. The detection based on the side peak for $\beta = 0.9$ is better than the detection on normal peak. Corresponding ED plots for a 10 ms signal are also included as a reference. It can be also seen that under uncertain noise estimation even 0.1 dB of noise uncertainty can affect the performance. Figure 3-48 also shows that compared to this detector, CD on side peaks performs better even for a very small CP (i.e., $T_G = T_D/16$). This result would not have been possible if the same CP would have been used and the detection would have been done on normal peaks instead of side peaks.

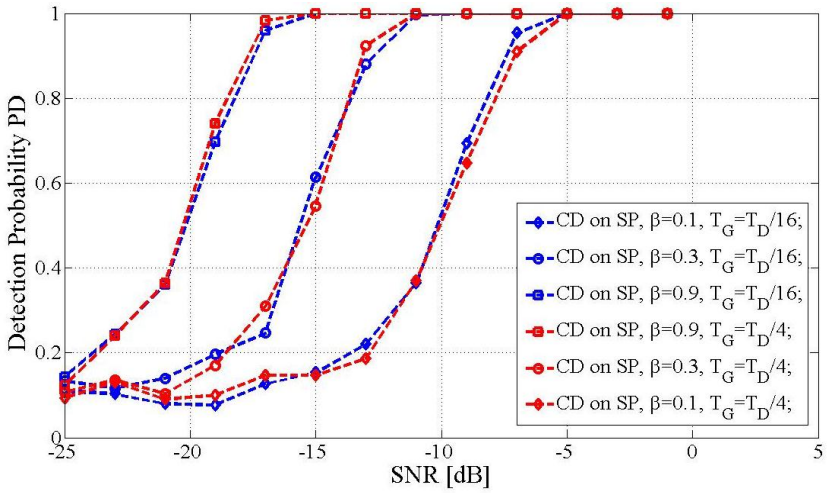

Figure 3-47: Detection probability for GFDM signals - Comparison of cyclostationary Detectors on the Side Peak (SP), for 10 ms GFDM signals, for different β and different cyclic prefix lengths. PFA_{target} has been considered 0.1

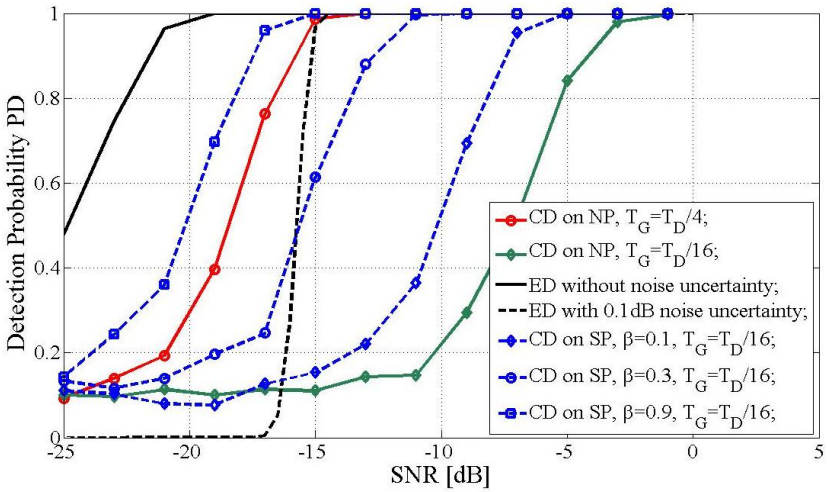

Figure 3-48: Detection probability for GFDM Signals - Comparison between energy and cyclostationarity detectors on both Side Peak (SP) and Normal Peak (NP), for 10 ms GFDM signals, for different β and different cyclic prefix lengths. PFA_{target} has been considered 0.1

Compared to OFDM, only the GFDM signal presents side peaks characteristics in the cyclostationary autocorrelation function (CAF). Following this observation, the impact of the roll-off factor on the detection result when the cyclostationarity detector uses the CAF side peaks is studied as well as the trade-off between the length of the CP and the roll-off factor for the detection performance. The results show that if the roll-off factor is properly designed, it can increase the detection capability even when the CP is very small, thus allowing transmitting more useful data in the same time without decreasing the detection.

3.1.5 Sensing in Code

3.1.5.1 Concept

In most cases, performing sensing corresponds to answering to the following question "In this geographic area, at this moment, is this frequency band used (and possibly by whom)?". It means that sensing is studied according to three dimensions: space, time and frequency. Nevertheless, there are additional dimensions which can be explored.

One of these new dimensions is the code dimension [Yücek09]. Indeed for all CDMA standards, the downlink bands are always fully used by common channels even if no user is using them. This means that there might be a potential available resource (unused orthogonal codes) that classical sensing algorithms do not see. Simultaneous transmission without interfering with the incumbent users could be possible in the code domain with codes that are orthogonal to the incumbent users' codes. In order to use these codes, the opportunistic system must be able to detect them (that is to detect the used spreading factors and spreading codes). In the following, several algorithms for the detection of UMTS and HSDPA downlink traffic channels are proposed and their performance evaluated.

3.1.5.2 UMTS/HSDPA Downlink Channels Structure

3.1.5.2.1 Structure of Logical Channels

UMTS and HSDPA are CDMA standards. For both of them, a Spreading Factor (SF) and a spreading sequence (which is a ± 1 sequence whose length is equal to the spreading factor) are associated to each logical channel. Each symbol to be transmitted is multiplied by the spreading sequence, thus producing a chip rate sequence. The chip sequences associated to the various logical channels are added. In order to get rid of the interference generated by the other base stations, the elements of this sequence are multiplied by the scrambling sequence, which is a cell specific sequence of period 38400 chips (that is one frame of 10 ms). Then the sequence is pulse shaped and transmitted by the base station. It is worth mentioning that the spreading sequences allocated to the logical channels of the same cell are orthogonal in order to improve the performance of the symbol detection algorithm. In UMTS and HSDPA, OVSF (Orthogonal Variable Spreading Factor) spreading sequences are used.

3.1.5.2.2 Structure of a Frame

Some logical channels are dedicated to the transmission of information to be broadcast to all the users of the cell. For the synchronization and the identification of a base station, four of them are mandatory. It is the P-SCH (Primary Synchronization CHannel), the S-SCH (Secondary Synchronization CHannel), the CPICH (Common PIlot CHannel) and the P-CCPCH (the Primary Common Control CHannel). These channels are common to UMTS and HSDPA.

For UMTS, DPCHs (Dedicated Physical CHannels) containing data (DPDCH (Dedicated Physical Data CHannel)) and control bits (DPCCH (Dedicated Physical Control CHannel)) are emitted. They are described in more details in section 3.1.5.2.3.

For HSDPA, HS-SCCHs (High Speed Shared Control CHannel) are signalling channels describing to the UE where the data dedicated to it is. This data is sent on HS-PDSCHs (High Speed Physical Downlink Shared CHannel).

3.1.5.2.3 UMTS Traffic Channels

In order to perform sensing in code on UMTS frequency channels, the DPCHs need to be detected and identified. Within one downlink DPCH, dedicated data is transmitted in time-duplex with control information (known pilot bits, TPC commands and optional TFCI) as shown in Figure 3-49. The number of bits N_{bit} in a slot depends on the spreading factor SF of the physical channel:

$$N_{bits} = 10 \times 2^k \text{ with } SF = 512/2^k$$

The spreading factor may range from 4 to 512.

It is important to mention that a DPCH can be desynchronized in comparison with the other physical channels. This offset, τ_{DPCH}, may vary from one DPCH to another and is a multiple of 256 chips.

$$\tau_{DPCH} = \alpha \times 256 \text{ chips with } \alpha \in \{0,1,\cdots,149\}$$

Each traffic channel can have a different offset.

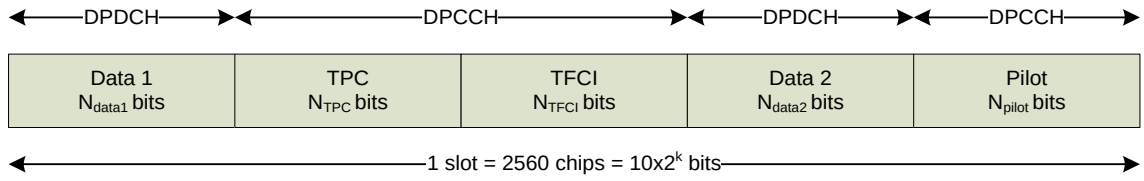

Figure 3-49: Structure of a DPCH

Moreover, for a given SF, the number of pilot bits and pilot bit patterns can change depending on the slot format as shown in Table 3-6.

Table 3-6: Number of different pilot patterns for a DPCH

SF	512	256	128	64	32	16	8	4
# of pilot patterns	1	3	2	1	1	1	1	1

3.1.5.2.4 HSDPA Traffic Channels

The traffic emission on HSDPA needs two types of channels: HS-SCCHs are signalling channels describing to the UE where is the data dedicated to it and the HS-PDSCH containing the data.

There are from 1 to 4 HS-SCCH. A constant SF of 128 allows 40 bits per slot to be carried (with QPSK modulation). There are no pilot or power control bits on the HS-SCCH. There is a time offset of two slots between the information given by the HS-SCCH and the corresponding data on the HS-PDSCH. This enables the HS-SCCH to carry time-critical signalling information which allows the terminal to demodulate and decode the correct codes. The HS-PDSCH use three different type of modulation, QPSK, 16QAM and 64 QAM, with a SF of 16.

3.1.5.3 UMTS Traffic Channel Detection

3.1.5.3.1 Introduction

Two UMTS traffic channel detectors are proposed. The first one is only based on the knowledge of the possible spreading sequences. The second one is based on the structure of a DPCH. For both methods, the scrambling code of the processed BTS is supposed to be known. It can be found from a classical UMTS synchronisation procedure. Both methods are using the demodulation structure described in Figure 3-50. The equalization part of the process will not be detailed in this document.

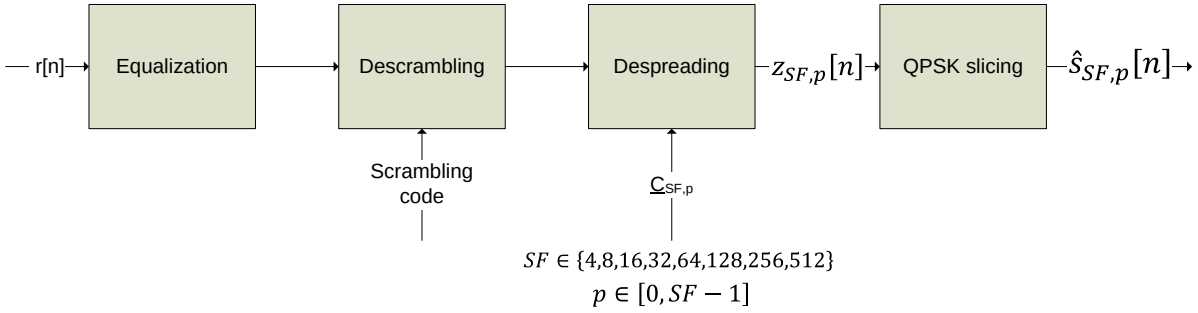

Figure 3-50: UMTS demodulator structure

3.1.5.3.2 Detection Without Pilot Bits

The first method performs the correlation between the despread symbols before and after decision. It computes the average distance between the demodulated symbols and the perfect constellation, as described in Eq. **3-87**. All the possible spreading factors and the spreading codes must be tested in order to find the ones that are used. In the UMTS case, it means that 4+8+16+32+64+128+256+512=1020 criterion points must be computed. This algorithm allows detecting the traffic channels but also any other spread channel (broadcast channels, pilot channel, etc.).

$$C_1(SF,p) = \frac{1}{\sqrt{N_{sym}}}\left(\sum_{n=1}^{N_{symb}} \Re\left(z_{SF,p}[n]\hat{s}^*_{SF,p}[n]\right)\right) \Bigg/ \left(\sqrt{\sum_{n=1}^{N_{symb}} \left|z_{SF,p}[n]\right|^2}\right) \qquad \text{Eq. 3-87}$$

N_{sym} is the number of symbols per slot, $N_{sym} = 2560/SF$. $\mathrm{C_1(SF, p)}$ is computed once a slot and averaged over N_{slot}. The other notations are described in Figure 3-50.

3.1.5.3.3 Detection with Pilot Bits

The second method is based on the knowledge of all the possible pilot bit patterns. It performs the correlation between the despread symbols and the known pilot symbols as described in Eq. 3-88. All the possible spreading factors, spreading codes, DPCH time offsets and pilot patterns must be tested in order to find the ones that are used. In the UMTS case, it means that $150 \times (512 + 3 \times 256 + 2 \times 128 + 64 + 32 + 16 + 8 + 4) = 249.000$ criterion points must be computed. This algorithm allows detecting only the DPCH but it gives more info than the other one that is the offset and the slot format.

$$C_2(SF,p,\tau_{DPCH}) = \frac{1}{\sqrt{N_{pilot}}}\left(\sum_{n=1}^{N_{pilot}} \Re\left(z_{SF,p}[n+\tau_{DPCH}]s^*[n]\right)\right) \Bigg/ \left(\sqrt{\sum_{n=1}^{N_{pilot}} \left|z_{SF,p}[n+\tau_{DPCH}]\right|^2}\right) \qquad \text{Eq. 3-88}$$

N_{pilot} is the number of pilot symbols per slot. It depends on the slot format. $\mathrm{C_2(SF, p, \tau_{DPCH})}$ is computed once a slot and averaged over N_{slot}.

3.1.5.3.4 Simulation Results

The simulations were run on a UMTS signal generated by Agilent software. Its CDMA channels configuration is summarized in Figure 3-51. The number into brackets corresponds to the spreading factor and to the scrambling code. As on real UMTS signal the P-CPICH and the P-CCPCH are always emitted by the BTS, these channels are not searched by the detection algorithm.

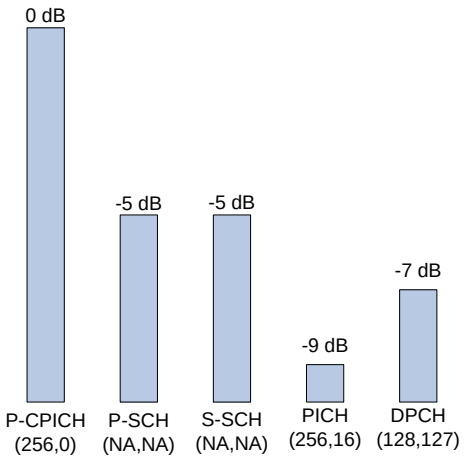

Figure 3-51: CDMA signal configuration for simulation

Figure 3-52 represents the detection criteria when using the method without pilot bits (on left hand side) and the method with pilot bits (on the right hand side). Each colour corresponds to a spreading factor. For the method with pilot bits, the criteria for each offset and pilot pattern are superposed.

When using the method without pilot bits, one can first notice that both the PICH and the DPCH are detected. Nevertheless, ambiguities are present. They correspond to spreading factors/spreading codes that are on the same branches than the CDMA channels to be detected. This is due to the way OVSF codes are generated. Indeed, the symbols on the same branch but with lower spreading factors are also correlated. Moreover, depending on the emitted symbols, the symbols of the same branch but with higher spreading factors can also be correlated. Hopefully, these ambiguities can be easily removed by adequate processing.

When using the method with pilot bits, no ambiguity shows up. Nevertheless, the number of point to compute can be unacceptable for cognitive device.

The detection thresholds are fixed by simulations, for a PFA equal to 10^{-2}. It is important to underline that the threshold is different for each spreading factor and of course for both methods.

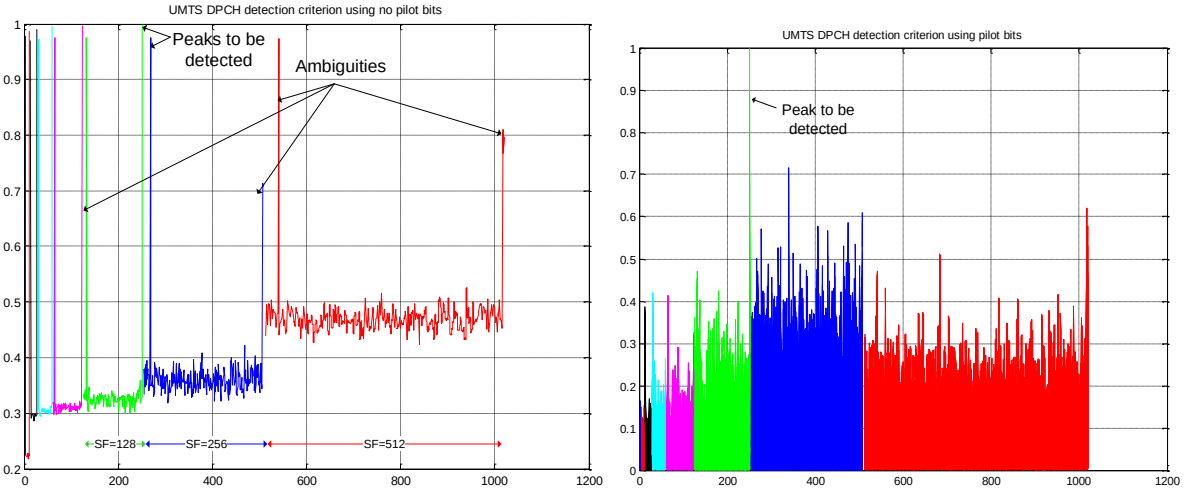

Figure 3-52: UMTS traffic detection criteria without pilot bits (left) and with pilot bits (right)

Figure 3-53 represents the detection performance of the DPCH present in the UMTS configuration described in Figure 3-51 when the SNR varies from -30 dB up to -5 dB. The red and blue plots correspond respectively to the method with and without pilot bits. The plain and dotted plots

correspond respectively to a stationary mono-path propagation channel and to a "vehicular A" propagation channel (Cf. Table 3-7). In the SNR, the signal part corresponds to the whole UMTS signal, not only the DPCH part.

Table 3-7: Vehicular A propagation channel characteristics

Delay [ns]	0	310	710	1090	1730	2510
Power [dB]	0	-1	-9	-10	-15	-20
Speed [km/h]	30					

First on can see that the method with pilot bits outperform the method without pilot bits from roughly 8 dB, whatever the propagation channel is. Moreover, the impact of the propagation channel on the performance is quite low (less than 1 dB). This is not due to the traffic detection algorithms but to the equalizer at the beginning of the process and how it deals with multi-path. A PD of 90% is reached for a SNR of -20 dB for the method with pilot bits and -12 dB for the method without pilot bits.

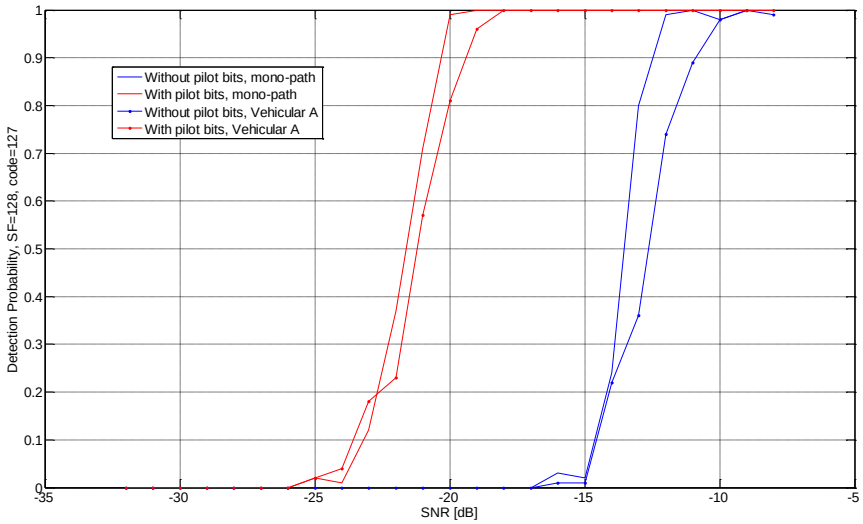

Figure 3-53: UMTS traffic detection performance when using the method with and without pilots bits, for a mono-path and a Vehicular A propagation channel

3.1.5.4 HSDPA Traffic Channel Detection

3.1.5.4.1 Proposed Method

In order to detect HSDPA used spreading codes, the HS-SCCHs and HS-PDSCHs must be detected and identified. The two methods presented for UMTS cannot be used. Indeed as not pilot bits are sent on the HS-SCCH and the HS-PDSCH, the method with pilot bit is useless. Moreover the method without pilot bits is also inefficient for HS-PDSCH detection. There are two reasons:

- Three types of modulation (QPSK, 16QAM and 64QAM) must be tested in the slicing block. If the wrong modulation is chosen ambiguities will appear that are quite difficult to reject.
- Calculating the distance of the despread symbols to the ideal constellation is inefficient with 64QAM and can only work at very high SNR.

Directly detecting the HS-PDSCH seems quite difficult. In the following, a method based on the detection and decoding of the HS-SCCH is proposed. Properly decoding the HS-SCCH allows knowing the spreading codes used for the HS-PDSCH (the SF is known as it is always 16). Figure 3-54 presents the channel coding chains of the HS-SCCH. It is important to underline that the HS-SCCH can be detected using the method without pilot bits.

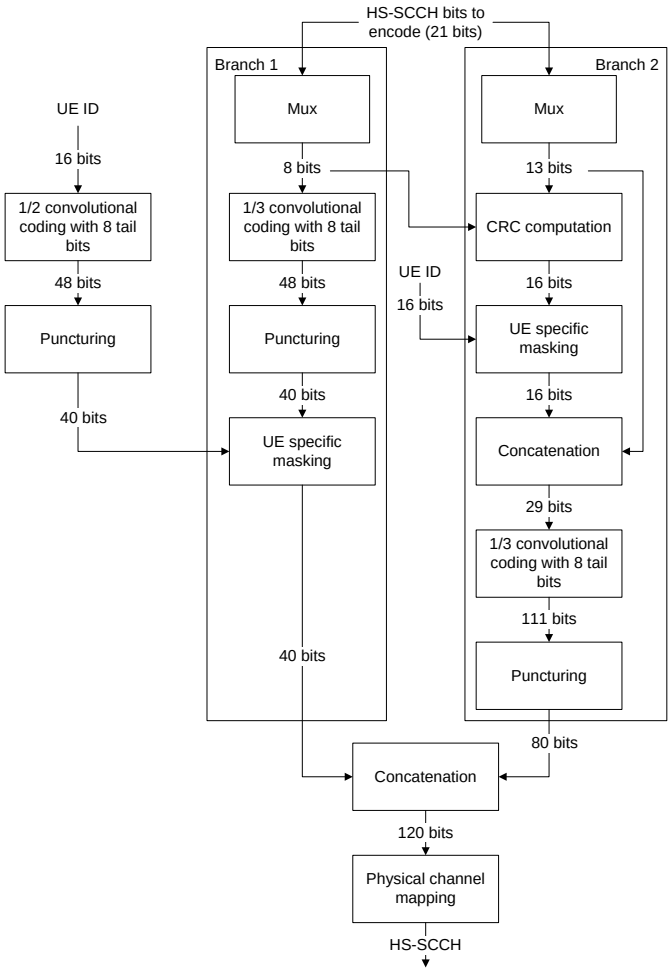

Figure 3-54: HS-SCCH channel coding chain

The tricky to detect the HS-SCCH part is that the ID of the UE, coded on 16 bits, must be known in order to perform the decoding. Obviously, it cannot be assumed that an opportunistic system knows this ID. Therefore the 2^{16} possible IDs must be tested. In practice, the right decoding is insured by the Cyclic Redundancy Check (CRC). Nevertheless, the 16-bits CRC is masked by the 16 bits of the UE ID. It means that if all UE IDs are tested, there will always be one for which the CRC is correct. The CRC is therefore not sufficient to validate the decoding chain. Therefore, in addition to the CRC, the Viterbi decoding weight is computed to verify that the decoding performed correctly.

The complete chain of the HS-PDSCH detection if presented in Figure 3-55. It can be seen that the whole decoding of the HS-SCCH is not performed for each UE ID. Indeed, in order to speed up the process, some tricks are used. As the Viterbi decoding of the convolutional code of the 2^{nd} branch does not involve the UE ID, it is performed first. The value of the decoding weight allows to state if the decoded channel is actually an HS-SCCH or not. Then the Viterbi decoding of the convolutional code of the 1^{st} branch is performed while testing the different UE ID. Once the decoding weight is low enough, the value of the UE ID is known. At the end, the CRC is checked to validate the correctness of the decoded bits.

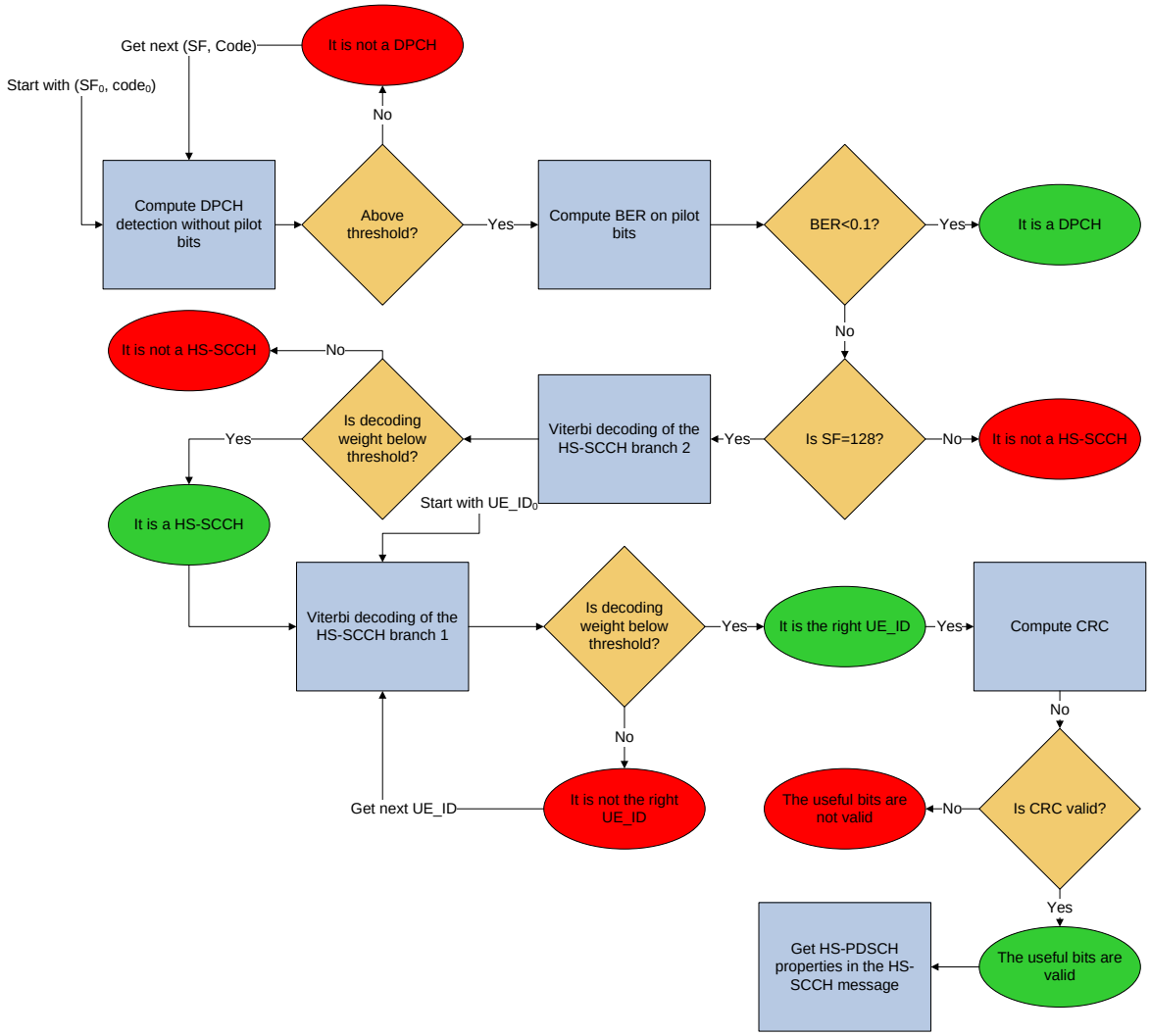

Figure 3-55: HS-PDSCH identification chain

3.1.5.4.2 Simulation Results

The simulations were run on a HSDPA signal generated by Agilent software. Its CDMA channels configuration is summarized in Figure 3-56. AWGN is added to the HSDAP signal in order to target an SNR from -20 dB to 0 dB. Two propagation channels were simulated; stationary mono-path and vehicular A.

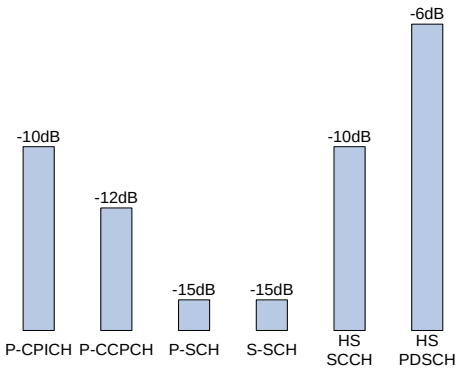

Figure 3-56: HSDPA signal configuration for simulation

First, the decoding weights for the two branches must be determined. In Figure 3-57, one can see the probability to have a correct or incorrect CRC depending on the decoding weight for the first branch (left figure) and the second branch (right figure). The blue curve is the probability to have a correct CRC when the decoded signal is an HS-SCCH while the black curve is the probability to have an incorrect CRC when the decoded signal is not an HS-SCCH. One can see that a good trade-off can be easily found. Indeed, on the first branch a decoding weight threshold of 40 insures a probability of right CRC of 97% for a probability of false CRC of 1%. For the second branch, a threshold of 76 insures a similar performance.

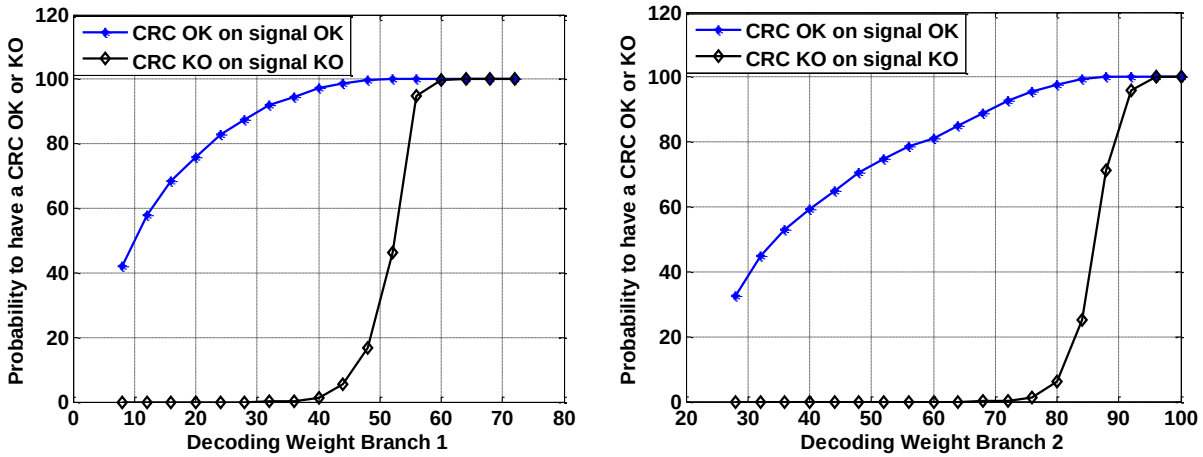

Figure 3-57: Probability to have a correct or incorrect CRC depending on the decoding weight

Figure 3-58 represents the percentage of correct CRC depending on the SNR for a stationary mono-path propagation channel (blue plain line) and a "vehicular A" propagation channel (red dotted line). A 90% rate of correct CRC is achieved for an SNR of -9 dB for the mono-path channel. The reachable SNR is degraded of 5 dB with the Vehicular A model.

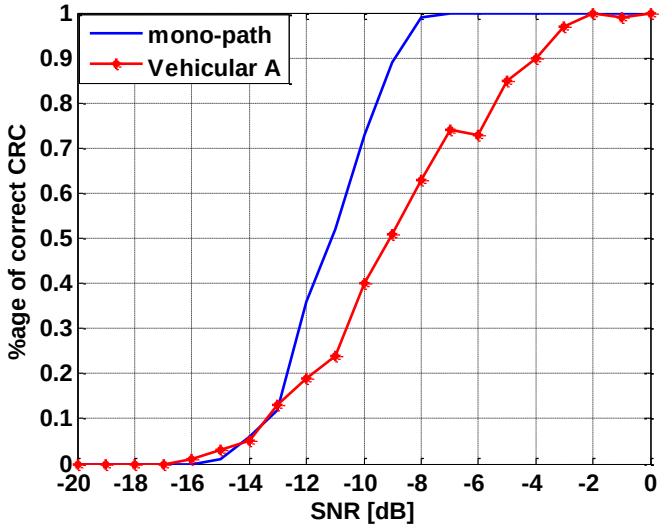

Figure 3-58: Percentage of correct CRC depending on the SNR

3.1.5.5 Conclusion

CDMA standards might have important unused resources that classical sensing methods cannot detect. In order to identify them, sensing in code must be performed. Three algorithms were proposed (two for UMTS and one for HSDPA) in order to detect the amount of traffic on CDMA frequency channels

and be able to identify the CDMA spreading codes that are unused and that could be a valuable resource for an opportunistic system.

On UMTS, the method without pilot bits offered good performance with limited complexity. The method with pilot bits outperformed the first one from 8 dB but with an important increase of complexity that may be unacceptable for a CR device.

The method without pilot bits cannot be transposed, with good performance, to HSDPA. This is due to the multiple possible modulations on the traffic channels (QPSK, 16QAM, 64QAM). Therefore, a new method was proposed based on the decoding of the control channels in order to have access to the traffic channels spreading codes. Due to the non-knowledge of the ID of the UE whose traffic channel is detected, the decoding of the control channels tends to be quite complicated even if the performance is good.

Sensing in code is a novel approach. Its possibilities can be very valuable as it deals with frequency bands that cannot be sensed with classical sensing methods and that are wide-band (as CDMA is a spread-spectrum waveform). Nevertheless, its implementation is complicated and seems, for the moment, unacceptable for a CR device. Additional approaches must be developed in order not to reject CDMA bands from cognitive radio.

3.2 Interference Monitoring

3.2.1 Overview of Interference Monitoring

One of the key functions enabling Opportunistic Spectrum Access (OSA) is spectrum management. One spectrum management method is a geo-location database approach, which has been adopted in the latest rules of Federal Communications Commission (FCC) in the US to allow OSA to use TV white space [FCC10]. In the FCC scenarios, the devices of the opportunistic systems identify their locations by using a geo-location capability and then query the database to determine which TV channels they can use at their locations. Similar approaches are investigated by CEPT [CEPT10]. From [CEPT10], to verify that the reuse of the TV channel does not cause harmful interference to the incumbent receiver, the database checks whether the Carrier to Interference Ratio (CIR) of the incumbent receiver can be kept at a required level. A transmit power which just satisfies the CIR requirement corresponds to an allowable transmit power of the opportunistic system. Thus, the opportunistic system (or the database) has to estimate the CIR of the incumbent receiver to determine the allowable transmit power. Path-loss prediction using propagation models is one CIR estimation method. However, the propagation model inevitably includes prediction error in actual radio environments, resulting in CIR estimation error. To absorb this error, a margin of the allowable transmit power has to be considered to keep the required CIR [OFCOM10]. Consequently, the allowable transmit power has to be limited, and thus white space utilization efficiency might be reduced. Therefore, it is important to improve the CIR estimation accuracy for expanding the white space opportunities.

Interference monitoring techniques can improve the CIR estimation accuracy. The concept of the interference monitoring is shown in Figure 3-59. In the interference monitoring techniques, actual measurements of both the interference signals and the incumbent signals are carried out to estimate the CIR of the incumbent receiver. This measurement is performed at a monitoring node of the opportunistic system located near the incumbent receiver at the edge of the incumbent service area. Using measurement results, the CIR of the incumbent receiver estimated by the path-loss prediction is compensated. In this way, the actual measurements are effectively used to improve the CIR estimation accuracy and thus to expand white space opportunities.

The interference monitoring can be considered as one spectrum sensing technique. However, its purpose is different from that of general spectrum sensing. General spectrum sensing performs the detection of incumbent signals or signals of other opportunistic systems to determine whether the active systems are around the opportunistic system. In other words, the opportunistic system is

supposed not to know whether the other system exists around. On the other hand, the interference monitoring determines how much interference is actually caused to the active system. In this case, to estimate the interference at the edge of the service area of the active systems, the opportunistic system obtains the location information of the active systems from the geo-location database and the monitoring node near the edge performs the measurements.

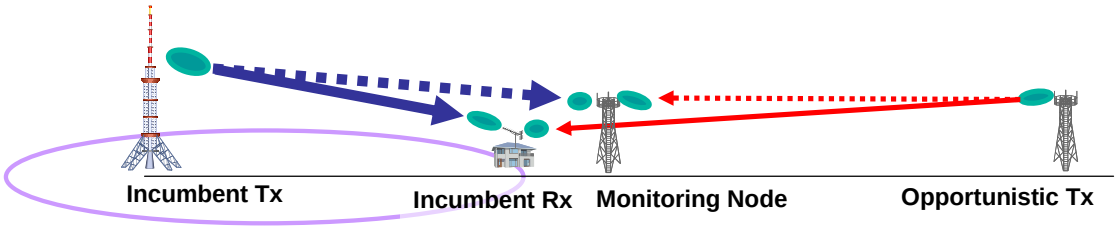

Figure 3-59: Concept of interference monitoring

One challenge for interference monitoring is to measure interference with a considerable accuracy. The accuracy of measurement needs to be at least higher than the accuracy of the path-loss prediction, because the measurement results of both the interference signals and the incumbent signals are used to compensate the path-loss prediction error. However, the monitoring node has to measure the interference signals under the condition that the incumbent signals with relatively high level exist in the measured band. For example, the protection ratio (the required CIR) of DTT is 21dB, which means that the incumbent signal level at the incumbent receiver is at least 21dB higher than the interference level. The Interference to Signal Ratio (ISR) of the monitoring node depends on its location, receiving antenna gain, the antenna height, and the transmit power of the interference signal etc. Although that condition is different from that of the incumbent receiver, ISR might be also low. Thus, the accurate interference measurement is important for the interference monitoring.

3.2.2 Interference Measurement Using Quiet Period-Based Power Estimation

This section provides a simple interference measurement technique and its evaluation results. Since a monitoring node receives incumbent signals and opportunistic signals within a measured band, it needs to separate the opportunistic signals from the incumbent signals to measure the received power of the interference. For this purpose, Quiet Period (QP) are utilized. They are assumed to be periodically allocated in the transmit signals for general spectrum sensing. An allocation of QP is shown in Figure 3-60. The opportunistic transmitter does not transmit any signal in QP so that it can perform general spectrum sensing. Since we assume that the opportunistic system knows the incumbent system in Figure 3-59 is active by the geo-location database information, this QP is used to detect the other incumbent systems or the other opportunistic systems.

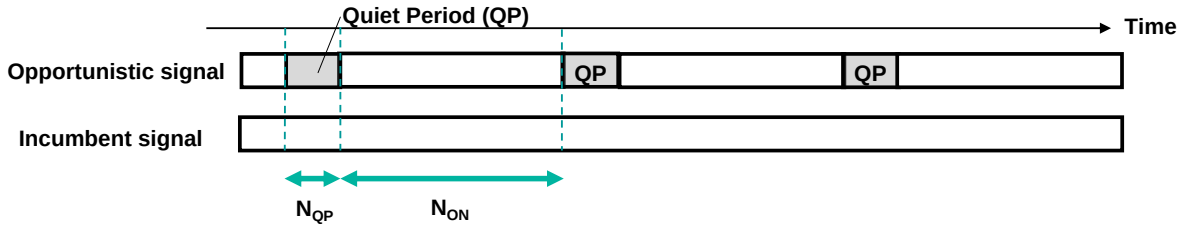

Figure 3-60: Quiet period allocation

It is assumed that the monitoring node knows the timing of QP and its duration. By using this information, the monitoring node separately measures the received power of signals in QP and that in transmission period. The difference of these received powers corresponds to the interference power. Thus, QP-based power estimation of the interference signals is performed by

$$\hat{I} = \frac{1}{N_{ON}} \sum_{k=N_{QP}}^{N_{QP}+N_{ON}-1} |r[k]|^2 - \frac{1}{N_{QP}} \sum_{k=0}^{N_{QP}-1} |r[k]|^2 \quad \text{Eq. 3-89}$$

where N_{QP} and N_{ON} are the number of samples in the QP and in the transmission period, respectively. $r[k]$ denotes the received signal at k^{th} sampling time and is expressed by

$$r[k] = i[k] + s[k] + n[k] \quad \text{Eq. 3-90}$$

where $i[k]$, $s[k]$, and $n[k]$ denote the interference signal, the incumbent signal, and white Gaussian noise, respectively. For simplification, it is assumed in Eq. 3-90 that the channels for the interference and the incumbent signals are AWGN channels.

As explained in the previous subsection, the measured interference power is used to compensate the path-loss prediction error. Since the path-loss prediction error is usually expressed in dB, it is convenient to also evaluate the measurement error in dB. Therefore, the measurement error represented by

$$e_{\mathrm{dB}} = \hat{I}_{\mathrm{dBm}} - I_{\mathrm{dBm}} = 10\log\hat{I} - 10\log I \quad \text{Eq. 3-91}$$

is used, where I, I_{dBm}, and $\hat{I}_{\mathrm{dBm}}$ denotes the actual interference power in the linear domain and the one in dB, and the estimated interference power in dB, respectively.

To evaluate the QP-based power estimation, simulations were conducted. The simulation conditions are shown in Table 3-8. The interference signals were set to be OFDM signals with 1024 FFT points and 72 guard interval points. Its power (I) was normalized to 1 in the simulation. For the structure of the interference signals, we assumed that one sub-frame was composed by 14 OFDM symbols. In addition, the total signal length to be measured was set to be 10 and 200 sub-frames. For example, in LTE systems, 10 and 200 sub-frames correspond to 10 ms and 200 ms. The QP duration was chosen to represent 10% of the total signal length, which corresponds to 14 OFDM symbols for 10 sub-frames and 280 symbols for 200 sub-frames. On the other hand, the incumbent signals were assumed to be white Gaussian noise for simplicity. As described in Section 2.3, SNR was set to 30 dB.

Table 3-8: Simulation conditions for QP-based power estimation

Interference signal	OFDM (FFT points: 1024, GI points: 72)
QP duration	14 / 280 OFDM symbols
Transmission duration	126 / 2520 OFDM symbols
Incumbent signal	Approximation by white Gaussian noise
SNR	30dB

The Root Mean Square Error (RMSE) of the interference measurement (Eq. 3-89) is shown in Figure 3-61. The RMSE can be a basic metric for evaluating the accuracy of the measurement techniques. From the figure, it can be seen that the RMSE decreases as ISR increases. When the ISR is higher than -10 dB, the RMSE of 10 sub-frames and 200 sub-frames gets close to 0. In this region, the measurement error does not impact the path-loss compensation accuracy in the interference monitoring. Meanwhile, when the ISR is lower than -20 dB, impacts caused by measurement error in the path-loss compensation needs to be considered. Such a measurement error has to be at least lower than the path-loss prediction error in order to improve the CIR estimation accuracy. For example, the error of ITU-R P.1546 propagation model is 13.2 dB in standard deviation [Grosskopf06]. In addition, the measurement error values might become negative under lower ISR conditions due to the estimation error which is caused by the inadequate averaging time. Since any power cannot be

negative, such a situation has to be considered in the path-loss compensation of the interference monitoring.

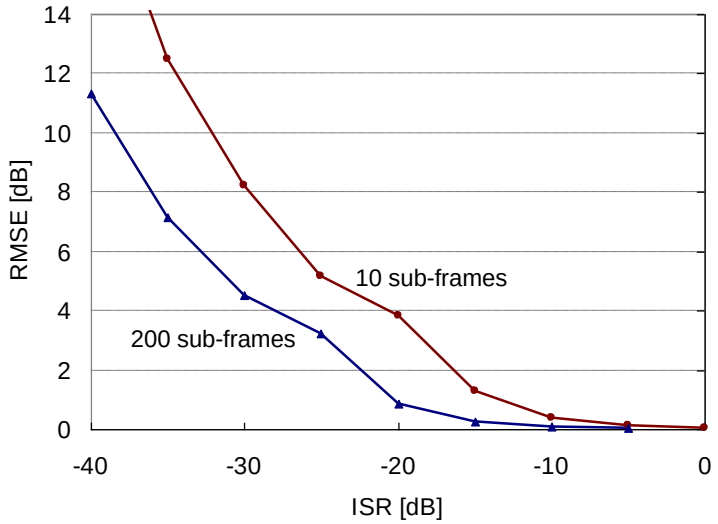

Figure 3-61: RMSE performance

3.2.3 Interference Measurement Using Cell-specific Reference Signals

Interference monitoring has been proposed aiming balanced realisation of incumbent protection and maximising capacity of opportunistic systems. Supposing cases where multiple opportunistic transmitters are operating in the same TV channel, the power of each interference signal needs to be known for the IM. Hence, the objective of the study is to develop algorithms which can accurately measure the power of each interference signal for LTE downlink signal. To achieve this objective, cell-specific Reference Signal (RS) based method is used. This method can distinguish each interference signal.

Cell-specific reference signals material can be recovered from [3GPP 36.211]. In [3GPP 36.211] it can be found that there are 4 cell-specific RS per Resource Block (RB), per antenna (when 1 antenna and 2 antennas are being used). Using the cell-specific RS lattice described in [3GPP 36.211], the UE is able to distinguish a cell from another neighbour cell.

The cell-specific RS sequences are QPSK modulated and defined by:

$$RS_{l,n_s}(m) = \frac{1}{\sqrt{2}}(1-2\cdot c[2m]) + j\frac{1}{\sqrt{2}}(1-2\cdot c[2m+1]), \quad m = 0,1,...,2N_{\mathrm{RB}}^{\max,\mathrm{DL}} - 1 \qquad \text{Eq. 3-92}$$

where n_s is the slot number within a radio frame and l is the OFDM symbol number within the slot. The pseudo-random sequences c are defined by a length-31 Gold sequence, and the pseudo-random sequence generator is initialised with

$$c_{init} = 2^{10}\cdot(7\cdot(n_s+1)+l+1)\cdot(2\cdot N_{ID}^{cell}+1)+2\cdot N_{ID}^{cell}+N_{CP} \qquad \text{Eq. 3-93}$$

at the start of each OFDM symbol, where N_{CP} = 1 for normal CP and 0 for extended CP. Please note that the value c_{init} is unique per cell.

3.2.4 Comparison of the QP Method with Cell-Specific RS Methods

Please note that for computing the RMSE of the interference measurement from Figure 3-61, the negative estimated values of Eq. 3-89 have been neglected. However, this is no longer the case for cell-specific RS-based methods. For this kind of methods, the estimated interference is computed in terms of absolute value. In the further paragraphs, two cell-specific RS methods have been considered:

- Cell-specific RS method I. This method assumes a perfect synchronization and is being employed after the FFT operation at the receiver side, after the CP is being removed.
- Cell-specific RS method II. This method is using a correlation of the received opportunistic signal in time-domain with a signal template known in advance by the receiver. This template is locally generated by the receiver and is has the usual OFDM structure but it contains only pilots without any useful data. This concept is further represented in Figure 3-62: the top figure represents an OFDM signal composed from useful data (blue) and RS (red), and the bottom figure represents the OFDM signal template composed from RS only (red).

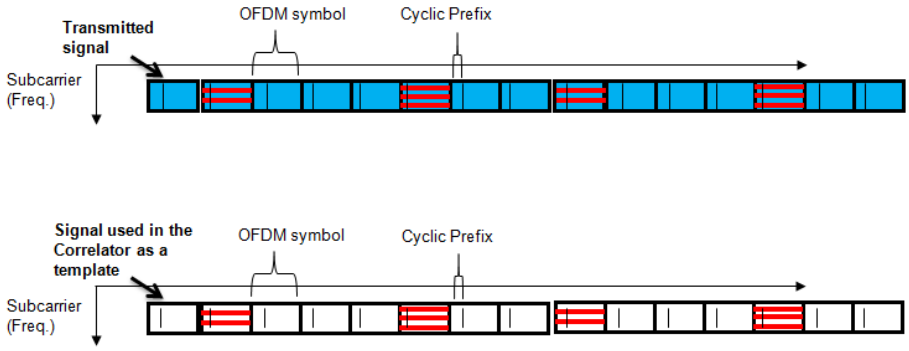

Figure 3-62: Description of cell-specific RS method using correlation in time-domain

Cell-specific RS method I used for estimating the interference can be described by

$$\hat{I} = \left| \frac{1}{N_{RS}} \sum_{j=0}^{N_{RS}-1} r[j] \cdot RS^*[j] \right|^2 = \left| \frac{1}{N_{RS}} \sum_{j=0}^{N_{RS}-1} \left(\sqrt{I} \cdot RS[j] + n[j] + s[j] \right) \cdot RS^*[j] \right|^2 \quad \text{Eq. 3-94}$$

where N_{RS} is the total number of RS from the lattice structure described in [3GPP 36.211]. As previously mentioned, the lattice structure provides the position of the RS after the FFT operation at the receiver side. r is the total received signal on the RS positions from the lattice, $RS[j]$ is the (known) cell-specific reference signal on the received sample j, $n[j]$ is the received noise sample on RS j, and $s[j]$ is the received DVB-T sample on RS j.

Cell-specific RS method II used for estimating the interference can be described by

$$\hat{I} = \max_{0 \le \tau \le N_{FFT}+N_{CP}-1} \left(\left| \frac{1}{N} \sum_{j=0}^{N} \left(\sqrt{I} \cdot i[j+\tau] + n[j+\tau] + s[j+\tau] \right) \cdot i_{RS}^*[j] \right| \cdot \frac{P_i}{P_{i_{RS}}} \right)^2 \quad \text{Eq. 3-95}$$

where N is the total time-domain number of samples used for estimation, $\sqrt{I} \cdot i$ is the received opportunistic signal of power I, i is the received normalized opportunistic signal, i_{RS} is the known signal template computed from the known cell-specific RS, $n[j]$ is the received noise sample j, and $s[j]$ is the received DVB-T sample j. P_i/P_{iRS} is the known power ratio between the opportunistic signal containing both useful data and RS, and between the signal containing only RS.

Figure 3-63 presents a comparison of cell-specific RS method I with cell-specific RS method II assuming perfect synchronization (τ=0). The comparison has been performed for a 5 MHz LTE signal, for a 10 ms and 200 ms measurement period respectively. The figure presents the RMSE and the standard deviation (STD) of the measurement error, versus ISR in dB. The ISR has been varied from -40 dB to 0 dB and it is the time-domain ISR, as in section 3.2.2. It can be easily seen that the performance of the two cell-specific RS methods is similar when assuming perfect synchronization. Since the cell-specific reference signals are not distributed in the entire frequency band, method I has the advantage of capturing less noise. However, compared with method I, method II beneficiates from the use of CP and therefore the performance is slightly better as confirmed by Figure 3-63.

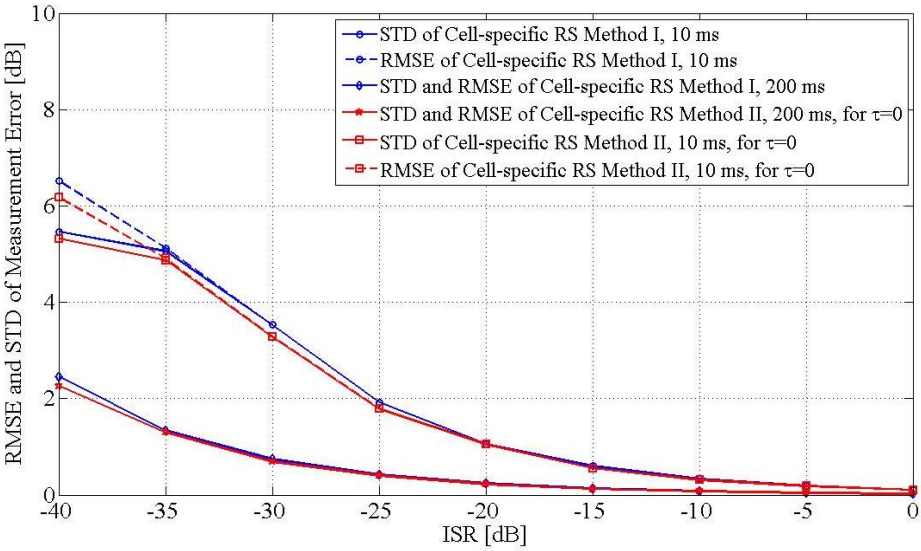

Figure 3-63: Comparison between cell-specific RS method I and cell-specific RS method II, assuming perfect synchronization (τ=0)

In Figure 3-64 it is represented the RMSE and the STD of the measurement error [dB] versus ISR [dB], for all the IM studied methods. The results from this figure have been obtained for one 5 MHz LTE transmitter. The measurement used 1 antenna, for 10 and 200 ms measurement durations, 10% quiet period (for QP-based method), SNR_{DVBT}= 30dB, 1000 realizations, without fading. The results for cell-specific RS method I have been obtained by supposing a perfect synchronization of the receiver used for measurement. However, cell-specific RS method II is not assuming perfect synchronization and the interference estimation plus the synchronization is performed by employing a correlation in time-domain. By comparison with Figure 3-63, one can easily see that the wrong synchronization modifies the RMSE, especially for 10 ms measurement duration when the receiver cannot synchronize perfectly for all realizations if the ISR is below -25 dB.

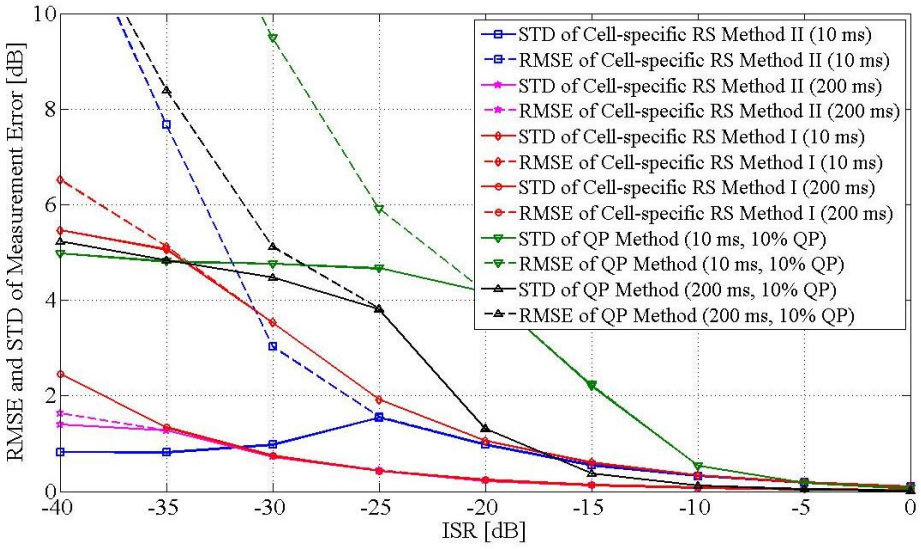

Figure 3-64: Comparison between cell-specific RS methods and QP methods

It has been found that for cell-specific RS methods, for 200 ms measurement duration, the RMSE is less than 3 dB. However, at low ISR, 10 ms seems to be an insufficient measurement duration since the RMSE is above 4 dB. It can be also seen that the QP-based method is better than cell-specific RS-

based method only for high values of ISR (above -10 dB). A similar result can be found when analyzing the PDF of the measurement error in Figure 3-65. The PDF peak of QP method is centered on 0 dB measurement error and is higher than the one of cell-specific RS method, indicating better performance of QP method at high ISR. The histograms have been further compared with reference Gaussians having the same variance and mean and it has been found that for ISR = 0 dB, the PDF of the measurement error [dB] is almost Gaussian.

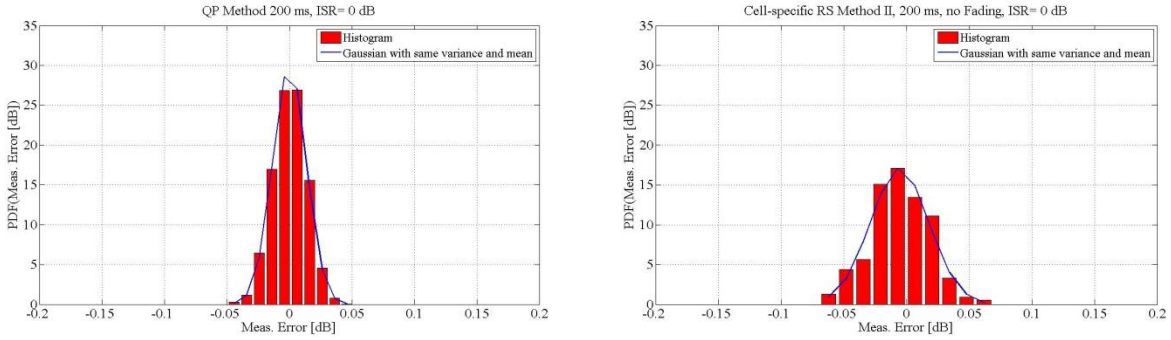

Figure 3-65: PDF of the measurement error [dB] for QP (left hand side) and cell-specific RS method II (right hand side) for 200 ms

For simulations under fading effect it was considered an Extended Pedestrian A model as in [3GPP 36.521] and [3GPP 36.141]. Figure 3-66 clearly shows that under fading, the performance of the cell-specific RS method is affected by an asymptotic bound and the RMSE does not reach 0 dB when ISR = 0 dB. In high ISR regions it is better to use QP method.

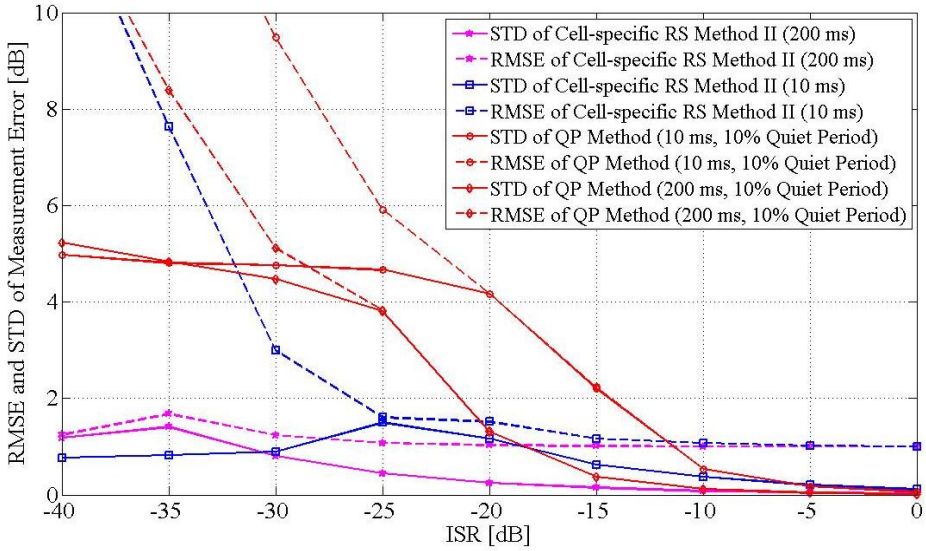

Figure 3-66: Comparison between cell-specific RS method II and QP method, under fading effect

3.3 Identification of Opportunistic Systems

3.3.1 Generalities

In September 2010, FCC published a second Memorandum [FCC10] that allows TVWS communication for the specific application of "super Wi-Fi hot spot" (See [QoSMOS_D13] for more details). For this application, spectrum sensing is no longer mandatory and only database solutions are

required to protect the incumbents. From [OFCOM10] it can be understood that the regulation in the UK is likely to follow the same trend.

The database solution catalogues the incumbents' bands and provides a portfolio of channels that could be used by CR systems. However, this portfolio, held by the regulator, is for protection purpose only and does not provide any information about a CR system that could appear in the "white" channels. A second tier database, aimed at opportunistic users, could be held by other stakeholders to complete the portfolio with real-time information about the whole spectrum at certain locations. The white space opportunistic usage is likely to end up with very dynamic situations where sensing may provide relevant information about achievable link quality and appropriate back up channel identification. As a consequence, white space monitoring by sensing is gaining importance in comparison to sensing for incumbent protection.

The requirements for opportunistic user detection differ from the ones to be considered for incumbent detection. In the case of incumbent detection, it is required to have an extremely high detection probability ratio which translates into high sensitivity detectors using a priori knowledge about the system to detect. Matched filters or feature based detectors fall into this category. On the other hand, opportunistic system waveforms may vary significantly and less a priori information can be exploited. The sensitivity requirement can be relaxed in this case though.

For these reasons, WP3 should carry on refining the requirements, the sensing method and the framework of the sensing device, and this section of the document will address these new considerations.

The first idea is related with the WP4 works which propose new techniques for the PHY layer modulation used by the opportunistic systems. In particular, FBMC (Filter-bank Multi-Carrier) modulation appears to be a promising alternative of OFDM modulation, and a solution is proposed to detect this new modulation in section 3.1.4. In the literature, a FBMC sensing technique has been proposed in [Zhang08]. They propose to insert cyclostationary signatures in the OFDM/OQAM transmitted signal in order to achieve efficient signal detection. A common work between WP3 and WP4 has been performed in order to have a joint design of the PHY layer and the sensing technique.

The second idea is to address the multi-band detection among the portfolio of channels that could be used by opportunistic systems. The multi-band technique should detect opportunistic signals over multiple frequency bands rather than over one band at a time. As the sensitivity requirement can be relaxed, a low complexity low latency method is developed in order to have a fast answer of which band could be used by a new opportunistic user.

Finally, as the opportunistic system waveforms may vary significantly, an opportunistic receiver could have the functionality of classifying and identifying the waveforms that are potentially present in a band. Many studies have been proposed to identify and characterize standards. However, they are locally optimal solutions, dedicated to a restricted number of standards (for example, standards based on OFDM modulation [Bouzegzi08]). The issue that shall be addressed is the definition of an algorithm which fits best with all the constraints of a multi-standard system. In this context, blind system identification could be proposed in order to extract and identify the characteristics of a generic waveform.

3.3.2 Watermarking

CR system can use different approaches to determine spectrum occupancy. The first is to query a database of the positions of the radio transmitters and their parameters (power, frequency) in order to deduce a map of the spectrum occupation. Another approach is to directly detect the signals using spectrum sensing approach. If the first can protect perfectly the incumbents, it could not help the management of resource allocation among opportunistic users. Detection techniques must be specifically adapted to the opportunistic users.

The detection of opportunistic users may be considered by the joint approach of the design of the physical layer of opportunistic users and the design of their detection.

In the literature, many detection techniques have been proposed. Those that offer the highest levels of sensitivity for a given detection time are those that use a priori information of the signal. However some signals do not contain many intrinsic signatures, in that case only blind algorithms can detect them.

The proposed solution relies on the following idea: the detection can be considered by the explicit introduction of specific signatures (or watermark) in the transmitted signal.

3.3.2.1 State of the Art

The introduction of signatures in the transmitted signal has already been addressed in the literature [Sutton08], [Zhang08]. They propose to insert cyclostationary signatures in some carriers of the signal to obtain an efficient detection of the signal. These solutions are highly dependent on the modulation used (OFDM, FBMC, etc.) and reduce the spectral efficiency of the system.

Unlike [Sutton08] and [Zhang08], the proposed scheme is to insert a signature independent of the modulation used. It does not insert cyclostationary features into the signal but adds a watermark. The detection scheme differs from conventional detectors because it relies on the detection of the watermark, not the detection of the useful signal.

In our approach, the watermark is inserted with a very low power in order to keep the transmitted signal. Thus, a receiver must be able to demodulate the signal without knowledge of the watermark. Only the detector uses the watermark to detect the signal.

3.3.2.2 Signal Detection Using Watermark Insertion

3.3.2.2.1 System Model

In order to introduce the system, the study case where an opportunistic user "User 2" wants to use the spectrum white spaces of incumbent systems is considered. Before performing its communication, this user must detect whether the free bands are already occupied by another opportunistic user "User 1" or not. The principle of the proposed detection is to insert a watermark in the transmitted signal and to use this watermark to help their detection by other opportunistic users.

Figure 3-67 describes the system model of the watermark insertion in the signal of user 1 and its detection by user 2. This figure describes two communication chains:

- The transmission of user 1 through channel 1 in order to test the influence of the watermark insertion on the quality of the user 1 demodulation.
- The transmission of user 2 through channel 2 in order to test the quality of the detection of user 1 by user 2.

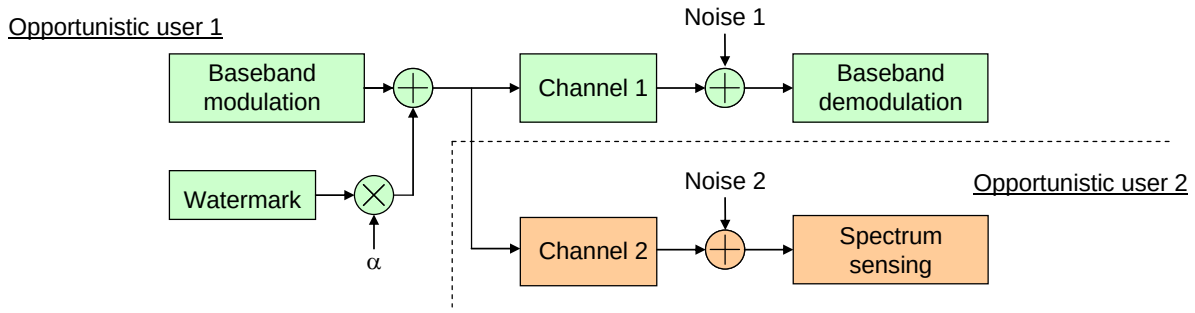

Figure 3-67: System model of the watermark insertion in the signal of User 1 and its detection by User 2

The proposed watermarking scheme is based on the watermarking of an audio signal described in [Baras06] where the hidden information is inserted into an audio signal.

The proposed watermarking consist in adding the signal *w(t)* with the signal *s(t)*. With the watermark power σ_w^2=1, the power of the watermark insertion in the signal *s(t)* depends only on the coefficient α and is characterized by the ratio WSR (Watermark to Signal Ratio) given by:

$$\mathrm{WSR} = 10.\log_{10}\left(\frac{\alpha^2}{\sigma_s^2}\right), \qquad \text{Eq. 3-96}$$

with σ_s^2 the power of the transmitted signal.

The watermark is defined by its power α and its length *L*. In a first step, we consider that the watermark follows a Gaussian distribution i.e., $w(t) \sim \mathrm{N}\left(0, \sigma_w^2\right)$.

The watermark inserted into user 1 should improve its detection by other users. The aim of the detector is to detect the presence of the watermark, not to detect the signal. Thus, the detection can be stated as the following hypothesis (in the case of an AWGN noise):

$$\begin{cases} \mathrm{H}_0 : \mathrm{r}_2(\mathrm{t}) = \mathrm{n}_2(\mathrm{t}), \\ \mathrm{H}_1 : \mathrm{r}_2(\mathrm{t}) = \alpha\, \mathrm{w}(\mathrm{t}) + \mathrm{s}(\mathrm{t}) + \mathrm{n}_2(\mathrm{t}). \end{cases} \qquad \text{Eq. 3-97}$$

$n_2(t)$ is the reception noise. The case where H_0 is the presence of a non-watermarked signal can also be considered, that is:

$$\mathrm{H}_0 : \mathrm{r}_2(\mathrm{t}) = s(t) + \mathrm{n}_2(\mathrm{t}) \qquad \text{Eq. 3-98}$$

The detection is performed by computing the correlation between the received signal and the watermark that must be known by the receiver. The output of the correlation is given by:

$$\mathrm{c} = \frac{\langle \mathrm{r}_2, \mathrm{w} \rangle}{\mathrm{L}} = \begin{cases} \dfrac{\langle \mathrm{n}_2, \mathrm{w} \rangle}{\mathrm{L}} & \text{si } \mathrm{H}_0, \\ \dfrac{\langle \mathrm{s} + \mathrm{n}_2, \mathrm{w} \rangle}{\mathrm{L}} + \alpha & \text{si } \mathrm{H}_1, \end{cases} \qquad \text{Eq. 3-99}$$

L is the length of the watermark and is also the number of samples used to compute the correlation.

The decision variable *T* is then computed:

$$\mathrm{T} = \max\left(E[c]\right) \qquad \text{Eq. 3-100}$$

where *E* [] is the mathematical expectation operator. In practice, the detector uses a total number of samples N_s to estimate the expectation value.

3.3.2.2.2 Implementation of the transmitter

Figure 3-68 shows the insertion of the watermark into the transmitted signal. It consists of adding the watermark to the digital transmitted signal. This is done so just before the Digital to Analog Conversion (DAC).

To set the system, the most important parameter is the insertion power α characterized by the ratio WSR defined by Eq. 3-96. This ratio should be as high as possible so that the insertion has the least influence on the useful transmitted signal. Typically, the simulation results show that a ratio of 15dB does not degrade system performance.

The choice of code is also important. It is characterized by its length *L* and must have good auto-correlation/cross-correlation properties to be easily detectable. It must also be uncorrelated with the useful signal.

In the simulations, a Gaussian random sequence (ideal autocorrelation property) is first used. Then, codes of literature conventionally used in spread spectrum systems [Kohno95] as in UMTS are utilized. These codes are orthogonal, however this feature is not essential. Pseudo-random non-orthogonal codes, such as the Gold codes, could have been used.

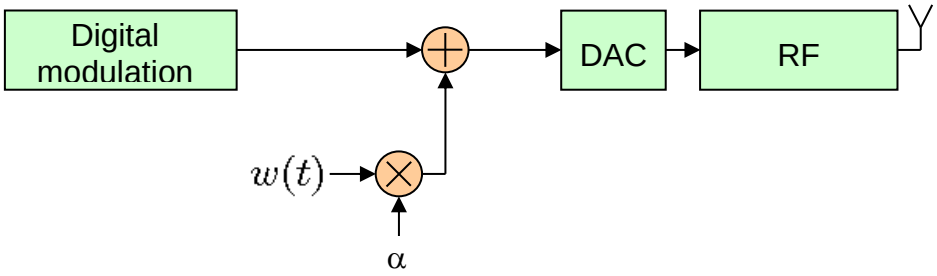

Figure 3-68: Implementation of the watermark insertion

3.3.2.2.3 Implementation of the Detector

Figure 3-69 presents the architecture of the detector. First, the correlation is performed between the received signal and the code used in the transmitter side. Then the expectation operation of Eq. 3-100 must be estimated. This operation could be performed by a first order IIR filter. The length of the filter is denoted *N* and is directly responsible of the time needed to provide the decision.

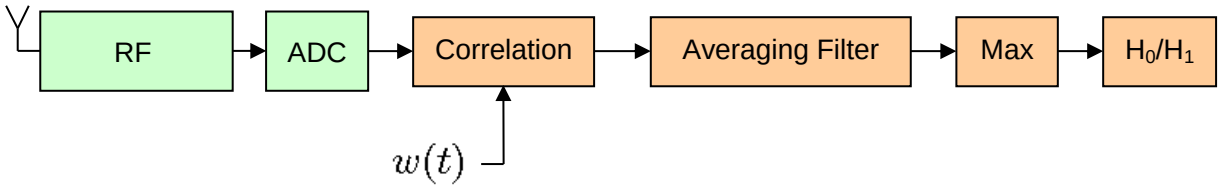

Figure 3-69: Implementation of the detector

By increasing *N*, the accuracy of the estimation is increasing and therefore the algorithm can detect the presence of the watermark with a lower signal to noise ratio. Once the average performed, the decision is done on the maximum output of the filter.

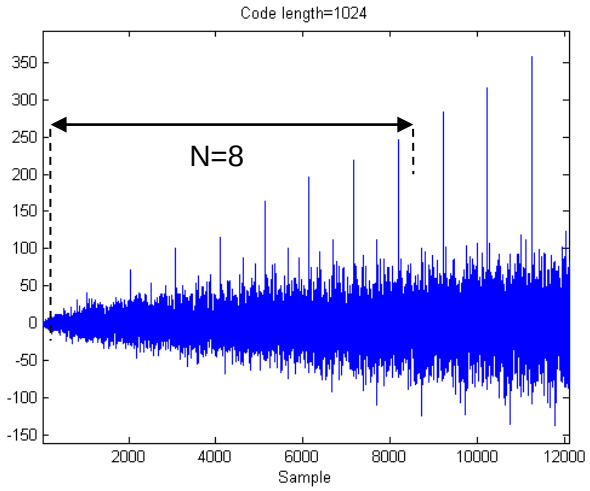

Figure 3-70: Output of the averaging filter

L being the length of the watermark, the number of samples *Ns* used for the detection is:

$$Ns=N.L \quad \text{Eq. 3-101}$$

Figure 3-70 illustrates how the detector operates by showing the output of the averaging filter. It shows the correlation peaks that increase gradually as the average is calculated.

3.3.2.3 Theoretical Performance

This section presents the theoretical performance of the proposed system and a validation with simulation results. These results are important to set the system's parameters.

3.3.2.3.1 Watermark Insertion Sensibility

First, the influence of the watermark on the transmission quality of user 1 must be evaluated. Taking Gaussian assumptions ($s(t) \sim N\left(0, \sigma_s^2\right)$), theoretical Bit Error Rate (BER_{th})is:

$$\mathrm{BER}_{\mathrm{th}} = \frac{1}{2}\mathrm{erfc}\left(\sqrt{\frac{E_b}{N_0 + 2a}}\right), \quad \text{Eq. 3-102}$$

with E_b the energy per bit, N_0 the spectral density of the noise $n_2(t)$ and erfc the well-known complementary error function.

Figure 3-71 shows the theoretical BER for different WSR. Performance is compared with simulation results. For the simulations, the signal *s*(t) is an OFDM modulation with 4-QAM non-coded symbols per sub-carriers. The number of sub-carriers is set to 1024, producing a zero-mean Gaussian signal due to the central limit theorem. The watermark *w*(t) is also a Gaussian signal.

Figure 3-71 shows that the simulation performance perfectly matches the theoretical curves. The results show that the watermark insertion leads to an E_b/N_0 degradation less than 1 dB (for a target BER of 10^{-3}) and for WSR less than -15 dB.

3.3.2.3.2 Signal Detection Characteristics

The performance of the watermark detection is evaluated. Taking Gaussian assumptions for the signal, the code and the noise, the correlation output statistics could be derived as:

$$u \sim \begin{cases} N\left(0, \frac{\sigma_n^2}{N_s}\right) & \text{if } H_0, \\ N\left(0, \frac{\sigma_s^2 + \sigma_n^2}{N_s}\right) + a & \text{if } H_1. \end{cases} \quad \text{Eq. 3-103}$$

Figure 3-72 shows the density of probability of the correlation output u for both hypothesis H_0 and H_1 (with Ns=128, WSR=-5 dB and SNR=-15 dB). H_0 density average is 0 while H_1 density average is 51 samples.

The probability of detection PD depends directly on the choice of the detection threshold λ. This choice is a trade-off between false alarms and good detections as shown in Figure 3-72.

Non-detections represent the red area in Figure 3-72. The non-detection probability PND is computed by:

$$\mathrm{PND} = \mathrm{Prob}(u < \lambda | H_1) = \frac{1}{2} - \frac{1}{2}\mathrm{erfc}\left(\frac{\lambda - \alpha}{\sqrt{2\frac{\sigma_s^2 + \sigma_n^2}{Ns}}}\right), \quad \text{Eq. 3-104}$$

Finally, the detection probability PD is given by:

$$PD = 1 - PND \qquad \text{Eq. 3-105}$$

False alarms represent the blue area on Figure 3-72. The theoretical false alarm probability is given by:

$$PFA = Prob(u \geq \lambda | H_0) = \frac{1}{2}\,\mathrm{erfc}\left(\frac{\lambda}{\sqrt{2}\,\frac{\sigma_n^2}{Ns}}\right), \qquad \text{Eq. 3-106}$$

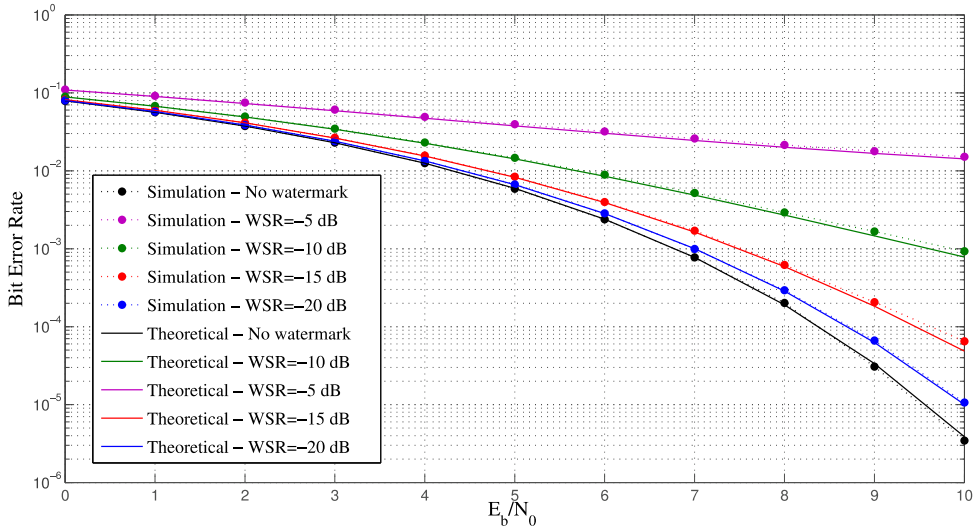

Figure 3-71: Insertion sensibility: BER versus E_b/N_0 for several watermark power WSR

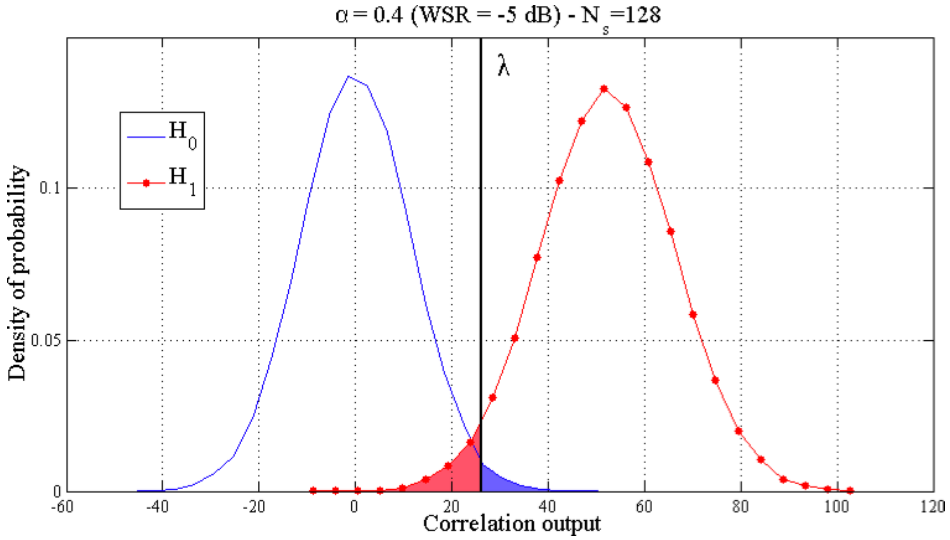

Figure 3-72: Density of probability of the correlation output for H_0 and H_1

Figure 3-73 shows the theoretical PFA and the theoretical PND for different WSR. Performance is compared with simulation results. The simulation settings are the same as for Figure 3-71. The detector uses N_s= 8192 samples with a code length L=1024. Figure 3-73 shows that the simulation performance perfectly matches the theoretical curves. The results show that Gaussian conditions (for the signal, the watermark and the noise) leads to an efficient detector where signals with SNR down to -20 dB could be detected.

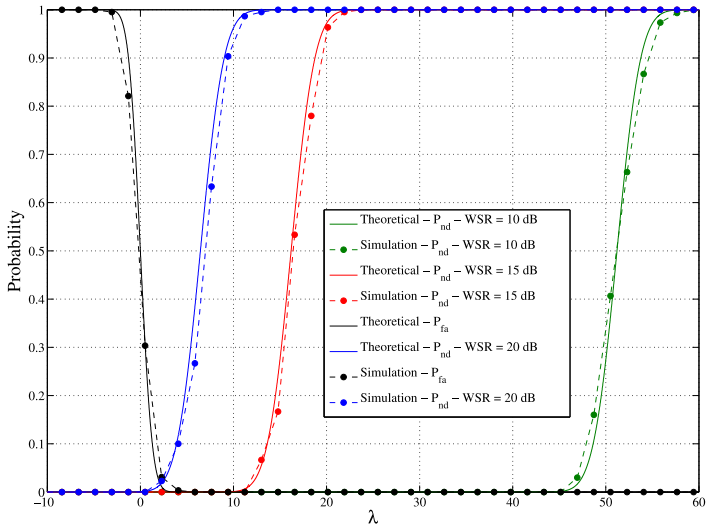

Figure 3-73: False alarm probability and non-detection probability versus detection threshold

3.3.2.4 Simulation Results

In this section, FBMC modulation with 256 sub-carriers is performed on 4-QAM non-coded symbols. It has been shown [Noguet11] that this modulation is a good candidate for the opportunistic use of the spectrum. Furthermore, this modulation suffers from its lack of cyclostationary features so being a good study case for the watermarking technique proposed herein. The watermarking is performed using a Hadamard code with L=1024.

The main feature of a detector is its sensitivity level expressed in SNR. In the following, the sensitivity is the minimum SNR that the detector could sense with PD = 95% and PFA = 10%.

The first results show how to increase the detection sensitivity using 2 parameters of the systems: the insertion strength WSR and the detection time *N*. Simulation results are introduced in Figure 3-74 and Figure 3-75.

Figure 3-74 shows the detection probability as a function of SNR for several insertion strengths WSR and for *N*=1. Figure 3-75 shows the detection probability as a function of SNR for a WSR of -15 dB and for several duration of detection *N*. In both results, the fixed threshold leads to a false alarm probability of 10%.

Simulations results in Figure 3-74 show that the watermark allows the detection of signals with SNR between to -1.5 dB and 11.5 dB for a WSR varying between -20 dB and -5 dB. The choice of WSR depends on the targeted link quality. In the following, WSR=-15dB will be used.

Results in Figure 3-75 show how improving the signal detection by increasing the integration time. Around 2 dB are gained by doubling the integration time leading to a detection sensitivity of -8.2 dB for *N*=8.

Then, performance of the proposed detector is compared with those of the energy detector. Figure 3-76 shows the sensitivity in SNR as a function of the integration time *N* for both watermark detector and energy detector. The sensitivity increases faster for the watermark detection than for the energy detection. Thus, for an integration time higher than 8, the watermark detector outperforms the energy detector. For *N*=16, a 3.4 dB gain is achieved.

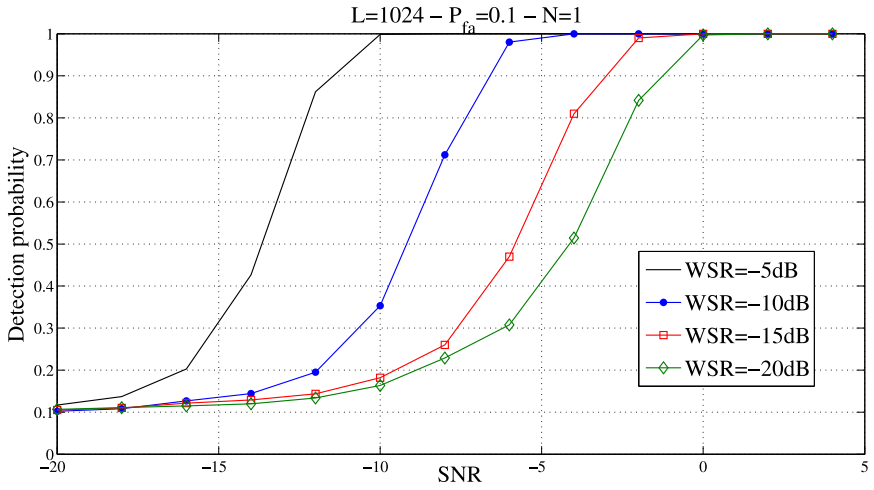

Figure 3-74: Detection probability versus SNR for different WSR

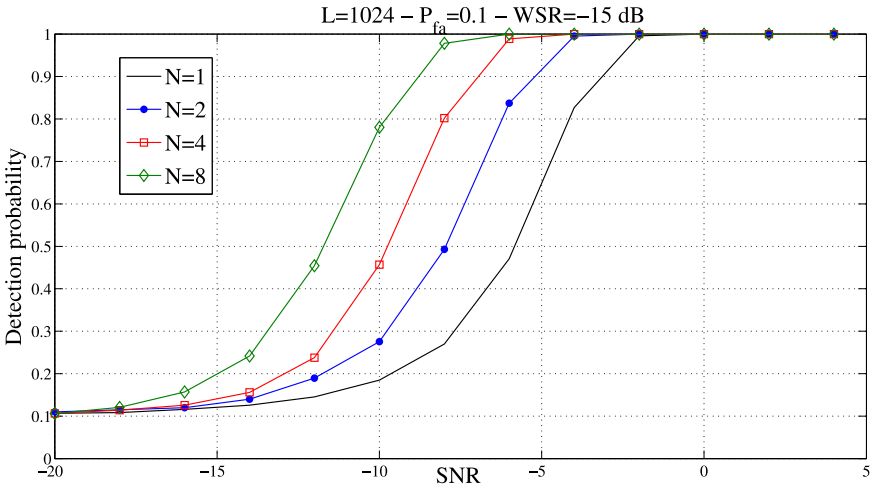

Figure 3-75: Detection probability versus SNR for different integration time N

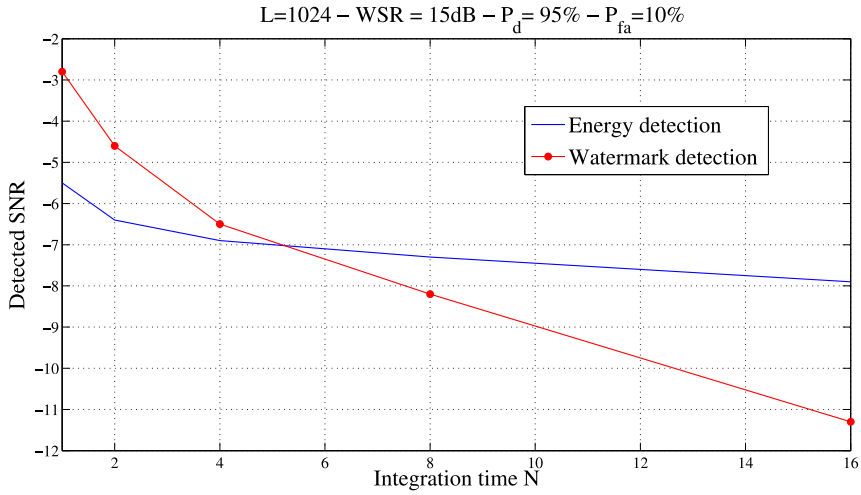

Figure 3-76: Detection sensibility in SNR versus integration time N

3.3.2.5 Conclusion

A new signal detector for cognitive radio systems has been introduced. It detects the watermark that has been inserted in the transmitted signal at a very low power. Theoretical performance and implementation discussion allow the setting of the system through the trade-off between the signal detection performance and the degradation of the communication quality. In realistic conditions, simulation results show that the proposed detector outperforms the energy detection and could detect SNR down to -11 dB with a reasonable detection duration.

3.4 Blind Frequency Localization

The Localization Algorithm based on Double-thresholding (LAD) method was originally proposed in [Vartiainen05]. The LAD method is a blindly operating signal detection method that can be used in spectrum sensing by detecting the presence or absence of a signal. It detects frequency domain signals whose relative bandwidth is less than 90% of the studied bandwidth. The purpose of the LAD method is to reduce the problems of falsely separated and detected signals. The LAD method is based on the usage of two thresholds, the upper and lower thresholds. The lower threshold avoids separating a signal, as the upper threshold avoids false signal detection. The LAD thresholds can be calculated, for example, using the Forward Consecutive Mean Excision (FCME) algorithm. The FCME algorithm is as an energy detector and, thus, not suitable for spectrum sensing purposes as such. However, the thresholds calculated by the FCME method can be used in the LAD processing.

The FCME algorithm is a forward type outlier detection method that obtains the detection threshold blindly, i.e., without the knowledge of the noise power or detected signal types. The iterative notch-type FCME algorithm uses the Constant False Alarm Rate (CFAR) principle used in the energy detection of unknown signals. In the CFAR type methods, the threshold setting is performed using a predetermined false alarm rate, so the probability of false alarm stays constant. The FCME algorithm separates the set of samples into two sets: noise sample set below the threshold and narrow-band signal sample set above the threshold. Threshold parameter γ_{cme} is selected based on the desired clean sample rejection rate [Vartiainen10_2] and squared (frequency domain) samples are rearranged in an ascending order according to their sample energy. About 10% of the smallest samples are selected to form the initial set Q. Iterative threshold calculation consists of two steps. At step one, threshold $\gamma_h = \gamma_{cme}\overline{Q}$ is calculated, where $\bar{\cdot}$ is the mean. At step two, samples $< \gamma_h$ are added to the set Q. Steps one and two are repeated until there are no new samples below the threshold. As a result, samples above the threshold are signal samples. The threshold setting is illustrated in Figure 3-77.

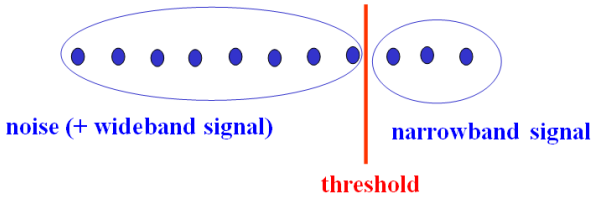

Figure 3-77: The FCME threshold setting procedure. The threshold separates signal samples (dots) into two sets: the noise set and thenarrow-band signal(s) set

In the LAD method, the threshold setting algorithm is run twice with two different threshold parameters, i.e., the upper (γ_1) and lower (γ_2) threshold parameters so that $\gamma_1 > \gamma_2$, to get the upper (γ_u) and lower (γ_l) thresholds. After the threshold calculation, adjacent samples above the lower threshold are grouped together to form a cluster. If the largest element of a cluster exceeds also the upper threshold, the cluster is decided to correspond to a signal. The LAD method can be used to estimate the bandwidths, centre frequencies and SNR values of several unknown signals. After the LAD processing, there are m' estimated sets of narrow-band signals and one noise set. The SNR estimate for the k^{th}, $k=1, \ldots, m'$, estimated narrow-band signal is [Vartiainen10_2]

$$\widehat{SNR}_k = \frac{\hat{P}_k^i}{\hat{P}_w} \quad \text{Eq. 3-107}$$

where $\hat{P}_k^i = \frac{1}{N_k}\sum |I_k(n)|^2$, where $\{I_k\}$ is the received frequency domain sample set belonging to the k^{th} estimated narrow-band signal set, N_k is the number of those samples, and $\hat{P}_w = \frac{1}{K}\sum |W(n)|^2$, where $\{W(n)\}$ is the received frequency domain samples belonging to the noise set, and K is the noise set size.

The LAD method has several enhancements. The LAD with Adjacent Cluster Combining (ACC) proposed in [Vartiainen07] uses an extra test after the LAD processing. That is, one or some samples are allowed to go below the lower threshold without breaking the signal into two parts. This reduces the frequency fluctuation and significantly improves the performance without increasing the probability of false alarm too much. The LAD and the LAD ACC methods are illustrated in Figure 3-78.

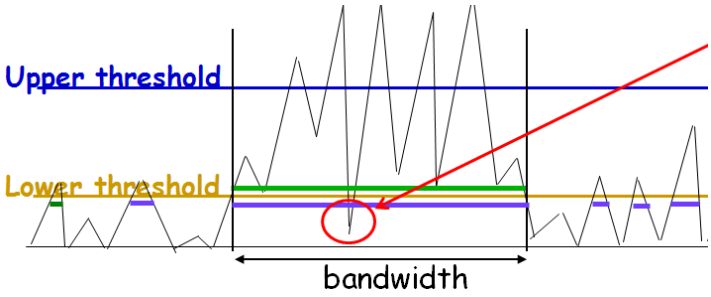

Figure 3-78: The LAD and the LAD ACC methods. Red circle denotes the sample(s) that ACC allows to go below the lower threshold without breaking the signal

The LAD with Normalized Thresholds (NT) was proposed in [Vartiainen07] to reduce the computational complexity. There, the threshold is calculated only once, and the upper and lower thresholds are derived from that using constant coefficient. The drawback is that the desired and obtained false alarm rates are not equal. This approach has been used in [Vartiainen12]. There, the mean from the one threshold was used and 10/6 dB was added to get the upper and lower thresholds, respectively. Doing this, the thresholds are not too sensitive to the changes in the noise.

The two-dimensional (2-D) LAD method originally proposed in [Vartiainen10_3] corresponds to binary detection that is used in radar systems. Once the LAD method has clustered the samples, there are *m'* clusters caused by unknown narrow-band signals. Because of the needless separation of signals, the number of estimated signals is usually larger than the number of present signals *m*, that is, *m'>m*. This problem can be solved using the 2-D processing. The 2-D processing considers *r* consecutive sweeps a.k.a. time instants (LAD/LAD ACC results) so that one frequency domain sample is considered in time. When a frequency domain sample belongs to the signal at least *p* times out of *r* time instants, that specific frequency domain sample is decided to belong to the signal. The goal is to reduce the time fluctuation. A flowchart of the LAD methods is illustrated in Figure 3-79.

The threshold parameters are usually calculated based on the desired clean sample rejection rate which is to be decided. The resulting threshold parameters vary according to the assumed noise distribution. For example, the larger the desired clean sample rejection rate is, the smaller the threshold parameter is. This yields to small threshold and large amount of false alarms. The proper choice of the desired clean sample rejection rate depends on the application and situation. In spectrum sensing applications, low threshold parameter causes falsely detected signals, as large threshold parameter may cause that the signal is not detected at all. The control of desired clean sample rejection rate is important in spectrum sensing, because it is directly related to the loss of spectral opportunities and to the interference caused. The proper threshold parameters are considered in [Vartiainen10_2]. The thresholds can be set also manually, but then the false alarm rate is not controlled if the noise level is

unknown as it usually is. In [Lehtomäki11], median filtering with the FCME algorithm (MED-FCME) was proposed in order to enable stable thresholds even in the cases when there are no signal-free reference samples. The performance of the MED-FCME which uses adaptive noise floor estimation was studied using indoor measurements in ISM-band.

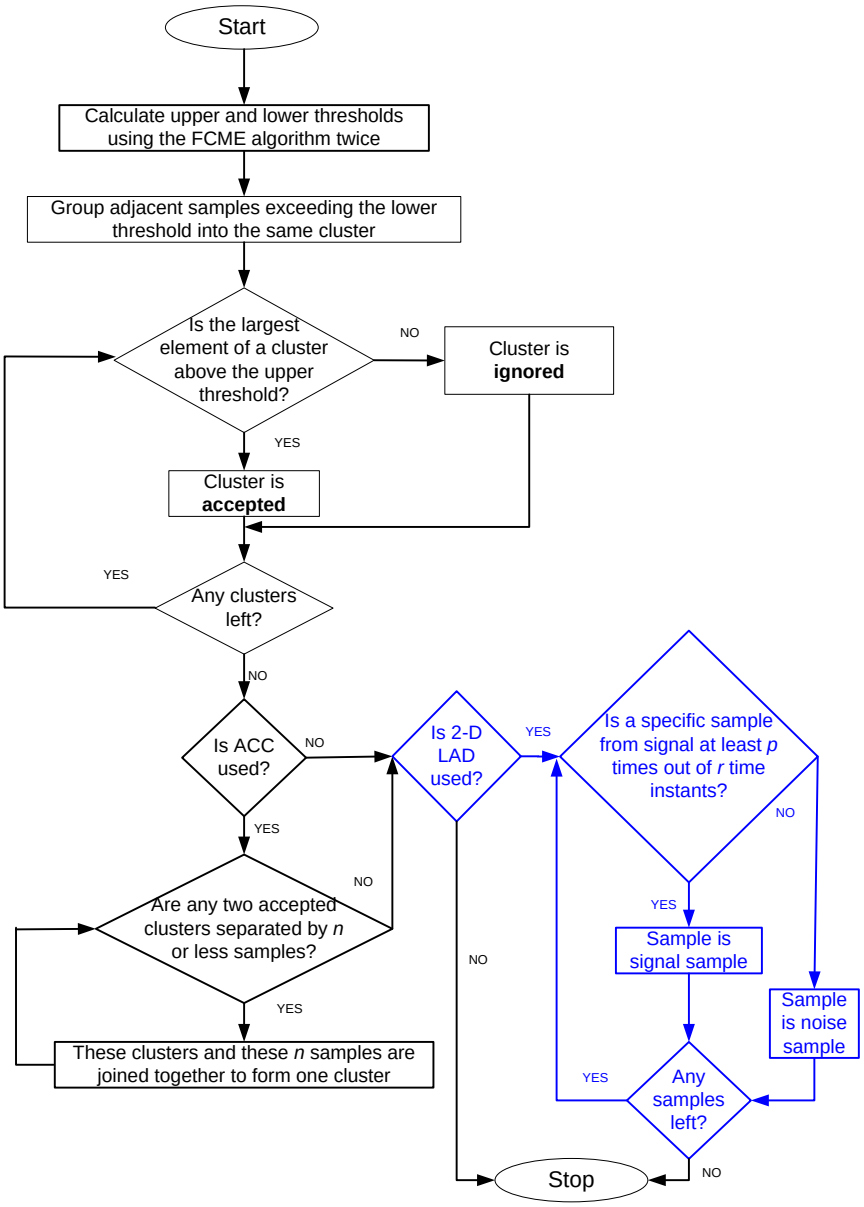

Figure 3-79: Flowchart of the LAD methods

The LAD methods have several benefits. First, no side-information is needed. In other words, no a priori information about the signals, their parameters, modulation, etc. is needed. Thus, the LAD methods are blind. The only requirement is that the signal(s) should be narrow-band with respect to the studied bandwidth. Second, the computational complexity of the LAD methods is relatively low. It is $N\log_2 N$ because of the fast Fourier transformation and sorting. The sorting can be done using, for example, Heapsort or Quicksort. The clustering and the 2-D processing have no effect to the overall complexity [Vartiainen10_2]. This enables real-life implementation. In 2010, the original LAD method was implemented on the wireless open-access research platform [Hänninen10].

The LAD methods calculate the thresholds using some assumption about the noise distribution. Usually it is assumed that the noise is Gaussian. However, this is not necessarily true in practice. It has been shown that the LAD methods are able to operate even though the noise is not pure Gaussian but from real-life measurements [Vartiainen10_2].

The LAD methods in multi-path situations have been considered, for example, in [Vartiainen11_2], [Vartiainen12]. In those papers, real-life WLAN bands were considered and real-life tests were performed. In [Vartiainen11_2], fixed phase shifts were used, as in [Vartiainen12], ETSI BRAN/WLAN channel models B and C with random phase shifts, Doppler effect and fading were used. In both papers, the LAD methods performed very well. As expected, the 2-D LAD method outperformed the LAD ACC method. However, no MATLAB simulations about a multi-path case have been presented until now. In the MATLAB simulations there were one sinusoidal signal with 0-2 multi-path components and AWGN noise. The mathematical model can be expressed as

$$s(t) = A(t)d(t) + \sum_{i=0}^{2} a_i d(t - \tau_{\alpha,i}) \qquad \text{Eq. 3-108}$$

where *A(t)*, *d(t)*, a_i and $\tau_{\alpha,i}$ denote amplitude, received sinusoidal signal, amplitude of i^{th} multi-path and delay of i^{th} multi-path. The length of the FFT was 512 samples, and the bandwidth of the sinusoidal signal was 0.2% of the considered bandwidth. The upper and lower threshold parameters were 13.81 and 2.66, respectively, and the ACC parameter was 3. These parameters have earlier been noticed to be proper choices [Vartiainen10_2]. There were one or two multi-path components with random phase shifts and with delays of 1/2/3/5/6/8/10/20 time domain samples and powers of 50% (1 multi-path component) and 25% (2 multi-path components) from non-multi-path component. The number of Monte Carlo iterations was 5000. The detection was performed if the method found the signal on the right frequency bin. Here, 98% detection probability means that in 98% of the cases, the signal was found. This is used instead of 100% detection probability because at multi-path case, the detection probability had some fluctuation around 100% because of the very narrow-band signal. The results for the LAD and LAD ACC methods are presented in Table 3-9. The results are the same for the LAD and LAD ACC methods because the studied signal was very narrow-band sinusoidal and clustering was not needed. It can be seen that in every studied case, there was no detection loss at 98% detection probability when compared to non-multi-path case. In other words, in order to detect the signal in 98% of the cases, equal power is required when compared to non-multi-path case.

Thus, the only difference between the non-multi-path and multi-path case is that when the signal is very narrow-band, i.e., covers one frequency bin, the probability of detection did not reach 100% in the multi-path case. Instead, there is some fluctuation between 99.8%...100%. When there were 2 multi-path components with delays of 2 and 5 time domain samples and the powers were equal which is quite an unrealistic case, the detection probability did not reach 100%. Instead, it was at most between 96-98%.

Table 3-9: Simulation results in the multi-path case for the LAD and LAD ACC methods

# of multi-path components	Power (From non-multi-path component)	Delay (Time domain samples)	98% detection probability compared to non-multi-path case
1	1/2	3	No loss
1	1/2	6	No loss
1	1/2	8	No loss
2	1/2, 1/4	1, 2	No loss
2	1/2, 1/4	2, 5	No loss
2	1/2, 1/4	10, 20	No loss

4 Distributed Processing and Data Fusion

In this section, the focus is made on distributed processing and data fusion. In this case, measurements come from spatially distributed sources.

This section is divided into three subsections corresponding to:

- The **influence of metrics parameterization** (latency of data transport, resolution of the data sent to the data fusion centre)
- Collaborative spectrum sensing based on **beta reputation system**
- **Impact of mobility** (which is one of the main concerns of QoSMOS) on spectrum sensing

4.1 Influence of Metrics Parameterization

4.1.1 Scenario and Main Issues

Figure 4-1 depicts the coexistence of an incumbent system with an opportunistic system. The incumbent system has a transmitter and the cognitive radio system has sensing nodes (which can be incorporated in the CR terminals). The nodes sense the spectrum and send the data (with eventually some processing) to the data fusion centre where a decision is made about the presence or absence of an incumbent transmitting source. The figure shows only one incumbent transmitter but in practice several incumbent systems may be considered as long as the CR sensors have the capability to scan several bands. The same principles apply whether considering one or multiple possible incumbent systems.

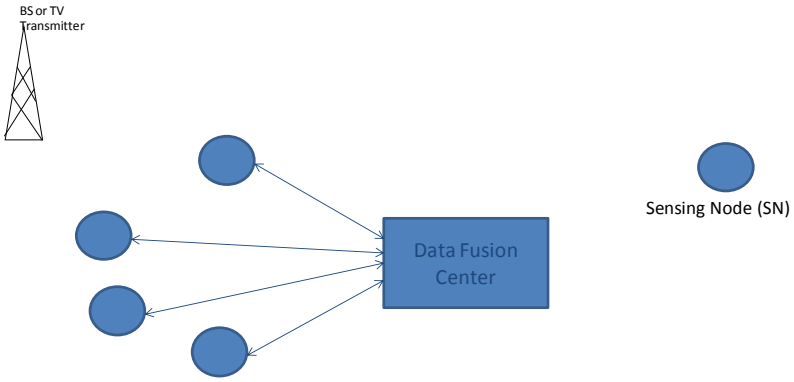

Figure 4-1: System and concept under analysis

There are several issues in sensing incumbent users in a mobile wireless environment. Some of them depend significantly on the nature of the incumbent user while others are caused by the variability of the wireless channel between the incumbent transmitter(s) and the opportunistic sensing node(s).

If the incumbent user is continuously transmitting or silent during a long period of time, as it happens with TV transmitters then there is not much concern with the time needed for detection. However, in some cases the incumbent may have bursty traffic with the on and off periods lasting a few milliseconds. This implies that the opportunistic user needs to detect onset of incumbent and switching off in real time to avoid causing harmful interference to the incumbent user. The sensing challenge is significantly larger in this latter case. For low interference to the incumbent and high spectral efficiency for the opportunistic user, the detection delay for on and off should be very small.

The issues that are caused by the nature of the propagation channel come from the time varying nature of mobile channels which cause the received signal power at the sensing node to fluctuate in time. These fluctuations can be considerable. Furthermore there is the hidden terminal problem where the

cognitive radio sensing node may be hidden from the incumbent transmitter. Moreover, the different incumbent users may use different modulation schemes, transmit powers, channel access technologies, etc.

Thus, spectrum sensing algorithms should be fast, robust and detect a signal at very low SNR. Therefore, signal detection by multiple cognitive sensing nodes at various places and collaborating with each other might be necessary, leading to the architecture shown in Figure 4-1. In Figure 4-1, we consider a hierarchical architecture where the edge nodes have only sensing capabilities, while decisions are performed centrally at the fusion centre. In this hierarchical architecture the sensing nodes report only to the fusion centre and do not exchange information between them. An alternative is to have a distributed architecture where the sensing nodes exchange information between them and collaboratively take decisions.

There are different types of sensing as energy detector, matched filtering, cyclostationary feature detection, etc. as described in section 2.1. However, when considering the formation for the architecture with multiple nodes and a fusion centre, the differences brought by the different sensing algorithms are reflected in different conditional probability functions. Let the observation at node *i* be X_i, where X_i can be the detected power in the case energy detection is employed or another statistic if other features are employed such as the cyclic correlation for a known cycle in the case of cyclostationarity detection. Let θ =0 be the hypothesis that an incumbent source is not present or not active and θ =1 the hypothesis that an incumbent source is present and active at the time sensing is performed. Because of the fact that the mobile channel is variable and because of the receiver noise at the sensing node, the variable X_i is random with a conditional distribution

$$p_{X_i|\theta}(x_i \mid \theta) \qquad \text{Eq. 4-1}$$

where θ is the value of the hypothesis.

The influence of the detection method arises in the specific conditional PDF in Eq. 4-1 , but formally there is no difference as far as the final fusion algorithm is concerned. The goal for the data fusion algorithm is based on the observations X_1, ...,X_n drawn from distributions $p_{x_i/\theta}(x_i/\theta)$ reported by the different sensing nodes to make a decision about the presence or not of the incumbent source.

In the hierarchical framework of Figure 4-1 we have two possibilities for the methodology to perform a decision and also several possibilities for the decision criteria. For the methodology they are basically one shot versus sequential, while for the criteria the most common is a Bayesian approach but others like the Neyman-Pearson can be used.

4.1.2 One Shot Detection

In the one shot decision, are considered:

- Observations: X_1, ...,X_n which come from distributions $p_{x_i/\theta}(x_i/\theta)$
- Two hypothesis corresponding to θ =0 or θ =1.

Based on this data the fusion centre decides on one of the two hypotheses and the performance criterion is based on the probability of correct detection

$$\Pr\left(\hat{\theta} = \theta \mid \theta\right) \qquad \text{Eq. 4-2}$$

where $\hat{\theta}$ is the decided hypothesis.

The criterion optimization can be done following several approaches. In the Bayesian approach [Chair86] one decides on the hypothesis θ if the a posteriori probability for θ is higher than the a posteriori probability for $\bar{\theta}$ ($\bar{\theta}$ is the complementary hypothesis of θ), i.e.

$$\frac{\Pr(1|x_1,...,x_N)}{\Pr(1|x_1,...,x_N)} \underset{0}{\overset{1}{\gtrless}} 1 \Leftrightarrow \frac{\Pr(x_1,...,x_N|1)}{\Pr(x_1,...,x_N|0)} \underset{0}{\overset{1}{\gtrless}} \frac{P_0}{P_1} \quad \text{Eq. 4-3}$$

where P_0 and P_1 are the a priori probabilities.

The criterion can be refined using different costs for the different types of errors. In fact, since it is mandatory to avoid harmful interference to the incumbent user it is meaningful to give a higher cost to the probability of a misdetection (i.e. there is an incumbent source but algorithm indicates that there is not) than to a false detection (there is no incumbent user but the algorithm indicates the presence of one).

Defining the costs associated with the different decisions as

$$C_{ij} = \Pr(\hat{\theta} = i | \theta = j) \quad \text{Eq. 4-4}$$

it is easy to verify that the decision rule that minimizes the average cost is given by:

$$\frac{\Pr(x_1,...,x_N|1)}{\Pr(x_1,...,x_N|0)} \underset{0}{\overset{1}{\gtrless}} \frac{P_0(C_{10}-C_{00})}{P_1(C_{10}-C_{11})} \quad \text{Eq. 4-5}$$

The Bayesian approach assumes that the a priori probabilities are known which may not be the case in a significant number of situations involving cognitive radios ([Chen07] finds these probabilities iteratively considering that the fusion decision is more accurate than the ones in each node). In such cases, a decision rule that does not depend on assumptions about the a priori probability of each hypothesis is needed. Here, the Neyman-Pearson (NP) criterion offers an alternative to the Bayesian framework. The NP criterion maximizes the probability of a correct decision conditioned to hypothesis 1 subject to a constraint on the probability of false alarm i.e.

$$\max \Pr(\hat{\theta} = 1 | \theta = 1) \qquad s.t. \quad \Pr(\hat{\theta} = 1 | \theta = 0) \le \alpha \quad \text{Eq. 4-6}$$

This leads to a decision region for hypothesis 1

$$R_1 : \left\{ \mathbf{x} : \frac{\Pr(x_1,...,x_N|1)}{\Pr(x_1,...,x_N|0)} > \gamma \right\} \quad \text{Eq. 4-7}$$

where the constant γ is chosen so that

$$\int_{R_1} \Pr(x_1,...,x_N|0) d\mathbf{x} \le \alpha \quad \text{Eq. 4-8}$$

This criterion is given by [Visotsky05]

$$\frac{\mathbf{1}^T \Sigma^{-1} \mathbf{SNR}_U}{\mathbf{1}^T \Sigma^{-1} \mathbf{SNR}_U} \underset{0}{\overset{1}{\gtrless}} T_m \quad \text{Eq. 4-9}$$

$\sum$ is the covariance matrix of the system. Suppose the one-tap channel from incumbent base station to node i be h_i then $\Sigma_{ij} = h_i h_j^*$ i,j=1…N. $\boldsymbol{SNR}_U$ is the vector of the relations signal to noise at the nodes and T_m is set so that $P_r[\theta = 1/0] = P_0$. The probability of false alarm P_0 is set by the system designer.

4.1.3 Sequential Detection

It is clear that each observation has a cost and therefore one would like to minimize the number of observations the sensing nodes have to take. This leads to the concept of sequential detection where samples are acquired until the fusion centre may be confident enough in making a final decision.

The sequential decision in cognitive radio can be applied in two ways:

- *N* sensing nodes are used among N_{max} available nodes. At each instant *t*, node *i* sends to the fusion centre x_i^t. Therefore, the fusion centre receives the vector of observations

$$\underline{x}^t = [x_1^t, \dots, x_N^t] \qquad \text{Eq. 4-10}$$

  The fusion centre receives sequentially $\underline{x}^1, \underline{x}^2, \dots, \underline{x}^K$ stopping when it has enough data to allow a decision.
- Polling scheme. The fusion centre polls sequentially nodes 1 to *L*, where *L* is the number of nodes polled ($1 \le L \le N_{max}$). The data fusion centre receives the observations from each node and stops when it has enough data to make a confident decision.

The difference between the two options is the following:

- In the first option, the number of nodes involved in the observations is defined a priori (*N* corresponding to *N* sensors involved at each time). Therefore it may occur situations where *N* is higher than necessary. In this case, data that would not be necessary are sent
- In the second option the data fusion centre receives one observation at each time. Therefore if the first or second observations have a very high level of confidence it can stop quite early.

In both cases the stopping criterion is defined as:

$$\begin{aligned} N_{stop} &= \min(n \ge 1) \\ L_n &= \frac{\Pr(x_1,\dots,x_n \mid 1)}{\Pr(x_1,\dots,x_n \mid 0)} > \gamma_H \ or < \gamma_L \end{aligned} \qquad \text{Eq. 4-11}$$

where $\gamma_H > 1 > \gamma_L > 0$ are chosen such that

$$\begin{aligned} \Pr(L_{N_{stop}} > \gamma_H) &= \alpha \\ \Pr(L_{N_{stop}} < \gamma_L) &= \beta \end{aligned} \qquad \text{Eq. 4-12}$$

In the case corresponding to Eq. 4-10, *n* is a multiple of *N*, since each node is involved at each instant. This test minimizes the number of observations needed under θ=0 and θ=1 while satisfying constraints on the above two types of error.

It is worth to note that in the case of Eq. 4-10, the space diversity (i.e. the number of nodes involved in the observation process) is fixed and therefore time diversity is added until decision is confident enough. In the case corresponding to the second option space diversity is added, adding one sensing node at each instant. Roughly speaking, if T_{max} is the maximum time allowed to make a decision (in period units) and assuming independent observations, the diversity order is $N \times T_{max}$. In the second case, time diversity can be added if after pooling all the available nodes and still not having enough data to make a decision, the first node is reconsidered.

The joint conditional probabilities can be derived, knowing the type of detector used in the sensing nodes.

In the case of the energy detector, let us assume that:

- the source to be detected is zero mean, Gaussian, with power per sample σ_s^2,

- the additive noise is Gaussian with power per sample σ_w^2,
- the attenuation between the source and the sensing node from which the i[th] observation[1] is taken is equal to α_i^2,
- the number of samples taken for the energy detector is *M*

Then, if *M* is high enough, the output *x* of the ED which follows a chi-square distribution can be approximated by a Gaussian distribution with parameters:

$$\begin{aligned} x &\sim Normal\left(M\sigma_w^2; 2M\sigma_w^2\right) && \text{in presence of signal} \\ x &\sim Normal\left(M\left(\alpha_i^2\sigma_s^2+\sigma_w^2\right); 2M\left(\alpha_i^2\sigma_s^2+\sigma_w^2\right)^2\right) && \text{in absence of signal} \end{aligned} \qquad \text{Eq. 4-13}$$

The correlation coefficient between the detector outputs at node *i* and node *j* is given by

$$\rho_{ij} = \begin{cases} 0 & \text{in presence of signal} \\ \dfrac{\alpha_i^2\alpha_j^2\sigma_s^2}{\left(\alpha_i^2\sigma_s^2+\sigma_w^2\right)^2\left(\alpha_j^2\sigma_s^2+\sigma_w^2\right)^2} = \dfrac{SNR_i SNR_j}{\left(1+SNR_i\right)\left(1+SNR_j\right)} & \text{in absence of signal} \end{cases} \qquad \text{Eq. 4-14}$$

The joint conditional probability used in Eq. 4-11 is given by

$$L_n = \frac{\Pr\left(x_1,...,x_n \mid 1\right)}{\Pr\left(x_1,...,x_n \mid 0\right)} = \frac{\dfrac{1}{\sqrt{\left|\mathbf{R}^{(0)}\right|}}\exp\left(-\dfrac{1}{2}\left(\left(\underline{x}-E(\underline{x}\mid 0)\right)^T\left(\mathbf{R}^{(0)}\right)^{-1}\left(\underline{x}-E(\underline{x}\mid 0)\right)\right)\right)}{\dfrac{1}{\sqrt{\left|\mathbf{R}^{(1)}\right|}}\exp\left(-\dfrac{1}{2}\left(\left(\underline{x}-E(\underline{x}\mid 1)\right)^T\left(\mathbf{R}^{(1)}\right)^{-1}\left(\underline{x}-E(\underline{x}\mid 1)\right)\right)\right)} \qquad \text{Eq. 4-15}$$

Where $\underline{x}$ is the vector of observations (output of the ED) sent to the fusion centre and $\mathbf{R}^{(i)}$ is the correlation matrix with element defined by Eq. 4-13 and Eq. 4-14 under hypothesis *i*.

4.1.4 Quantization

The previous theory considered that the observation is sent without distortion to the fusion centre. It is clear that the more accurate is the observation transmitted to the fusion centre the more resources in terms of bandwidth will be required by the signalling channels. Therefore, one significant matter of interest is how much the information of the sensing nodes can be compressed so that the bandwidth required by the signalling channels is minimized with acceptable penalty degradation. In fact, in a practical system, the samples are not sent in analogue format but are digitized. It is obvious that if a high number of bits are used in the quantization the degradation relatively to the ideal case is negligible, but the interest is to know how far in the quantization process can be used while still guaranteeing that the degradation is below a given threshold.

We have to further distinguish between two cases:

- Conventional quantization of the analogue observation samples collected by the sensing nodes.
- Binary decision at the sensing nodes.

In the first approach there is no difference relatively to the analogue treatment addressed in the previous section, the only difference is the fact that the samples are corrupted by quantization noise. The samples *x* collected by the sensing nodes are based on noisy measurements and can therefore be written as:

[1] In the case of the Eq. 4-11, the i[th] observation is given by node $k=i \bmod N$

$$x = x_v + w_R \quad \text{Eq. 4-16}$$

where x_v is the value the observation would take in the hypothetical situation where noise free measurements were available, and w_R is the disturbance caused by the noise existing in the measurements.

When quantizing the quantized sample transmitted to the fusion centre is given by:

$$x_Q = x_v + w_R + w_Q \quad \text{Eq. 4-17}$$

where w_Q is the quantization noise.

In the second case when the sensing nodes perform a decision by themselves (which is not used for communication purposes but only to report to the fusion centre), there are new possibilities of processing at the fusion centre. Namely it opens the door to simplified data fusion techniques as:

- Majority logic, when an incumbent is declared present when the majority of sensing nodes report its presence.
- Minimum indication of incumbent activity. As referred previously, because of the need to strictly avoid harmful interference at the incumbent system, the probability of a miss is more serious than a false alarm, and therefore one can go to a more conservative criterion than the majority logic one. In the extreme case, a single indication of presence would be enough to decide on the presence.

In the decision case, the same level of importance is attributed to the decisions made at all the sensing nodes. However, it is clear that in some nodes the signal may be weaker than that in others because of shadowing and therefore one should give a larger weight to nodes that receive a clean signal. Transmitting directly the final decision neglects of course the likelihood of the decision taken. Also in the case of quantization of several levels, one may use high number of levels which are necessary to discriminate at very low levels but are irrelevant when the signal has strong power. Let us consider that for a given band the threshold level to discriminate from the existence or absence of an incumbent is -100dBm. It is clear that there would be interest in a clear discrimination around the -100dBm, but distinction between let us say -70dBm and -50dBm is completely irrelevant, and therefore a uniform quantizer could still be inefficient in terms of required bandwidth. The alternative would be to use non-uniform quantizers, but it is prefered to resort to another strategy: we quantify the likelihood of this binary decision, and transmit its quantized version.

4.1.5 Selective Reporting Algorithm

One significant issue in collaborative sensing is the overhead required for the localized sensors to transmit the information to the fusion centre. Although the information by itself may be a simple binary indication, it always requires the set-up of dedicated channels which requires resources. Moreover the transmissions from the sensors require energy. It is therefore highly convenient for energy reduction and overhead minimization purposes to devise distributed sensing schemes that minimize the number of transmissions from the localized sensors to the fusion centre. In this section, the scenario of Figure 4-1 is considered. A distributed sensing scheme that divides the sensors into two classes is proposed and analysed. This allows reducing the average number of transmissions by 50% without any loss in the performance. This algorithm has been selected for implementation in WP6 and is part of the proof of concept.

4.1.5.1 Review of the Basics

The mathematical model for binary hypothesis testing problem in the scenario of Figure 4-1 is the following

$$\begin{aligned} &\text{Primary User absent } H_0: \quad y[n] = w[n] \\ &\text{Primary User present } H_1: \quad y[n] = ax[n] + w[n] \end{aligned} \quad \text{Eq. 4-18}$$

where the following notation is used:

$n = 0,1,\cdots(N\text{-}1)$ with N the number of samples in the observation window of received signal

$x[n]$: transmitted signal, usually modelled as zero – mean AWGN with variance σ_x^2

$w[n]$: noise (zero – mean AWGN with variance σ_w^2)

$y[n]$: received signal

a: complex multiplier accounts for fading

Considering an energy detector, the decision statistic is formed summing up the energy of the received samples during the observation interval, i.e. considering that N samples are collected, the decision statistic U is given by:

$$U = \frac{1}{N}\sum_{n=0}^{N-1} |y[n]|^2 \qquad \text{Eq. 4-19}$$

and using this statistic the classical decision rule is simply

$$\begin{cases} \text{Decide } H_0 \text{ if } U < L \\ \text{Decide } H_1 \text{ if } U \geq L \end{cases} \qquad \text{Eq. 4-20}$$

Let us now consider the distributed sensing scheme for the scenario of Figure 4-1. Assuming the localized sensing variables that are sent to the fusion centre, one may have several processing algorithms, i.e. one can make a majority logic decision, use an AND or an OR for example. The most common one, for scenarios where subject to a given probability of false alarm the goal is to reduce the probability of miss detection is to the OR function. At each sensor, from Eq. 4-20:

$$\begin{cases} \text{Decide } H_0 \text{ if } U < L \text{ and send } 0 \\ \text{Decide } H_1 \text{ if } U \geq L \text{ and send } 1 \end{cases}$$

The final decision is made at the fusion centre by employing the OR rule: if at least one sensor reports 1 decides H_1 otherwise H_0. With such a rule and assuming K identical sensors, the global probabilities of false alarm are given by:

$$PFA = 1 - (1-q)^K \qquad \text{Eq. 4-21}$$

where q is the localized (at each sensor) probability of false alarm.

Similarly the probability of miss-detection is simply expressed as a function of the localized miss-detection probabilities

$$PMD = \prod_{i=1}^{K} v_i \qquad \text{Eq. 4-22}$$

where v_i is the localized probability of false alarm for sensor i (i=1,2,...K).

Eq. 4-21 can be to extended, in the case of non-identical sensors, to:

$$PFA = 1 - \prod_{i=1}^{K} (1-q_i) \qquad \text{Eq. 4-23}$$

where q_i is the localized probability of false alarm for sensor i (i=1,2,...K).

The localized probabilities for the case of energy detection considered here can be amenable to analytical formulation under some conditions. Assuming that the number of samples N is high, one can resort to the Gaussian hypothesis and we get [Cabric06]

$$\begin{cases} q = Q\left(\dfrac{K-\sigma_w^2}{\sigma_w^2\sqrt{2}}\sqrt{N}\right) \\ v_i = Q\left(\dfrac{K-\left(\sigma_w^2+|a_i|^2\sigma_x^2\right)}{\sqrt{2\left(\sigma_w^2+|a_i|^2\sigma_x^2\right)^2}}\sqrt{N}\right) \end{cases} \quad \text{Eq. 4-24}$$

where Q(.) is the complementary error function $Q(x)=\frac{1}{\sqrt{2\pi}}\int_x^\infty e^{-x^2/2}dx$.

In the case of non-identical sensors the asymptotic localized probability of false alarm is simply modified by using $\sigma_{w(i)}^2$ in the expression of q in Eq. 4-24.

4.1.5.2 Cooperative Sensing with Censorship

Several works published in the literature ([Axe10], [Lunden07], [Maleki11]), motivated by the need of reducing overhead and energy consumption at the sensors, have considered the use of a censoring policy at each sensor. Roughly speaking, the local decisions made at each sensor are sent to the FC only if they are informative.

The most common procedure defines two thresholds as shown in Eq. 4-25. Information is sent only if:

$$U>L_u \text{ (and 1 sent)}$$
$$\text{or } U<L_l \text{ (and 0 zero sent)} \quad \text{Eq. 4-25}$$

If the statistic U belongs to the interval $[L_l \;\; L_u]$ then no reporting is performed because the binary information corresponding to the local decision is not reliable enough to justify the usage of transmitted power and radio resources.

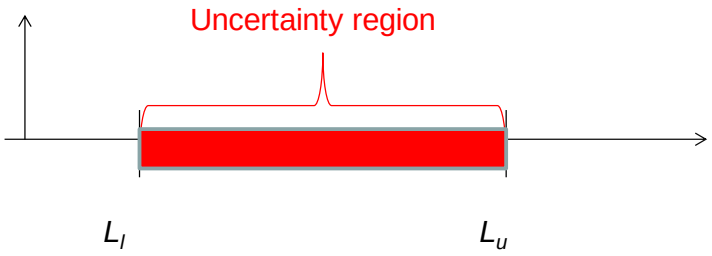

Figure 4-2: Two thresholds for cooperative sensing with censorship

Although one can significantly reduce the overhead with such a scheme, optimization requires a careful setting of the thresholds L_u and L_l , which are dependent of the probabilities of having an incumbent signal or not. If such a priori probabilities are not known or cannot be guessed, then a random choice of the thresholds does not guarantee a good ROC. This can be improved with learning procedures but this again takes time to stabilize.

4.1.5.3 Cooperative Sensing with Silence Periods

To overcome the problem associated with the conventional "censorship policy" scheme, a new distributed scheme is proposed, that essentially relies on basic information theory principles, that say silence periods may also convey information.

The basis of the proposal relies on the use of two types of sensors, that report if different events occur at each one, i.e.:

- **Type 1**: report only if decide for H_1. Do not report if decide for H_0

- **Type 2**: report only if decide for H_0. Do not report if decide for H_1

The operating mode of the type 1 sensor is shown in Figure 4-3 (left). In this figure the columns represent the hypothesis that is really occurring and the lines the decision made. The cells contain the type of message that is sent along the joint probability of $\left(\hat{H}_i;\ H_j\right)\ i, j \in \{0;1\}$. The equivalent table for a type 2 sensor is shown in Figure 4-3 (right). In these table, E indicates that no message is sent (from the word erasure) and M that a message is sent. The type of message (M) is rather irrelevant.

The only thing that counts is the identification of the transmitting node. In fact upon receiving a message, the FC knows that if it is coming from a type 1 sensor it means that this node has detected an incumbent signal, whereas if it is coming from a type 2 sensor it means that no incumbent signal was locally detected.

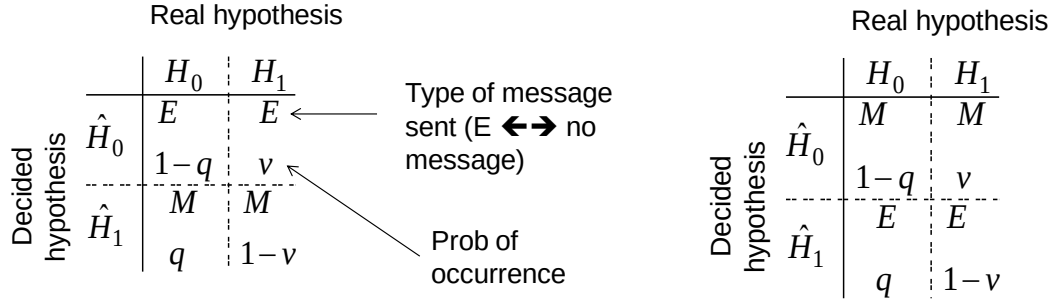

Figure 4-3: Operation of type 1 (left) sensor and type 2 (right)

Figure 4-4 illustrates the operation of the scheme considering that there are only two sensors, one type 1 and the other type 2.

Type 1 sensor			Type 2 sensor			
Local decision	Message sent to FC	Interpretation at FC	Local decision	Message sent to FC	Interpretation at FC	FC Decision (OR Rule)
0	E	0	0	M	0	0
0	E	0	1	E	1	1
1	M	1	0	M	0	1
1	M	1	1	E	1	1

Figure 4-4: Illustration of the selective reporting scheme with two sensors of different types

Let us consider the number of messages that are transmitted assuming that $K/2$ sensors of type 1 and $K/2$ sensors of type 2 are deployed. As a starting assumption it is considered that localized miss detection and false alarm probabilities are equal for all sensors.

i) Hypothesis H_0

Let us assume hypothesis H_0 where no incumbent signal is present. Conditioned to this hypothesis a type 1 sensor transmits if it makes an erroneous detection, and thus the average number of messages (T_1) coming from type 1 sensors is given by

$$E\left(T_1 \middle| H_0\right) = \frac{K}{2} q \qquad \text{Eq. 4-26}$$

while type 2 sensors transmit when they make the correct decision and then the average number of messages (T_2) coming from type 2 sensors is given by

$$E(T_2|H_0)=\frac{K}{2}(1-q) \quad \text{Eq. 4-27}$$

Therefore the average number of transmitted messages is given by

$$E(T_1+T_2|H_0)=\frac{K}{2}q+\frac{K}{2}(1-q)=\frac{K}{2} \quad \text{Eq. 4-28}$$

That is, irrespective of the localized probabilities of false alarm, the average number of transmissions is *K*/2, i.e. in average only half of the sensors transmit.

ii) Hypothesis H_1

Under hypothesis $\boldsymbol{H_1}$ type 1 sensors transmit if they make the correct detection, while type 2 sensors transmit if they miss the detection. Thus the average number of messages coming from type 1 and type 2 sensors is given by

$$\begin{cases} E(T_1|H_1)=\frac{K}{2}(1-\nu) \\ E(T_2|H_1)=\frac{K}{2}\nu \end{cases} \quad \text{Eq. 4-29}$$

Therefore the average number of total transmissions is again *K*/2,

$$E(T_1+T_2|H_1)=\frac{K}{2} \quad \text{Eq. 4-30}$$

Irrespective of the localized probabilities of miss detection, the average number of transmissions is *K*/2, i.e. in average only half of the sensors transmit.

From Eq. 4-27 and Eq. 4-30, one concludes that irrespective of the hypothesis the average number of transmissions from sensors to the fusion centre is *K*/2, which means that when there is no fading, the average number of messages when using a total of *K* sensors with half being of type 1 and half of type 2 is equal to *K*/2.

As the probability of false alarm and miss detection coincide with the ones of *K* sensors with classical transmission / detection employing an OR rule at the fusion centre, it can be concluded that with the proposed scheme the number of transmissions can be reduced by a factor of 2 without any penalty in the ROC.

4.1.5.4 Analysis

Let us now consider the distribution of the number of transmitted messages.

i) Hypothesis H_0

Under the assumptions of no fading and identical sensors, the distribution of the number of transmitted messages conditioned to H_0 is given by:

$$f_0(m)=(1-q)^{K/2}q^{K/2}\left(\frac{1-q}{q}\right)^m\sum_{l=0}^{m}\binom{K/2}{l}\binom{K/2}{m-l}\left(\frac{q}{1-q}\right)^{2l} \quad \text{Eq. 4-31}$$

from which the average and variance can be computed

$$\begin{cases} E[T\mid H_0]=K/2 \\ Var[T\mid H_0]=Kq(1-q) \end{cases} \quad \text{Eq. 4-32}$$

ii) Hypothesis H_1

Under the assumptions of no fading and identical sensors, the distribution of the number of transmitted messages and respective average and variance conditioned to H_1 is given by:

$$\begin{cases} f_1(m) = (1-\nu)^{K/2}\nu^{K/2}\left(\frac{\nu}{1-\nu}\right)^m \sum_{l=0}^{m}\binom{K/2}{l}\binom{K/2}{m-l}\left(\frac{1-\nu}{\nu}\right)^{2l} \\ E[T \mid H_1] = K/2 \\ Var[T \mid H_1] = K\nu(1-\nu) \end{cases} \quad \text{Eq. 4-33}$$

For typical designs the number of transmissions is much more concentrated around the mean for hypothesis 0 than for hypothesis 1. Let us just point out some numbers for a scenario with 10 sensors (5 of each type). If the global probability of false alarm is designed to be $p_F = 0.2$, this requires a localized probability of false alarm at each sensor $p_{locF} = 0.022$, and therefore $\sigma_{H_0} = \sqrt{Var[T \mid H_0]} = \sqrt{10 \times 0.022 \times (1-0.022)} = 0.46$, whereas designing for a global probability of miss detection 10^{-5}, gives $\sigma_{H1} = \sqrt{Var[T \mid H_1]} = \sqrt{10 \times 10^{-5/10} \times (1-10^{-5/10})} = 1.47$

4.1.5.5 Information Theoretic Interpretation of the Sensing Scheme

It may be surprising that with the selective reporting scheme one get, with fewer transmissions, the same ROC as in the case of a conventional distributed detector where the results of the local detection are always sent. This may be explained using basic concepts of information theory where it is learnt that no transmission (silent periods) may carry information. Let us consider two sensors (1 type 1 and 1 type 2) as shown in Figure 4-5 where E stands for no transmission.

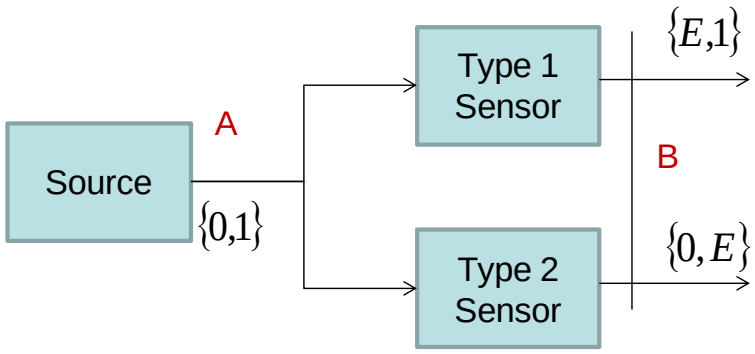

Figure 4-5: Two sensor scheme for interpretation of the behaviour of the selective reporting algorithm

It is easy to verify using the basic formulas from information theory, that the mutual information between A and B is the same if one replaces in the output alphabet of type 1 sensors E by 0 and for the type 2 sensors E by 1.

The mutual information can be increased if instead of using E as 0 for type 1 and E as 1 for type 2, we allow the use of 3 symbols, which make the promise that using a double threshold can improve the performance.

4.1.5.6 Algorithm Behaviour with Fading Channels

Let us now consider the case of fading between the incumbent system and the sensors. It is clear that when the incumbent signal is absent nothing changes. Assuming the sensors to be identical, the

formulas given by Eq. 4-31 and Eq. 4-32, can be used i.e. it can expected that the average number of transmissions is still equal to half the number of sensors.

However the things change when the hypothesis is H_1. As the signal from the incumbent system arrives at the sensors with different powers, the probability of miss detection is different for the various sensors.

Let us now consider hypothesis H_1, assume K sensors labelled as 0,1,..., K/2-1 for sensors of type 1 and as K/2, K/2+1, ...; K-1. for sensors of type 2. The probability of miss detection at sensor i ν_i, is given (under the asymptotic Gaussian approximation) by Eq. 4-24. Sensors of type 1 transmit therefore with probability (1-ν_i) and sensors of type 2 with probability ν_i. Although an analytic expression for the distribution of the number of transmissions is not amenable, the first and second order moments are quite easy to derive since it is a sum of Bernoulli variables that are independent. The additivity of the mean and variance can be invoked. The average number of transmissions for sensor i is given by

$$E[T_i \mid H_1] = \begin{cases} 1-\nu_i & 0 \le i \le K/2-1 \\ \nu_i & K/2 \le i \le K-1 \end{cases} \quad \text{Eq. 4-34}$$

Therefore

$$E[T \mid H_1] = \sum_{i=0}^{K/2-1} 1-\nu_i + \sum_{i=K/2}^{K-1} \nu_i = \frac{K}{2} + \sum_{i=0}^{K/2-1} \nu_{i+K/2} - \nu_i \quad \text{Eq. 4-35}$$

Over the long term if the environment is stationary, the average value of transmissions will be K/2, but for the reporting at a specific instant this will depend on the specific distributions of the fading from the incumbent source to the sensors.

The variance can be computed in the same way

$$\text{var}[T \mid H_1] = \sum_{i=0}^{K-1} (1-\nu_i)\nu_i \quad \text{Eq. 4-36}$$

By introducing a new level of randomness in the probabilities of miss detection, the variability of the number of transmissions will clearly increase.

4.1.5.7 Numerical Results

In this section numerical results related to the number of transmissions achieved with the proposed algorithm are presented.

The following parameters were used for the simulations:

- Number of sensing nodes: 10
  - Type 1 nodes: 5
  - Type 2 nodes: 5
- Global probability of false alarm designed for $p_F = 0.1$
- Transmitted signal and noise Gaussian
- Signal to noise ratio at the sensors in the case an incumbent signal is present
  - 0dB for the case no fading is considered
  - Uniformly distributed between [-8; 12] dB for the case fading is considered
- Number of samples used in the energy detector: 20

Figure 4-6 and Figure 4-7 report the distribution of the number of transmissions for the two different types of nodes for the case where no incumbent signal is present.

Figure 4-6 clearly shows the expected asymmetry between the distributions. The type 1 nodes are silent most of the time whereas the type 2 nodes are transmitting with a high probability.

In Figure 4-7 it is clear to identify the symmetry around the average value which is equal to half the number of sensors, i.e. 5, with the distribution highly concentrated near this value.

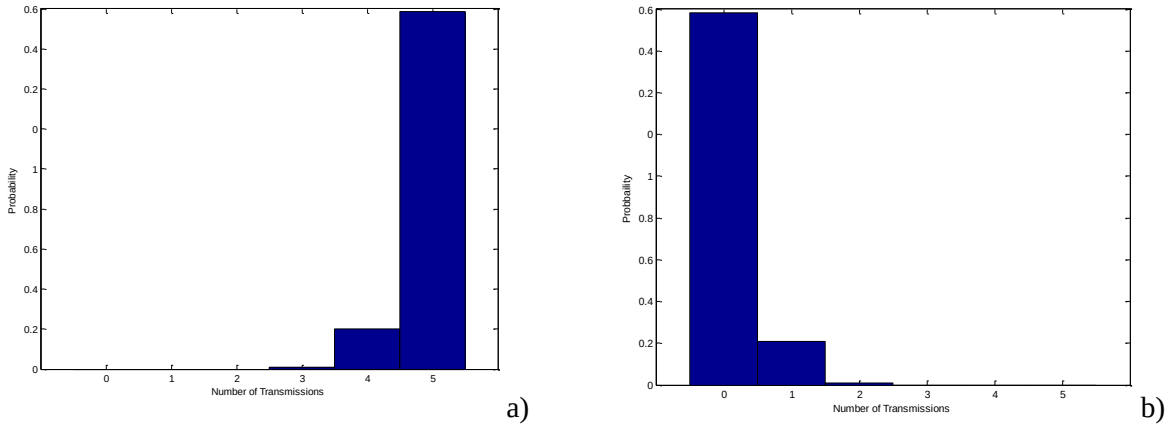

a) b)

Figure 4-6: Distribution of the number of transmissions for the type 2 nodes a) and type 1 b), Hypothesis H_0

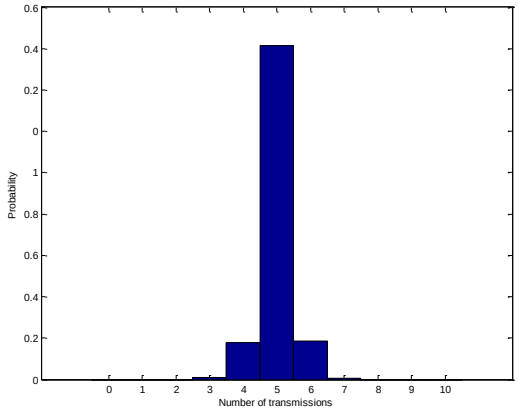

Figure 4-7: Distribution of the total number of transmissions. Hypothesis H_0

The average value if transmissions in the case reported in Figure 4-7 is very close to the statistical mean as it can be seen by the high concentration of transmissions around 5 and the symmetry of the histogram. A wider spread will occur if the threshold is changed to give a larger probability of false alarm. However, to notice significant asymmetry one has to increase the probability of false alarm to 0.3, which is a design value seldomly used in practical systems. This is shown when a much larger dispersion around the mean and an asymmetry can be seen (in this particular simulation for values above the mean).

Figure 4-9 and Figure 4-10 report the distribution of the number of transmissions for the two different types of nodes for the case where the incumbent signal is present. No fading is assumed and the path loss is such that the SNR at each node is equal to 0dB. In these figures, it can be seen a larger spread in the distributions as it was anticipated in the theoretical analysis. However the mean is very close to half the number of nodes in Figure 4-10.

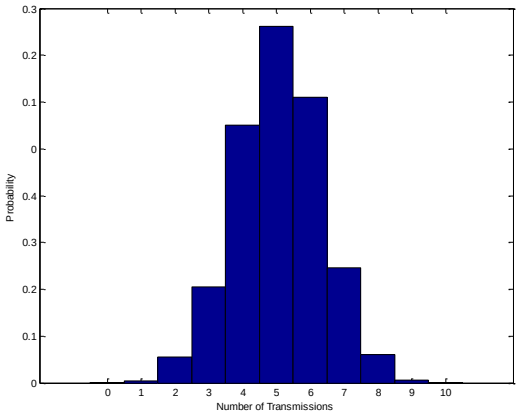

Figure 4-8: Distribution of the total number of transmissions. Hypothesis H_0 and probability of false alarm designed for 0.3

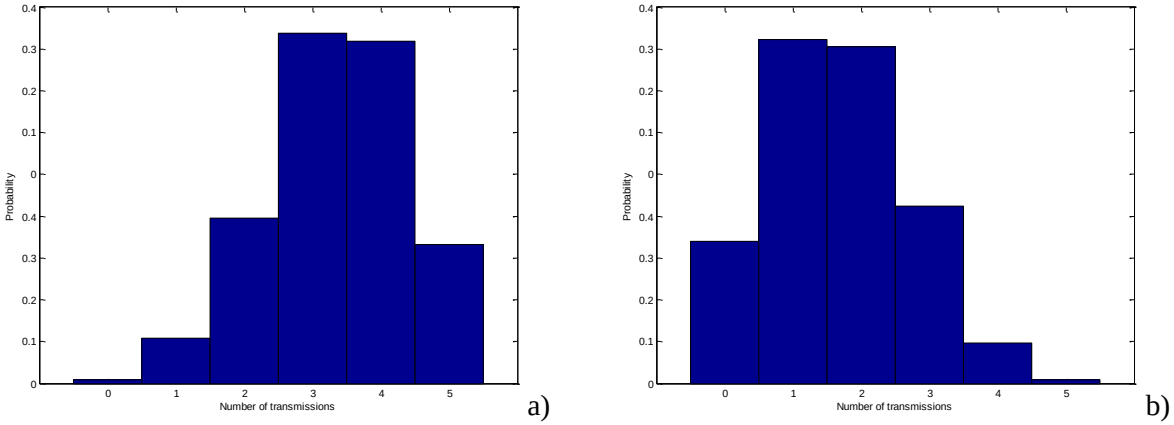

Figure 4-9: Distribution of the number of transmissions for the type 2 nodes a) and type 1 b). Hypothesis H_1 and no fading

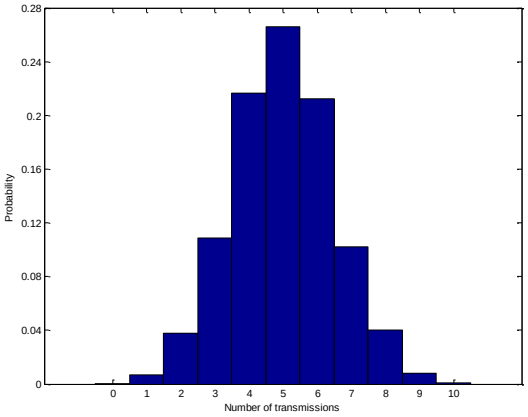

Figure 4-10: Distribution of the total number of transmissions. Hypothesis H_1

In Figure 4-11, the behaviour in the average number of transmissions is evaluated as a function of the SNR which is equal for all nodes. The figure shows that within a 12dB fluctuation range the results are very close to the theoretical statistical mean.

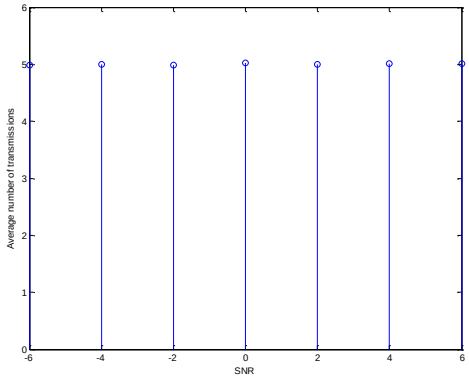

Figure 4-11: Average number of transmissions as a function of the SNR. Hypothesis H_1 and no fading

Figure 4-12 and Figure 4-13 show the probability distributions in presence of fading, i.e. the SNRs at each node may be different. For these figures the SNR is assumed to vary uniformly in the interval [-8; 10] dB. Figure 4-12 shows a wider spread in the number of transmissions. In both plots (a) and (b) one can notice, at the opposite edge of the point where the probability is expected to be maximum, an increase in the density. This arises because, for the type 1 sensors, there may be nodes with very low SNR that simply cannot detect the incumbent signal and contribute to an enhancement for the value of 0. The opposite arises for the type 2 nodes. Nevertheless the distribution of Figure 4-13 turns out to be very symmetric and the mean is very close to 5.

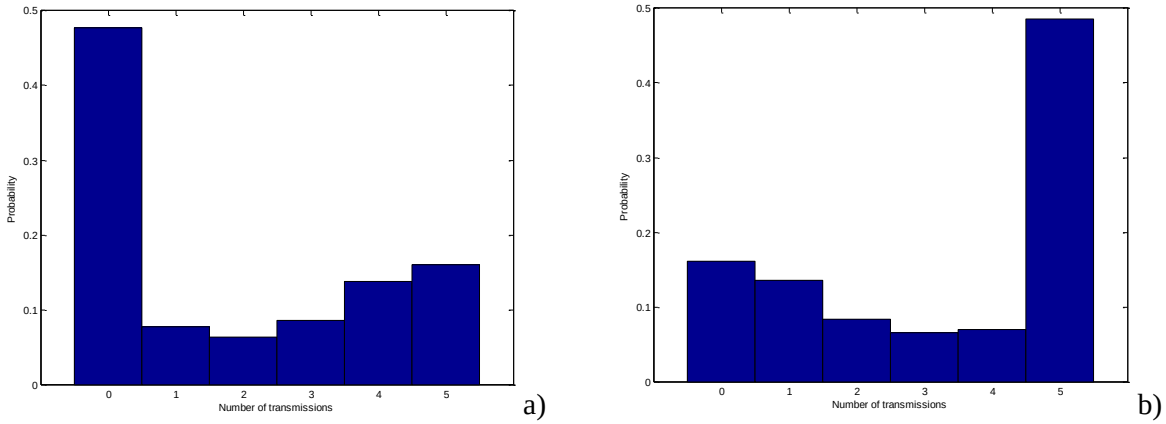

Figure 4-12: Distribution of the number of transmissions for the type 2 nodes a) and type 1 b). Hypothesis H_1 and fading leading to SNR uniformly distributed in [-8; 10] dB

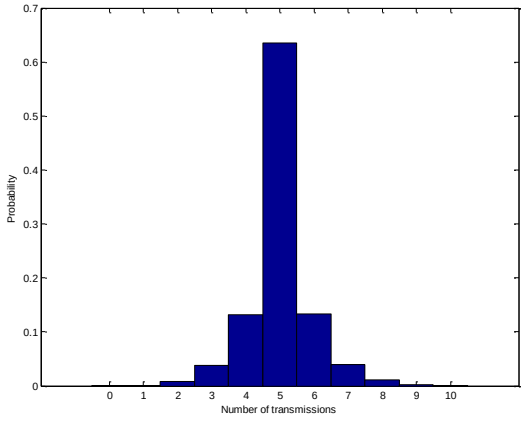

Figure 4-13: Distribution of the total number of transmissions. Hypothesis H_1 and fading leading to SNR uniformly distributed in [-8; 10] dB

To evaluate the expected value of the number of transmissions, higher deviations in the SNR span were considered. in Figure 4-14, four cases are presented. The SNRs at the different nodes may vary in the intervals [-8*k*; 10*k*] dB with *k* taking the values 1, 2, 3, 4. The results show that although the SNRs vary, the average number of transmissions is still very close to the theoretical statistical value. In general one can say that for the parameters of interest that can summarized in a PFA lower than 0.1 and a PND 10^{-3}, and for a moderately large number of sensors, the distributions are quite sharp and the number of transmissions very close to the mean.

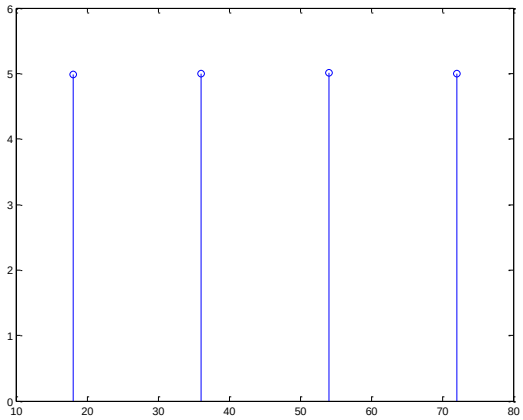

Figure 4-14: Average number of transmissions as a function of the SNR. Hypothesis H_1 and fading leading to different spans for the SNR

4.1.6 Selective Reporting Based on State Transitions

The second considered selective algorithm is state-based. There are a wide number of scenarios where the states "absence" / "presence" can be considered as long term. For example in the case of TV transmitters, the shut-down of the transmitter is in most of the cases a permanent event. Even if it is temporary, the shutdown will take place for a long time compared to the duration of elementary radio resources of most common wireless systems. The same occurs if the incumbent system is a cellular base station that can be shut down temporarily or in the case of more sophisticated power saving schemes like putting the station in a sleep mode [Sake10]. These two events can also be categorized as long term. It is clear that if the probability of state transition from " incumbent signal present" to " incumbent signal absent" or vice-versa is low, it is much more meaningful to report the information to the fusion centre in the scenario of Figure 4-1 only in cases where each node detects a state transition rather than the true value each time a detection is performed.

4.1.6.1 State Models for the Case of Constant Underlying Process

In the following, let us consider that the underlying process (i.e. the presence or absence of an incumbent signal) is stationary. It means that the incumbent signal is on in a permanent basis. In such a case the transition diagram conditioned to either H_0 or H_1 is quite simple and the stationary probabilities can be easily computed.

Let us consider a given node, for which the transmission from the node to the fusion centre is error free. Let us also consider that the fusion centre performs the OR operation based on the binary information corresponding to the detection or not of an incumbent signal. Furthermore, let us consider that the nodes only transmit to the fusion centre when there is a change in the detection at the node. This can be easily modelled with a two state diagram where the states are R (right) which means that the last decision of the node was correct, or W (wrong) which means that the last decision at the node was incorrect.

i) Hypothesis H_0

With such an underlying hypothesis, the state diagram is shown in Figure 4-15, where $P_{F_{loc}}$ is the localized probability of false alarm.

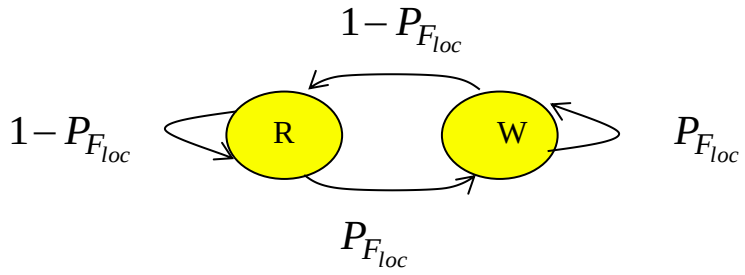

Figure 4-15: State diagram for underlying hypothesis H_0

The stationary probabilities for the R and W states can be easily written as:

$$\begin{cases} \Pr(R \mid H_0) = 1 - p_{F_{loc}} \\ \Pr(W \mid H_0) = p_{F_{loc}} \end{cases} \quad \text{Eq. 4-37}$$

ii) Hypothesis H_1

With such an underlying hypothesis, the state diagram is shown Figure 4-16 where $P_{M_{loc}}$ is the localized probability of miss detection. The two diagrams are identical only the labelling is different. One is using the localized probability of false alarm and the other one the localized probability of miss detection.

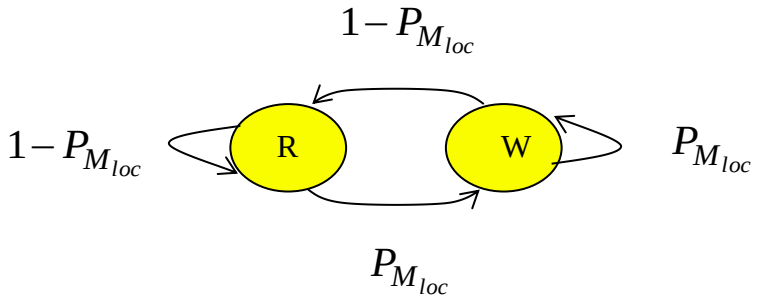

Figure 4-16: State diagram for underlying hypothesis H_1

The stationary probabilities for the R and W states are then given by:

$$\begin{cases} \Pr(R \mid H_1) = 1 - p_{M_{loc}} \\ \Pr(W \mid H_1) = p_{M_{loc}} \end{cases} \quad \text{Eq. 4-38}$$

The analysis of the expressions given by Eq. 4-37 and Eq. 4-38 indicates that the same performance as with a conventional cooperative sensor will be achieved. In fact the previous state diagrams are the ones of the nodes and nothing is different.

Let us now consider the reporting. This is illustrated in Figure 4-17. Once again E means no message transmitted and M message transmitted. The state diagram covers both cases where p is the localized probability of false alarm under H_0 and the localized probability of miss detection under H_1.

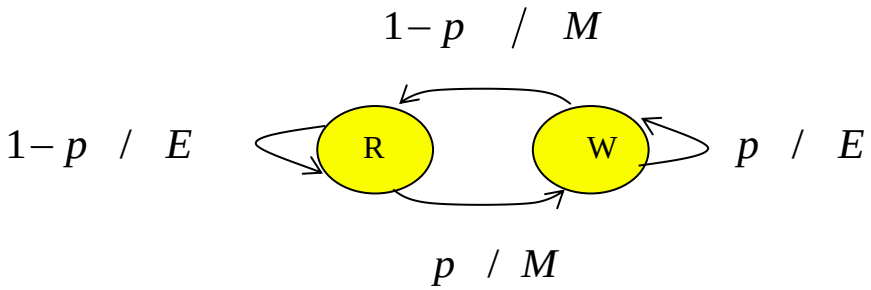

Figure 4-17: State diagram with message labelling

It is clear from elementary theory on Markov chains that, irrespective of the initial state, the stationary probabilities will be identical. However, if at the beginning the fusion centre has the wrong information about the state of the node, all decisions are reversed.

However, assuming that at the beginning the fusion centre receives not the information of a transition but the initial state of the node and that this information is sent without error, then the ambiguity is removed. The probability of transmitting one message is therefore the probability of the two transitions in Figure 4-17. Thus we get:

$$\begin{cases} \Pr(M \mid H_o) = 2p_{F_{loc}}(1-p_{F_{loc}}) \\ \Pr(M \mid H_1) = 2p_{M_{loc}}(1-p_{M_{loc}}) \end{cases} \quad \text{Eq. 4-39}$$

This means that the number of required transmissions is reduced relatively to the conventional scheme always reporting from K to $2Kp(1-p)$, where p is the localized probability of false alarm under H_0 and the localized probability of miss detection under H_1.

4.1.6.2 Influence of the Reliability of the Reporting Channel

For the case of the conventional cooperative sensing algorithm that reports the state of the node each time a measurement is made, or for the scheme presented in the previous section that includes two classes of sensors, if the channel from the node to the fusion centre is highly reliable this channel does not affect the ROC. Basically if the channel from the node to the fusion centre has a probability of error q, or a probability that the message is not received q, the effect corresponds to use the following modified probabilities of false alarm and miss detection:

$$\begin{cases} P'_{F_{loc}} = P_{F_{loc}}(1-q) + (1-P_{F_{loc}})q \\ P'_{M_{loc}} = P_{M_{loc}}(1-q) + (1-P_{M_{loc}})q \end{cases} \quad \text{Eq. 4-40}$$

and therefore if $q << (P_{F_{loc}};\ P_{M_{loc}})$, the effect is negligible.

The things change in the case of the cooperative sensing scheme that only reports the state transitions at the nodes. Let us consider that q is the probability that a message reporting a state transition is not received. In such a case and if the node is at the correct state but has entered a state where the information at the fusion centre is wrong, then if $(q; P_{F_{loc}};\ P_{M_{loc}}) << 1$, then it can stay in such a state for a quite long time.

This is illustrated in Figure 4-18, where the states (XY) are defined, where X represents the state of the node (Right (R) or wrong (W)) and Y represents the indication the fusion centre has about the state of the node. In Figure 4-18, p represents the localized probability of false alarm in the hypothesis H_0 and the localized probability of miss detection in the case of H_1. The state diagram shows that after entering the state RW the probability of staying there is 1-p which will be high if $(P_{F_{loc}}; P_{M_{loc}}) \ll 1$. Therefore the system can stay in this state for a very long time.

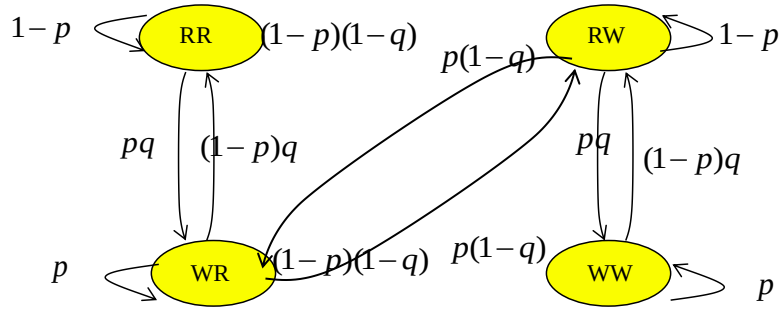

Figure 4-18: State diagram including errors in the reporting channel

The matrix of the probabilities of transition numerically labelling the states as $[RR\ \ RW\ \ WR\ \ WW] = [1\ \ 2\ \ 3\ \ 4]$ is given by

$$\mathbf{P} = \begin{bmatrix} 1-p & 0 & p(1-q) & pq \\ 0 & 1-p & pq & p(1-q) \\ (1-p)q & (1-p)(1-q) & p & 0 \\ (1-p)(1-q) & (1-p)q & 0 & p \end{bmatrix} \qquad \text{Eq. 4-41}$$

and solving the usual equation $\boldsymbol{\pi} = \boldsymbol{\pi}\mathbf{P}$ for the determination of the stationary probabilities (vector $\boldsymbol{\pi}$), one gets

$$\boldsymbol{\pi} = \begin{bmatrix} p_{RR} \\ p_{RW} \\ p_{WR} \\ p_{WW} \end{bmatrix} = \begin{bmatrix} \frac{1-p}{2} \\ \frac{1-p}{2} \\ \frac{p}{2} \\ \frac{p}{2} \end{bmatrix} \qquad \text{Eq. 4-42}$$

That is the state R(W) of the node is at the fusion centre divided into two states with equal probability $(1-p)/2$ or($p/2$). The stationary probabilities are independent of the reporting channel reliability. This means of course that the system will be completely ineffective if one is not able to identify the correct sub-state.

To cope with such a problem let us consider that, in addition to report the state transitions, the nodes periodically report the value of their state. Let us consider that the value of the state is reported once every *N* measurements. With such an arrangement the number of transmission is increased by 1/N for each detection performed. The average number of transmissions per node and energy measurement is therefore given by

$$E(T)/Node/Detection = \begin{cases} \frac{1}{N} + 2p_{F_{loc}}(1-p_{F_{loc}}) & H_0 \\ \frac{1}{N} + 2p_{M_{loc}}(1-p_{M_{loc}}) & H_1 \end{cases} \qquad \text{Eq. 4-43}$$

4.1.6.3 Numerical Results

Figure 4-19 presents the ROC for the transition reporting algorithm complemented with a periodic reporting of the node state.

The following assumptions were assumed

- Number of nodes: 10
- No fading
- SNR=0dB
- Reporting channel reliability: $q=10^{-6}$
- Fusion algorithm employed: OR

Figure 4-19 presents the cases where the true state reporting is done at $1/N$ where N=4 and 8, and also included is the ROC curve for the conventional cooperative sensing algorithms that reports the state at each measurement (which is also the performance achieved by the selective reporting scheme of the previous section).

The results show the expected degradation as N increases, but the penalty in the ROC is much less than what would be achieved by halving the number of nodes in the conventional detector while the number of transmissions is reduced by a factor that is always higher than 2.6.

As a final conclusion, it can be pointed out that selective reporting based on the transitions is quite promising.

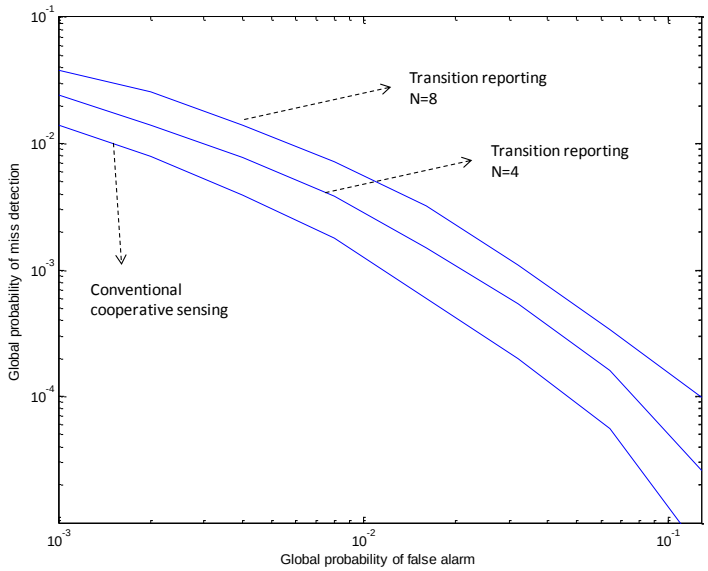

Figure 4-19: ROC for the conventional detector and transition / periodic reporting

4.1.7 Conclusions

In this subsection cooperative sensing schemes, with reduced signalling to report the state to the fusion centre, is considered.

Two schemes are proposed: based on two dual types of sensors. One reports only the presence or only the absence of incumbent users, and the second one reports only the state transitions of the nodes.

The first scheme allows achieving in average a reduction of 50% in the number of transmissions when compared with a conventional scheme while providing exactly the same performance. Furthermore the arrangement when using a single threshold is very simple and only requires the definition of the threshold to provide the desired probability of false alarm, unlike the schemes based on a censorship

policy that only achieve good performance if the thresholds are adjusted based on some a priori information about the probability of having an incumbent user present. Due to its simplicity and predictable behaviour this scheme has interest for practical implementations and has been implemented in WP6 to be a part of the different proofs of concept defined for QoSMOS.

The second scheme has to be used with an extension where updates about the true state of the node are provided from time to time. Otherwise, even if the reporting channel is highly reliable, an ambiguity between two states will appear. The proposal was to periodically, in addition to the transition reporting, update the true state of the nodes. The results show a degradation in the ROC but for the cases simulated this is more than compensated by the reduction in the required number of transmissions.

4.2 Collaborative Spectrum Sensing Based on Beta Reputation System

The research demonstrated here is a collaborative spectrum sensing scheme exploiting spatial diversity of users. However, in the presence of malfunctioning or misbehaving users, the performance of collaborative schemes deteriorates significantly. Proposed therefore is a credibility based mechanism using beta reputation system in which the fusion centre assigns weights to each user observation based on individual credibility score with significant improvement in reliability of aggregated information in the presence of falsified users.

4.2.1 Introduction

One of the most crucial tasks of a CR is to identify the presence of incumbent users with high reliability over wide range of spectrum. This is challenging as CR needs to identify various incumbent users using different modulation schemes and data rates in presence of variable propagation losses and thermal noise. The burden on sensing algorithms can be alleviated to a large extent by exploiting spatial diversity among CR users. In Collaborative Spectrum Sensing (CSS) all CRs send their sensing reports directly to a fusion centre [Arshad10] while in cooperative spectrum sensing CRs relay sensing reports from each other and decision can be made in a distributed manner [Atapattu09]. Collaboration or cooperation among few CR users adequately distant from each other can help to reduce the individual requirements on sensitivity by countering the deleterious channel effects [Arshad09].

In CSS, CR users either send their local observations (for example measured energy in case of energy detector) to the fusion centre (soft decision combining) or may send just their decision e.g. 1 (incumbent present) or 0 (incumbent absent) to the fusion centre, called Hard Decision Combining (HDC). In general, HDC is a better choice due to its significantly lower communication overhead [Ghasemi07]. The fusion centre makes a final decision about the presence or absence of incumbent user based on the information received from the CRs participating in CSS. The work presented here uses energy detection for local spectrum sensing and hard decision based collaborative spectrum sensing (HD-SS) but similar arguments are equivalently applicable for the case of the cooperative spectrum sensing.

Most of the current collaborative spectrum sensing schemes assume that all CRs are honest, trustworthy and are without any hardware fault [Arshad10], [Ghasemi07]. However, in reality a CR user may send false information to the fusion centre. A user may be maligned due to device malfunctioning or there may be some selfish reasons. For example, a selfish user might send the information to the fusion centre that an incumbent signal is present so that the fusion centre makes a wrong decision and later on the selfish user can transmit its own signal on the free channel. Similarly, a CR might send wrong information unintentionally due to the defects or faults in its hardware. Such CR users are hitherto called dubious users and it is assumed that they send wrong sensing data due to any reason. It has been shown in the literature that the presence of Dubious Cognitive Radios (DCR) can severely degrade the performance of collaborative spectrum sensing [Mishrai06].

There is a limited literature available that address the problem of collaborative spectrum sensing in the presence of DCR users. Robust and reliable collaborative spectrum sensing based on outlier detection

techniques has been proposed in [Kaligineedi10]. An outlier is a sensing observation which is far away from the rest of the observations from the other CR users. Identification of DCR users based on outlier detection is only applicable when CR users share their sensing observations with the fusion centre. Hence, outlier detection schemes cannot be directly implemented for the case of HD-CSS.

In [Mishrai06], a simple approach was proposed in which CRs report yes or no indicates incumbent user present or absent respectively. If there are k DCRs, fusion centre declares yes only if there are at least $k+1$ users reporting yes. This approach has many disadvantages e.g. it requires exact number of DCR to be known at the fusion centre and approach is only applicable for the case of HD-CSS only. In [Yang07], the trust of each cognitive user was taken into consideration that is based on each CR detection and false alarm rate, but do not consider potential cheating behaviours. Similarly, the approach proposed in [Wang09_2] can differentiate honest and DCRs when there is only one dubious CR and scheme cannot be applied when multiple DCRs exists.

Herein proposed is a novel robust credibility based collaborative detection scheme to alleviate the vicious aspects of DCRs. In our proposed approach, fusion centre assign credibility score (ς) to each CR participating in CSS. A centralised approach is considered in which the fusion centre calculates the value of all CRs using a Bayesian formulation, specifically a beta reputation system, for the evaluation of credibility of different users in a CR network. Credibility score of each user is used to calculate the weight coefficient of the corresponding sensing result of that user at the fusion centre. Initially, all the users are considered as reliable with same initial value of ς. Credibility of users is updated at each sensing interval by checking consistency between global and local sensing decisions.

Based on credibility score, each user's information is weighted at the fusion centre and hence less credible users have less effect on the global decision about the existence of incumbent user.

4.2.2 System Model

Considered is a group of K CRs each equipped with an energy detector and is able to perform local spectrum sensing. The CRs perform spectrum sensing periodically and send their sensing decision to a fusion centre through control channels. Let us also assume error free control channels for the transmission of sensing decision information. Based on the information received from the collaborating users, the fusion centre makes a global decision regarding the presence or absence of an incumbent user using a decision fusion rule. Also assumed is that the incumbent signal received by the CRs is independent from each other because of location diversity and the sensing channel corrupts the incumbent signal by adding additive white Gaussian noise with zero mean and variance σ^2. These assumptions are reasonable for IEEE 802.22 networks, whose coverage area has a radius of 33 to 100 km and CRs are widely distributed in this area [IEEE802.22].

Spectrum sensing problem for the j^{th} user is represented as below:

$$\mathbf{y}_j = \begin{cases} \mathbf{n}, & \boldsymbol{\mathcal{H}_0} \\ \sqrt{\rho_j}\,\mathbf{s} + \mathbf{n}, & \boldsymbol{\mathcal{H}_1} \end{cases} \qquad \text{Eq. 4-44}$$

where $\mathcal{H}_0$ and $\mathcal{H}_1$ are defined in Eq. 3-63. Assume $\mathbf{n} = [n(1), n(2), \ldots., n(N)]^T \in \boldsymbol{\mathcal{R}}^N$ and $y_j = [y_j(1), y_j(2), \ldots, y_j(N)]^T \in \boldsymbol{\mathcal{R}}^N$ represent noise and received samples vectors respectively where the number of received samples is N in one sensing interval. Without loss of generality, the incumbent transmitted signal $\mathbf{s}$ can assume $\mathbf{s} = \mathbf{1}_N^T$, where $\mathbf{1}_N^T$ is a column vector of all ones of size $N \times 1$. Let us also assume $\sigma^2 = 1$ for all users and hence ρ_j is the received SNR at the j^{th} CR. Let $\mathfrak{T}_j$ represent the test statistics of energy detector at j^{th} CR, such that $\mathfrak{T}_j = \mathfrak{T}_{\mathrm{ED}}$ and $\lambda_j = \lambda_{\mathrm{ED}}$ as defined in Eq. 3-71 , where λ_j is the decision threshold at the j^{th} user which satisfied the required probability of false alarm, PFA [Arshad10].

The goal of spectrum sensing is to make a decision between $\mathcal{H}_0$ and $\mathcal{H}_1$. Local decision at j^{th} user i.e. d_j is calculated as:

$$d_j = \begin{cases} 1, & \mathfrak{T}_j \geq \lambda_j \\ 0, & \text{otherwise} \end{cases} \quad \text{Eq. 4-45}$$

In HD-CSS scheme, each CR user transmits d_j to the fusion centre through a control channel in an orthogonal manner. Fusion centre combines all the received information $d = [d_1, d_2, \dots, d_k]^T$ and makes a global decision D such that:

$$D = \mathfrak{g}(\mathbf{w}, \mathbf{d}) \quad \text{Eq. 4-46}$$

where $\mathbf{w} = [w_1, w_2, \dots, w_3]^T$ is the weight vector calculated by the fusion centre based on each user (ς) value and $\mathfrak{g}$ is the fusion rule. Here, let us define the fusion rule $\mathfrak{g}$ as in [Arshad10]:

$$\mathfrak{g}(\mathbf{w}, \mathbf{d}) = \begin{cases} 1, & \sum_{j=1}^{K} (w_j \times d_j) \geq \left\lceil \frac{K}{2} \right\rceil \\ 0, & \text{otherwise} \end{cases} \quad \text{Eq. 4-47}$$

4.2.3 Beta Reputation System

Reputation systems are used to foster good behaviour by providing incentives for honest users and help some entity to make decisions about who to trust. In the context of a cognitive radio network, the fusion centre can employ a reputation system to identify dubious users quickly and minimise their contributions in global decision making by assigning an appropriate ς (and hence weight) to each user. The beta reputation system models the behaviour of each CR as a binary event modelled by the beta distribution [Josang02]. Hence, it provides a sound mathematical basis for combining observations and decisions for distributed users and for expressing the credibility of each user. Since the true probability of a CR user to act maliciously, say ε, is unknown, ς is estimated from the data obtained at the fusion centre. Take $p(\varepsilon)$ from the beta family, whose probability function is given by:

$$P(\varepsilon) = \frac{\Gamma(\alpha + \beta)}{\Gamma(\alpha)\Gamma(\beta)} \varepsilon^{\alpha-1}(1-\varepsilon)^{\beta-1} \qquad 0 \leq \varepsilon \leq 1, \qquad \alpha \geq 0, \beta \geq 0 \quad \text{Eq. 4-48}$$

with the restriction that $p \neq 0$ if $\alpha < 1$ and $p \neq 1$ for $\beta < 1$ [Josang02]. In Eq. 4-48 $\Gamma(\cdot)$ represents gamma function. The first order statistics of the beta distribution is given as:

$$\mathrm{E}[p(\varepsilon)] = \frac{\alpha}{\alpha + \beta} \quad \text{Eq. 4-49}$$

$$\mathbf{Var}[p(\varepsilon)] = \frac{\alpha\beta}{(\alpha + \beta)^2(\alpha + \beta + 1)} \quad \text{Eq. 4-50}$$

The advantage of the beta reputation system is that it only needs two parameters that are continuously updated as decisions are reported to the fusion centre. Furthermore, the beta distribution is the most suitable option because of its flexibility and ability to pick any value in $[0, 1]$ with arbitrarily small variance.

In HD-CSS, the fusion centre has two possible outcomes for each user in every sensing interval; the fusion centre either categorizes the j^{th} user contribution as positive rating or negative rating. Let ζ represent the total number of *positive ratings* and η represent the total number of negative ratings then the probability density function of the outcome that the j^{th} user has a positive rating is obtained by setting $\zeta = \alpha + 1$ and $\eta = \beta + 1$ [Josang02]:

$$P(\varepsilon) = \frac{\Gamma(\zeta + \eta + 2)}{\Gamma(\zeta + 1)\Gamma(\eta + 1)} \varepsilon^{\zeta}(1 - \varepsilon)^{\eta} \qquad \zeta, \eta \geq 0 \qquad \text{Eq. 4-51}$$

The probability expectation value is defined as $\mathbb{E}[p(\varepsilon)]$ which is interpreted as the most likely value of $p(\varepsilon)$.

4.2.4 Proposed Reputation Based Mechanism at Fusion Centre

An opportunistic or cognitive radio user can be classified either as reputable or dubious based on its current decision d_j and the global decision D. A reputable CR user is always honest i.e. transmitting its actual spectrum sensing observation or decision to the fusion centre and its spectrum sensing observations are normally reliable. While on the other hand, a dubious CR user is the one who may be dishonest or honest but its sensing results is not always correct because of many factors like the sensing algorithm used, the capability of the hardware etc. In order to achieve a high credibility score i.e. ς value, a CR user needs to be honest and able to provide accurate sensing observations. Each CR user has its credibility database stored at the fusion centre. When a new observation i.e. d_j at the k^{th} sensing interval is reported, the fusion centre first decides if the j^{th} user is a collaborative or a dubious user using Eq. 4-46 and Eq. 4-47. The fusion centre, then, updates the values of ζ_j and η_j by incorporating new observation d_j as follows:

$$\zeta_j(k) = \zeta_j(k-1) + \tau_1, \qquad \eta_j(k) = \eta_j(k-1) + \tau_2 \qquad \text{Eq. 4-52}$$

Where:

$$\tau_1 = \begin{cases} 1, & \text{if } d_j(k) = D(k) \\ 0, & \text{otherwise} \end{cases} \qquad \text{Eq. 4-53}$$

$$\tau_2 = \begin{cases} 1, & \text{if } d_j(k) \neq D(k) \\ 0, & \text{otherwise} \end{cases} \qquad \text{Eq. 4-54}$$

Hence, based on Eq. 4-49 to Eq. 4-54, the credibility score ς_j of j^{th} user can be written as:

$$\varsigma_j \triangleq \mathrm{E}[p(\varepsilon)] = \frac{\zeta_j + 1}{\zeta_j + 2 + \eta_j} \qquad \text{Eq. 4-55}$$

Finally, the weighting coefficients for the observations of each CR user are defined as:

$$\mathbf{w} = \frac{\boldsymbol{\varsigma}}{\sum_{j=1}^{k} \varsigma_j} \qquad \text{Eq. 4-56}$$

where $\varsigma_j = [\varsigma_1, \varsigma_2, \ldots, \varsigma_K]^{\mathrm{T}}$. Hence, the weight vector defined in Eq. 4-56 is updated in each sensing interval and once a CR user is regarded as unreliable, its observations received by the fusion centre has less effect on the global decision because of its low credibility score.

4.2.5 Simulation Results and Discussions

For the simulations, we consider K=20 collaborating users in a cognitive radio network. Each CR user sample the local observation N=10 times and process N received samples to generate test statistic $\mathfrak{T}_{\mathrm{i}}$ as defined in Eq. 3-71. Mean received SNR of the cognitive users is uniformly distributed in the range of -5 to 5dB. Let us assume that the noise variance σ_{n}^2 is known to each user and is equal to 1. Moreover, initially all the users as trusted users and initialise weight vector w as a vector of all ones. From simulations, we observed that the weights of all users converge after 10 to 15 sensing intervals provided channel conditions remained constant. However, to estimate values of probability of false alarm and probability of detection, 10,000 iterations are considered. In our simulations, dubious CRs do not perform spectrum sensing and send random data to the fusion centre.

In Figure 4-20 (a), a collaborative spectrum sensing system is considered, having no DCR, 2 DCRs and 4 DCRs and study the impact of dubious users on the performance of collaborative spectrum sensing. ROC curves are plotted for performance evaluation i.e. plots probability of miss detection versus probability of false alarm [Arshad10]. It is clear from Figure 4-20 (a) that presence of dubious users significantly affects the performance of collaborative spectrum sensing. For example, for a given probability of false alarm $\mathrm{PFA} = 20\%$ under parameters given in last paragraph, probability of detection with no DCR is 99.18%. However, in the presence of 2 and 4 dubious cognitive users, probability of detection reduces to 96.27% and 89.13% respectively.

The performance of the proposed credibility based CSS scheme is compared with the case of Equal Weight Combining (EWC). In EWC, same weight is assigned to each user regardless of its credibility score, hence in this scheme all users have equal share of contributions in global decision about the existence of incumbent users. Proposed scheme of credibility score based collaborative spectrum sensing (CF-CSS) assigns weighted coefficients to users that are helpful in nullifying the effect of false information in order to enhance to credibility of global decision. User weights are calculated according to Eq. 4-56 that are based on the credibility of each user as defined in Eq. 4-55.

Figure 4-20 (b) and (c) show the performance of CSS in the presence of 2 and 4 DCR respectively. The performance with EWC is shown in each figure as a reference for comparison purposes. Compared to EWC in the presence of dubious users, the proposed CF-CSS scheme demonstrates significant performance gain and completely nullifying the effects of misbehaved users. It should be noted from Figure 4-20 (b) and (c) that with CF-CSS sensing performance is even better than the performance without any dubious user (see Figure 4-20 (a)). This is due to the reason that all CRs are uniformly distributed in an area and have different values of mean SNR. Hence, some of the users although trusted (i.e. neither selfish nor malfunctioning), cannot make reliable decisions most of the time due to bad channel conditions. Hence, proposed scheme assigns less weight to such users and more weight to users who frequently make correct decisions. Figure 4-20 (d) plots probability of miss detection versus detected SNR that can be reliably detected by cognitive radio network for a given probability of false alarm of 50%. Here, it is assumed that all CR users received same mean SNR (i.e. close to each other and distant from the incumbent transmitter). It is clear from the Figure 4-20 (d) that with proposed scheme 20 users can detect signal as low as $-15\mathrm{dB}$ for $\mathrm{PMD} = 48.5\%$ while with EWC signals up to only $-11\mathrm{dB}$ can be detected for the same PMD.

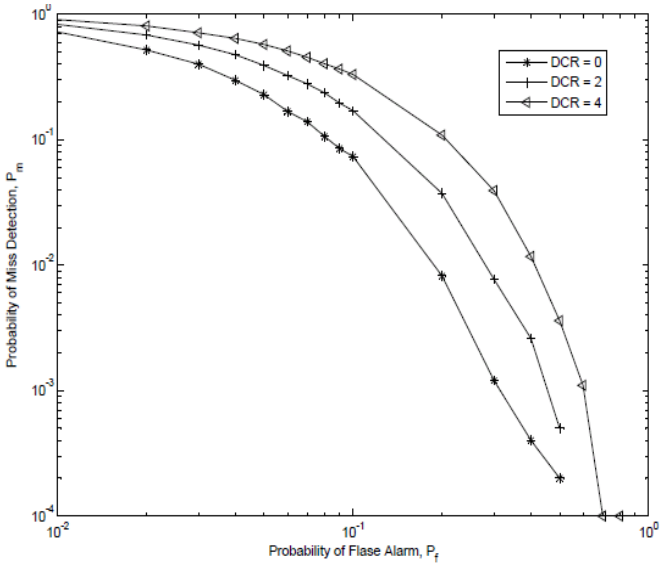

(a) Effect of Dubious CR users on CSS performance $K = 20, N = 10$ and $\rho = -5$ to 5 dB

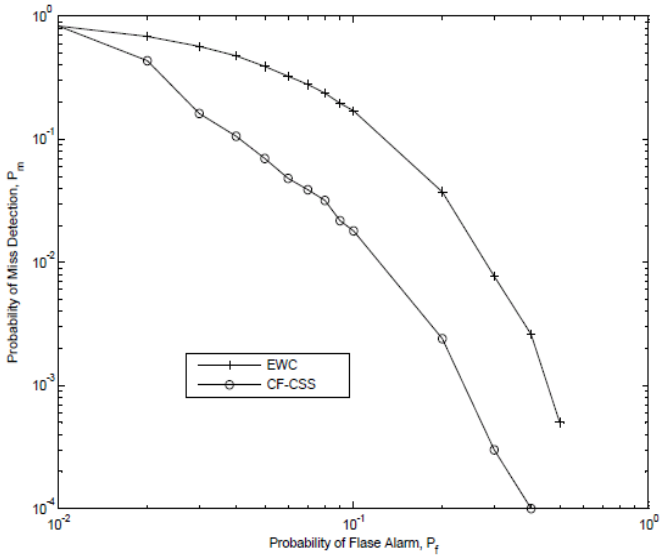

(b) ROC curve with 2 DCR, $K = 20$, $N = 10$ and $\rho = -5$ to 5dB

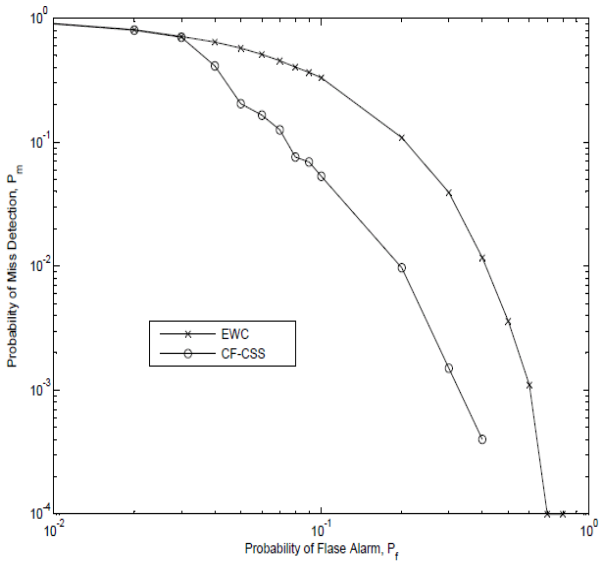

(c) ROC curve with 4 DCR, $K = 20$, $N = 10$ and $\rho = -5$ to 5 dB

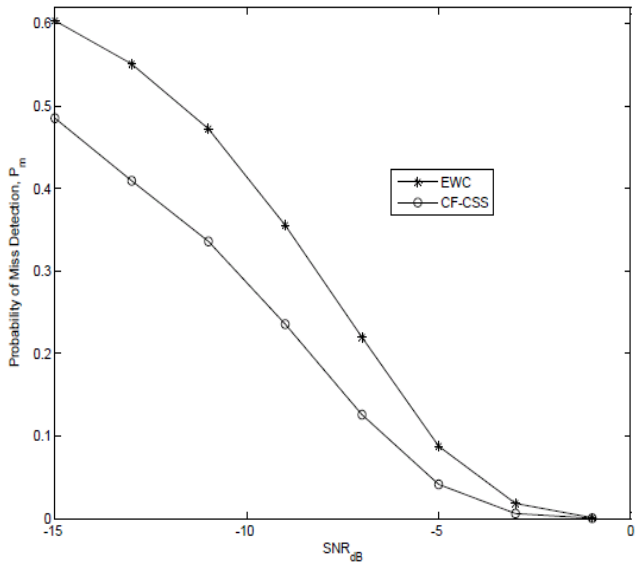

(d) P_m Vs SNR with 2 DCR, $K = 20$, $N = 10$ and PFA $= 0.5$

Figure 4-20: Simulation results showing the performance of CF-CSS

4.3 Distributed Processing to Handle Mobility

In this section the impact of the time variance caused by the mobility of CRs on the sensitivity of spectrum sensing algorithm is considered. A framework for local spectrum sensing is proposed in order to exploit spatio-temporal diversity due to the user mobility where cognitive radios make multiple spectrum measurements and makes a decision about the existence of a licensed user.

4.3.1 Introduction

A number of spectrum sensing algorithms are available in literature as explained in section 2.1. However, existing studies on spectrum sensing have focused on a model in which CRs are stationary but it is expected that in future, most of the wireless traffic will be generated from mobile devices as the user wants services on the go. Spectrum sensing algorithms that perform outstanding in stationary environments may be totally inept when user mobility exists. Hence, a proper model is needed which is more suited to rigid constraints encroached by user mobility. According to our best knowledge, this area has not been much explored in the literature.

Recently, impact of user mobility on the performance of spectrum sensing has been presented in [Min09]. However, the presented analyses have inaccurate expressions and numerical results. For example, the inverse of the covariance matrix (defined in [Min09] as a sum of an identity matrix **I** and a symmetric Toeplitz matrix, say **M**) cannot be expressed as a sum of an identity matrix and a tri-diagonal matrix i.e. $[\mathbf{I} + \mathbf{M}]^{-1} \neq \mathbf{I} + \mathbf{M}^{-1}$.

In this section, a mobility driven collaborative spectrum sensing mechanism using Neyman-Pearson's (NP) criteria is presented. It is shown that a mobile CR can achieve better spectrum sensing performance by exploiting its mobility. In the considered system, each CR makes multiple spectrum measurements to exploit spatial diversity. Local test statistics and an optimal detection rule in the presence of mobility are also derived in this section.

4.3.2 System Model

Let us consider a scenario in which a CR user is moving with speed *v* and makes a decision on the presence of the Incumbent User (IU) signal collaboratively. The IU is assumed to be a TV transmitter

and the CR is detecting the IU signal in a certain bandwidth *B* in time *T*. The CR makes multiple measurements *N* in a discrete time interval Δt before sending its observation to the central controller (e.g. fusion centre) which makes a final decision about the existence of an IU. Let us make the following assumptions:

- Direction of CR will not change during any two consecutive measurements
- Average received signal power at a CR from an IU or any other CR is less than the noise power as documented in IEEE 802.22 [IEEE802.22].

The log-normal correlated shadowing is taken into account as well as a distance dependent path loss. Iit should be noted here that the effect of small scale fading is negligible because of the larger bandwidth of TV channels i.e. 6MHz [IEEE802.22]. The received power at a CR can be expressed as,

$$P = P_r e^{Y} \quad \text{Eq. 4-57}$$

where P_r is the average received power, $Y \sim \mathcal{N}(0, \sigma_n^2)$ and σ_n is the standard deviation of Y. Log-normal shadowing is normally characterised in terms of $\sigma -$ dB which is related with σ as, $\sigma_n = 0.1 \log(10)\sigma$ dB. Let us consider correlated log-normal shadowing and use exponential correlation model $R(v) = e^{-av\Delta_t}$ where *a* is an environment constant [Gudmundson91].

4.3.3 Spectrum Sensing

4.3.3.1 Measurement Statistics

Spectrum sensing can be formulated as a binary hypothesis testing problem by assuming hypothesis of the IU inactive and active as $\mathcal{H}_0$ and $\mathcal{H}_1$ respectively [Arshad10]. Following previous work [Quan08], for a large value of $m = T \times B$, the statistical model of received energy for the i^{th} measurement is given by [Min09],

$$r \sim \begin{cases} \mathcal{N}\left(\sigma_n^2, \frac{\sigma_n^4}{m}\right) & ; \mathcal{H}_0 \\ \mathcal{N}\left(P + \sigma_n^2, \frac{(P+\sigma_n^2)^2}{m}\right) & ; \mathcal{H}_1 \end{cases} \quad \text{Eq. 4-58}$$

Let us define $\underline{r} = [r_1, r_2 \cdots, r_N]^T$ as a multi-variate Gaussian random variable having *N* measurements. Its joint distribution under each hypothesis is given as,

$$\underline{r} \sim \begin{cases} \mathcal{N}\left(\underline{\mu}_0, \mathbf{\Sigma}_0\right) & ; \mathcal{H}_0 \\ \mathcal{N}\left(\underline{\mu}_1, \mathbf{\Sigma}_1\right) & ; \mathcal{H}_1 \end{cases} \quad \text{Eq. 4-59}$$

where $\underline{\mu_j}$ and $\mathbf{\Sigma}_j$ are mean vector and covariance matrix of $\underline{r}$ for $j = 0,1$. From Eq. 4-58 and Eq. 4-59,

$$\underline{\mu}_0 = \sigma_n^2 \times \underline{1}; \quad \underline{\mu}_1 = (P + \sigma_n^2) \times \underline{1} \quad \text{Eq. 4-60}$$

$$\mathbf{\Sigma}_0 = \frac{\sigma_n^4}{m}\mathbf{I}_N, \quad \mathbf{\Sigma}_1 = \frac{\sigma_n^4}{m}\mathbf{I}_N + \frac{2P\sigma_n^2}{m}\mathbf{\Lambda} \quad \text{Eq. 4-61}$$

where $\mathbf{I}_N$ and $\mathbf{\Lambda}$ are $N \times N$ identity and covariance matrices with elements of $\mathbf{\Lambda}$ are $\Lambda_{a,b} = \rho^{|a-b|}$, ρ is a measure of the correlation coefficient between two positions of a node separated by a distance of $v\Delta_t$, here $\rho = e^{-av\Delta_t}$, and $\underline{1}$ is a $N \times 1$ column vector of all ones. In Eq. 4-60, the assumption is made that the average received signal power is less than the noise power (lower values of signal to noise ratios) as envisioned in IEEE 802.22 [IEEE802.22].

4.3.3.2 Hypothesis Testing

After collecting measurements at each time step $n\times\Delta t$, where $n \in \{1,2,\dots,N\}$, the NP test can be applied which is optimal in maximising probability of detection for a given probability of false alarm [IEEE802.22]. The likelihood ratio of $\underline{r}$ is given as,

$$L(\underline{r}) \triangleq \frac{h(\underline{r};\mathcal{H}_1)}{h(\underline{r};\mathcal{H}_0)} \qquad \text{Eq. 4-62}$$

where $h(\underline{r};H_j)$ represents the probability density function of $\underline{r}$ under hypothesis $\mathcal{H}_j$ where j=0,1. After some mathematical manipulations, Eq. 4-62 can be simplified as,

$$L(\underline{r}) = \frac{1}{2}\underline{r}^{T}\left(\boldsymbol{\Sigma}_0^{-1} - \boldsymbol{\Sigma}_1^{-1}\right)\underline{r} + \underline{\mu}_1^{T}\boldsymbol{\Sigma}_1^{-1}\underline{r} - \underline{\mu}_0^{T}\boldsymbol{\Sigma}_0^{-1}\underline{r} + \varphi \qquad \text{Eq. 4-63}$$

where φ is a constant. For a given threshold, η, spectrum sensing test can be formulated as,

$$\frac{1}{2}\underline{r}^{T}\left(\boldsymbol{\Sigma}_0^{-1} - \boldsymbol{\Sigma}_1^{-1}\right)\underline{r} + \underline{\mu}_1^{T}\boldsymbol{\Sigma}_1^{-1}\underline{r} - \underline{\mu}_0^{T}\boldsymbol{\Sigma}_0^{-1}\underline{r} \gtrless \eta - \varphi \qquad \text{Eq. 4-64}$$

It should be noted that the test statistics defined in Eq. 4-64 consists of a quadratic term in $\underline{r}$, which makes mathematical analysis intractable [Shellhammer06]. However, test statistics can be transformed in linear form by assuming $\boldsymbol{\Sigma}_0 = \boldsymbol{\Sigma}_1 = \boldsymbol{\Sigma}$ which is possible if we assume non-zero received power P_r under hypothesis $\mathcal{H}_0$. Let us assume $P_r \neq 0$ which can be considered as power of interfering signals. This assumption results in the following optimal decision fusion rule,

$$\underline{\tilde{\mu}}^{T}\underline{r} \gtrless \tilde{\eta} \qquad \text{Eq. 4-65}$$

where $\underline{\tilde{\mu}}^{T} = \left(\underline{\mu}_1 - \underline{\mu}_0\right)^{T}\Sigma^{-1}$ and $\tilde{\eta}$ is a constant. Based on the decision rule defined in Eq. 4-65, the structure of the detector can be proposed which is shown in Figure 4-21.

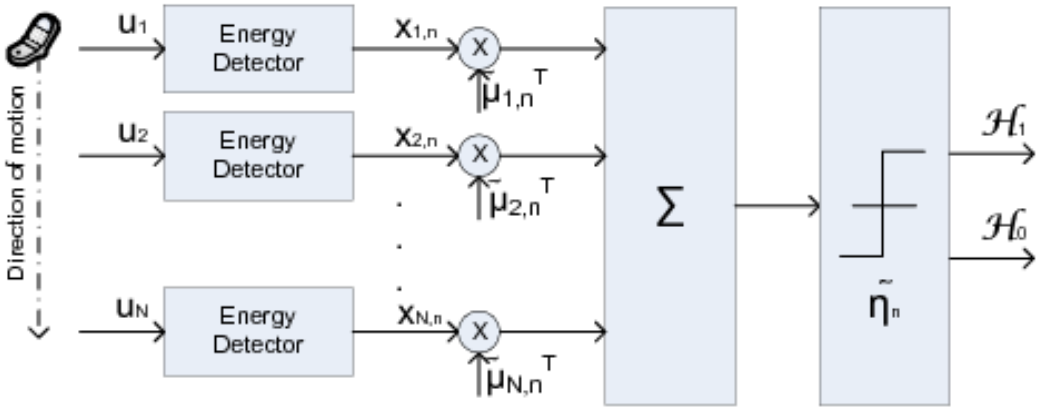

Figure 4-21: Proposed structure of detector

4.3.3.3 Performance Analysis

In this section, the closed form equation of the probability of detection, PD and the probability of false alarm, PFA are given based on the decision rule From Eq. 4-65, PFA and PD are given by,

$$\mathrm{PFA} = \mathcal{Q}\left(\frac{\tilde{\eta} - \mathrm{E}\left[\underline{\tilde{\mu}}^{T}\underline{r}|\mathcal{H}_0\right]}{\sqrt{\mathrm{Var}\left(\underline{\tilde{\mu}}^{T}\underline{r}|\mathcal{H}_0\right)}}\right) \qquad \text{Eq. 4-66}$$

$$\mathrm{PD} = \mathcal{Q}\left(\frac{\tilde{\eta} - \mathrm{E}\left[\underline{\tilde{\mu}}^T \underline{\mathrm{r}} | \mathcal{H}_1\right]}{\sqrt{\mathrm{Var}\left(\underline{\tilde{\mu}}^T \underline{\mathrm{r}} | \mathcal{H}_1\right)}}\right)$$

where $\mathrm{E}[\cdot]$ and $\mathrm{Var}(\cdot)$ denotes the expectation and variance operators respectively and $\mathcal{Q}(\cdot)$ is the right tail probability of standard normal distribution. First order statistics of $\underline{\tilde{\mu}}^T \underline{\mathrm{r}}$ can be calculated easily under both hypothesis $\mathcal{H}_0$ and $\mathcal{H}_1$ and hence a close form expression of PFA and PD is given by:

$$\mathrm{PD} = \mathcal{Q}\left(\mathrm{Q}^{-1}(\mathrm{PFA}) - \sqrt{\underline{\tilde{\mu}}^T \mathbf{\Sigma} \underline{\tilde{\mu}}}\right) \qquad \text{Eq. 4-67}$$

where $\mathbf{\Sigma}\, \underline{\tilde{\mu}}^T = \underline{\mu}_1 - \underline{\mu}_0$. Now consider,

$$\begin{aligned} \underline{\tilde{\mu}}^T \mathbf{\Sigma} \underline{\tilde{\mu}} &= \left(\underline{\mu}_1 - \underline{\mu}_0\right)^T \mathbf{\Sigma}^{-1} \mathbf{\Sigma}\, \mathbf{\Sigma}^{-1} \left(\underline{\mu}_1 - \underline{\mu}_0\right) \\ &= \left(\underline{\mu}_1 - \underline{\mu}_0\right)^T \mathbf{\Sigma}^{-1} \left(\underline{\mu}_1 - \underline{\mu}_0\right) \\ &= {P_r}^2\, \underline{1}^T \mathbf{\Sigma}^{-1} \underline{1} \end{aligned} \qquad \text{Eq. 4-68}$$

4.3.4 Numerical Results

In this section, the proposed mobility driven spectrum sensing framework is evaluated numerically and results are presented. In most of the results, the Probability of Miss-detection (PM), $\mathrm{PM} = 1 - \mathrm{PD}$ against various quantities is plotted and the impact of CR mobility on the performance of spectrum sensing is studied. The following parameters are used in numerical evaluation (as typically assumed in IEEE 802.22 [IEEE802.22]) until stated otherwise: σ_n^2 = −95.2dBm, $T = 1ms$, $W =$ 6MHz, $\sigma =$ 1.0dB, P_r = −114 dBm, PFA= 10^{-3} and $\Delta_t = 1s$.

Figure 4-22 illustrates the effect of CR speed on the probability of miss detection for a fixed probability of false alarm in an urban and a suburban environment, corresponding to a = 1⁄50 /m and a = 1⁄150 /m respectively. As expected, while increasing the number of measurements, the PD increases (or PM decreases). For a given speed and a number of measurements N, the CR can detect an incumbent user signal better in urban environment rather than suburban environment. This is due to the fact that in urban environment there is more scattering of incumbent signal and hence with mobility multiple measurements decorrelate over shorter distances. Intuitively, it is also obvious that for a fixed N and at a very high speed, PM will approach to the case of N independent sensors placed at a distance of $v\Delta_t$ and it can not go down to zero.

Figure 4-23 plots PM versus a number of measurements for different speeds and it can be seen easily that by increasing the number of times a CR will perform spectrum sensing, PM can approach zero. Figure 4-24 depicts PM versus averaged received power from the incumbent TV transmitter and for a fixed speed v and N. It is clear from Figure 4-24 that performance of spectrum sensing is highly sensitive to the average received power.

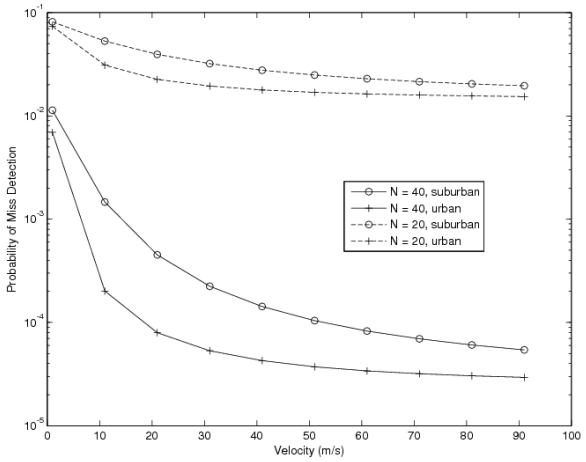

Figure 4-22: Probability of miss detection versus speed

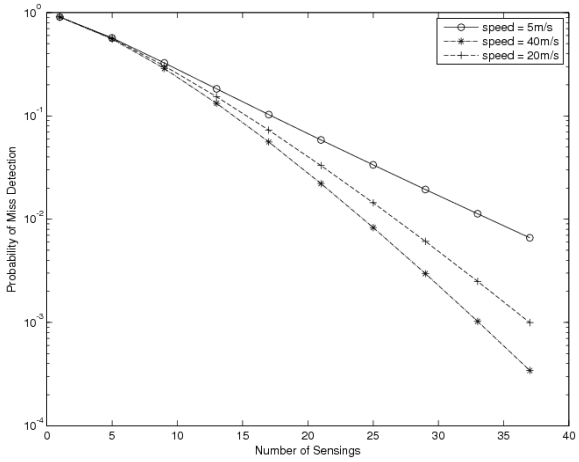

Figure 4-23: Probability of miss detection versus number of measurements N

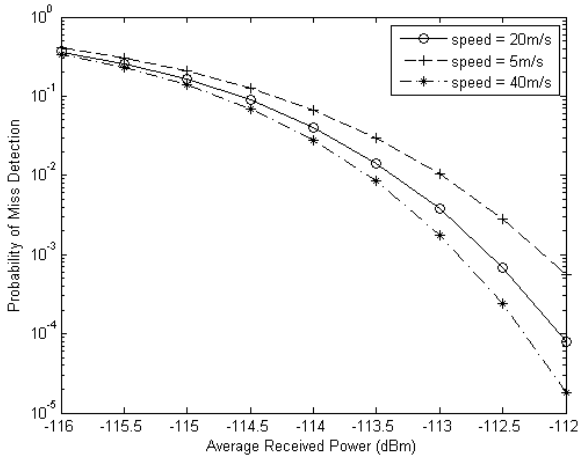

Figure 4-24: Probability of miss detection versus received power

4.3.5 Remark

A large number of spectrum sensing and collaborative spectrum sensing algorithms are available but few of them considered mobility of cognitive radios so far. In this section, a theoretical analysis of energy detection based collaborative spectrum sensing in the presence of user mobility is presented. The main conclusion of this section is that a cognitive radio can improve spectrum sensing performance if user mobility is exploited by performing multiple measurements. A suitable detector structure which is optimal in a Neyman-Pearson sense is presented and the expressions for probability of detection for spectrum sensing are derived.

5 Conclusions

This deliverable provides a complete set of algorithms for sensing in the framework of the QoSMOS project. It focuses on both radio context acquisition where sensing is performed on one location and disseminated sensing where exchange problematic of collaboratively or cooperatively collected data is crucial.

Classical sensing techniques such as energy detection and cyclostationary feature detection are improved using several methods:

- Hybrid detection mixing ED and CFD outperforming the performance of both algorithms taken separately.
- The use of the properties of speech for more efficient energy detection on PMSE.
- High order cyclostationary feature detection.
- Antenna processing increasing sensitivity and allowing the opportunistic user to perform sensing on incumbent network without quiet period, directly on its communication data.
- Statistical tests theory is used to improve noise level estimation and also to verify if the processed samples have noise distribution properties. In order to do so the Anderson-Darling and the Kolmogorov-Smirnov are used.

Innovative sensing approaches are described:

- As GFDM waveform is an important contribution of QoSMOS from WP4, GFDM sensing algorithms were developed using its cyclostationarity characteristics.
- The detection of opportunistic users can be performed by watermaking. It consists in the introduction of a specific signature in the transmitted signal, signature that will be detected.
- Classical sensing methods are useless for CDMA standards for which common channels are always broadcast. The concept of sensing in code is presented as well as detection algorithms for CDMA traffic channels.
- For blind frequency localization, a method based on double thresholding is proposed.

Moreover, in the case of the TV white space reuse, classical sensing (meaning the detection of the presence of a signal in a given frequency band) is not sufficient. Indeed, to verify that the reuse of the TV channel does not cause harmful interference to the incumbent receiver, the opportunistic system has to estimate the CIR of the incumbent receiver to determine the allowable transmit power. That is why reliable CIR estimation technique is presented.

In order to improve local sensing performance (in case of shadowing for example), distributed sensing is presented. The main problematic is no longer the detection algorithm performance but how to merge numerous / various sensing metrics. Three aspects are considered:

- The quantization of the metrics sent to the fusion centre : what is the resolution to use in order not to degrade the sensing performance.
- What is the impact of mobility (key point of the QoSMOS project) on sensing performance and how this mobility can be used to improve sensing performance?
- How can the fusion centre deals with malfunctioning or misbehaving sensing nodes? A solution based on beta reputation system is proposed.

6 Acronyms

16QAM	16-state Quadrature Amplitude Modulation
2-D	Two-dimensional
64QAM	64-state Quadrature Amplitude Modulation
ACC	Adjacent Cluster Combining
AD	Anderson Darling
ADC	Analog to Digital Conversion
AMC	Automatic Modulation Classification
AWGN	Additive White Gaussian Noise
BER	Bit Error Rate
BPSK	Binary Phase Shift Keying
BS	Base Station
BTS	Base Transceiver Station
CAF	Cyclic Autocorrelation Function
CD	Cyclostationarity Detector
CDMA	Code Division Multiple Access
CFAR	Constant False Alarm Rate
CFD	Cyclostationary Feature Detection
CIR	Carrier to Interference Ratio
CPCC	Cyclic Prefix Correlation Coefficient
CPICH	Common PIlot CHannel
CR	Cognitive Radio
CRC	Cyclic Redundancy Check
CSS	Collaborative Spectrum Sensing
DAC	Digital to Analog Conversion
DCR	Dubious Cognitive Radio
DFT	Discrete Fourier Transform
DPCCH	Dedicated Physical Control CHannel
DPCH	Dedicated Physical CHannels
DPDCH	Dedicated Physical Data CHannel
DSA	Dynamic Spectrum Access
DTT	Digital Terrestrial Television
DVB-T	Digital Video Broadcasting Terrestrial
ED	Energy Detector
EM	Expectation Maximization

EPA	Extended Pedestrian A
EWC	Equal Weight Combining
EWC	Equal Weight Combining
FB	Feature-Based
FBMC	Filter-Bank Multi Carrier
FC	Fusion Centre
FCME	Forward Consecutive Mean Excision
FDMA	Frequency Division Multiple Access
FFT	Fast Fourier Transform
FM	Frequency Modulation
FPGA	Field Programmable Gate Array
FWT	Fast Wavelet Transform
GFDM	Generalized Frequency Division Multiplexing
GI	Guard Interval
GLRT	Generalized Likelihood Radio Test
HDC	Hard Decision Combining
HSDPA	High Speed Downlink Packet Access
HS-PDSCH	High Speed Physical Downlink Shared CHannel
HS-SCCH	High Speed Shared Control CHannel
IFFT	Inverse Fast Fourier Transform
IIR	Infinite Impulse Response
INR	Interference to Noise Ratio
ISR	Interference to Signal Ratio
IU	Incumbent User
KS	Kolmogorov Smirnov
LAD	Localization Algorithm based on Double-thresholding
LB	Likelihood-Based
LRT	Likelihood Radio Test
LTE	Long Term Evolution
MED	MEDian
MF	Matched Filter
MJD	Multi-band Joint Detection
ML	Maximum Likelihood
MLE	Maximum Likelihood Estimate
MOD ID	MODulation IDentification

NP	Neyman Pearson
NP	Normal Peak
NT	Normalized Threshold
OFDM	Orthogonal Frequency Division Multiplexing
OFDMA	Orthogonal Frequency Division Multiple Access
OQAM	Offset Quadrature Amplitude Modulation
OR	Overlapping Ratio
OSA	Opportunistic Spectrum Access
OVSF	Orthogonal Variable Spreading Factor
P-CCPCH	Primary Common Control CHannel
PD	Probability of Detection
PDF	Probability Density Function
PFA	Probability of False Alarm
PM	Probability of Misdetection
PMSE	Programme Making and Special Events
PND	Probability of Non-Detection
P-SCH	Primary Synchronization CHannel
PSD	Power Spectral Density
PU	Primary User
QP	Quiet Period
QPSK	Quadrature Phase Shift Keying
RaSSSD	Receiver-aided Spectrum Sensing scheme with Spatial Differentiation
RAT	Radio Access Technology
RB	Resource Block
RC	Raised Cosine
RF	Radio Frequency
RMSE	Root Mean Square Error
RRC	Root Raised Cosine
RS	Reference Signal
SC-FDMA	Signal Carrier Frequency Division Multiple Access
SF	Spreading Factor
SIMO	Single Input Multiple Output
SINR	Signal to Interference plus Noise Ratio
SIR	Signal to Interference Ratio
SNR	Signal to Noise Ratio

SP	Side Peak
STD	STandard Deviation
S-SCH	Secondary Synchronization CHannel
TFCI	Transport Format Combination Indiactor
TPC	Transmit Power Control
TVWS	TV White Space
UE	User Equipment
UHF	Ultra High Frequency
UMP	Uniformly Most Powerful
WARP	Wireless open-Access Research Platform
WLAN	Wireless Local Area Networks
WSR	Watermark to Signal Ratio

7 References

[3GPP 36.141] 3GPP TS36.141. "Technical Specification Group Radio Access Network; Evolved Universal Terrestrial Radio Access (E-UTRA); Base Station (BS) conformance testing".

[3GPP 36.211] 3GPP TS 36.211 V9.1.0 (2010-03). "Technical Specification Group Radio Access Network; Evolved Universal Terrestrial Radio Access (E-UTRA); Physical Channels and Modulation".

[3GPP 36.521] 3GPP TS 36.521-1 V9.1.0. "Technical Specification Group Radio Access Network; Evolved Universal Terrestrial Radio Access (E-UTRA); User Equipment (UE) conformance specification; Radio transmission and reception; Part 1: Conformance Testing**".**

[Abdelmonem10] M. Abdelmonem, M. H. Ismail, M. S. El-Soudani and M. Nafie. "Coarse spectrum sensing for LTE systems". IEEE 17th International Conference on Telecommunications (ICT), pp.116-121, 4-7 April 2010.

[Aka01] A. Akansu and R. Haddad. "Multi-resolution Signal Decomposition: Transforms, Subbands and Wavelets". Academic Press, 2001.

[Aldirmaz09] S. Aldirmaz, A. Birol, I. Demirdogen and H. Arslan. "On suitability of PSD method for opportunity detection in OFDM(A) based cognitive radio systems". IEEE Workshop on Mobile Computing and Networking Technologies 2009.

[Anderson52] T. W. Anderson and D. A. Darling. "Asymptotic Theory of Certain "Goodness of Fit" Criteria Based on Stochastic Processes". Annals of Mathematical Statistics, vol. 23, no. 2, pp. 193–212, 1952.

[Arshad09] K. Arshad and K. Moessner. "Collaborative Spectrum Sensing for Cognitive Radio". IEEE International Conference on Communications Workshops, pp. 1-5, June 2009.

[Arshad10] K. Arshad, M. A. Imran, and K. Moessner, "Collaborative Spectrum Sensing Optimisation Algorithms for Cognitive Radio Networks". International Journal of Digital Multimedia Broadcasting, vol. 2010, no. 424036, 2010.

[Atapattu09] S. Atapattu, C. Tellambura, and H. Jiang. "Relay Based Cooperative Spectrum Sensing in Cognitive Radio Networks". IEEE Global Telecommunications Conference, 2009.

[Axe10] E. Axell, G. Leus and E. Larsson. "Overview of Spectrum Sensing for Cognitive Radio", 2010 IAPR Workshop on Cognitive Information Processing.

[Bacut84] P. Bacut and et. al. "Signal Detection Theorey. Radio and Svyaz". 1984.

[Baras06] C. Baras, "Tatouage informé de signaux audio numériques". PhD thesis, Télécom Paris (June 2006).

[Birru10] D. Birru, K. Challapali and B. Dong. "Detection of the presence of television signals embedded in noise using cyclostationary toolbox". US Patent 2010/0157066.

[Boccuzzi07] J. Boccuzzi. "Signal Processing for Wireless Communications, volume 1". McGraw-Hill Professional, 2007.

[Bokharaiee10] S. Bokharaiee, H. H. Nguyen, and E. Shwedyk. "Spectrum Sensing for OFDM-Based Cognitive Radio". Vehicular Technology Conference Fall (VTC 2010-Fall),

2010.

[Bouzegzi08] A. Bouzegzi, P. Jallon, and P. Ciblat. “A second order statistics based algorithm for blind recognition of OFDM based systems”. IEEE Global Communications Conference (GLOBECOM2008), December 2008.

[Cabric06] D. Cabric, A. Tkachenko, and R. Brodersen. “Spectrum sensing measurements of pilot, energy, and collaborative detection”. IEEE Military Communications Conference, MILCOM’06, Oct. 2006, pp. 1–7.

[Candes06] E. Candes, J. Romberg and T. Tao, “Robust uncertainty principles: exact signal reconstruction from highly incomplete frequency information”. IEEE Transactions on Information Theory 52 (2) (2006) 489–509.

[CEPT10] “Radio systems in the white space of the frequency band 470–790 MHz,” Annex 3 to Doc. SE43(09)34, September 2010.

[Chair86] Z. Chair and P. Varshney, “Optimal Data Fusion in Multiple Sensor Detection Systems”. IEEE Transactions on Aerospace and Electronic Systems, vol. AES-22, no. 1, pp. 98–101, January 1986.

[Chen07] L. Chen, J. Wang and S. Li, “An Adaptive Cooperative Spectrum Sensing Scheme Base on the Optimal Data Fusion Rule”. 4th International Symposium on Wireless Communication Systems (ISWCS), 17-19 October 2007, Trondheim, Norway.

[Chen08_1] H.-S. Chen, W. Gao and D. Daut. “Spectrum sensing for wireless microphone signals”. IEEE Sensor, Mesh and Ad Hoc Communications and Networks Workshops (SECON08), June 2008.

[Chen08_2] H. S. Chen, W. Gao and D. G. Daut. “Spectrum Sensing for OFDM Systems Employing Pilot Tones and Application to DVB-T OFDM”. IEEE International Conference on Communications (ICC'08).

[Clarke68] R. H. Clarke. “A statistical theory of radio-mobile reception”. Bell Syst. Tech. J. 47, pp. 957-1000 (1968).

[Conover99] W. J. Conover. “Practical Nonparametric Statistics”. 3rd edition, John Wiley and Sons, 1999.

[Dandawate94] A. Dandawate and G. B. Giannakis. “Statistical tests for presence of cyclostationarity”. IEEE Trans. Signal Processing, 42, 2355-2369 (1994).

[Demirdogen10] I. Demirdogen, A. Birol, S. Aldirmaz, H. Arslan and L. Durak. “Cognitive OFDMA: Exploring a new FFT based detection technique for opportunistic usage”. IEEE RWS 2010.

[Dobre05] O. A Dobre, A. Abdi, Y. Bar-Ness and W. Su, “Selection combining for modulation recognition in fading channels”. Proceedings of IEEE Military Communications Conference (MILCOM), pp. 2499-2505, Vol. 4, October 2005.

[Donoho06] D. Donoho. “Compressed sensing”. IEEE Transactions on Information Theory 52 (4) (2006) 1289–1306.

[Durbin73] J. Durbin. “Distribution Theory for Tests Based on the Sample Distribution Function”. Society for Industrial Mathematics, 1973.

[E3_D5.3] E3 D5.3, “First Draft Report on Cognition Enablers Schemes”, March 2009. ICT-2007-216248

[ETS06] ETSI TR 102 546, v.1.1.1_1.0.3 (2006-12), Technical Report.

[FCC10] Federal Communications Commission, "Second memorandum opinion and order". FCC 10-174, Sept. 2010.

[Fraser57] D. A. S. Fraser. "Nonparametric Methods in Statistics". Wiley, 1957.

[Gardner88] W. A. Gardner "Signal interception, a unifying theoretical framework for feature detection". IEEE transaction on communications, Vol. 36 N°8, August 1988.

[Gardner90] S. V. Schell and W. A. Gardner "Detection of the number of cyclostationarity signals in unknown interference and noise". 24th Asilomar conference on Signal, systems and computers, Pacific Grove, CA, November 1990.

[Gautier10] M. Gautier, M. Laugeois, and D. Noguet, "Teager-Kaiser energy detector for narrow-band wireless microphone spectrum sensing". IEEE International Conference on Cognitive Radio Oriented Wireless Networks and Communications (CROWNCOM), June 2010.

[Ghasemi07] A. Ghasemi and E. S. Sousa, "Opportunistic Spectrum Access in Fading Channels through Collaborative Sensing". IEEE Journal of Communications, vol. 2, no. 2, pp. 71–81, March 2007.

[Ghosh08] M. Ghosh, V. Gaddam, G. Turkenich, and K. Challapali, "Spectrum Sensing Prototype for Sensing ATSC and Wireless Microphone Signals". International Conference on Cognitive Radio Oriented Wireless Networks and Communications (CROWNCOM08), May 2008.

[Gilbert02] A. C. Gilbert, S. Guha, P. Indyk, S. Muthukrishnan and M. Strauss. "Near-optimal sparse Fourier representations via sampling". Proceedings of the 34th annual ACM symposium on Theory of computing, STOC '02, 2002, pp. 152–161.

[Goh07] L.P. Goh, Z. Lei and F. Chini. "DVB detector for cognitive radio". Proceedings of the IEEE International Conference on Communications (ICC'07), pp. 6460–6465, Glasgow, UK, June 2007.

[Gradshteyn80] I. S. Gradshteyn and I. Ryzhik. "Table of integrals, series and products". New-York: Academic Press, 1980.

[Gronsund09] P. Gronsund, H. N. Pham and P. E. Engelstad. "Towards dynamic spectrum access in primary OFDMA systems". IEEE 20th International Symposium on Personal, Indoor and Mobile Radio Communications, pp.848-852, 13-16 September 2009.

[Grosskopf06] R. Grosskopf. "Deterministic propagation prediction method developed by the European broadcasting union". Proceedings of the First European Conference on Antennas and Propagation (EuCAP), November 2006.

[Gudmundson91] M. Gudmundson. "Correlation Model for Shadow Fading in Mobile Radio Systems". Electronics Letters, vol. 27, no. 23, pp. 2145–2146, November 1991.

[Han06] N. Han, S. H. Shon, J. O. Joo and J. M. Kim. "Spectral correlation based signal detection method for spectrum sensing in IEEE 802.22 WRAN systems". International Conference on Advanced Communication Technology, February 2006.

[Hänninen10] T. Hänninen, J. Vartiainen, M. Juntti and M. Raustia. "Implementation of Spectrum Sensing on Wireless Open-Access Research Platform". International Workshop on Cognitive Radio and Advanced Spectrum Management COGART 2010, Rome, Italy, November 2010.

[Huan95] C.-Y. Huan and A. Polydoros. "Likelihood methods for MPSK modulation classification". IEEE Transactions on Communications, vol. 43, no. 234, pp. 1493-

1504, Feb/Mar/Apr. 1995.

[IEEE802.22] IEEE802.22, "Working Group on Wireless Regional Area Networks (WRAN)," IEEE, Tech. Rep., 2009.

[Josang02] A. J Sang and R. Ismail. "The beta reputation system". Proceedings of the 15th Bled Electronic Commerce Conference, 2002.

[Kaiser90] J. F. Kaiser. "On simple algorithm to calculate the energy of signal". IEEE International Conference on Acoustics, Speech, and Signal Processing (ICASSP90), April 1990.

[Kaligineedi10] P. Kaligineedi, M. Khabbazian, and V. Bhargava. "Malicious User Detection in a Cognitive Radio Cooperative Sensing System". IEEE Transactions on Wireless Communications, vol. 9, no. 8, pp. 2488 -2497, 2010.

[Khambekar07] N. Khambekar, L. Dong and V. Chaudhary. "Utilizing OFDM Guard Interval for Spectrum Sensing". WCNC 2007.

[Kohno95] R. Kohno, R. Meidan, and L. B. Milstein. "Spread spectrum access methods for wireless communications". IEEE Communications Magazine, vol. 33, no. 1, pp. 58–67, January 1995.

[Kolmogoroff33] A. Kolmogoroff. "Sulla determinazione empirica di una legge di distribuzione". Giorn. 1st. Ital. Attuari, vol. 4, pp. 83–91, 1933.

[Koufos09] K. Koufos, K. Ruttik R. and Jantti. "Signal model for OFDM sensing in cognitive radio". IEEE 20th International Symposium on Personal, Indoor and Mobile Radio Communications (PIMRC) 2009.

[Le06] B. Le, T. W. Rondeau, D. Maldonado, D. Scaperoth, and C. W. Bostian, "Signal Recognition for Cognitive Radios". Proceedings of SDR Forum 06 Technical Conference, Orlando, FL, 2006.

[Lehmann05] E. L. Lehmann and J. P. Romano. "Testing statistical hypotheses". Springer Texts in Statistics. Springer, New York, 3rd edition, 2005.

[Lehtomäki11] J. J. Lehtomäki, J. Vartiainen, R. Vuohtoniemi and H. Saarnisaari. "Adaptive FCME-Based Threshold Setting for Energy". International Workshop on Cognitive Radio and Advanced Spectrum Management COGART 2011, Barcelona, Spain, October 2011.

[Leinonen04] J. Leinonen and M. Juntti. "Modulation classification in adaptive OFDM systems". Proceedings of IEEE Vehicular Technology Conference (VTC), vol. 3, pp. 15541558, May 2004.

[Li09] G. N. Li, L. Yang, N. Zhang and K. Cui. "A New Primary User Sensing Approach Based on LTE Wireless Sensor Networks". 5th International Conference on Wireless Communications, Networking and Mobile Computing, 2009. WiCom '09.

[Lien10] S.-Y. Lien, C.-C. Tseng, K.-C. Chen and C.-W. Su. "Cognitive Radio Resource Management for QoS Guarantees in Autonomous Femtocell Networks". IEEE International Conference on Communications (ICC), pp. 1-6, 23-27 May 2010

[Lotze09] J. Lotze, S. A. Fahmy, B. Özgul, J. Noguera and L. Doyle. "Spectrum sensing on LTE femtocells for GSM spectrum re-farming using Xilinx FPGAs". Proceedings of the SDR'09 Technical Conference and Product Exposition 2009.

[Lunden07] J. Lunden, V. Koivunen, A. Huttunen, and H. V. Poor. "Censoring for Collaborative Spectrum Sensing in Cognitive Radios". Conference Record of the Forty-First

Asilomar Conference on Signals, Systems and Computers, 2007. ACSSC 2007.

[Lunden08] J. Lunden, S. Kassam and V. Koivunen. "Nonparametric cyclic correlation based detection for cognitive radio systems". Cognitive Radio Oriented Wireless Networks and Communications (CrownCom), pp. 1–6, May. 2008.

[Maleki11] S. Maleki and G. Leus. "Censored truncated sequential spectrum sensing for cognitive radio networks". 17th International Conference on Digital Signal Processing (DSP), 2011

[Marchand98] P. Marchand. "Detection and recognition of numerical modulations by means of higher order cyclostationarity" (Translation from French), PhD Thesis, 1998.

[Marks78] R. Marks, G. Wise, D. Haldeman and J. Whited. "Detection in Laplace Noise". IEEE Transactions on Aerospace and Electronic Systems, AES-14(6):866 –872, November. 1978.

[Massey51] F. Massey "The Kolmogorov-Smirnov test for goodness of fit". Journal of the American Statistical Association, vol. 46, no. 253, pp. 68–79, 1951.

[Min09] A. W. Min and K. G. Shin. "Impact of Mobility on Spectrum Sensing in Cognitive Radio Networks". Proceedings of the ACM workshop on Cognitive radio networks. ACM, 2009, pp. 13–18.

[Mishrai06] S. Mishra, A. Sahai, and R. Brodersen. "Cooperative Sensing among Cognitive Radios". IEEE International Conference on Communications, vol. 4, pp. 1658-1663, June 2006.

[Moon06] T. K. Moon. "The Expectation-Maximization Algorithm". IEEE Signal Processing Magazine, November 2006.

[Mustafa03] H. Mustafa, M. Doroslovacki and H. Deng. "Algorithms for emitter detection based on the shape of power spectrum". Proceedings of the Conference on Information Sciences and Systems, The Johns Hopkins University, Baltimore, MD, USA, 2003.

[Neihart07] N. M. Neihart, S. Roy, and D. J. Allstot. "A parallel multi-resolution sensing technique for multiple antenna cognitive radios". IEEE International Symposium on Circuits and Systems, May 2007.

[Noguet11] D. Noguet, M. Gautier, and V. Berg. "Advances in Opportunistic Radio Technologies for TVWS". EURASIP Journal on Wireless Communications and Networking, November 2011.

[Noh08] G. Noh, J. Lee, H. Wang, S. You and D. Hong, "A New Spectrum Sensing Scheme using Cyclic Prefix for OFDM-Based Cognitive Radio Systems". Vehicular Technology Conference VTC Spring 2008.

[OFCOM10] Digital Dividend: Cognitive Access, http://www.ofcom.org.uk/consult/condocs/cognitive

[Öner04] M. Öner, F. Jondral. "Cyclostationairy based air interface recognition for software radio systems". Radio and Wireless Conference, 2004 IEEE

[Öner07] M. Öner. F. Jondral. "Air interface identification for software radio systems". International Journal of Electronic Communications, vol. 61, pp. 104–117, February 2007.

[Panaitopol10_1] D. Panaitopol, J. Fiorina, P.-Y. Kong and C.-K. Tham. "The Effect of Impulsiveness in Inter-Cell Interference on Throughput of TH-IR-UWB Networks". WCNC 2010.

[Panaitopol10_2] D. Panaitopol, J. Fiorina and T. Erseghe. "A Comparison of IR-UWB Receivers Adapted to MUI with Mixture Based Distributions". WCNC, 2010.

[Panaitopol12] D. Panaitopol, R. Datta and G. Fettweis. "Cyclostationary Detection of Cognitive Radio Systems using GFDM Modulation". Wireless Communication and Networking Conference, WCNC IEEE, 2012.

[Pha10] H. N. Pha, P. Gronsynd, P. E. Engelstad and O. Grondalen. "A Dynamic Spectrum Access Scheme for Unlicensed Systems Coexisting with Primary OFDMA Systems". 7th annual consumer communications and networking conference (CCNC), Las Vegas, Nevada, January 2010.

[Proakis95] J. G. Proakis. "Digital Communications", 3rd edition McGraw-Hill, 1995.

[QoSMOS_D1.3] QoSMOS D1.3. "QoSMOS initial system requirements". FP7-ICT-2009-4/248454

[QoSMOS_D4.3] QoSMOS D4.3. "Flexible PHY concepts for white spaces – Final Report". FP7-ICT-2009-4/248454

[Quade65] D. Quade. "On the Asymptotic Power of the One-Sample Kolmogorov-Smirnov Tests". The Annals of Mathematical Statistics, vol. 36, no. 3, pp. 1000–1018, June 1965.

[Quan08] Z. Quan, S. Cui, and A. Sayed. "Optimal Linear Cooperation for Spectrum Sensing in Cognitive Radio Networks". IEEE Journal of Selected Topics in Signal Processing, vol. 2, no. 1, pp. 28–40, February 2008.

[Quan09] Z. Quan, S. Cui, A. Sayed and H. Poor. "Optimal multi-band joint detection for spectrum sensing in cognitive radio networks". IEEE Transactions on Signal Processing 57 (3) (2009) 1128–1140.

[Renard10] J. Renard, J. Verlant-Chenet, J-M. Dricot, P. De Doncker and F. Horlin. "Higher-Order Cyclostationarity Detection for Spectrum Sensing", Draft 2010, EURASIP Journal.

[Sahin10] M. E. Sahin, I. Guvenc and H. Arslan. "Uplink User Signal Separation for OFDMA-Based Cognitive Radios". EURASIP Journal on Advances in Signal Processing, vol. 2010, Article ID 502369, 11 pages, 2010.

[Sake10] L. Saker and S. Elayoubi. "Sleep mode implementation issues in green base stations". 21st International Symposium on Personal Indoor and Mobile Radio Communications (PIMRC), 2010 IEEE

[Shellhammer06] S. J. Shellhammer, N. S. Shankar, R. Tandra, and J. Tomcik. "Performance of Power Detector Sensors of DTV Signals in IEEE 802.22 WRANs". Proceedings of the first international workshop on Technology and policy for accessing spectrum. New York, NY, USA: ACM, 2006, p. 4.

[Shellhammer08] S. J. Shellhammer. "Spectrum sensing in IEEE 802.22," IAPR Workshop on Cognitive Information Processings, June 2008.

[Sohn07] S. H. Sohn, N. Han, J. M. Kim and J. W. Kim. "OFDM signal sensing method based on cyclostationarity detection," Cognitive Radio Oriented Wireless Networks and Communications (CrownCom), pp. 63–68, August 2007.

[Stephens74] M. A. Stephens. "Edf statistics for goodness of fit and some comparisons". Journal of the American Statistical Association, vol. 69, no. 347, pp. 730–737, 1974.

[Sutton08] P. D. Sutton, K. E. Nolan and L. E. Doyle. "Cyclostationary signatures in practical cognitive radio applications". IEEE Journal on Selected Areas in Communications,

vol. 26, no. 1, pp. 13–24, 2008.

[Swami00] A. Swami and B. M. Sadler. "Hierarchical digital modulation classification using cumulants". IEEE Transactions on Communications, vol. 48, no. 3, pp.416-429, March 2000.

[Tachwali10] Y. Tachwali, W. Barnes, F. Basma and H. Refai. "The feasibility of a fast Fourier sampling technique for wireless microphone detection". IEEE 802.22 air interface, INFOCOM IEEE Conference on Computer Communications Workshops, 2010, 2010, pp. 1–5.

[Tandra08] R. Tandra and A. Sahai. "SNR Walls for Signal Detection". IEEE Journal of Selected topics in Signal Processing, vol. 2, no. 1, pp. 4 –17, February 2008.

[Teager89] H. M. Teager and S. M. Teager. "Evidence for nonlinear speech production mechanisms in the vocal tract" Proceedings of the NATO Advanced Study Institute on Speech Production and Speech Modelling, pages 214–261, July 1989.

[Tian07] Z. Tian and G. Giannakis. "Compressed sensing for wide-band cognitive radios". Proceedings of IEEE ICASSP 2007, Vol. 4, 2007, pp. 1357–1360.

[Tropp07] J. Tropp and A. Gilbert. "Signal recovery from random measurements via orthogonal matching pursuit". IEEE Transactions on Information Theory 53 (12) (2007) 4655–4666.

[Tu07] S. Y. Tu, K. C. Chen and R. Prasad. "Spectrum sensing of OFDMA systems for cognitive radios," International Symposium on Personal, Indoor and Mobile Radio Communications (PIRMC), pp. 3–7, September 2007.

[Urkowitz67] H. Urkowitz. "Energy detection of unknown deterministic signals". IEEE Proceedings, vol. 55, no. 4, pp. 523–531, April 1967.

[Vartiainen05] J. Vartiainen, J. J. Lehtomäki, and H. Saarnisaari, "Double-threshold based narrow-band signal extraction". IEEE 61st Semiannual Vehicular Technology conference VTC 2005 Spring, Stockholm, Sweden, May/June 2005.

[Vartiainen07] J. Vartiainen, H. Sarvanko, J. Lehtomäki, M. Juntti and M. Latva-aho. "Spectrum Sensing with LAD based Methods". IEEE International Symposium on Personal, Indoor and Mobile Radio Communications PIMRC 2007, Athens, Greece, September 2007.

[Vartiainen10_1] J. Vartiainen, M. Höyhtyä, J. Lehtomäki, and T. Bräysy. "Priority channel selection based on detection history database" 5th International Conference on Cognitive Radio Oriented Wireless Networks & Communications (CROWNCOM), pp.1-5, June 2010.

[Vartiainen10_2] J. Vartiainen. "Concentrated signal extraction using consecutive mean excision algorithms". PhD thesis, University of Oulu, Finland, 2010.

[Vartiainen10_3] J. Vartiainen, J. Lehtomäki, H. Saarnisaari, M. Juntti and K. Umebayashi. "Two-Dimensional Signal Localization Algorithm for Spectrum Sensing". IEICE Transactions on Communications, E93-B(11), November 2010.

[Vartiainen11_1] J. Vartiainen, J. Lehtomäki, H. Saarnisaari and M. Juntti. "Analysis of the Consecutive Mean Excision Algorithms". Journal of Electrical and Computer Engineering, 2010.

[Vartiainen11_2] J. Vartiainen, J. Lehtomäki and R. Vuohtoniemi. "Performance of the LAD Methods Under Channel Impairments". International Workshop on Cognitive Radio and Advanced Spectrum Management COGART 2011, Barcelona, Spain, October

2011.

[Vartiainen12] J. Vartiainen, J. Lehtomäki and R. Vuohtoniemi, "The LAD Methods in WLAN Indoor Multipath Channels". CrownCom 2012, Stockholm, Sweden, June 2012.

[Visotsky05] E. Visotsky, S. Kuffner and R. Peterson. "On Collaborative Detection of TV Transmissions in Support of Dynamic Spectrum Sharing". 2005 1st IEEE

[Wang09] H. Wang, E.-H. Yang, Z. Zhao, and W. Zhang. "Spectrum Sensing in Cognitive Radio using Goodness of Fit testing". IEEE Transactions on Wireless Communications, vol. 8, no. 11, pp. 5427–5430, November 2009.

[Wang10] W. Wang, J. Cai and A. S. Alfa. "Receiver-Aided Spectrum Sensing Scheme with Spatial Differentiation in OFDM Based Cognitive Radio Networks". IEEE Conference on Computer Communications Workshops, 2010.

[WangH09] W. Wang, H. Li, Y. Sun, and Z. Han. "Attack-proof Collaborative Spectrum Sensing in Cognitive Radio Networks". 43rd Annual Conference on Information Sciences and Systems, pp. 130-134, 2009.

[Wei00] W. Wei and J. M. Mendel. "Maximum-likelihood classification for digital amplitude-phase modulations". IEEE Transactions on Communications, vol. 48, no. 2, pp. 189-193, February 2000.

[Wei04] T. A. Weiss and F. K. Jondral. "Spectrum pooling: an innovative strategy for the enhancement of spectrum efficiency". IEEE Communications Magazine, March 2004.

[Wiley93] R. G. Wiley. "Electronic intelligence: the analysis of radar signals". Artech House, London, 2nd edition, 1993.

[Xu08] S. Xu, Y. Shang and H. Wang. "SVD based Sensing of a Wireless Microphone Signal in Cognitive Radio Networks". IEEE International Conference on Communications Systems, November 2008.

[Yangi07] W. Yang, Y. Cai and Y. Xu. "A Fuzzy Collaborative Spectrum Sensing Scheme in Cognitive Radio". International Symposium on Intelligent Signal Processing and Communication Systems, pp. 566-569, 2007.

[Yücek07] T. Yücek and H. Arlsan. "OFDM Signal Identification and Transmission Parameter Estimation for Cognitive Radio Applications". Global Telecommunications Conference, 2007. GLOBECOM '07. IEEE

[Yücek09] T. Yücek and H. Arslan. "A Survey of Spectrum Sensing Algorithms for Cognitive Radio Applications". IEEE Communications Surveys & Tutorials, vol. 11, no. 1, pp. 116–130, 2009.

[Zahedi10] A. Zahedi-Ghasabeh, A. Tarighat and B. Daneshrad. "Spectrum Sensing of OFDM Waveforms Using Embedded Pilot Sub-carriers". IEEE ICC 2010.

[Zarrin09] S. Zarrin and T. J. Lim. "Composite hypothesis testing for cooperative spectrum sensing in cognitive radio". Proceedings of IEEE ICC 2009, 2009, pp. 1–5.

[Zhang08] H. Zhang, D. Le Ruyet and M. Terre. "Signal detection for OFDM/OQAM system using cyclostationary signatures". IEEE International Symposium on Personal, Indoor and Mobile Radio Communications, (PIMRC08), September 2008.

[Zheng09] Y. Zheng, X. Xie, and L. Yang. "Cooperative Spectrum Sensing based on Blind Source Separation for Cognitive Radio". First International Conference on Future Information Networks, October 2009, pp. 398–402.

[Zhou10] X. Zhou, G. Y. Li, D. Li, D. Wang and A. C. K. Soong. “Probabilistic resource allocation for opportunistic spectrum access”. IEEE Transactions on Wireless Communications, vol. 9, no. 9, September 2010.